WEAR AND CORROSION BEHAVIOUR OF ELECTROLESS Ni-P BASED NANOCOMPOSITE COATINGS

Ph.D. THESIS

by

PREETI MAKKAR

DEPARTMENT OF METALLURGICAL AND MATERIALS ENGINEERING
INDIAN INSTITUTE OF TECHNOLOGY ROORKEE
ROORKEE – 247667, INDIA
MARCH, 2015

WEAR AND CORROSION BEHAVIOUR OF ELECTROLESS Ni-P BASED NANOCOMPOSITE COATINGS

A THESIS

Submitted in partial fulfilment of the requirements for the award of the degree of

DOCTOR OF PHILOSOPHY

in

METALLURGICAL AND MATERIALS ENGINEERING

by

PREETI MAKKAR

DEPARTMENT OF METALLURGICAL AND MATERIALS ENGINEERING
INDIAN INSTITUTE OF TECHNOLOGY ROORKEE
ROORKEE – 247667, INDIA
MARCH, 2015

INDIAN INSTITUTE OF TECHNOLOGY ROORKEE
ROORKEE

CANDIDATE'S DECLARATION

I hereby certify that the work which is being presented in the thesis, entitled **"Wear and Corrosion behaviour of Electroless Ni-P based Nanocomposite Coatings"** in partial fulfilment of the requirements for the award of the degree of Doctor of Philosophy and submitted in the Department of Metallurgical and Materials Engineering, Indian Institute of Technology Roorkee, Roorkee is an authentic record of my own work carried out during the period from July, 2010 to March, 2015 under the supervision of **Dr. R.C. Agarwala**, Former Professor and **Dr. Vijaya Agarwala**, Professor, Department of Metallurgical and Materials Engineering, Indian Institute of Technology Roorkee, Roorkee.

The matter presented in this thesis has not been submitted by me for the award of any other degree of this or any other institute.

(**PREETI MAKKAR**)

This is to certify that the above statement made by the candidate is correct to the best of our knowledge.

(Dr. R.C. Agarwala)
Supervisor

(Dr. Vijaya Agarwala)
Supervisor

Date:

ABSTRACT

Wear and corrosion resistance is counted as the basic requirements for reliable and efficient service life of the engineering system. The purpose of conducting wear and corrosion tests of the coatings is to understand behavior of a particular family of materials under tribological applications and corrosive environments. Nickel based dispersion coatings are used in multitude applications where corrosion and wear resistance is required. Electroless coating technology is a controlled chemical reduction process which has emerged as a leading growth area in surface engineering, metal finishing. Here the driving force is supplied by chemical reducing agent in solution (sodium hypophosphite). The reaction continues as long as the surface remains in contact with the bath solution or solution gets depleted of metallic ions. Electroless nickel coatings are widely used in different industries because of their physical properties, such as good hardness, coating uniformity, wear and corrosion resistance, and capability of depositing on either conductive or nonconductive substrates. Nanocomposite coatings are the ones in which either the thickness of coatings or size of second phase particles that are embedded into the matrix is of nanosized. EL composite coatings can be developed when either the second phase(s) can be added during the coating or the second phase(s) can be generated to nucleate and grow within the bath. The incorporation of nanosized ceramic particles like alumina, zirconia and titania in Ni-P matrix offers many advantages in terms of hardness, friction coefficient, chemical inertness, and thermal stability of the resulting composite coatings. Hence a quest for improved wear and corrosion performances has led many researchers to develop and investigate either newer variants of electroless nickel based nanocomposite coatings or provide modification in the coating process parameters. Moreover, due to complexity of the structure, wide variety of wear and corrosion apparatus, distinct environment, substrate and counterface medium used during the wear and corrosion tests, there is always a need regarding the systematic studies of wear and corrosion behavior of Ni-P-X nanocomposite coatings. Therefore, an effort to develop EL N-P-X [X= Al_2O_3, ZrO_2 and TiO_2] nanocomposite coatings by conventional and non-conventional means on mild steel substrate for wear and corrosion applications has been made in this thesis.

The objective of the present work is to provide a better understanding of preparation methods used for the synthesis of nanoparticles incorporated in Ni-P matrix. This study also aims to develop EL Ni-P-X [X= Al_2O_3, ZrO_2 and TiO_2] nanocomposite coatings through conventional and non-conventional methods. These developed coatings are characterized,

heat treated and subjected to wear, friction and corrosion tests and compared with Ni-P alloy coatings.

The thesis is divided into nine chapters. **Chapter 1** presents an introduction to the electroless Ni-P and Ni-P-X coating technology for enhancing the service life of components used in various industries. It also gives an insight into the reinforcements used along with their synthesis routes. This chapter also provides a brief idea about the need, aim and scope for the present work.

Chapter 2 outlines a brief review of literature, discussing the advantages, mechanisms, condition required and limitations of EL Ni-P coating technology. The significance of EL Ni-P-X nanocomposite coatings to yield desired properties is also featured. It also discusses the beneficial aspects of reinforcements like Al_2O_3, ZrO_2 and TiO_2 into Ni-P matrix and a brief survey on their preparation modes are outlined. An extensive survey on studies where Al_2O_3, ZrO_2 and TiO_2 particles are incorporated in Ni-P matrix especially for wear and corrosion applications has also been presented. All these lead to formulation of problem for undertaking the present work.

The proposed formulation of the problem is discussed in **chapter 3**. It defines the scope of present work based on literature review and the adopted methodology and the gaps of information found in the area of development of EL Ni-P-X [X=Al_2O_3, ZrO_2 and TiO_2] nanocomposite coatings for wear and corrosion resistance applications.

Experimental details including raw materials used, experimental set-up, equipments used, process parameters employed in synthesis of Al_2O_3, ZrO_2 and TiO_2 nanoparticles by two approaches are discussed in **chapter 4**. The details including the development of EL Ni-P based nanocomposite coatings by two different means are also featured. The characterization techniques along with details of mechanical and physical properties tested are also presented in this chapter.

Chapter 5 describes the synthesis of nanosized Al_2O_3, ZrO_2 and TiO_2 powders using two different approaches namely Bottom up and Top down. The chemical precipitation method was employed to synthesize Al_2O_3, ZrO_2 and TiO_2 nanoparticles. The thermal studies of the dried powders were carried out. Al_2O_3, ZrO_2 and TiO_2 nanoparticles of average particle size of 12nm, 7nm and 10nm were synthesized by this bottom up approach. Al_2O_3, ZrO_2 and TiO_2 nanoparticles were also prepared separately by mechanical milling in high energy ball mill at 250 rpm for 40h. The variation of particle size with respect to different extents of milling (5h, 10h, 20h, 30h and 40h) was also studied. Increase in milling time lowered the particle size and formed amorphous phases. The Al_2O_3, ZrO_2 and TiO_2

nanopowders of size range 15nm, 21nm and 39nm respectively were achieved after 40h of milling. The prepared nanopowders 'X' were used as the reinforcement for development of Ni-P-X [X= Al_2O_3, ZrO_2 and TiO_2] nanocomposite coatings as discussed in the chapter 6.

Chapter 6 features the development of electroless Ni-P-X [X= Al_2O_3, ZrO_2 and TiO_2] nanocomposite coatings by conventional and non-conventional means where nanosized chemically prepared and milled powders are employed as reinforcements in conventional route. The optimal concentration of 'X' particles for sound Ni-P-X coatings in non-conventional route is determined. Its heat treatment effect (400^oC for 1h) on morphology, phase and hardness studies are analysed with respect to Ni-P alloy coatings. The results revealed that the codeposition of 'X' nanoparticles into Ni-P matrix by conventional route results in surface modification of the coatings with presence of nodular protrusions as analysed by FESEM micrographs. A typical globular type morphology with no clear 'X' [X= Al_2O_3, ZrO_2 and TiO_2] particles can be observed on the surface of the *insitu* Ni-P-X nanocomposite coatings. The existence of nanosized 'X' particles can be confirmed by virtue of EDAX, X-ray mapping and XRD analysis. AFM studies depicts that non-conventional Ni-P-X nanocomposite coatings have relatively smooth surface over the conventional Ni-P-Al_2O_3 coatings. The thickness of the developed coatings is ~ 30μm showing good adhesion between the mild steel substrate and the coating. The optimum 'X' concentration is found to be 15g/l for sound non-conventional EL Ni-P-X coatings with higher hardness. All developed Ni-P-X nanocomposite coatings exhibits higher hardness than Ni-P deposits due to the reinforcement of hard second phase 'X' in Ni-P matrix and achieves maximum on heat treatment due to the precipitation of Ni_3P phase. AFM studies reveal that the roughness of the coatings decreases after heat treatment. Non-conventional Ni-P-X nanocomposite coatings attained highest hardness over the two conventionally developed coatings. However, the conventional coatings containing milled nanopowders exhibited higher hardness over chemically prepared particles on account of its better adhesion on Ni-P surface.

Chapter 7 discusses the results obtained on the friction, wear and corrosion resistance of EL Ni-P-X [X= Al_2O_3, ZrO_2 and TiO_2] nanocomposite coatings developed by conventional and non-conventional means and compared with Ni-P alloy coatings. The effect of loads (1, 1.5 and 2N) and sliding velocities (0.1 and 0.2m/s) on the specific wear rate of EL Ni-P and Ni-P-X nanocomposite coatings in heat treated condition are discussed. The results indicates an improvement in wear resistance and lower coefficient of friction for all EL Ni-P-X nanocomposite coatings with respect to Ni-P alloy coatings, both at different

loads and sliding velocities owing to its higher hardness. Mild adhesive wear is the predominant mechanism taking place during wear for all Ni-P-X nanocomposite coatings. The electrochemical polarization curves for EL Ni-P and Ni-P-X nanocomposite coatings in 'as coated' and 'heat treated' conditions under different environments (pH-4.5 & 8) are analysed. EL Ni-P-X nanocomposite coatings are found to have a higher corrosion potentials (E_{corr}) and lower corrosion currents (I_{corr}) than those of Ni-P coating, indicating an improved corrosion protection in both acidic (pH-4.5) and alkaline (pH-8) atmosphere. The heat treatment also enhances the corrosion resistance due to formation of compact, smooth and homogenous coatings and the trend is followed in both acidic and alkaline environments. The lower wear rate, friction coefficient and corrosion rate is showed by EL Ni-P-X nanocomposite coatings developed by *insitu* route compared to conventional ones. However, the inclusion of milled nanoparticles on Ni-P surface imparts slightly lower friction coefficient and wear rate but higher corrosion rate with respect to chemically prepared nanoparticles. The corroded surfaces are analysed with the help of FESEM micrographs. Comparatively, better corrosion resistance is observed in alkaline (pH-8) atmosphere as compared to acidic (pH-5) one.

Chapter 8 draws the conclusion from this work and contribution made in this thesis on development of Ni-P-X [X=Al_2O_3, ZrO_2, TiO_2] nanocomposite coatings with respect to its hardness, wear, friction and corrosion characteristics.

The scope for the future work on the area of EL Ni-P based nanocomposite coatings is suggested in **Chapter 9.**

ACKNOWLEDGEMENT

I would like to express my heartiest thanks and deepest gratitude to my respected supervisors Dr. R.C. Agarwala, Former Professor, Department of Metallurgical and Materials Engineering (MMED) and Dr. V. Agarwala, Professor, MMED & Joint faculty, Center of Excellence- Nanotechnology (CON) for their inspiration, expert guidance and indefatigable efforts at every stage of this thesis work. This thesis could not have been completed without their support and encouragement. Their timely help, constructive criticism, positive attitude, painstaking efforts, humanistic and warm personal approaches made me capable to compile the thesis in its present form. Prof. R.C. Agarwala spent his precious time and efforts directing the research work. I believe that the things that I learned from him will benefit me over the course of my lifetime. I would also like to express special thanks to Prof. Vijaya Agarwala for her invaluable discussions and suggestions despite her very busy schedule. Her motivation and energy has always been a driving force for bringing confidence and successful completion of this thesis work.

I am highly grateful to Prof. S. K. Nath, Head, MMED, IIT Roorkee and all faculty members of the department for their help and support throughout the course of my research work. Profound sense of appreciation acknowledged to all the members of my Student Research Committee (SRC), Dr. G.P. Chaudhary (Chairman), Dr. K.L. Yadav (External member) and Dr. B.S.S. Daniel (Internal member) for their valuable suggestions, encouragement and motivation to improve the quality of my research work. My special thanks are due to Dr. V.V. Dabhade, Dr. B.V. Manoj Kumar and Dr. Ujjawal Prakash, MMED for their ever kind string of help, moral support and encouragement.

Deep sense of admiration acknowledged to the Head, Institute Instrumentation Centre (IIC), for their co-operation in extending the necessary facilities and supports during the course of characterization work. A special thanks to all the IIC technical staff members for giving their full assistance for all characterization facilities. I would like to thank all the technical and administrative staff of MMED and CON for their corporation during the tenure of the work.

Sincere appreciation and special thank to all my friends and colleagues for their moral support and memorable stay at IIT Roorkee. I enjoyed working with Dr. Abhishek Kumar, Dr. Debesh Devdutta Mishra, Ms. Nidhi Rana, Mr. Ram Kishore, Dr. Siddharth Jain, Mr. Sunil Kumar, Mr. Tilak Joshi, Mr. Himanshu Panjiar, Mr. Ravikant, Mr.V.M.R. Mutthaiah, Mr. Ashish Selokar, Mr. Sanjay Rathore, Mr. Ravi Panwar, Mr. S. Vidyasagar

and Mohd. Najim in MMED; and Dr. Mini Namdeo Giri, Post Doctoral Fellow and Mr. Rahul Saini from Centre of Excellence-Nanotechnology. Thanks are due to, Ms. Reena Gupta, Ms. Poornima Dubey and Mr. Nilesh Dorkar for helping me directly or indirectly during the entire period of this work.

I would like to express heartiest gratitude to my parents, Shri R.L. Makkar and Smt. Sushma Makkar, for showering their blessings over me. My heartiest thanks to my elders, Mr. Jatinder Makkar, Ms. Sunita Makkar, Dr. Jyoti Makkar, Ms. Aarti Makkar and my younger brother Mr. Rajeev Makkar for their extended support and making me free from my social responsibilities during my Ph.D. work. I am thankful to my nephew Gaurav and niece Khushi whose smiling, loving and innocent faces has always refreshed me and relieved the stress of my research work.

Finally, I would like to express my sincere thanks to the, "Women Scientists Scheme (WOS-'A')", Department of Science & Technology (DST), New Delhi and Uttarakhand State Council for Science and Technology (UCOST), Dehradun, India for providing me with the financial support during the tenure of my research work.

Above all, I express my sincere thanks to GOD from the core of my heart for giving the strength and patience to accomplish my research work.

Roorkee
Dated:

(**PREETI MAKKAR)**

TABLE OF CONTENTS

Page No.

CANDIDATE'S DECLARATION

ABSTRACT i

ACKNOWLEDGEMENT v

TABLE OF CONTENTS vii

LIST OF FIGURES xiii

LIST OF TABLES xix

LIST OF PUBLICATIONS xxi

ACROMYNS xxv

1 INTRODUCTION 1

2 LITERATURE REVIEW 7

2.1 Introduction 7

2.2 Development of Electroless Deposition- A brief history 7

2.3 Classification of Electroless Coatings 8

2.3.1 Electroless Metallic Coatings 8

2.3.2 Electroless Alloy Coatings 8

2.3.2.1 *Electroless Nickel Bath - Its Fundamental Aspects* 9

2.3.2.2 *Bonding mechanisms of electroless nickel coatings* 13

2.3.2.3 *Factors affecting the EL nickel coating process* 15

2.3.2.4 *Structure of EL Ni-P alloy Coatings* 16

2.3.3 Electroless Composite Coatings 17

2.4 Brief Overview on the synthesis of metal oxide ceramics nanoparticles 19

2.4.1 Methods for synthesis of alumina, zirconia and titania nanoparticles 20

2.4.1.1 *Chemical precipitation- bottom up approach* 21

2.4.1.2 *Mechanical milling- top down approach* 22

2.5 Performance of Ni-P-X [X=Al_2O_3, ZrO_2 and TiO_2] nanocomposite coatings 24

2.5.1 Properties of Ni-P-Al_2O_3 nanocomposite coatings 24

2.5.2 Properties of Ni-P-ZrO_2 nanocomposite coatings 28

2.5.3 Properties of Ni-P-TiO_2 nanocomposite coatings 31

2.6 Summary 34

3 PROBLEM FORMULATION 35
3.1 Backgrounnd 35
3.2 Proposed Methodology 36
4 EXPERIMENTAL DETAILS 39
4.1 Introduction 39
4.2 Synthesis of Nanoparticles 39
4.2.1 Bottom-up Approach (Chemical route) 39
4.2.1.1 *Synthesis of Al_2O_3 particles* 40
4.2.1.2 *Synthesis of ZrO_2 particles* 40
4.2.1.3 *Synthesis of TiO_2 particles* 40
4.2.2 Top-down Approach (Mechanical Milling route) 41
4.3 Characterization of Nanoparticles 41
4.3.1 Field Emission Scanning Electron Microscopy (FESEM) 41
4.3.2 Transmission Electron Microscopy (TEM) 42
4.3.3 X-Ray Diffraction (XRD) 42
4.3.4 Thermal Analysis 42
4.4 Substrate Preparation 43
4.4.1 Degreasing and Etching of substrate 43
4.4.2 Pretreatment of substrate 44
4.5 EL Bath 44
4.5.1 Ni-P Alloy Coating 45
4.5.2 Ni-P-X Composite Coating 46
4.5.2.1 *Conventional Composite Coating* 46
4.5.2.2 *Non-Conventional Composite Coating* 46
4.5.3 Heat Treatment (HT) of Coatings 47
4.6 Characterization of EL Coatings before and after HT 47
4.6.1 FESEM 47
4.6.2 XRD 47
4.6.3 AFM 47
4.6.4 MicroHardness 48
4.6.5 Wear and Friction Studies 48
4.6.5.1 *Wear Track Studies* 48
4.6.6 Corrosion Studies 48
4.6.6.1 *Electrochemical Corrosion* 48

4.7 Summary 49
5 SYNTHESIS AND CHARACTERIZATION OF NANOPARTICLES 51
5.1 Introduction 51
5.2 Synthesis and Characterization of Nanoparticles by Bottom up Approach (Chemical Precipitation Route) 51
5.2.1 Alumina (Al_2O_3) nanoparticles 51
5.2.1.1 *Thermal Analysis* 51
5.2.1.2 *Morphological Study* 52
5.2.1.3 *XRD Analysis* 54
5.2.2 Zirconia (ZrO_2) nanoparticles 54
5.2.2.1 *Thermal Analysis* 54
5.2.2.2 *Morphological Study* 54
5.2.2.3 *XRD Analysis* 56
5.2.3 Titania (TiO_2) nanoparticles 56
5.2.3.1 *Thermal Analysis* 56
5.2.3.2 *Morphological Study* 57
5.2.3.3 *XRD Analysis* 58
5.3 Synthesis and Characterization of Nanoparticles by Top down Approach (Mechanical Milling Route) 59
5.3.1 Alumina (Al_2O_3) nanoparticles 59
5.3.1.1 *Morphological Study* 59
5.3.1.2 *XRD Analysis* 62
5.3.2 Zirconia (ZrO_2) nanoparticles 63
5.3.2.1 *Morphological Study* 63
5.3.2.2 *XRD Analysis* 65
5.3.3 Titania (TiO_2) nanoparticles 66
5.3.3.1 *Morphological Study* 66
5.3.3.2 *XRD Analysis* 68
5.4 Summary 70
6 DEVELOPMENT OF Ni-P AND Ni-P-X NANOCOMPOSITE COATINGS USING ELECTROLESS TECHNIQUE 71
6.1 Introduction 71
6.2 Development of EL Ni-P alloy coatings 71
6.2.1 Composition of Substrate Material 71

6.2.2 Morphological studies of 'as coated' and HT alloy coatings 72
6.2.3 XRD Analysis of 'as coated' and HT alloy coatings 72
6.3 Development of EL Ni-P-X [X= Al_2O_3, ZrO_2, TiO_2] nanocomposite coatings 74
6.3.1 Development of EL conventional Ni-P-Al_2O_3 nanocomposite coatings 74
6.3.1.1 *Morphological studies of 'as coated' and HT, (C_1 and M_1) nanocomposite coatings* 74
6.3.1.2 *XRD analysis of 'as coated' and HT , (C_1 and M_1)coatings* 77
6.3.2 Development of non-conventional (*insitu*) EL Ni-P-Al_2O_3 nanocomposite coatings and optimization of concentration of second phase particles 79
6.3.2.1 *Morphological studies of 'as coated' and HT, I_1 nanocomposite coatings* 80
6.3.2.2 *XRD analysis of 'as coated' and HT, I_1 nanocomposite coatings* 84
6.3.3 Development of Ni-P-ZrO_2 nanocomposite coatings 85
6.3.3.1 *Morphological studies of 'as coated' and HT, (C_2, M_2 and I_2) nanocomposite coatings* 85
6.3.3.2 *XRD analysis of 'as coated' and HT, (C_2, M_2 and I_2) nanocomposite coatings* 90
6.3.4 Development of Ni-P-TiO_2 nanocomposite coatings 90
6.3.4.1 *Morphological studies of 'as coated' and HT, (C_3, M_3 and I_3) nanocomposite coatings* 91
6.3.4.2 *XRD analysis of 'as coated' and HT, (C_3, M_3 and I_3) nanocomposite coatings* 95
6.3.5 Thickness of heat treated Ni-P based nanocomposite coatings 95
6.4 Hardness studies of EL Ni-P alloy and Ni-P-X nanocomposite coatings 97
6.4.1 Hardness of EL *insitu* Ni-P-Al_2O_3 nanocomposite coatings developed at various concentrations 97
6.4.2 Hardness of EL Ni-P and Ni-P-X [Al_2O_3, ZrO_2 and TiO_2] nanocomposite coatings 98
6.5 Summary 100
7 WEAR AND CORROSION STUDIES OF EL Ni-P AND Ni-P-X NANOCOMPOSITE COATINGS 103
7.1 Introduction 103
7.2 Wear and Friction studies of EL Ni-P alloy coatings 103

7.2.1 Wear rate 103
7.2.2 Friction studies 104
7.2.3 Morphological studies of worn surfaces 105
7.3 Wear and Friction studies of EL Ni-P-X [Al_2O_3, ZrO_2 and TiO_2] nanocomposite coatings 106
7.3.1 EL Ni-P-Al_2O_3 nanocomposite coatings (C_1, M_1 and I_1) 106
7.3.1.1 *Wear rate* 106
7.3.1.2 *Friction studies* 107
7.3.1.3 *Morphological studies of worn surfaces* 108
7.3.2 EL Ni-P-ZrO_2 nanocomposite coatings (C_2, M_2 and I_2) 110
7.3.2.1 *Wear rate* 110
7.3.2.2 *Friction studies* 111
7.3.2.3 *Morphological studies of worn surfaces* 112
7.3.3 EL Ni-P-TiO_2 nanocomposite coatings (C_3, M_3 and I_3) 114
7.3.3.1 *Wear rate* 114
7.3.3.2 *Friction studies* 115
7.3.3.3 *Morphological studies of worn surfaces* 116
7.4 Corrosion studies of EL Ni-P alloy coatings 119
7.4.1 Potentiodynamic polarisation studies 119
7.4.2 Microstructural analysis 120
7.5 Corrosion studies of EL Ni-P-X [Al_2O_3, ZrO_2 and TiO_2] nanocomposite coatings 121
7.5.1 EL Ni-P-Al_2O_3 nanocomposite coatings (C_1, M_1 and I_1) 121
7.5.1.1 *Potentiodynamic polarisation studies* 121
7.5.1.2 *Microstructural analysis* 124
7.5.2 EL Ni-P-ZrO_2 nanocomposite coatings (C_2, M_2 and I_2) 126
7.5.2.1 *Potentiodynamic polarisation studies* 126
7.5.2.2 *Microstructural analysis* 128
7.5.3 EL Ni-P-TiO_2 nanocomposite coatings (C_3, M_3 and I_3) 130
7.5.3.1 *Potentiodynamic polarisation studies* 130
7.5.3.2 *Microstructural analysis* 132
7.6 Summary 136
8 CONCLUSION 137
8.1 Synthesis and Characterisation of reinforcements ‘X’ used in Ni-P-X system 137
8.2 Synthesis and Characterisation of EL Ni-P and Ni-P-X Nanocomposite Coatings 137

8.3 Properties of EL Ni-P and Ni-P-X Nanocomposite Coatings 138
9 SUGGESTIONS FOR FUTURE WORK 141
REFERENCES 143

LIST OF FIGURES

Figure No.	Description	Page No.
Fig. 2.1	Schematic representation of growth and bonding mechanism of EL nickel coating with the substrate	14
Fig. 2.2	Schematic representation of diffusion bonding mechanism showing, (a) Interface of EL Ni-P coating in 'as coated' condition and (b) Diffusion layer of Ni-P at the interface after heat treatment	14
Fig. 3.1	Flow chart showing the experimental details of proposed research plan	38
Fig. 4.1	Experimental set up for EL Coatings	44
Fig. 5.1	Thermal analysis of (a) Precursor $AlCl_3$, (b) Dried Al_2O_3 powder from room temperature to 1500^oC	52
Fig. 5.2	Microstructures of Al_2O_3 powder under, (a) FESEM and (b) TEM (*inset* SAD pattern).	53
Fig. 5.3	EDAX analysis along with surface morphology of calcined Al_2O_3 powders	53
Fig. 5.4	XRD patterns of $AlCl_3$, dried Al_2O_3 and calcined Al_2O_3 at 1200^oC for 2h	53
Fig. 5.5	DTA/TG traces from room temperature to 1000^oC of (a) precursor $ZrOCl_2$ and (b) Dried ZrO_2 powder	55
Fig.5.6	Micrographs of calcinated ZrO_2 powder (a) FESEM and (b) TEM (*inset* SAD pattern)	55
Fig. 5.7	EDAX analysis and surface morphology of calcined ZrO_2 powders	55
Fig. 5.8	XRD patterns of $ZrOCl_2$, dried ZrO_2 and calcined ZrO_2 at 400^oC for 4h	56
Fig. 5.9	DTA/TG traces of dried TiO_2 powder from room temperature to 1000^oC	57
Fig. 5.10	TiO_2 powder examined (a) FESEM (b) TEM (*inset* SAD pattern)	57
Fig. 5.11	EDAX analysis with morphology of calcined TiO_2 powders	58

Fig. 5.12	XRD patterns of Dried TiO_2 and calcined TiO_2 at 500^oC for 1h	58
Fig. 5.13	FESEM micrographs of Al_2O_3 powder (a) As received, milled for different extents of time (b) 5 h (c) 10 h (d) 20 h (e) 40 h, (f) TEM micrograph of 40h milled Al_2O_3 powder with SAD pattern	61
Fig. 5.14	(a) Effect of milling hours on the particle size of Al_2O_3 powder by FESEM quantitative analysis, (b) EDAX analysis along with surface morphology of 40h milled Al_2O_3 powders	62
Fig. 5.15	XRD patterns of As received and Milled Al_2O_3 powder for 5h, 10h, 20h, 30h and 40h	62
Fig. 5.16	FESEM micrographs of ZrO_2 powder (a) As received, milled for different extents of time (b) 5 h, (c) 10 h, (d) 20 h, (e) 40 h and (f) TEM micrograph of 40h milled ZrO_2 powder with SAD pattern	64
Fig. 5.17	(a) Effect of milling hours on the particle size of ZrO_2 powder by FESEM quantitative analysis, (b) EDAX analysis along with surface morphology of 40h milled ZrO_2 powders	65
Fig. 5.18	XRD patterns of (a) As received and Milled ZrO_2 powder for 5h, 10h, 20h, 30h and 40h	66
Fig. 5.19	FESEM micrographs of TiO_2 powder (a) As received, milled for different extents of time (b) 5 h, (c) 10 h, (d) 20 h, (e) 40 h and (f) TEM micrograph of 40h milled TiO_2 powder with SAD pattern	67
Fig. 5.20	(a) Effect of milling hours on the particle size of TiO_2 powder by FESEM quantitative analysis, (b) EDAX analysis along with surface morphology of 40h milled TiO_2 powders	68
Fig. 5.21	XRD patterns of As received and Milled TiO_2 powder for 5h, 10h, 20h, 30h and 40h	69
Fig. 6.1	FESEM micrographs of EL Ni-P alloy coatings, (a) As coated and (b) HT conditions	72
Fig. 6.2	AFM morphologies of EL Ni-P coatings (a) As coated, (b) HT	73
Fig. 6.3	XRD patterns of EL Ni-P alloy coating in ‘as coated’ and HT conditions	73

Fig. 6.4	FESEM micrographs of EL conventional Ni-P-Al_2O_3 coatings, (a) C_1, (b) C_1 HT, (c) M_1 and (d) M_1 HT	75
Fig. 6.5	EDAX and X-ray Mapping Analysis of heat treated EL Ni-P-Al_2O_3 coatings in the selected region under FESEM (a) C_1 and (b) M_1 showing particle entrapment	76
Fig. 6.6	AFM studies of Ni-P-Al_2O_3 nanocomposite coatings, (a) C_1, (b) C_1 HT, (c) M_1 and (d) M_1 HT	78
Fig. 6.7	XRD patterns of Ni-P-Al_2O_3 nanocomposite coatings with different Al_2O_3, C_1 and M_1 in 'as coated' and HT conditions	79
Fig. 6.8	FESEM micrographs showing surface morphology of EL *insitu* Ni-P-Al_2O_3 nanocomposite coatings at different concentrations, (a) A_1, (b) A_2 and (c) A_3	81
Fig. 6.9	EDAX analysis of EL *insitu* Ni-P-Al_2O_3 nanocomposite coatings at different concentrations under FESEM (a) A_1, (b) A_2 and (c) A_3	82
Fig. 6.10	Effect of reactant, $AlCl_3$ concentration, in EL bath on Al_2O_3 content in the deposit	83
Fig. 6.11	Area mapping studies of optimized heat treated *insitu* EL Ni-P-Al_2O_3 nanocomposite coating (A_2) in the selected region under FESEM showing particle entrapment	83
Fig. 6.12	AFM micrographs of optimized EL *insitu* Ni-P-Al_2O_3 nanocomposite coating in (a) 'as coated', (b) HT conditions	84
Fig. 6.13	XRD patterns of *insitu* Ni-P-Al_2O_3 nanocomposite coatings at different concentrations A_1, A_2 and A_3 in 'as coated' and HT conditions	85
Fig. 6.14	FESEM micrographs of EL Ni-P-ZrO_2 nanocomposite coatings, (a) C_2, (b) C_2 HT, (c) M_2, (d) M_2 HT, (e) I_2, (f) I_2 HT	87
Fig. 6.15	EDAX and X-ray Mapping analysis of heat treated EL Ni-P-ZrO_2 nanocomposite coatings in the selected region under FESEM (a) C_2, (b) M_2 and (c) I_2	88
Fig. 6.17	XRD patterns of Ni-P-ZrO_2 coatings with different mode of synthesis C_2, M_2 and I_2 in 'as coated' and HT conditions	90
Fig. 6.18	FESEM micrographs of EL Ni-P-TiO_2 nanocomposite coatings, (a) C_3, (b) C_3 HT, c) M_3, (d) M_3 HT, (e) I_3, (f) I_3 HT	92

Fig. 6.19	EDAX and X-ray Mapping analysis of heat treated EL Ni-P-TiO_2 nanocomposite coatings in the selected region under FESEM, (a) C_3, (b) M_3 and (c) I_3 showing particle entrapment	93
Fig. 6.20	AFM studies of Ni-P-TiO_2 nanocomposite coatings, (a) C_3, (b) C_3 HT, (c) M_3, (d) M_3 HT, (e) I_3 and (f) I_3 HT	94
Fig. 6.21	XRD patterns of Ni-P-TiO_2 nanocomposite coatings with different mode of synthesis, C_3, M_3 and I_3 in 'as coated' and HT conditions	96
Fig. 6.22	FESEM micrograph showing the cross section of heat treated EL Ni-P based nanocomposite coating using (a) secondary electrons and (b) back scattered electrons	96
Fig. 6.23	Microhardness of *insitu* EL Ni-P-Al_2O_3 nanocomposite coatings at various concentrations	98
Fig. 6.24	Hardness of EL coatings (a) Ni-P (b) Ni-P-Al_2O_3 (C_1, M_1, I_1) (c) Ni-P-ZrO_2 (C_2, M_2, I_2) (d) Ni-P-TiO_2 (C_3, M_3, I_3) in 'as coated' and HT conditions	100
Fig. 7.1	Variation in wear rate of heat treated EL Ni-P alloy coatings at varying (a) Loads (b) Sliding velocities	104
Fig. 7.2	(a) Effect of sliding distance on the friction coefficient of EL Ni–P alloy coating at varying loads (b) Variation of friction coefficient of EL Ni–P alloy coating with sliding velocities	104
Fig. 7.3	FESEM micrographs of EL Ni-P coatings under loads (a) 1N (b) 1.5 N (c) 2N at 0.1 m/s sliding velocity (d) Under 1N load at 0.2 m/s sliding velocity after wear tests	105
Fig. 7.4	Variation in wear rate of heat treated C_1, M_1 and I_1 nanocomposite coatings at varying (a) Loads and (b) Sliding velocities	107
Fig. 7.5	Effect of sliding distance on the coefficient of friction of (a) C_1, (b) M_1 and (c) I_1 nanocomposite coatings at varying loads	108
Fig. 7.6	Variation of friction coefficient of (a) C_1, (b) M_1 and (c) I_1 nanocomposite coatings with sliding velocities	109
Fig. 7.7	FESEM micrographs of C_1 nanocomposite coatings under loads (a) 1N, (b) 2N at 0.1 m/s sliding velocity and (c) Under 1N load at 0.2 m/s sliding velocity after wear tests	109

Fig. 7.8	FESEM micrographs of M_1 nanocomposite coatings under loads (a) 1N, (b) 2N at 0.1m/s sliding velocity and (c) Under 1N load at 0.2 m/s sliding velocity after wear tests	110
Fig. 7.9	FESEM micrographs of I_1 nanocomposite coatings under loads (a) 1N, (b) 2N at 0.1m/s sliding velocity and (c) Under 1N load at 0.2m/s sliding velocity after wear tests	110
Fig. 7.10	Variation in wear rate of heat treated C_2, M_2 and I_2 nanocomposite coatings at varying (a) Loads and (b) Sliding velocities	111
Fig. 7.11	Effect of sliding distance on the coefficient of friction of (a) C_2, (b) M_2 and (c) I_2 nanocomposite coatings at varying loads	112
Fig. 7.12	Variation of friction coefficient of (a) C_2, (b) M_2 and (c) I_2 nanocomposite coatings with sliding velocities	113
Fig. 7.13	FESEM micrographs of C_2 nanocomposite coatings under loads (a) 1N, (b) 2N at 0.1m/s sliding velocity and (c) Under 1N load at 0.2m/s sliding velocity after wear tests	113
Fig. 7.14	FESEM micrographs of M_2 nanocomposite coatings under loads (a) 1 N, (b) 2 N at 0.1 m/s sliding velocity and (c) Under 1N load at 0.2 m/s sliding velocity after wear tests	114
Fig. 7.15	FESEM micrographs of I_2 nanocomposite coatings under loads (a) 1N (b) 2N at 0.1m/s sliding velocity and (c) Under 1N load at 0.2m/s sliding velocity after wear tests	114
Fig. 7.16	Variation in wear rate of heat treated C_3, M_3 and I_3 nanocomposite coatings at varying (a) Loads (b) Sliding velocities	115
Fig. 7.18	Variation of friction coefficient of (a) C_3, (b) M_3 and (c) I_3 nanocomposite coatings with sliding velocities	117
Fig. 7.19	FESEM micrographs of C_3 nanocomposite coatings under loads (a) 1N, (b) 2N at 0.1m/s sliding velocity and (c) Under 1N load at 0.2 m/s sliding velocity after wear tests	118
Fig. 7.20	FESEM micrographs of M_3 nanocomposite coatings under loads (a) 1N, (b) 2N at 0.1m/s sliding velocity and (c) Under 1N load at 0.2m/s sliding velocity after wear tests	118

Fig. 7.21	FESEM micrographs of I_3 nanocomposite coatings under loads (a) 1N, (b) 2N at 0.1m/s sliding velocity and (c) Under 1N load at 0.2m/s sliding velocity after wear tests	118
Fig. 7.22	Tafel Polarisation curves of EL Ni-P alloy coatings in varied environments with pH (a) 4.5 and (b) 8.0	120
Fig. 7.23	Morphologies of EL Ni-P alloy coatings after corrosion tests at pH-4.5 (a) As coated, (b) HT and at pH-8 (c) As coated, (d) HT conditions under FESEM	121
Fig. 7.24	Tafel polarisation curves of C_1, M_1 and I_1 nanocomposite coatings in 'as coated' and HT conditions under environments with pH (a) 4.5 and (b) 8.0	123
Fig. 7.25	Morphologies of nanocomposite coatings after corrosion tests at pH-4.5, (a) C_1, (b) C_1 HT, (c) M_1 and (d) I_1 under FESEM	125
Fig.7.26	Morphologies of nanocomposite coatings after corrosion test at pH-8, (a) C_1, (b) C_1 HT, (c) M_1 and (d) I_1 under FESEM	125
Fig. 7.27	Tafel polarisation curves of C_2, M_2 and I_2 nanocomposite coatings in 'as coated' and HT conditions under environments with pH (a) 4.5 and (b) 8.0	127
Fig. 7.28	Morphologies of nanocomposite coatings after corrosion tests at pH-4.5, (a) C_2, (b) C_2 HT, (c) M_2 and (d) I_2 under FESEM	129
Fig. 7.29	Morphologies of nanocomposite coatings after corrosion test at pH-8, (a) C_2, (b) C_2 HT, (c) M_2 and (d) I_2 under FESEM	129
Fig. 7.31	Morphologies of nanocomposite coatings after corrosion tests at pH-4.5, (a) C_3, (b) C_3 HT, (c) M_3 and (d) I_3 under FESEM	133
Fig. 7.32	Morphologies of nanocomposite coatings after corrosion tests at pH-8, (a) C_3, (b) C_3 HT, (c) M_3 and (d) I_3 under FESEM	133

LIST OF TABLES

Table No.	Description	Page No.
Table 2.1	Brief overview of developed nickel alloy coatings types with its features	11
Table 2.2	Components of EL nickel bath and their respective functions	12
Table 2.3	Phases present in EL Ni-P films at various phosphorous contents	16
Table 2.4	Brief overview of developed Ni-P nanocomposite coatings with nanosized ceramic particles as reinforcement referred in the literature	19
Table 4.1	Bath Components for EL Ni-P Based Coatings	45
Table 4.2	Operating Conditions for EL Ni-P Based Coatings	45
Table 5.1	Milling and mixing parameters	59
Table 5.2	Effect of milling hours on the crystallite size of Al_2O_3 (M) powder by XRD analysis	63
Table 5.3	Effect of milling hours on the crystallite size of ZrO_2 (M) powder by XRD analysis	66
Table 5.4	Effect of milling hours on the crystallite size of TiO_2 (M) powder by XRD analysis	69
Table 6.1	Composition of Mild steel (wt. %)	71
Table 6.2	The details of Ni-P-X [Al_2O_3, ZrO_2, TiO_2] nanocomposite coatings developed by various routes with their sample IDs	74
Table 6.3	Concentrations of Al_2O_3 particles precipitated inside EL bath for *insitu* method	80
Table 7.1	Corrosion characteristics of EL Ni-P alloy coatings in 'as coated' and HT conditions	120
Table 7.2	Corrosion characteristics of EL Ni-P-Al_2O_3 nanocomposite coatings (C_1, M_1 and I_1) in 'as coated' and HT conditions	124
Table 7.3	Corrosion characteristics of EL Ni-P-ZrO_2 nanocomposite coatings (C_2, M_2 and I_2) in 'as coated' and HT conditions	128
Table 7.4	Corrosion characteristics of EL Ni-P-TiO_2 nanocomposite coatings (C_3, M_3 and I_3) in 'as coated' and HT conditions	132

Table 7.5 Wear resistance of EL Ni-P and Ni-P-X nanocomposite coatings in heat treated condition 134

Table 7.6 Corrosion resistance of EL Ni-P and Ni-P-X nanocomposite coatings in ‘as coated’ and heat treated conditions 135

LIST OF PUBLICATIONS

PUBLICATIONS IN JOURNALS

1. **Preeti Makkar,** R.C. Agarwala and Vijaya Agarwala, "Wear and Corrosion Characteristics of Alumina dispersed Ni-P nanocomposite coating developed by Electroless technique", Journal of Material Science, (2015), Vol. 50, pp. 2813–2823.
2. **Preeti Makkar,** R.C. Agarwala and Vijaya Agarwala, "Wear Characteristics of Mechanically milled TiO_2 Nanoparticles incorporated in Electroless Ni-P coatings", Advanced Powder Technology, (2014), Vol. 25, pp. 1653-1660.
3. **Preeti Makkar,** R.C. Agarwala and Vijaya Agarwala, "Chemical synthesis of TiO_2 nanoparticles and their inclusion in Ni-P Electroless coatings", Ceramics International, (2013), Vol. 39, Iss. 8, pp. 9003-9008.
4. **Preeti Makkar,** R.C. Agarwala and Vijaya Agarwala, "Development of Electroless Ni-P-ZrO_2 Nanocomposite Coatings by Codeposition of Mechanically Reduced ZrO_2 Nanoparticles", Advanced Materials Research, (2013), Vol. 740, pp. 545-549.
5. **Preeti Makkar,** R.C. Agarwala and Vijaya Agarwala, "Studies on Electroless Coatings at IIT Roorkee-A Brief Review", Materials Science Forum, (2013), Vol. 736, pp. 275-288.
6. **Preeti Makkar,** R.C. Agarwala and Vijaya Agarwala, "Morphological and Hardness Studies of Electroless Ni-P-ZrO_2 Nanocomposite Coatings on Mild Steel" Advanced Materials Research, (2012), Vol. 585, pp. 478-482.
7. **Preeti Makkar,** R.C. Agarwala and Vijaya Agarwala, "Wear and corrosion studies of *insitu* synthesized Ni-P-Al_2O_3 nanocomposite coatings", to be communicated.
8. **Preeti Makkar,** R.C. Agarwala and Vijaya Agarwala, "Electroless deposition of sol-enhanced Ni-P-TiO_2 nanocomposite coatings and their properties", to be communicated.

PUBLICATIONS IN CONFERENCES

1. **Preeti Makkar**, R.C.Agarwala and Vijaya Agarwala; "Mechanical Preparation of TiO_2 Nanoparticles and their Incorporation in Electroless Ni-P Coatings", an oral presentation at 5th International Conference on Nanotechnology: Fundamentals and Applications held at Clarion Congress Hotel Prague, Prague, Czech Republic, during August 11-13, 2014.
2. **Preeti Makkar**, R.C.Agarwala, "Wear Behavior of Electroless Ni-P-ZrO_2 NanoComposite Coatings", an oral presentation at 2nd International Conference on Science and Technology (ICST), held at Grand Seasons Hotel, Kuala Lumpur, during June 17, 2014.
3. **Preeti Makkar**, R.C.Agarwala and Vijaya Agarwala, "Development of Electroless Ni-P-Al_2O_3 Nanocomposite Coatings for Wear Applications", an oral presentation at International Conference on Processing & Fabrication of Advanced Materials (PFAM XXII), held at NUS University, Singapore, during December 18-20, 2013.
4. **Preeti Makkar**, R.C.Agarwala and Vijaya Agarwala; "Development of Electroless Ni-P-ZrO_2 Nanocomposite Coatings by Codeposition of Mechanically Reduced ZrO_2 Nanoparticles", an oral presentation at International Conference on Materials, Mechatronics and Automation (ICMMA 2013), held at Singapore, during April 21-22, 2013.
5. **Preeti Makkar**, R.C.Agarwala and Vijaya Agarwala, "Development of Electroless Ni–P-TiO_2 nanocomposite coatings for wear applications", a poster presentation at National Conference on advances in Naval Materials (ADNAM-2013), held at National Institute of Ocean Technology, Chennai, during February 22-23, 2013.
6. **Preeti Makkar**, R.C.Agarwala and Vijaya Agarwala, "Studies of Electroless Ni–P-TiO_2 nanocomposite coatings on mild steel" an oral presentation at 7th Uttarakhand State Science & Technology Congress (USSTC-2012), held at Graphic Era University, Dehradun, during November 21-23,2012 .
7. **Preeti Makkar**, R.C.Agarwala and Vijaya Agarwala; "Morphological and Corrosion Studies of Electroless Ni-P-ZrO_2 Nano-Composite Coatings on Mild Steel", an oral presentation in International Conference on Advances in Materials and Processing Challenges and Opportunities (AMPCO-2012) held at IIT Roorkee, during November 2-4, 2012.

8. **Preeti Makkar**, R.C.Agarwala and Vijaya Agarwala; "Electroless plating of Ni-P-ZrO_2 composite coatings" an oral presentation at National Conference on Recent trends in Design, manufacturing and thermal science (NCRDMT'12) held at SRM University, NCR Campus, Meerut, during 22-23 March, 2012.
9. **Preeti Makkar**, R.C.Agarwala and Vijaya Agarwala; "Preparation and characterization of mechanically alloyed Ni-P-Al_2O_3 composite coatings developed by electroless technique", an oral presentation at National Seminar on Microstructure-2011 held at IIT Roorkee, during November 4-5, 2011.
10. **Preeti Makkar**, R.C.Agarwala and Vijaya Agarwala; "Synthesis of Electroless Ni-P nano-coating on mild steel and their further heat treatment", a poster presentation at the Third International conference on Frontiers in Nanoscience and Technology (Cochin Nano-2011) held at Cochin University of Science and Technology, Cochin, during August 14-17, 2011.

Symbol	Description
am	Amorphous
Å	Angstrom
A_n	Nominal area
AFM	Atomic force microscopy
At%	Atomic percent
b	Burger vector
CR	Corrosion rate
d	Interplanar spacing
D	Mean grain diameter
DMAB	Di methyl aminoborane
DTAB	Dodecyl trimethyl ammonium bromide
DEAB	Di ethyl aminoborane
DTA	Differential thermal analysis
DTG	Differential thermal gravimetry
EDAX	Energy dispersive X-ray spectroscopy
EL	Electroless
EL Ni-P	Electroless nickel-phosphorous
EL Ni-B	Electroless nickel-boron
EL Ni-P-X	Electroless 'X' reinforced nickel-phosphorus matrix nanocomposite coatings
E_{corr}	Corrosion potential
EIS	Electrochemical impedance spectroscopy
EW	Equivalent weight of specimen
F	Applied load
FESEM	Field emission scanning electron microscopy
G	Grain size
h	Hour
HEBM	High Energy Ball Milling
HT	Heat treatment
HV	Vickers Pyramid Number
I_{corr}	Corrosion current density

JCPDS	Joint Committee on Powder Diffraction Standards
k	strengthening coefficient
K	Specific wear rate
K_a	constant
L	Distance between specimen and screen
M_{40}	Mechanical milled for 40h
mc	Microcrystalline
MS	Mild Steel
mpy	Miles per year
μm	Micrometer
N	Newton
nm	Nanometer
Ni-P-Al_2O_3	Alumina reinforced nickel-phosphorus matrix nanocomposite coatings
Ni-P-ZrO_2	Zirconia reinforced nickel-phosphorus matrix nanocomposite coatings
Ni-P-TiO_2	Titania reinforced nickel-phosphorus matrix nanocomposite coatings
OCP	Open circuit potential
R	Ring radius
s	Sliding distance
SDS	Sodium dodecyl sulfate
TEM	Transmission electron microscopy
TGA	Thermo-gravimetric analysis
TTAC	1,3 toloyl triethanol ammonium chloride
V	Wear volume
v	Sliding velocity
VHN	Vickers Hardness Number
Wt %	Weight percent
XRD	X-ray diffraction
Y	Shear modulus
W	Wear rate
β	Line broadening
λ	Wavelength of electron beam
θ	Bragg's Angle

σ	Yield stress
P	Density of specimen
t	Dispersed particles distance

CHAPTER 1

INTRODUCTION

Wear and corrosion issues are of great relevance in an extensive range of industrial applications as the outcome is progressive deterioration and at worst, failure of components. It diminishes operating efficiency, service life of components and even aids to component replacement frequencies. The reliability of serviceable engineering components not only depends on their bulk material properties but also on their surface design and characteristics. For the most part, it is hard to discover all these features in a single material with favourable economics. So, the surface modification of materials is widely used in present day manufacturing to convert low cost materials into valuable engineering materials. Coatings are one such form of surface treatment where the surface of bulk material is given a protective layer of an alternate material having superior properties than those of the bulk material. Coatings play an essential part in decreasing the expense of wear and corrosion losses in industrial applications and inturn to improve the performance of any engineering system [Strafford et al. (1990); Hogmark et al. (1997)].

The technological advancement demands the development of newer coating materials with improved resistance against wear and corrosion. Mild steel (MS) is widely used as a structural material in various engineering applications due to its lower cost, yet, the properties like hardness, wear and corrosion resistance are not excellent [Habig (1989); Rabinowicz (1965)]. The use of coatings is specially recommended to protect these alloys at moderate temperatures in order to make them strengthen and become less prone to wear and corrosion over time [Sidky and Hocking (1999)]. The wear tests of the coatings can be carried out for a number of reasons such as materials evaluation, lubricants evaluation, friction assessment, fundamental tribological studies, and component life evaluation [Holmberg et al. (1998)]. The high need for coatings with improved resistance to highly aggressive environments is due to the growing demand for extended safe service life of industrial components. Therefore, it becomes critically important in the testing of coated components where the presence of the coatings can change the operating wear and corrosion mechanisms [Bull (1997); Chitty et al. (1997)].

The surface modification processes that are currently used range from low cost processes like electroplating and electroless plating used for mass production to high cost processes like physical vapour deposition (PVD), chemical vapor deposition (CVD) introduced over the last two decades [Karwan et al. (2010)]. Electroless (EL) nickel coating, credited mainly to Brenner and Riddell (1946), has long been adopted as a kind of effective surface modification

technology for its unique physiochemical and mechanical properties for which they are being increasingly used in industrial applications. The advantages of simple processing, easy implementation with the modest equipment demand, relatively lower cost, fast kinetics, controllability as well as reproducibility of the bath solution and its suitability to large scale plating, makes this coating process highly potential to fit in that space. EL nickel plating is an autocatalytic chemical technique depending on the catalytic reduction of nickel ions in an aqueous solution and subsequent deposition on substrate without the use of electrical energy [Agarwala (1987); Baudrand (1994)]. It significantly differs from the conventional electroplating process that depends on an external source of direct current (dc) to reduce nickel ions in the electrolyte for nickel deposition. The key benefit is its uniform thickness throughout the coating over the whole area, ranging from 2.5 to 500μm, even on complex shaped geometrical components unlike electroplating which provides uneven coating thickness at corners and awkwardly located areas, so expensive jigging and machining is required after deposition [Gawne and Ma (1989); Husheng et al. (1991)]. Other predominant features of electroless nickel coating include its feasibility of deposition on non-conductors, offer properties like high solderability, high reflectivity, excellent wear resistance due to high hardness after suitable heat treatment and effective barrier properties and corrosion resistance owing to their amorphous nature and pore free networks. It strikes the best balance between finished component's performances, quality and cost effectiveness i.e. lengthens working life and improves component's cost effectiveness. It competes with electrolytic nickel plating for brightness and chromium plating for hardness and wear resistance when properly designed for service [Groshart (1983)]. Hardness, wear resistance and corrosion protection are the attributes that make EL nickel popular [Baudrand (1994)].

The ability to codeposit fine particulate substance(s) within an EL nickel deposit has led to new promising era of composite coatings i.e. Ni-P-X, where ‘X’ is the second phase particles can be tailored to obtain desired properties. It was initially developed by Odekerken (1966) where aluminum oxide (Al_2O_3) and polyvinyl chloride resin (PVC) were codeposited in nickel matrix for improved corrosion resistance. Embedding various soft/hard particles onto EL Ni-P matrix enhances the physiochemical and mechanical properties are well established [Balaraju et al. (2003); Grosjean et al. (1997)]. The scope of composite coatings is more broadened with the inclusion of nanosized particles into EL Ni-P matrix owing to their unique properties [Sahoo et al. (2011)]. Nanocomposite coatings are the ones in which either the thickness of coatings is in nanometer range or size of second phase particles that are embedded into the matrix is of nanosized range. EL Ni-P based nanocomposite coatings are presently the high end coatings in the field of wear and corrosion resistance applications with their extreme demands.

EL composite coatings can be developed by two ways, depending upon the compatibility of reactions and the process parameters of EL bath. Conventional composite coatings i.e. 'X' present in the composite coatings can be added during the coating (codeposition of particles of micrometer to nanometer in range) and non-conventional composite coatings i.e. 'X' can be generated to nucleate and grow within the bath during coating (*insitu* particles precipitated of nanometer in size). Successful codeposition is reliant on various factors including particle characteristics like charge, catalytic inertness nature, its size distribution, EL bath composition, compatibility of the particles with the nickel matrix, bath reactivity and the plating rate [Balaraju et al. (2003); Sharma et al. (2006)]. According to past studies, non-conventional (*insitu*) route provides more beneficial effect on surface properties over the conventional route as the 'X' particles were found to have better dispersion with Ni-P matrix [Sharma et al. (2002), (2005)].

The use of hard ceramic particles namely SiC, SiO_2, Al_2O_3, Si_3N_4, B_4C, ZrO_2, TiN, TiO_2 etc. offers many advantages in terms of hardness, wear, friction coefficient, chemical inertness and thermal stability of the resulting composite coatings [Balaraju et al. (2003); Sahoo and Das (2011)]. Therefore, the thrust is progressively being given on the development of newer variants of nanocomposite coatings and understanding of their tribological and corrosion behaviour. Among reinforcements used, alumina (Al_2O_3), zirconia (ZrO_2) and titania (TiO_2) are choosen in the present work as these are the most cost effective and versatile advanced ceramic materials widely used in industries due to their high strength, excellent wear resistance, high chemical corrosion resistance, low thermal expansion coefficient and ease of availability [Patnaik (2002)]. Second phase nanosized 'X' [X= Al_2O_3, ZrO_2 and TiO_2] powders can be prepared through different methods such as mechanical milling, vapor phase reaction, precipitation, sol-gel, hydrothermal etc. However, in EL Ni-P-X composite coating systems, the preparation method of nanoparticles codeposited on Ni-P matrix is less focussed.

Most studies on EL Ni-P-X [X= Al_2O_3, ZrO_2 and TiO_2] composite coatings are focussed upon the incorporation of micron sized particles in Ni-P matrix. Although, fewer investigations have been conducted using nanosized 'X' particles as reinforcement, still due to complexity of the structure, extensive variety of wear and corrosion apparatus, different environments employed for the wear and corrosion tests, wide substrate and counterface (electrolyte) materials used, the proper knowledge of tribological studies and corrosion mechanism of these Ni-P-X coatings are troublesome. There is a need to give more consideration regarding the systematic studies of wear and corrosion behaviour of Ni-P-X nanocomposite coatings. Moreover, the comparative studies on wear and corrosion behaviour of EL N-P-X nanocomposite coatings developed by conventional and non-conventional means on mild steel substrate have not yet

received adequate attention from research community.

Thus, the present investigation has been focused with an aim (i) To develop EL conventional Ni-P-X [X=Al_2O_3, ZrO_2 and TiO_2] nanocomposite coatings where second phase 'X' nanoparticles are synthesized separately by chemical precipitation (bottom up) and mechanical milling (top down) methods. (ii) To develop EL non-conventional *(insitu)* Ni-P-X nanocomposite coatings using the same chemical method for comparison. All the developed Ni-P-X coatings are subjected to heat treatment (400^oC for 1h) for better adherence with the mild steel substrate. (iii) To examine the microhardness of EL Ni-P-X nanocomposite coatings before and after heat treatment. (iv) To investigate the wear and friction charcatersistics of all heat treated Ni-P-X nanocomposite coatings (iv) To determine the corrosion behaviour of EL Ni-P-X nanocomposite coatings in 'as coated' and 'heat treated' conditions. (v) To compare the performance of Ni-P-X nanocomposite coatings in terms of hardness, wear and corrosion with Ni-P alloy coatings.

The thesis has been organised in nine chapters summarized as follows:

The role of electroless nickel coating technique for enhancing the service life of engineering components in industries is introduced with their properties and benefits over electroplating. The significance of EL Ni-P-X nanocomposite coatings for wear and corrosion applications and methods used for their preparation are overviewed. It provides an insight into the reinforcements used along with their advantages and the process methods employed for their synthesis. Chapter 1 also gives a brief idea about the aim and scope of the present work.

In chapter 2, literature review on EL nickel coating technology, their advantages, classifications, mechanisms involved, limitations etc. have been carried out. A survey on EL Ni-P based composite coatings with their key benefits, classification and properties are presented. The importance of Al_2O_3, ZrO_2 and TiO_2 nanoparticles, their usage in coatings and the review on their fabrication modes are included in this chapter. Also extensive survey on the studies carried out on incorporation of Al_2O_3, ZrO_2 and TiO_2 particles in Ni-P matrix for wear and corrosion resistant properties is outlined.

The literature review identifies gaps of information. It leads to the formulation of problem, which defines the total scope of present work and has been presented in chapter 3.

The experimental details such as raw materials, experimental conditions, equipments, process parameters used for synthesis of Al_2O_3, ZrO_2 and TiO_2 nanosized powders and EL Ni-P based composite coatings by two means are presented in chapter 4. The details of characterisation techniques used for morphology, phases and thermal analysis of powders and coatings are discussed. The hardness, wear and corrosion testing parameters with equipment details are also outlined in this chapter.

In chapter 5, the results based on synthesis and characterization of Al_2O_3, ZrO_2 and TiO_2 nanoparticles separately using top down and bottom up approaches are discussed. The morphology, particle size, thermal studies and phase structures of Al_2O_3, ZrO_2 and TiO_2 nanoparticles synthesized by chemical precipitation route are presented. The chapter also features the results obtained by mechanically milling of Al_2O_3, ZrO_2 and TiO_2 nanoparticles at different extents of milling time (5h, 10h, 20h, 30h and 40h) with their morphological characterizations and phase analysis studies. Al_2O_3, ZrO_2 and TiO_2 nanoparticles produced by above methods are used as the second phase 'X' for the development of EL Ni-P-X nanocomposite coatings.

Chapter 6 focusses on the development of EL Ni-P, conventional Ni-P-X [X= Al_2O_3, ZrO_2 and TiO_2] and non-conventional Ni-P-X [X= Al_2O_3, ZrO_2 and TiO_2] nanocomposite coatings by electroless technique where in conventional ones, 'X' reinforcements used are chemically synthesized and 40 h milled powders. Also, the optimal concentration studies of the 'X' particles reinforced in non-conventional Ni-P-X coatings are described. Heat treatment of all Ni-P and Ni-P-X coatings are carried at 400^oC for 1h in argon atmosphere. The results based on morphology, phase structure and microhardness studies of all developed EL Ni-P-X nanocomposite coatings before and after heat treatment are discussed in detail with respect to Ni-P alloy coatings.

Chapter 7 discusses the results obtained by the wear, friction and corrosion studies of all developed EL conventional and non-conventional Ni-P-X [X= Al_2O_3, ZrO_2 and TiO_2] nanocomposite coatings and compared with Ni-P alloy coatings. The influence of varying loads (1, 1.5 and 2N) and sliding velocities (0.1 and 0.2m/s) on specific wear rate of all heat treated Ni-P-X and Ni-P coatings are determined. The variation in friction coefficient with sliding distance of Ni-P and Ni-P-X coatings under 1, 1.5 and 2N loads are studied. The results on electrochemical polarization studies of Ni-P and Ni-P-X coatings in 'as coated' and 'heat treated' conditions under varied environments (pH-4.5 & 8) are discussed. The morphologies of worn and corroded surfaces of Ni-P and Ni-P-X coatings are analysed.

The conclusions are drawn from the present work in chapter 8. It outlines the results obtained by morphological, phase analysis and thermal studies of nanosized [X= Al_2O_3, ZrO_2 and TiO_2] powders. The results concluded from morphology, phase, hardness, wear, friction and corrosion characteristics of EL Ni-P and Ni-P-X nanocomposite coatings are also presented.

In chapter 9, suggestions and scope for future work in the area of EL Ni-P based nanocomposite coatings for wear and corrosion applications are outlined.

CHAPTER 2

LITERATURE REVIEW

2.1 INTRODUCTION

Electroless coating technology is a controlled chemical reduction process which has emerged as one of the thrust zone of surface engineering and metal finishing. Electroless coatings have unique physicochemical and mechanical properties for which they are being utilized progressively. The quest for enhanced physical and mechanical properties prompted an era of composite coatings. A brief literature survey in the area of electroless coatings, Ni-P based nanocomposite coatings has been carried out. Moreover, little emphasis on nanoparticles synthesis modes especially for materials namely alumina, zirconia and titania has been done. The survey regarding the incorporation of above mentioned particles into Ni-P coatings and their impact on physical and mechanical properties has also been carried out in the present chapter.

2.2 DEVELOPMENT OF ELECTROLESS DEPOSITION- A BRIEF HISTORY

The electroless deposition of metallic nickel in the vicinity of hypophosphite compound from aqueous solution was first noticed in 1844, by Wurtz, as a chemical curiosity [Gaurilow (1979)]. In 1911, Breteau had precipitated the metal in powder form and deposited on the surface of reaction vessels as bright finished coatings. Roux, in 1911, had done a similar work but lacks practical applications [Gillespie (1997)]. However, no further developments were carried out during its intial stages until the electroless nickel deposition was reinvented by Brenner and Riddell in 1946. They developed the process to coat the inner walls of tubes with nickel-tungsten alloy using citrate and hypophosphite based reducing bath. The coating process was a controlled autocatalytic chemical reduction process where nickel (Ni) deposition prevails only on the catalytic substrates immersed into the bath [Brennerand Riddell (1947)]. Later, during the period of 1954-59, Gutzeit worked on electroless plating process as an alternative to conventional electroplating process by the use of acidic baths apart from alkaline baths used earlier. The composite coatings were initially developed by Odekerken, in 1966. Here, in an intermediate layer, fine powder particles of aluminum oxide (Al_2O_3) and polyvinyl chloride resin (PVC) were distributed within electrodeposited nickel-chromium matrix for improved corrosion resistance. Alumina particles as reinforcement in electroless nickel coating were articulated by Metzger et al. (1966). Additionally, their continuous efforts attributed to the first commercial implementation of electroless Ni-SiC composite coating on the Wankel (rotary)

internal combustion engine. Further, with appropriate course of time, in 1981, polytetrafluoroethylene (PTFE) based composite coating was introduced with commercial application [Sharma et al. (2006)]. In 1983, Feldstein et al. suggested that the incorporation of alumina (Al_2O_3) or silicon carbide (SiC) in nickel matrix were accomplished without much challenges as opposed to the difficulties experienced with codeposition of diamond and polytetrafluoroethylene (PTFE) particles. Since then, the codeposition of second phase particles, from micron to nano size range, within a metal/alloy matrix has begin a new era of composite coatings to achieve desired properties.

2.3 CLASSIFICATION OF ELECTROLESS COATINGS

Electroless coatings can be divided into three main categories i) metallic coatings ii) alloy coatings and iii) composite coatings. Significant efforts by various investigators have been devoted to identify the wide range of metals/alloys/composites that can be deposited by the EL (autocatalytic) deposition route.

2.3.1 Electroless Metallic Coatings

The particularly useful metals that have been demonstrated to be of practical importance are nickel, cobalt, copper, silver etc. Among them, electroless copper coatings are widely used on plastics, ceramics, polymers and non-conducting materials [Henry (1985); Pedraza and Godbole (1990); Ramasubramanian et al. (1999)]. EL copper coating is also utilized in shielding electronic devices. The thickness of the coatings is varied from 0.12 to 3µm. The plating bath contains a source of metallic ions, a reducing agent, a complexing agent and a stabilizer. Copper sulphates, nitrates or acetates are the source of copper ions. The reducing agent commonly used is formaldehyde but reducing agents such as DMAB, sodium hypophosphite ($NaPO_2H_2$) etc. can be employed for the same. Sodium hydroxide/potassium tritarate and thiourea/vanadium oxide are used as complexing agents and stabilizers respectively. The coating can also be carried out at room temperature to the temperature of the bath as high as 70^oC. The pH should be maintained at higher levels of about 12 to obtain bright coatings, although, the stability of the bath is higher at 9.0 pH [Henry (1985)].

2.3.2 Electroless Alloy Coatings

The electroless technique is one of the distinguished processes to deposit nickel based alloy coatings. Apart from plating by reduction reaction, two other methods have also been reported, these include immersion plating on steel from solutions of nickel chloride and boric acid, and decomposition of nickel carbonyl vapor on steel substrate [Gaurilow (1979)]. However, the

later is hazarous and the first one has a poor adherent and non-protective. The overall uniformity in composition and thickness of the substrate which is independent of roughness are counted as the main advantages for the usage of the autocatalytic reduction process [Agarwala (1987)]. The autocatalytically deposited Ni-P based alloys have numerous industrial applications due to high hardness, excellent wear and corrosion resistance, their paramagnetic properties etc [Graham et al. (1965); Duchnaiya et al. (2011)]. Nickel based ternary and quaternary alloys are termed as polyalloys by few researchers [Szczygieł et al. (2008); Valova et al. (2001); Wang et al. (1992)]. Polyalloys are generally employed where electrical, magnetic or non magnetic properties or high temperature resistance applications are required. Distinctive alloy combinations are coated onto the substrate in order to get desired mechanical and physical properties. The alloy selection purely relies on the application front and its economic contemplations [Ganesan (1998); Karwan and Rosso (2006); Karwan (2011)]. Several nicked based binary, ternary and quaternary alloys have been deposited and reported with the relevant features are summarized briefly in table 2.1. Nickel stems out to be the single widely coated element with phosphorus (P) or boron (B) derived from the reducing agent in the bath.

2.3.2.1 Electroless Nickel Bath - Its Fundamental Aspects

Electroless nickel coatings are generated by chemical reduction of metallic ions on a catalytic substrate surface in a controlled manner. The electroless process is an autocatalytic process i.e. coating itself is catalytic to reduction reaction, consequently, the reaction continues as long as the surface remains in contact with the bath solution or the bath solution gets depleted of solute ions [Gaurilow (1979)]. The coating layer is formed by repeated nucleation and grows laterally and vertically by virtue of atom-by-atom deposition. Therefore, have equal probability of getting an ion of nickel be deposited in all parts of the surface area of substrate, which are immersed in the bath [Park and Lee (1988); Sharma et al. (2005)]. Thus, uniformity of the coating throughout the contours of the substrate is achieved making it distinguishable from electroplating which provides uneven coating thickness at corners and awkwardly located areas, so expensive jigging and machining is required after deposition. It significantly differs from the conventional electroplating process that depends on an external source of direct current (dc) to reduce nickel ions in the electrolyte for nickel deposition [Gawne and Ma (1989); Husheng et al. (1991)]. Electroless nickel coatings are widely used in different industries because of their physicochemical and mechanical properties, such as good hardness, coating uniformity, wear and corrosion resistance, and capability of depositing on either conductive or nonconductive substrates [Gawne and Ma (1987)]. For EL nickel depositions,

mainly two types of baths are being used i.e. acidic and alkaline which differing in bath pH. Pretreatment of substrate which includes its sensitization and activation is one of the crucial factors for sound electroless nickel deposition [Guo et al. (2010)]. In general, surface of substrate is first sensitized with stannous chloride ($SnCl_2$) and then activated by immersing it in palladium chloride ($PdCl_2$) solution for a specific time at room temperature. Here, first, tin ions (Sn) deposits onto the surface, over that palladium ions (Pd) can be deposited where it acts as a nucleus/catalyst for EL deposition to starts with [Henry (1985); Sharma et al. (2006)].

The basic components for an electroless nickel bath include an aqueous solution of metal (nickel) ions, reducing agent(s), complexing agent(s) and bath stabilizer(s) operating at a specific metal ion concentrations. Apart from these, a sensitized and activated target substrate with pH and temperature controller for maintaining pH and temperature is also required. EL nickel bath solution kept at stipulated temperature comprises of different chemicals where each performing an important function is illustrated in table 2.2 [Agarwala (1987); Sharma et al. (2006)].

(a) Reducing Agents- The driving force in an electroless process is a reducing agent (electron donors) which reduces metal ions (electron acceptors) to metal. Generally, four kinds of reducing agents have been commercialized for deposition of electroless nickel alloy, namely, sodium hypophosphite, amineboranes, sodium borohydride and hydrazine. Sodium hyphosphite reduced baths are commonly employed (more than 70%) for EL nickel deposition. The key advantage of using hypophosphite over other reducing agents involve its lower cost, ease of process control to greater extent and provide better corrosion resistance. Two mechanisms have been proposed for nickel ions reduction by hypophosphite, namely, electrochemical bonding mechanisms and atomic hydrogen mechanism. However, the chemical reactions involving in electroless deposition is found to be controlled by an electrochemical mechanism [Gutzeit (1959)] and are discussed in section 2.3.2.2. Generally, an amount of sodium hypophosphite, 1kg, is required for reduction of 200g of nickel with an almost 37% efficiency on an average [Gaurilow (1979); Mallory (1974)]. The amineboranes baths are limited to the use of two commercialized compounds i.e. N-dimethyl amineborane (DMAB $(CH_3)_2NHBH_3$) and H-diethyl amineborane (DEAB $(C_2H_5)_2NHBH_3$). DEAB required to be mixed with a aliphatic alcohol before immersing into nickel bath whereas DMAB exhibits good solubility in aqueous soultions. These are effective over a much wider pH range than the borohydride baths. 1kg dimethyl amineborane, in general, reduces about 1kg of nickel [Gaurilow (1979); Mallory (1979)].

Table 2.1: Brief overview of developed nickel alloy coatings types with its features

Coating	Reference and Year	Usage
Ni-P	Brenner and Riddell (1946), (1947); Graham et al. (1962), (1965); Henry (1985); Harris et al. (1985); Agarwala (1987); Husheng et al. (1991); Chitty et al. (1997); Staia et al. (1997); Puchi et al. (1993); Bozzini et al. (1997), (2002); Krishnan et al. (2006)	Hardness Wear resistance Corrosion resistance Solderability Thermal properties Fatigue strength Tensile strength
Ni-B	Bedingfield et al. (1991); Srivastava et al. (1992); Giampaolo et al. (1997); Krishnan et al. (2006)	Hardness Wear resistance
Ni-B-P	Ivanov et al. (2001)	Wear resistance Electrical properties
Ni-Cu-P	Wang et al. (1992) Hameed and Fekry (2010)	Corrosion resistance Ductility
Ni-Re-P Ni-Re-W-P	Valova et al. (2001)	Electrical resistance Corrosion resistance
Ni-W-P	Li et al. (1996); Valova et al. (2001); Szczygieł et al. (2008)	Corrosion resistance Electrical resistance
Ni-Sn-P Ni-Sn-Cu-P	Bangwei and Haowen (2000)	Corrosion resistance
Ni-Co-P Ni-Fe-Co-P	Narayanan et al. (2003) Yang et al. (2012)	Magnetic properties Microwave absorbtion
Ni-Fe-P Ni-Fe-P-B	Wang et al. (2000), (2002)	Corrosion resistance Magnetic properties
Ni-Zn-P	Oulladj et al. (1999)	Corrosion resistance

Table 2.2: Components of EL nickel bath and their respective functions [Sharma et al. (2006)]

Ni-P Bath Constituents	Source	Function
Nickel Sulphate ($NiSO_4.5\ H_2O$)	Metal ions	Source of Nickel
Sodium Hypophosphite ($NaH_2PO_2.\ H_2O$)	Reducing agent	Supply electrons for reduction
Sodium tri-citrate ($Na_3C_6H_5O_7.H_2O$)	Complexing agent	To control the free nickel available to the reaction
Ammonium Sulphate $(NH_4)_2\ SO_4$ & Ammonium Chloride (NH_4Cl)	Stabilizers	To control the reduction and avoid EL bath decomposition
Ammonia (NH_4OH)	pH Buffers	To maintain pH

Sodium borohydride bath is considered as the most effective reducing agent for deposition of electroless nickel. Borohydrides are easily hydrolyzed in acidic range, however, in alkaline medium, it causes difficulties and spontaneous bath decomposition may takes place and thus not suited for aluminium substrates as reported [Mallory (1974); Morales et al. (2005)]. In general, sodium borohydride (600g) reduce1kg of nickel with purity of deposits above 92.97%. Hydrazine has likewise been utilized for deposition of electroless nickel but due to its instability at high temperatures, these baths have a tendency to become unstable and thus, hard to control. The substrate lacks lustre even after coating. The deposits are highly stressed and brittle for commercial applications [Levy (1963); Juarez and Morales (2008)].

(b) Complexing Agents- One of the major challenges of electroless deposits is its bath stability throughout the coating process. As the coating progresses, there is continual reduction of nickel ion concentration in the bath. The precipitation of nickel phosphite inside the bath weakens the coating quality bringing about rough and dull deposits. Also, induces instability of the bath leading to bath decomposition. Complexing agents are generally added to control free nickel available in bath for reaction. It retards the possibility of nickel phosphite formation so that nickel deposits only on the catalytic substrate, in turn, avoids the total bath decomposition. It also buffers the bath solution and improves the quality of the deposit. Additives like salts of succinic, glyconic or malomic acids can be used as complexing agents although they fail to avoid the nickel phosphite precipitation in the bath. The best alkaline nickel phosphorus

deposits are obtained with sodium citrate concentration of about 30g/l. The accelerators such as soluble fluorides, salts of carbonic acids can also be added in lesser amounts to enhance the deposition rate [Gutzeit (1959)].

(c) Stabilizers- The addition of stabilizers stabilizes the deposition rate and brightness of the coating. It can be added to further control the reduction reaction rate and to avoid the total decomposition of the bath. Heavy metals like As, Pb, Cd, Bi and sulfides like cyanides and thiourea are commonly used as stabilizers for EL nickel deposition reactions [Lanzoni et al. (1997)].

2.3.2.2 Bonding mechanisms of electroless nickel coatings

During the electroless deposition process, the bonding mechanisms reported at the interface of substrate and coating are chemical and mechanical bonding. Apart from these, on heat treatment, diffusion bonding also takes palce at the inferface [Sharma et al. (2006)].

(a) Electrochemical bonding mechanisms

The basic chemical reactions involved in the reduction mechanism of nickel ions under the catalytic action of palladium and hypophosphite for the deposition of nickel and phosphous onto substrate are given in equations 2.1-2.4. Here, the catalytic oxidation of the hypophosphite yields electrons at the catalytic surface which inturn reduces nickel and gaseous hydrogen ionsat the catalytic suraface. The hypophosphite ion also itself gets reduced and liberates phosphorus. Thus, a layer of nickel and phosphorus is deposited on the surface of substrate [Gutzeit et al. (1959)].

$$H_2PO_2^- + H_2O \longrightarrow H_2PO_3^- + 2H^+ + 2e^- \quad (2.1)$$

$$Ni^{++} + 2e^- \longrightarrow Ni \quad (2.2)$$

$$2H^+ + 2e^- \longrightarrow H_2 \quad (2.3)$$

$$H_2PO_2^- + 2H^+ + e^- \longrightarrow P + 2H_2O \quad (2.4)$$

(a) Mechanical bonding mechanisms

On account of good adherence of EL copper and Ni-P coatings with different substrates such as ceramic powder, glass and Al sheet, a model is proposed and schematic representation of the growth mechanism/ bonding at the interface of substrate and coating is shown in figure 2.1. The EL coating is shown to grow uniformly inside and outside the surface pores layer by layer. The nano-globules of EL coating are getting filled into nanopores at the surface of the

substrate to start with [Fig 2.1]. As the anchoring of the growth of the coating into the pore occur, the coating remains stable and thus adhere to the surface of the substrate. Thus it is suggested that the EL coating adhere to the substrates due to the mechanical bonding [Sharma et al. (2006)]. Apart from mechanical bonding, at the interface of the substrate and the coating, the chemical bonding is also possible due to the pretreatment given to the substrate and the reactions occurring inside the bath [equation 2.1-2.4].

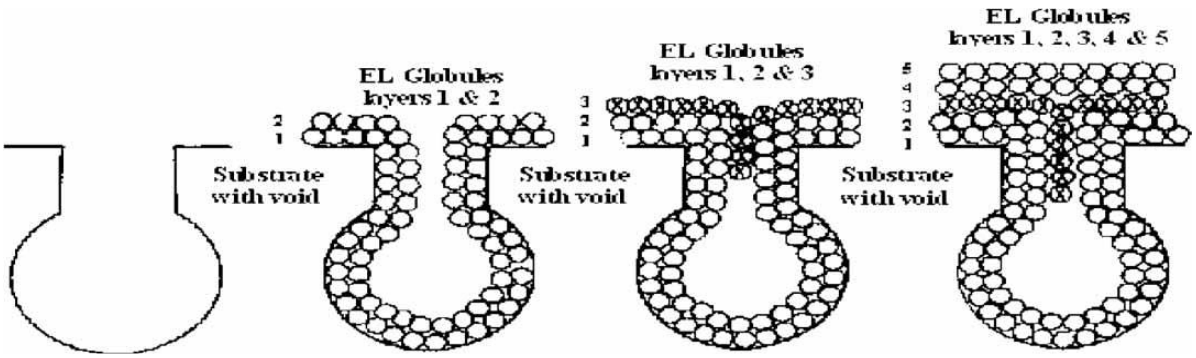

Fig 2.1- Schematic representation of growth and bonding mechanism of EL nickel coating with the substrate [Sharma et al. (2006)].

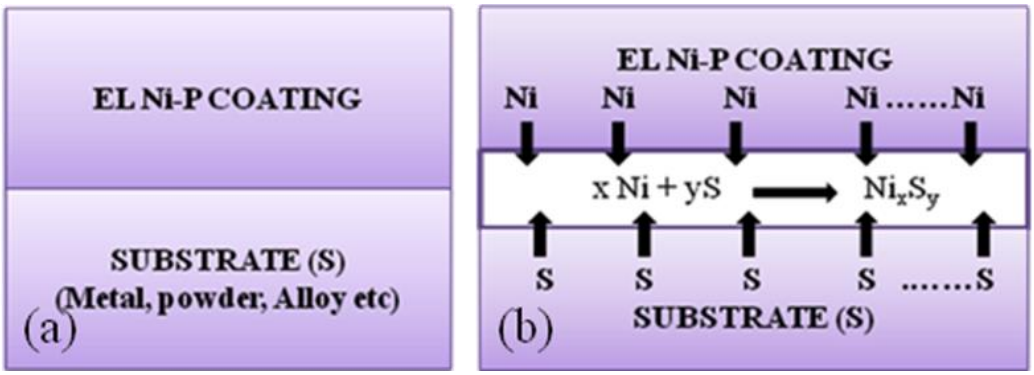

Fig 2.2- Schematic representation of diffusion bonding mechanism showing, (a) interface of EL Ni-P coating in 'as coated' condition and (b) diffusion layer of Ni_xM_y at the interface after heat treatment [Sharma et al. (2006)].

(a) Diffusion bonding mechanisms

Heat treatment is recommended for the EL coatings to achieve better bonding with the substrate and to improve the strength of the EL coatings. The diffusion bonding with the substrate along with the chemical and mechanical bonding occurs on heat treatment of 'as coated' metallic substrates like Al, Cu, Steel, etc. [Fig 2.2a]. During heat-treatment, the diffusion of atoms at the interface of the two layers (metallic layer, M and coated layer, Ni-P) takes place, allowing to form an intermetallic layers like Ni_xM_y due to diffusion bonding

[Fig 2.2b]. Diffusion bonding mechanism is applicable only for the metallic surfaces as the heating temperature and time will not affect the substrates like ceramics, glass etc. Hence, the chemical and mechanical bonding mechanisms prevail for these kinds of substrates [Ganesan et al. (1984); Ping et al. (1997); Sharma et al. (2006)].

2.3.2.3 Factors affecting the EL nickel coating process

The performance of EL deposits not only depends upon the bath constituents and its chemistry but also governed by various factors such as pH, operating temperature, bath loading factor, etc. Nickel salt concentrations do not affect the rate of reduction of nickel but the variation of hypophosphite concentrations influence the process considerably. Very high nickel concentration intake in the bath may make bath turbid due to hydrolysis of Ni_2P, hence, an optimum amount of about 30-40g/l concentration is used. The increase in the hypophosphite concentrations although improves the rate of reduction of nickel but, on the other hand, extra amounts of the reducing agents should not be used as this may cause the reduction to take place in the bulk of the solution. Hence, the appropriate amount of hypophosphite can be chosen by observing the bath condition during the reaction. The weak hydrogen evolution is an indication of a low concentration of hypophosphite and excess hypophosphite in an EL bath results in a vigorous hydrogen evolution. With the increase in alkalinity of the bath, the nickel content increases or the phosphorus content of the deposit decreases where phosphorus may be present as a phosphite or as solid solution. The concentration of nickel salts slightly affects the rate of deposition. Large concentration of the nickel salts results in deterioration in the quality of the coatings due to the formation of rough deposits. Also the solution pH decreases due to evolution of hydrogen during the plating process. Most of the EL nickel processes used buffers by adding ammonium chloride to minimize pH swings, however, periodic additions of ammonia to maintain the pH within the operating limits is required for alkaline bath. As pH has a profound effect on phosphorus content, hence monitoring and controlling of solution pH is critical in producing a consistent, high quality EL nickel deposit. Increasing pH increases plating rate, but it decreases bath stability and also results in decreased phosphite solubility. The rate of the EL process increases with increase in temperature and attains a maximum at about 92^{o}C. Beyond this temperature, it becomes difficult to maintain the pH of the bath solution and, therefore, the quality of the coating deteriorates. Apart from temperature and pH, the bath loading is one of the most crucial factors affecting the performance of an EL nickel process. It is defined as the ratio of total exposed surface area being plated to the volume of plating solution in the tank. It has a profound influence on coating rate and as well as on phosphorus content of the resulted coating. It is seen from practice that the coating thickness of

Ni-P deposits tends towards an optimum value after which the coating rate starts reducing [Henry (1985); Sharma et al. (2006)].

2.3.2.4 Structure of EL Ni-P alloy Coatings

Structural studies, magnetization and crystallization behavior at various temperature have been studied for EL Ni-P deposits containing phosphorus (P) in the range of 10.8 to 23.4 at%. [Agarwala (1987)]. The Ni-P coatings exhibit smooth and shining surfaces. It was observed that the film having lower phosphorus concentration adheres well at the surface of substrate while the higher phosphorus concentration film (Ni-23.4 at%P) has fallen off at number of places and the substrate has been exposed. A hemispherical globular nature of surface topography was observed by various researchers under SEM micrographs [Agarwala (1987); Abraham et al. (1990); Henry (1985); Hur et al. (1990)]. To determine the structure of the 'as deposited' film at varying P content, diffraction patterns were recorded. The sharp intensity peak was observed at lower P content of the film whereas the peak diffused at high P content and a broad hump was seen near the angular position of (111) peak of crystalline nickel at Ni-23.4 at%P film. It was suggested that the film remain crystalline at low P content and become microcrystalline at medium phosphorus and finally amorphous at higher phosphorus content [Agarwala (1987); Mahoney and Dynes (1985)]. The possible phases at different P concentrations were examined as confirmed by XRD and TEM analysis is shown in table 2.3 [Agarwala (1987)]. The studies by various researchers showed that heat treatment promotes phase transformation and found to improve the physiochemical and mechanical properties within the deposit [Agarwala and Ray (1992); Apachitei et al. (1998/1); Karwan et al. (2003); Sorkhabi and Rafizadeh (2004); Staia et al. (1997)].

Table 2.3: Phases present in Ni-P films at various phosphorus contents [Agarwala (1987)]

S.No	Composition	Common Phase	Less common Phase
1.	Ni-10.8 at .%P	Ni (mc)	Ni_5P_4, $Ni_{12}P_5$, Ni (am)
2.	Ni-14.3 at .%P	Ni (mc)	Ni_5P_4, $Ni_{12}P_5$, Ni (am)
3.	Ni-15.3 at .%P	Ni (mc)	$Ni_{12}P_5$, Ni (am)
4.	Ni-17.8 at .%P	Ni (am)	Ni_5P_2, $Ni_{12}P_5$, NiP_2, Ni (mc)
5.	Ni-19.8 at .%P	Ni (am)	$Ni_{12}P_5$, Ni_7P_3, Ni (mc)
6.	Ni-22.4 at .%P	Ni (am)	Ni_5P_2, Ni_3P, $Ni_{12}P_5$, Ni (mc)
7.	Ni-23.4 at .%P	Ni (am)	Ni_3P, Ni_7P_3, $Ni_{12}P_5$, Ni (mc)

2.3.3 Electroless Composite Coatings

The codeposition of fine particulate substance(s) within an EL nickel deposit is termed as electroless composite coatings. The incorporation of particulates within EL nickel coatings was initiated in 1960s as discussed in section 2.2. The quest for improved physiochemical properties such as higher hardness, anti-wear and anti-corrosion properties gives an idea of codeposited second phase particles in the matrix of electroless nickel deposits. The combination of properties of second phase material along with the inherent uniformity, hardenability, wear and corrosion resistance properties of nickel matrix has led to the development of electroless nickel composite coatings. The particles normally codeposited so far within EL nickel are either lubricants (like PTFE, MoS_2) or hard load bearings such as oxides, carbides, ceramics, diamond etc., which physically get entrapped in a growing Ni-P layer on the substrate surface [Moonir et al. (1997); Michalski et al. (2003)] . The improvement in surface properties is achieved by the incorporation of micron to nanosized particles onto the Ni-P matrix [Balaraju et al. (2003); Sharma et al. (2006); Sahoo and Das (2011)]. The properties of Ni-P composite coatings depends upon the type of second phase particle dispersed in the Ni-P matrix. Nanocomposite coatings are the ones in which either the thickness of coatings is in nanometer range or size of second phase particles that are embedded into the matrix are of nanosized range. According to past studies, EL composite coatings can be produced in two ways, depending upon the compatibility of reactions and the process parameters of EL bath, namely,

(a) Conventional composite coatings – The second phase(s) present in the composite coatings can be added during the coating (codeposition of particles of micrometer to nanometer in range).

(b) Non- conventional(*insitu*) composite coatings - The second phase particles can be nucleated and grown within the bath during coating (*insitu* particles precipitated are of nanometer in size).

Non-conventional (*insitu*) route is found to be more advantageous over the conventional route as the particles embedded in the Ni-P matrix are of nano sized range, avoids the possibility of agglomeration of nanoparticles in the coating matrix and uniform distribution of second phase particles are seen in Ni-P matrix [Sharma et al. (2005); Gupta et al. (2010)]. The incorporation of particles does not change the structure of the electroless Ni-P matrix deposit [Balaraju et al. (2003); Bozzini et al. (1999)].

The key requirements for sound EL nickel based composite coatings are outlined as-

(1) Particle characteristics- Characteristics of second phase particle such as its size, shape, density, hardness, concentration and method of suspension in EL bath play a vital role in the deposit [Apachitei et al. (1998/2)]. Beyond certain concentration, probability of agglomeration of second phase particles increases as mean distance between them decreases causing settlement of the particles at the bottom of EL bath, hence, lower its codeposition efficiency [Balaraju et al. (2003)].

(2) Bath stability- The dispersion of second phase particles in EL bath increases the surface area of EL bath and this brings instability or bath decomposition [Reddy et al. (2000)].

(3) Agitation- Agitation of the electroless bath solution is a key factor for sound coating. The particles are kept in suspension by agitation and thus codeposit within the Ni-P deposit. Otherwise hard particles such as SiC, diamond, etc. are settled at the bottom and not readily available for codeposition. Rate of agitation, substrate position and movement also affect the deposition [Apachitei et al. (1999); Vasudvan et al. (1998)]

(4) Surfactants- These are generally significant in case of soft particles incorporation in Ni-P matrix such as graphite, polytetrafluoroethylene (PTFE), and molybdenum disulfide (MoS_2) [Balaraju et al. (2003)].

In recent years, the composite coatings provide an important means of enlarging the range of attainable mechanical, tribological and anticorrosive properties by incorporation of hard second phase micron sized particles in Ni-P matrix [Balaraju et al. (2003); Li (1997)]. The use of nanosized particles (range 2 to 50 nanometers) enhances the synergy between particle and matrix and thus increases the degree of codeposition to a specific limit. The scope of coatings is further broadened with the inclusion of ceramic nanosized particles codeposited into the EL Ni-P matrix to obtain high performance nanocomposite coatings in terms of high hardness, improved corrosion and wear resistance [Sahoo et al. (2011); Sharma et al. (2006)]. Work on electroless Ni-P composite coatings containing nanosized hard ceramic particles as reinforcement into the Ni-P matrix find wide applications, especially, as high hardness, antiwear and anticorrosion is listed briefly in table 2.4.

Table 2.4: Brief overview of developed Ni-P nanocomposite coatings with nanosized ceramic particles as reinforcement referred in the literature

Reinforcements 'X' used in Ni-P-X	**Reference and Year**
Al_2O_3	Zhou et al. (2008); Hamdy et al. (2007): Sharma et al. (2013)
SiC	Jiaqiang et al. (2006); Bigdeli et al. (2009); Yuan et al. (2009)
WC	Liu et al. (2007); Zhao et al. (2014)
SiO_2	Dong et al. (2009); Rabizadeh et al. (2011); Hazan et al. (2010)
Si_3N_4	Balaraju et al. (2008), (2010)
CNT	Chen et al. (2002); Wang et al. (2003); Alishahi et al. (2012)
ZrO_2	Song et al. (2008); Yang et al. (2011)
TiO_2	Chen et al. (2010); Guo et al. (2011)
Diamond	Xu et al. (2005); Mazaheri et al. (2012); Sorkhabi et al. (2013)
TiN	Mafi et al. (2011); Yu et al. (2011)

2.4 BRIEF OVERVIEW ON THE SYNTHESIS OF METAL OXIDE CERAMICS NANOPARTICLES

Nanopowders have made enormous enthusiasm in recent years by virtue of their unusual electronic, electrical, magnetic, optical and mechanical properties due to their smaller size and high surface area to volume ratio [Padmanabhan (2001); Basu and Chakravorty (2006)]. Nanocrystalline ceramic oxides owing to their unique physical, mechanical, structural, magnetic and optical properties have gained much attention [Vaben and Stover (1999); Shahbazian et al. (2002)]. Many researchers have taken interest on the preparation methods of nanocrystalline metal oxide ceramics due to their unique special features such as increased strength, ductility, diffusivity, specific heat, reduced density, elastic modulus, higher thermal expansion coefficient, electrical resistance, lower thermal conductivity and superior magnetic properties [Bjgrkval et al. (2000); Gupta et al. (2012); Kikandi et al. (2007)]. Due to these remarkable properties, nanocrystalline ceramic oxides find wide applications in various fields like protective coatings, biocompatible coatings, composite materials, antifogging coatings and antimicrobial finishing [Bin et al. (1996); Wong and Gupta (2007)]. Nanosized metal oxide ceramics codeposited on metal coating delivers improved ceramic characteristics such as wear and corrosion resistance, reduced brittleness and higher bonding ability to metals [Hamid and Elkhair (2002); Zhong and Gupta (2005); Miao and Ben (2000)]. The most promising versatile ceramic metal oxides, namely alumina (Al_2O_3), zirconia (ZrO_2) and titania (TiO_2) are

widely used in surface protective coatings for industrial applications.

2.4.1 Methods for synthesis of alumina, zirconia and titania nanoparticles

Alumina (Al_2O_3), zirconia (ZrO_2) and titania (TiO_2) nanoparticles has been intensively produced on account of their numerous technological applications due to its superior chemical, thermal, optical, electrical, catalytic, mechanical properties and ease of availability [Patnaik (2002)]. Significant physicochemical properties of Al_2O_3 ceramics such as its higher mechanical strength, excellent wear resistance, high chemical resistance, good dimensional stability and its ease of availability promotes its wide use in varied fields like coatings, cutting materials, abrasive grains refractory and composites [Lin et al. (1997); Vidacak et al. (2001); Eriksson and Seetharaman (2004)]. ZrO_2 is also well attracted ceramic known for its outstanding characteristics like high hardness, toughness, chemical corrosion resistance, thermal shock resistance and wear resistance. Hence, zirconia based coatings find wide applications in automobile engine components, cutting tools and wire drawing dies [Nai et al. (2006); Shibli et al. (2006); Song et al. (2007)]. TiO_2 ceramic, owing to its good mechanical and chemical properties have also gained major interest in view of its high performance ranging from photocatalytic to wear and corrosion resistant components for industrial applications [Gerasopoulos et al. (2010); Novakovic et al. (2006); Shibli and Dilimon (2007); Zhou et al. (2012)]. Significant efforts are focused to synthesize nanosized Al_2O_3, ZrO_2 and TiO_2 particles via novel approaches. Bottom up and top down approaches are commonly employed to synthesize these nanoparticles. In bottom up approach, particles are generated atom by atom and grow in size. The chemical process methods depend upon the kinetics of nucleation and growth of the particles in aqueous suspension on electrostatic stabilization [Segal (1997)]. On the other hand, micron sized powders are reduced to nano level by top down approach using conventional ball mill [Indris et al. (2000)]. Various processes methods namely precipitation [Hong et al. (1998); Li and Sun (2000)], sol-gel [Mirjalili et al. (2010); Tyagi et al. (2006)], hydrothermal [Li et al. (2009), Yuxiang et al. (2010)], mechanical milling [Adam et al. (2008)], vapour phase reaction [Varma et al. (1994)], auto-combustion [Casanova et al. (2007)], mechanochemical [Šepelák et al. (2012)] and spray pyrolysis [Yuan et al. (1998); Ganesan et al. (2003)] etc. are used for the synthesis of second phase nanometric Al_2O_3, ZrO_2 and TiO_2 nanopowders. Among variety of explored techniques, chemical precipitation and mechanical milling are more effective in terms of their simple and economical processing to produce nanoparticles. Both methods control the texture, homogeneity, composition and structural properties of ceramic particles.

2.4.1.1 Chemical precipitation- Bottom up approach

The chemical precipitation method is a simple and convenient method of producing Al_2O_3, ZrO_2 and TiO_2 nanoparticles. The nanoparticles are derived from aqueous inorganic salt solutions (chlorides, sulfates, nitrates) by the addition of a precipitating agent at room temperature and under specific pH. The morphology and composition of nanoparticles are mainly reliable on precursor type and its concentration, the reaction pH and temperature and ionic strength of the medium. Uniform particle size distribution can be achieved by controlling the reaction parameters such as reagent concentration, pH, time, temperature and surfactants [Li and Sun (2000); Tabriz and Nassaj (2009)]. The chemical precipitation method for fabrication of nanosized ceramics such as Al_2O_3, ZrO_2, TiO_2 and others has gained significant research interest.

Debsikdar (1987) synthesized $Al_2O3.ZrO_2$ (80:20 wt%) powders using three different chemical processes namely, chemical polymerization, destabilization of mixed sols and coprecipitation. It was found that the particles of size range 1.5 to 3.0nm were produced by each process and were noted to be amorphous by electron diffraction.

Hong et al. (1998) prepared Al_2O_3/20 mol% ZrO_2 powders by co-precipitation method and separately Al_2O_3 and ZrO_2 powders by precipitation method using aqueous solutions of $AlCl_3$, $ZrOCl_2$ and ammonia solution. The results show a series of partitioning and transformation processes in the solid solution with respect to rise in temperature.

Seo and Kim (2003) prepared TiO_2 nanoparticles by homogeneous precipitation process using urea and compared with particles synthesized by conventional precipitation using ammonia along with its characteristics. It was reported that the homogeneously precipitated powder attained lower particle size and more uniform particle shape than the conventional one with increase in heat treatment temperature.

Nanocrystalline ZrO_2 particles were synthesized using both precipitation and sol-gel techniques by Tyagi et al. (2006). Zirconium oxychloride and zirconium propoxide were used as the precursors for precipitation and sol-gel method respectively. The results revealed that particles were found to be spherical and cubic/rectangular shaped geometries in sol-gel and precipitation technique respectively. Thermal drying of gel in an oven (110°C, 12h) showed lower crystallite size (11-13nm) with respect to drying in vacuum (50 mbar, 70°C) where higher crystallite size (20-21nm) was noticed in both sol-gel and precipitation synthesis methods.

Ambrus et al. (2008) prepared Fe (III)-doped TiO_2 photocatalysts from aqueous $TiCl_3$ and $FeCl_3$ solutions by coprecipitation method. It was presented that the photocatalytic efficiency of Fe doped TiO_2 was superior than bare TiO_2 under UV-vis irradiation. However, the performance was worse at higher iron contents (6.0-10.0 at.%).

Wang et al. (2008) prepared nanosized γ-alumina powder using precipitation procedure. The reactant concentration, its molar ratio and the calcination temperature were investigated. The γ-alumina nanoparticles (5-9nm) without agglomeration were obtained. It was noticed that ethanol can avoid agglomeration during precipitation and calcination temperature plays a major role to determine various factors like surface area, the phase composition, size and diameter of the final product.

Tabriz and Nassaj (2009) synthesized Al_2O_3 nanoparticles using $AlCl_3 \cdot 6H_2O$ and Al by using precipitation method. The influence of heat treatment (60-1200°C) on the precipitate was examined. The results revealed the Al_2O_3 nanoparticles (30-95nm) were obtained and α-Al_2O_3 phase achieved above 1100^{o}C temperature.

The key advantage of chemical precipitation route is its simple processing where complex experimental procedures are not required. Further, the method is cheap in terms of starting materials used. The method is used to achieve high purity nanoparticles with controlled particle size with less agglomeration and thus highly favoured for the commercial production of nanosized metal oxides [Seo and Kim (2003)].

2.4.1.2 Mechanical milling- Top down approach

Mechanical milling (ball milling) is a simple, popular as well as comparatively cost effective method used for the mass production of nanosized Al_2O_3, ZrO_2 and TiO_2 powders. Ease of manufacturing elemental mixtures of any composition (mechanical alloying) or readily available nano powders (mechanical milling) makes the technique popular. High energy planetary ball mill has been employed for particle size reduction [Kumar et al. (2014)]. Ball mill is commonly used for mixing or grinding the materials such as ceramics, chemicals, ores and paints. Ball mills are filled partially with the material to be grinded along with the grinding media and then are mechanically rotated on their horizontal axis. It works on the principle of critical speed. The parameters of control are such as milling time, media, ball and powder ratio, speed etc. also ensures reproducible results. A variety of material is choosen for jars and grinding media like alumina, zirconia, agate, hardened steel and stainless steel jars and balls depending upon the grinding material used. Various researchers work on the preparation of nanosized metal oxides using mechanical route.

Panchula and Ying (1997) studied the mechanical preparation of nanocrystalline α-Al_2O_3 from γ-Al_2O_3. The influence of milling time on crystallite size, transformation kinetics, temperature, was evaluated. The results showed that the mechanical treatment induce significant increase in transformation kinetics in shorter time intervals.

Indris et al. (2000) examined the grain size effect of oxide ceramics Li_2O, $LiNbO_3$, $LiBO_2$,

B_2O_3, TiO_2 and the composite system Li_2O: B_2O_3 during the milling process. It was reported that the ball milling is an efficient technique for the analysis of grain size effect in nanocrystalline materials. The characteristics of milling like grain size reduction and subsequent grain growth are found similar in all oxides although in some materials, chemical reactions and phase transitions induced by mechanochemical treatment were noticed.

Colin et al. (2002) studied the kinetics and mechanisms of the phase transformation of anatase into TiO_2-II by milling of two types of TiO_2 powders separately and these were compared. It was found that formation of TiO_2-II crystallites occurred at the particle surface (150nm) for one powder and in bulk for the second one (25nm). The surface properties change was noticed in the ground powders compared to as-received powders after grinding.

The effect of milling process on three different types of ZrO_2 nanoparticles were studied by Adam et al. (2008) where 3,6,9-Trioxadecanoic acid (TODA) is used as an electrosterically acting surface modifier for the colloidal stabilization. It was concluded that the processing of zirconia nanoparticles in stirred media mills with an insitu surface modification is effective technique for the production of stable colloids with almost completely deagglomerated particles. Another research group, Reid et al. (2008) extensively studied the milling of Al_2O_3 powders using hardened steel, tungsten carbide, alumina and zirconia as different milling media. The degree of contamination from each media was compared and its effectiveness in reducing the crystallite size of the powders was examined. It was concluded that among all, the lowest contamination (3-4%) was observed in using zirconia media and in certain cases, the contamination may enhance the toughness of the material.

Muslimin and Yusoff (2009) investigated the infuence of high energy milling to the crystallite size of α-Al_2O_3 with milling time (0 to 60 min) and speed (400 to 1100 rpm). It was concluded that milling parameters (speed and time) plays a vital role on the crystallite size. The optimum milling speed and time was found to be 1000 rpm and 60 minutes respectively for the lowest crystallite size. A number of transition nano metal oxides such as TiO_2, ZnO, ZrO_2 and Al_2O_3 have also been prepared by mechanochemical reactions [Šepelák et al. (2012)].

The major advantage of mechanical milling is production of large quantities of nanosized powders, its easy handling and the disaggregation of nanosized aggregated powders at lower temperatures. The large scale production of these nanosized powders is an essential requirement for their industrial usage in surface protective coatings. However, the limitation is inclusion of fewer impurities as during milling, abrasion of the milling tools can occur. However, the choice of appropriate milling parameters (milling media, ball-to-powder weight ratio, milling time) can avoid or minimize the impurities in the samples [Kumar et al. (2014)].

2.5 PERFORMANCE OF Ni-P-X [X=Al_2O_3, ZrO_2 and TiO_2] NANOCOMPOSITE COATINGS

Wear is defined as loss of material from a surface by means of some mechanical action where as the deterioration of material by reaction to its environment is termed as corrosion. Wear and corrosion problems are of great relevance in a wide range of industrial applications as they result in progressive destruction and eventually failure of components [Morales et al. (2005); Pathak and Mohan (2005); Gadhikar et al. (2014)]. The use of coatings is specially recommended to protect these alloys at moderate temperatures to improve its corrosion and wear resistance properties and reduce the cost of losses generated by it [Dennis and Sagoo (1991); Elsener et al. (2008); Wang et al. (2011)]. Advances in materials performance require the development of nanocomposite coatings. Nanocomposite coatings are presently the high end coatings in the field of wear and corrosion resistance with their extreme demands as discussed briefly in table 2.3. Al_2O_3, ZrO_2 and TiO_2 nanoparticles owing to their high hardness, superior wear resistance, good chemical stability and ease of availability, as discussed in section 2.4, believed to be an effective second phase material in electroless Ni-P coatings to fabricate wear and corrosion resistant parts. For the stability and durability of the engineering system, the wear and corrosion tests of the coatings can be carried out as the presence of the coatings can change the operating wear and corrosion mechanisms. Various research communities from Iran, Poland, Japan, China, New Zealand, Netherlands, Taiwan, Egypt, India and USA are doing phenomenal research in development of nanocomposite coatings for wear and corrosion applications by reinforcement of Al_2O_3, ZrO_2 and TiO_2 in Ni-P matrix. The work done so far on improvement of mechanical and corrosion properties by inclusion of Al_2O_3, ZrO_2 and TiO_2 particles in the electroless Ni-P coating is discussed briefly in the following sub-sections.

2.5.1 Properties of Ni-P-Al_2O_3 nanocomposite coatings

The hardness studies on Ni-P-γAl_2O_3 and Ni-P-αAl_2O_3 were carried out by Pushpavanam (1992) where γAl_2O_3 (1.6μ) and αAl_2O_3 (3μ) particles were prepared by ball mill. The effect of heat treatment temperatures (473 K to 1273 K) on hardness of the composite coating was examined and compared with electrodeposits. It was concluded that EL Ni-P-αAl_2O_3 are much harder than Ni-P-γAl_2O_3 composites and it enhances with heat treatment (673K). It was also seen that electroless composites were three times harder than Ni-Al_2O_3 electrodeposits.

Lin et al. (1997) studied the difference in tribological behavior of alumina coatings prepared by plasma spraying with and without electroless film as underlayer. The results revealed that deposition of electroless nickel film with the steel substrate has much longer wear life and

adhesion strength unless the alumina layer is thinner than 0.3mm. It was also reported that lower the surface roughness of the steel substrate better the wear life of the alumina layer either with electroless nickel film or without.

Apachitei et al. (1998) investigated the hardness studies of incorporated micron sized hard particles namely SiC, B and Al_2O_3 with different irregular, spherical shaped composition and fibers within Ni-P matrix on Al (6063-T6) substrate. It was concluded that Ni-P coating containing spherical Al_2O_3 particles exhibited highest hardness among others before (743 HV_{100}) and after heat treatment (1248 HV_{100}) at 400^oC for 1h.

Hamid and Elkhair (2002) examined electroless Ni-P deposits incorporating ZrO_2, TiO_2, and Al_2O_3 particles (0-12g/l, 7-10µm size) on Al alloy (6061) from acidic bath. The mechanism of incorporation of particles was suggested and mechanical properties such as hardness and wear resistance were studied. The results showed that the optimal addition of surfactant 1,3 toloyl triethanol ammonium chloride (TTAC) enhanced the incorporation and increase in hardness values of Ni-P-Al_2O_3 (1400 HV) and wear resistance about five times in heat treated condition (400^oC, 1h) was observed compared to Al alloy substrate.

Electroless Ni-P-Al_2O_3 coatings were prepared on AISI 1045 steel by Alirezaei et al. (2004) and effect of alumina content (5, 10, 15, 20 and 25g/l) on deposition rate, morphology, roughness and hardness were investigated. The results showed the decrease in deposition rate and phosphorus content in coating whereas an enhancement in roughness and hardness with increase in alumina particles content. It was also found that on heat treatment at 400^oC for 1h, hardness attains maximum value (~ 1050 HV).

Shrestha et al. (2004) developed Ni-P-Al_2O_3 composite coating on copper substrate by 'two-step' technique where first alumina particles on Ni-P were deposited by electrophoretic deposition and then was again coated with layer of electroless Ni-P. It was revealed that the particle incorporated composite coatings exhibited better antiwear performance than the particle free coatings and heat treatment further enhanced the wear characteristics.

Crystallization and hardness behaviour of electroless Ni-P-nanoAl_2O_3 coating was studied on copper sheets by Jiaqiang et al. (2005). It was concluded that the activation energy and Avrami exponent of crystallization were lowered while microhardness of the composite coatings was greatly increased due to codeposited Al_2O_3 particles (50-150nm) and attained maximum (HV_{50} 1150) when heat treated at 230^oC for 24h.

Balaraju et al. (2006) studied the influence of the particle sizes (50nm, 0.3µm and 1.0µm) on the microstructure, hardness and corrosion resistance properties of electroless Ni-P-Al_2O_3 coatings on mild steel. It was concluded that a marginal improvement in hardness was noticed in composite coatings which enhances (about 15%) on heat treatment (400^oC, 1h). A slight

enhancement in corrosion resistance was reported in composite coatings with signs of uniform and localized corrosion after potentiodynamic polarization tests in 3.5% sodium chloride solution.

Alirezaei et al. (2007) studied hardness and wear resistance of electroless Ni-P and Ni-P-Al_2O_3 coatings on AISI 1045 steel along with their heat treatment effect at varied temperatures (200, 400, 600^{o}C). It was concluded that the existence of Al_2O_3 particles (5-15μm) in Ni-P coating matrix resulted in improved hardness and wear resistance and the achievement was maximum when heat treated at 400^{o}C for 1h.

Hamdy et al. (2007) studied the corrosion protection performance of electroless Ni-P, Ni-P-W, Ni-P-nanoAl_2O_3 coatings on low carbon steel with its heat treatment effect. Electrochemical impedance spectroscopy and polarization measurements were employed for corrosion tests in 3.5% NaCl solution before and after heat treatment. It is reported that Ni-P-W coatings showed best surface resistance (12.0×104 Ωcm^2) as double than for Ni-P-Al_2O_3 (7.00×104 Ωcm^2) and twenty times better than Ni-P (0.78×104 Ωcm^2). Also, it was found that corrosion resistance decreased after heat treatment.

Zhou et al. (2008) studied the microhardness and the wear resistance properties of EL Ni-P-nanoAl_2O_3 electroless composite coatings on low carbon steel and its heat treatment effect at various temperatures (200, 300, 400, 500 and 600^{o}C for 1h). The wear tests were carried using block-on-ring tribometer and compared with Ni-P and Ni-P-micro Al_2O_3 coatings. It was revealed that nanosized Al_2O_3 particles (20nm) were distributed uniformly in Ni-P matrix and attained largest hardness and wear resistance values among others and achieved best properties on heat treatment at 400^{o}C.

Luo et al. (2009) prepared alumina film on carbon steel surface with electroless Ni-P plating as an intermediate layer and oxidation kinetics was reported by measuring weight gain at 800^{o}C for 100h. It was revealed that adhesion strength to the substrate is up to 20N and higher oxidation resistance of coated steel than uncoated one.

The corrosion and oxidation resistance tests of electroless Ni-P and Ni-P-Al_2O_3 composite coatings on low carbon steel (Q235) sheets were studied by Sun et al. (2010). Corrosion resistance was examined by immersion and electrochemical tests using 10 vol.% H_2SO_4 and 3.5 wt% NaCl solutions respectively. Oxidation resistance was evaluated by weight gain analysis at 923K for 6h. An improvement of corrosion resistance and oxidation resistance by 35% were reported by dispersion of Al_2O_3 particles (sized 3~10μm) as compared with the carbon steel substrate.

Similar group also investigated the effects of amount of Al_2O_3 particles (6, 8, 10, 12g/l) and heat treatment temperatures (300, 350, 400 and 450°C for 1h) on the corrosion behaviour of

the coatings. It was presented that corrosion resistance is best at 8g/l concentration and enhancement is seen at temperature raises to 450°C.

Nova´k et al. (2010) reported the tribological properties of electroless Ni-P and Ni-P-Al_2O_3 coatings on Al-10Si-0.3Mg casting alloy after heat treatment at temperatures 400-550^oC for 1-8h uses pin on disc method at 5N load and 0.05m/s sliding velocity. It was observed that the coating performance was best when heat treated at 400^oC, 1h and coating wear resistance was reduced when annealed at temperatures above 400^oC. It was also found that reinforcement of Al_2O_3 saffil fibers reduces the scaling and increases wear resistance of coatings as compared to Ni-P coatings.

Heat treatment effect on microstructure, phase composition and adhesion using scratch test with an initial load of 8.80N was also investigated by the above similar group. It was presented that high temperature annealing (450°C and above) results in poor coating adhesion and wear resistance than optimal annealing at 400°C for 1h and Al_2O_3 fiber reinforcement greatly reduces the coating delamination.

The corrosion studies on electroless Ni-P and Ni-P-Al_2O_3 alloy coatings were carried on carbon steel substrate by León et al. (2010). The influence of varied annealing temperatures (100, 200, 300, 400 and 500°C) on the corrosion parameters was examined in artificial seawater (pH 5.0 and 8.1) media using electrochemical impedance spectroscopy and potentiodynamic polarisation tests. It was reported that crystallised Ni-P and Ni-P-Al_2O_3 (Al_2O_3-5μm size) exhibited higher corrosion resistance than the coating in the amorphous form. Coatings annealed at 400 and 500°C for 1h represented the most noble corrosion potential with highest R_{ct} and the lowest C_{dl} values.

Zhang et al. (2010) proposed laser strengthening technique on stainless steel (3Cr13) after EL Ni-P-nanoAl_2O_3 electroless plating and coating performance in terms of microhardness and wear resistance were measured using pin-on disc with a load of 900N and speed of 1100r/min. It was concluded that with high laser power (4kW) and velocity, the electroless deposit with finer Al_2O_3 particles (20nm) exhibit excellent properties as microhardness increases about threetimes and the wear resistance about two times more than the stainless steel substrate.

Afroukhteh et al. (2012) studied the corrosion behaviour of electroless Ni-P-Al_2O_3 nanocomposite coatings with and without polymeric surfactant (0-1g/l) at varied concentrations of 70nm sized Al_2O_3 particles (3-30g/l) on low carbon steel plates. Corrosion tests were carried out by using electrochemical impedance spectroscopy and polarization methods in 3.5% NaCl solution. It was concluded that the codeposition of 3g/l Al_2O_3 particles showed much better corrosion resistance in the presence of surfactant than 20g/l Al_2O_3 particles without any surfactant.

Wear and corrosion resistance of electroless Ni-P and Ni-P-Al_2O_3 nanocomposite coatings were investigated by Sharma and Singh (2013) on mild steel substrate at varied concentrations (5 to 20g/L). Electrochemical and immersion tests were conducted in 3.5% NaCl solution for corrosion studies and pin-on-disc method was employed for wear studies. It was concluded that inclusion of Al_2O_3 particles (80-90nm size) showed improved wear resistance, hardness, corrosion resistance and higher friction coefficient which further enhanced with increase in its alumina content as compared to Ni-P coating.

Li et al. (2013) developed EL Ni-P-Al_2O_3 nanocomposite coatings on steel substrate. α-Al_2O_3 nanoparticles were prepared by milling in a high energy mill and influence of nanoparticle concentration on the microhardness, wear resistance and corrosion resistance of the coatings was studied in as deposited and heat treated conditions. The wear and corrosion tests were carried out using tribometer at a load of 20N and polarization method in 3.5 wt.% NaCl solution respectively. The results showed that the reinforcement of milled Al_2O_3 nanoparticles (13nm) improved the microhardness and wear resistance but affect the corrosion resistance of nanocomposite coatings.

Karthikeyan and Ramamoorthy (2014) recently studied the characteristics and properties such as roughness, hardness and wear of electroless Ni-P and Ni-P-nanoAl_2O_3 coatings with varying reducing agent concentration. Wear tests were conducted using pin on disc apparatus with constant 300 rpm speed and a 20N load. It was concluded that Al_2O_3 dispersion enhances the surface roughness of the coating (1.613µm) than Ni-P (0.924µm) coating. Also, codeposition of Al_2O_3 increased hardness upto 460 HV and 1083 HV with reduced specific wear rate by 52.62% and 32.38% before and after heat treatment respectively.

2.5.2 Properties of Ni-P-ZrO_2 nanocomposite coatings

He et al. (1997) studied the tribological properties of tetragonal zirconia (Y-TZP), alumina dispersed in Y-TZP (ADZ), ZrO_2 dispersed in Al_2O_3 (ZTA) and Al_2O_3 with MgO and revealed that ADZ had better wear resistance among all.

Sharma et al. (2002) developed electroless Ni-P-X (ZrO_2-Al_2O_3) by conventional and *insitu* methods on aluminium substrate and studied its wear and friction behaviour using pin on disc method before and after heat treatment. It was concluded that composite coatings exhibited higher wear performance than aluminum in as coated and heat treated condition. It was also found that the friction coefficient decreases with increase in applied load.

Similar group [Sharma et al. 2002] investigated the application of Ni-P-ZrO_2-Al_2O_3-Al_3Zr electroless coatings on aluminium, low carbon steel and carbon fabric substrates in terms of tribological behaviour.

Sharma et al. (2003) developed an empirical model for coating weight in Ni-P-X (X= ZrO_2-Al_2O_3-Al_3Zr) composite coating at the specified bath composition. The non-isothermal crystallisation kinetics studies for Ni-P and Ni-P-X composite coatings were also carried out. The model representated that the coating weight of the composite coating is around 32.5-112.5 cm^2/l.

Sharma et al. (2005) developed the pioneered route for synthesis of electroless Ni-P-X (X=ZrO_2-Al_2O_3-Al_3Zr) composite coating and studied its morphological and hardness characteristics. It was reported that EL Ni-P-X composite coatings attained a microcrystalline structure around 648 K crystallization temperature. The microhardness of the composite was about two fold than Ni-P coating on heat treatment at 673K for 1h.

A different work was introduced by Shibli et al. (2006) by reinforcement of electroless Ni-P plate with ZrO_2 where the plate used as potential catalytic electrode for hydrogen evolution reaction in alkaline media.

Gay et al. (2007) prepared electroless Ni-P-ZrO_2 composite coatings on brass plates and the influence of the incorporation rate of ZrO_2 particles (0 to 90gl^{-1}) on the mechanical and tribological properties of the composite coatings was investigated. Friction coefficient and wear resistance measurements of the composite coatings were examined using pin on disc tests at 2 N loads. It was found that the incorporation of ZrO_2 particles (0.9µm) in Ni-P coating with a concentration of 7.4% represented high hardness (1150 $kgmm^{-2}$), low friction coefficient (0.52) and good wear resistance after heat treatment of 400°C for 1h as compared to Ni-P coating.

Hardness, wear and corrosion studies of electroless Ni-P-ZrO_2 composite coatings were studied by Song et al. (2007) on AZ91D magnesium alloys. It was concluded that the hardness of Ni-P-ZrO_2 composite coatings achieved a maximum after heat treated at 350°C followed by decay at 400°C. The wear and corrosion resistance of Ni-P-ZrO_2 composite coatings was found superior than Ni-P coatings.

A similar group [Song et al. 2007] also investigated the detailed corrosion protection properties of Ni-P-ZrO_2 composite coatings using EIS, potentiodynamic curves, salt spray and immersion tests of the coated magnesium alloy in 3.5% NaCl solution. It was mentioned that ZrO_2 incorporated composite coating showed higher corrosion performance due to open corrosion pits than that of Ni-P coating where blocked corrosion pit was the main corrosion form.

Similar research group, in 2008, [Song et al.] developed a multilayer Ni-P-ZrO_2 (15µm)/electroplating Ni (20µm)/Ni–P (5µm) coating on AZ91D magnesium alloys. The corrosion behaviors were examined by immersion (3.5 wt% NaCl), salt spray (5 wt% NaCl) and electrochemical (0.6M NaCl, Na_2SO_4 and 0.6M NaOH) tests. The results revealed that an

improvement in corrosion resistance occurred in ZrO_2 (20nm) incorporated composite coatings (more than 1000h for the salt spray test). Also, it was found that composite coatings suffered attack in NaCl solution but displayed passivation characteristics in Na_2SO_4 and NaOH solutions.

Szczygieł et al. (2008) studied electroless binary Ni-P, ternary Ni-W-P alloy coatings and composite (Ni-P-ZrO_2 and Ni-P-W-ZrO_2) coatings on alloy steel substrate (AISI 304). AT-10 tester machine with a constant pressure of 50 MPa and the sliding speed of 0.56ms^{-1} was used to determine the abrasion resistance of the coatings. The results showed that all the coatings exhibited higher hardness (over 800 HV) than substrate and the improvement of wear resistance was stronger in ZrO_2 (5μm) than tungsten.

A similar group [Szczygieł and Turkiewiczet (2008)] also studied the composition, structure and topography of the Ni-P-W-ZrO_2 coatings and its heat treatment (400^{o}C, 1h) effect. The results showed a nodular compact structure (nodule size 2 to 10mm) and degree of crystallinity increases to nearly two fold on heat treatment.

The oxidation behaviour of ZrO_2 (3.0μm) particles incorporated electroless Ni-P coating was examined on low carbon steel substrate by Tan et al. (2011) by weight gains evaluation during high temperature (923K) oxidation test. The results showed that the embeddment of ZrO_2 particles in Ni-P matrix greatly enhanced oxidation resistance of the steel substrate than Ni-P coating.

Yang et al. (2011) developed a novel technique to produce Ni-P-ZrO_2 nanocomposite coatings by adding ZrO_2 sol into conventional electroless Ni-P plating bath on AZ31 Mg alloy sheet. Wear tests were conducted on a tribometer with a load of 7N and a sliding speed of 50mm/s. The *insitu* nanocomposite coating showed increased microhardness (1045 HV_{200}) than conventional Ni-P-ZrO_2 (759) and Ni-P (619) coating and better wear resistance.

The surfactant effect was studied on electroless Ni-P-ZrO_2 (100nm) coatings by Zielin´ska et al. (2012). The impact of addition of dodecyl trimethyl ammonium bromide (DTAB) surfactant on the rate of deposition, composition and topography of coatings was examined. It was concluded that better dispersion of zirconia (21.88–22.10 wt.%) were noticed in coatings with baths containing DTAB.

Ranganatha et al. (2012) investigated the corrosion behavior of electroless Ni-P, Ni-P-ZrO_2 and Ni-Cu-P-ZrO_2 coatings with varied concentrations of Cu and ZrO_2 (30-35nm). Anodic polarization, Tafel plots and EIS methods were choosen for corrosion tests evaluation in 3.5% NaCl solution. It was concluded that Ni-Cu-P-ZrO_2 was the most noble among all coatings and the corrosion rate decreased by twice and 7 times than Ni-P-ZrO_2 and Ni-P coatings respectively.

2.5.3 Properties of Ni-P-TiO_2 nanocomposite coatings

Balaraju et al. (2001) studied the corrosion resistance characteristics of Ni-P, Ni-P-Si_3N_4, Ni-P-CeO_2 and Ni-P-TiO_2 composite coatings using EIS technique in 3.5 wt.% NaCl solutions. It was reported that the charge transfer resistance for all the coatings were in the range of 32, 253, 700 Ωcm^2 and capacitances were in the order of 11-17 $\mu f/cm^3$. It was found that corrosion resistance were in the order of Ni-P-Si_3N_4 = Ni-P-CeO_2 > Ni-P-TiO_2.

Song et al. (2004) developed the new technique of sol enhanced electroless Ni-P-TiO_2 composite coatings on carbon steel followed by heat treatment at 550^oC. The results showed that TiO_2 modified film have good corrosion resistance in 0.5mol/L H_2SO_4 and in 0.5mol/L NaCl solutions.

Balaraju et al. (2006) discussed the structural characteristics and phase transformation behaviour of plane electroless Ni-P coating and electroless Ni-P-Si_3N_4, Ni-P-CeO_2 and Ni-P-TiO_2 composite coatings and concluded that incorporation of Si_3N_4, CeO_2 and TiO_2 particles in Ni-P matrix donot have any influence on the structure and phase transformation behaviour of electroless Ni-P coatings.

Novakovic et.al (2006) prepared electroless Ni-P and Ni-P-TiO_2 composite coatings on brass substrate followed by heat treatment in vacuum (800^oC for 10 min). The hardness tests were conducted and corrosion behaviour was studied using linear polarisation curves in 3.5% NaCl solution. The results showed that the composite coatings with TiO_2 particles (200-300nm) as reinforcement acquired higher microhardness (1450 HV) than Ni-P (1200 HV) although the corrosion resistance almost remained unaffected after vacuum heat treatment.

Shibli and Dilimon (2007) explored electroless Ni-P plates for hydrogen evolution reaction (HER) and the role of phosphorus content on the physicochemical and electrocatalytic properties of electroless Ni-P plates was studied and concluded that the plates with optimum phosphorus content were found to consist of a mixture of amorphous and crystalline phase and TiO_2 reinforced plates exhibited high electrocatalytic activity during HER.

Yu et al. (2007) studied electroless Ni-P-nanoTiO_2 (anatase type) composite plating and its effects on the deposition rate, corrosion resistance and pitting corrosion potential by using weight loss and electrochemical methods. The results indicated that the corrosion resistance of composite coatings increased by 8 times in salt media than Ni-P although it remains constant in basic and acidic corrosive medium.

Song et al. (2008) prepared Ni-P/TiO_2 composite film on sintered NdFeB permanent magnet by dispersion of TiO_2 sol in electroless nickel coating. The corrosion resistance was studied by potentiodynamic polarization and EIS techniques. It was concluded that the corrosion current density (i_{corr}) of composite film is about 33% of that of Ni-P coating in 0.5mol/L H_2SO_4

solution and about 14% that of Ni-P coating in 0.5mol/L NaCl solution indicated that composite film showed better corrosion resistance than Ni-P coating.

Microhardness and corrosion behavior of elecroless Ni-P and Ni-P-TiO_2 composite coatings was studied by Novakovic and Vassiliou (2009) on carbon steel substrates using low TiO_2 bath concentrations (0.5-2.0g/l). The corrosion studies were carried using linear polarisation curves in 3.5% NaCl solution. It was concluded that the TiO_2 particles (200-300nm) incorporation increases with increase in their concentration in the bath. The results indicated an improvement in microhardness (20%) in composite coatings compared to Ni-P coatings and decrease in the corrosion resistance in both coated and vacuum heat treated condition.

Wu et al. (2009) prepared Ni-P-TiO_2 composite coating on substrates and showed when TiO_2 content in bath was 4g/l, plating speed was fast with deposit amount (12.2μm/h) and photocatalytic effect was best. An improvement in microhardness of heat-treated composite coating (HV 1180) was observed with respect to the Ni-P alloy coating (HV 950).

Chen et al. (2010) proposed a novel TiO_2 sol enhanced Ni-P electroless composite coatings on AZ31 Mg alloy samples where transparent TiO_2 sol was added into Ni-P solution leading to *insitu* synthesis of Ni-P-TiO_2 nanocomposite coating. The wear tests were conducted using a microtribometer with load of 7N and sliding speed of 50mm/s. It was concluded that TiO_2 particles (15nm) were well dispersed into Ni-P matrix. The properties like microhardness (1025 HV_{200}) and the wear resistance of the composite coatings were found to be greatly increased than conventional (710 HV_{200}) composite method.

Similar group Chen et al. (2010) also studied TiO_2 sol enhanced Ni-P electroless composite coatings on steel substrate. The results revealed that the hardness (10 GPa) and Young modulus (200 GPa) of the composite coating were found to be improved than plane Ni-P coating which is of the order 6 and 110 GPa respectively.

Guo et al. (2011) prepared electroless Ni-P/TiO_2 metal matrix composite (MMC) coatings combined with sol-gel method on magnesium alloys (Mg-3.0Nd-2.0Zn-0.4Zr wt.%). It was found that the TiO_2 nanoparticles were well dispersed in the coating matrix. The microhardness of composite coating (734 HV_{100}) was higher than Ni-P (501 HV_{100}) and Mg substrate (67 HV_{100}). The corrosion resistance of composite in 3.5 wt % NaCl solution is higher than substrate but no significant change was noticed with respect to Ni-P coating.

Electroless Ni-P/TiO_2 and Ni-Sn-P/TiO_2 nanocomposite coatings with varied contents were prepared by Khalifa et al. (2011). The corrosion resistance of the deposits was studied by potentiodynamic polarization in 3.5% NaCl solution. The results revealed that composite films attained good corrosion resistance. Heat treatment was resulted in crystalline structure with Ni and Ni_3P phases apart from TiO_2.

Hardness and corrosion resistance of Ni-P-TiO_2 nanocomposite coatings with varied nanosized TiO_2 particles contents was studied by Momenzadeh and Sanjabi (2011). The surfactant sodium dodecyl sulfate (SDS) effect on chemical composition of the coatings was also investigated. It was concluded that the surfactant enhances the particle dispersion in the coating. Also it was presented that corrosion resistance and hardness (1050 HV) of Ni-P-TiO_2 nanocomposite coatings was improved greatly compared to Ni-P coating (805 HV) after heat treatment at 400^oC for 1h.

Allahkaram et al. (2012) codeposited TiO_2 nanoparticles (20nm) with Ni-P matrix using electroless technique on API-5L-X65 steel substrates and its hardness and corrosion behaviour were studied using linear polarization method in 0.5M sulfuric acid solution. It was presented that inclusion of TiO_2 nanoparticles enhanced coating's microhardness but corrosion resitance was found to be lower than Ni-P although higher than substrate.

Lee (2012) compared the corrosion resistance between electroless Ni-P/nanoTiO_2 and Ni-P/CNT composite coatings on 5083 aluminum alloy. The corrosion tests were investigated by potentiodynamic polarization and immersion tests in 3.5 wt.% NaCl solution. It was revealed that TiO_2 (15nm) and CNT (5nm) nanoparticles incorporated composite coatings exhibited better corrosion resistance than plane Ni-P coating and the substrate. It was also found that CNT reinforcement possessed superior corrosion resistance than TiO_2 reinforced composite coating.

In the same year, [Zhou et al. (2012)] developed Ni-P/TiO_2 bilayer coating using combined electroless plating and sol-gel method on A3 low carbon steel. Photocathodic protection properties were examined by electrochemical method. The results showed that the open circuit potential (OCP) of the composite coating was shifted to -0.42 V under UV irradiation which is found to be lower than the corrosion potential of carbon steel.

Gawad et al. (2013) studied the performance of nanocomposite coatings containing second phase Al_2O_3 (70nm) and TiO_2 (50nm) particles on copper sheets. Corrosion tests were performed using electrochemical method exposed to 3.5% NaCl solution. Both coatings were reported improved hardness and corrosion resistance as compared to Ni-P coating. It was also found that coatings with alumina reinforcement (490 HV_{50}) were much harder as compared to titania (490 HV_{50}) while titania reinforce coating showed slightly better corrosion resistance.

Georgiza et al. (2013) studied hardness and corrosion behavior of three different types of electroless nickel coatings on AZ31 wrought magnesium alloy. The first one was plane Ni-P coating, the second one was duplex coating comprising of different phosphorus content layers. The third one was duplex layer incorporated with TiO_2 (0.3-0.5μm) and ZrO_2 (5μm) particles. Tafel polarization curves were employed for corrosion tests in 3.5% NaCl solution. The results

revealed that all the coatings protect the Mg alloy substrate. It was also found that the composite coatings enhanced hardness and corrosion resistance after heat treatment at 200°C for 2h.

2.6 SUMMARY

The present chapter outlines a brief review of literature, discussing the development, advantages, classification, mechanisms, essential conditions required and process parameters influencing electroless nickel coating technology. The survey on the development of EL Ni-P based composite coatings systems (Ni-P-X) used for wear and corrosion resistant applications have been presented. The significance of inclusion of Al_2O_3, ZrO_2 and TiO_2 reinforcements on the protective Ni-P coatings are outlined and various synthesis modes have been discussed. A brief literature based on process methods, namely chemical precipitation and ball milling used for the synthesis of nanosized Al_2O_3, ZrO_2 and TiO_2 reinforcements has been carried out. The review on studies of EL Ni-P-X [X=Al_2O_3, ZrO_2 and TiO_2] nanocomposite coatings developed by inclusion of nanosized 'X' particles in Ni-P matrix through various means especially for wear and corrosion applications has been extensively done.

CHAPTER 3

PROBLEM FORMULATION

3.1 BACKGROUND

An extensive literature review has been carried out on EL Ni-P alloy and Ni-P based composite coating systems for wear and corrosion applications and discussed in the previous chapter. The enhancement of wear and corrosion resistance by embedding hard ceramic particles in nickel matrix as composites and a suitable heat treatment were studied to some extent [Balaraju et al. (2003); Sahoo and Das (2011)]. The promising ceramic materials namely alumina (Al_2O_3), zirconia (ZrO_2) and titania (TiO_2) due to their excellent mechanical and good chemical resistance properties are believed to be used as the second phase for improving the properties like hardness, wear and corrosion resistance of Ni-P coatings [Hamid and Elkhair (2002); Gay et al. (2007); Novakovic et al. (2006)]. It has been observed that most studies on EL Ni-P-X [X= Al_2O_3, ZrO_2 and TiO_2] composite coating systems were mainly focused upon the incorporation of micron sized 'X' particles into the Ni-P matrix to yield better coating properties. Only fewer investigations have been conducted using nanosized 'X' particles, though, preparation methods of reinforcement of nanosized particles are not much focused. Studies on reinforcement of nanosized 'X' particles prepared by chemical precipitation route into an EL Ni-P matrix have not been reported to date. Mechanical milling is mainly employed for preparation of nanosized particles in bulk quantities. The idea of incorporation of mechanically milled 'X' nanopowders into EL Ni-P matrix is less focused. It was studied only for Ni-P-Al_2O_3 [Li et al. (2013)] though the systematic studies on milling parameters of reinforcement are not yet discussed. Non-coventional (*Insitu*) synthesis of EL Ni-P-X nanocomposite coatings is rarely focussed. The studies were carried out recently on *insitu* synthesis of EL Ni-P-ZrO_2 [Yang et al. (2011)], Ni-P-TiO_2 [Chen et al. (2010)] using different reagents. However, *insitu* synthesis of Al_2O_3, ZrO_2 and TiO_2 nanoparticles prepared by precipitation followed by codeposition within EL Ni-P bath to form EL Ni-P-X nanocomposite coatings is not yet studied. The detailed tribological studies employing ball-on disc method on nanosized 'X' particles reinforced EL Ni-P matrix nanocomposite coatings are not yet discussed. The corrosion characteristics of these EL Ni-P-X nanocomposite coatings in acidic and saline atmosphere are not fully featured.

3.2 PROPOSED METHODOLOGY

In view of literature survey, the present investigation is an attempt to develop EL Ni-P-X [X= Al_2O_3, ZrO_2 and TiO_2] nanocomposite coatings by different means for wear and corrosion applications. The details of the proposed research plan are mentioned in the flowchart in figure 3.1. Following studies are proposed accordingly in this regard:

- Al_2O_3, ZrO_2 and TiO_2 nanoparticles are proposed to be synthesized by Bottom up and Top down approaches. In case of Bottom up approach (chemical route), chemical precipitation method is used with an appropriate heat treatment for separately producing nanoparticles of Al_2O_3, ZrO_2 and TiO_2. In case of Top down approach (mechanical milling), high energy planetary ball mill is employed for reducing the particles to nanometer size range from commercially available micron sized Al_2O_3, ZrO_2 and TiO_2 particles. All nanosized powders 'X' are proposed to be characterized using instrumental tools like XRD, FESEM with EDAX, TEM, DTA/TG/DTG.
- The above prepared nanosized 'X' particles are then proposed to be used as second phase particles in Ni-P matrix to develop conventional Ni-P-X [X= Al_2O_3, ZrO_2 and TiO_2] nanocomposite coatings by EL technique. EL technique is the one where the coating proceeds in autocatalytic manner just by controlling pH and temperature. Hence, six different types of EL conventional Ni-P-X nanocomposite coatings are proposed to be developed by reinforcing the distinct 'X' nanoparticles.
- At another set of experiments, an *insitu* method is proposed to be employed which can precipitate Al_2O_3, ZrO_2 and TiO_2 nanoparticles in the environment suitable for depositing EL Ni-P. In this way, *insitu* synthesis of 'X' nanoparticles occurs within the EL Ni-P bath followed by its codeposition into Ni-P matrix to develop non-conventional *(insitu)* Ni-P-X nanocomposite coatings is proposed. These *insitu* Ni-P-X nanocomposite coatings are compared with conventional coatings for the same reactions.
- All EL Ni-P-X nanocomposite coatings developed by conventional and non-conventional means are proposed to be heat treated at 400^oC for 1 h in argon atmosphere to improve the adhesion along with mechanical and physiochemical properties.
- All the above mentioned EL Ni-P-X nanocomposite coatings are proposed to be characterized in 'as coated' and 'heat treated' conditions. The characterizations carried out are for evaluating morphology (FESEM), elemental analysis (EDAX), phase analysis (XRD) and surface topography (AFM). The properties like microhardness (Hardness tester), wear resistance, friction coefficient (Ball-on disc method) and

corrosion resistance (Electrochemical polarization) are to be studied.

- The characteristics and performance of EL Ni-P-X nanocomposite coatings in terms of hardness, wear and corrosion is compared with EL Ni-P alloy coatings.

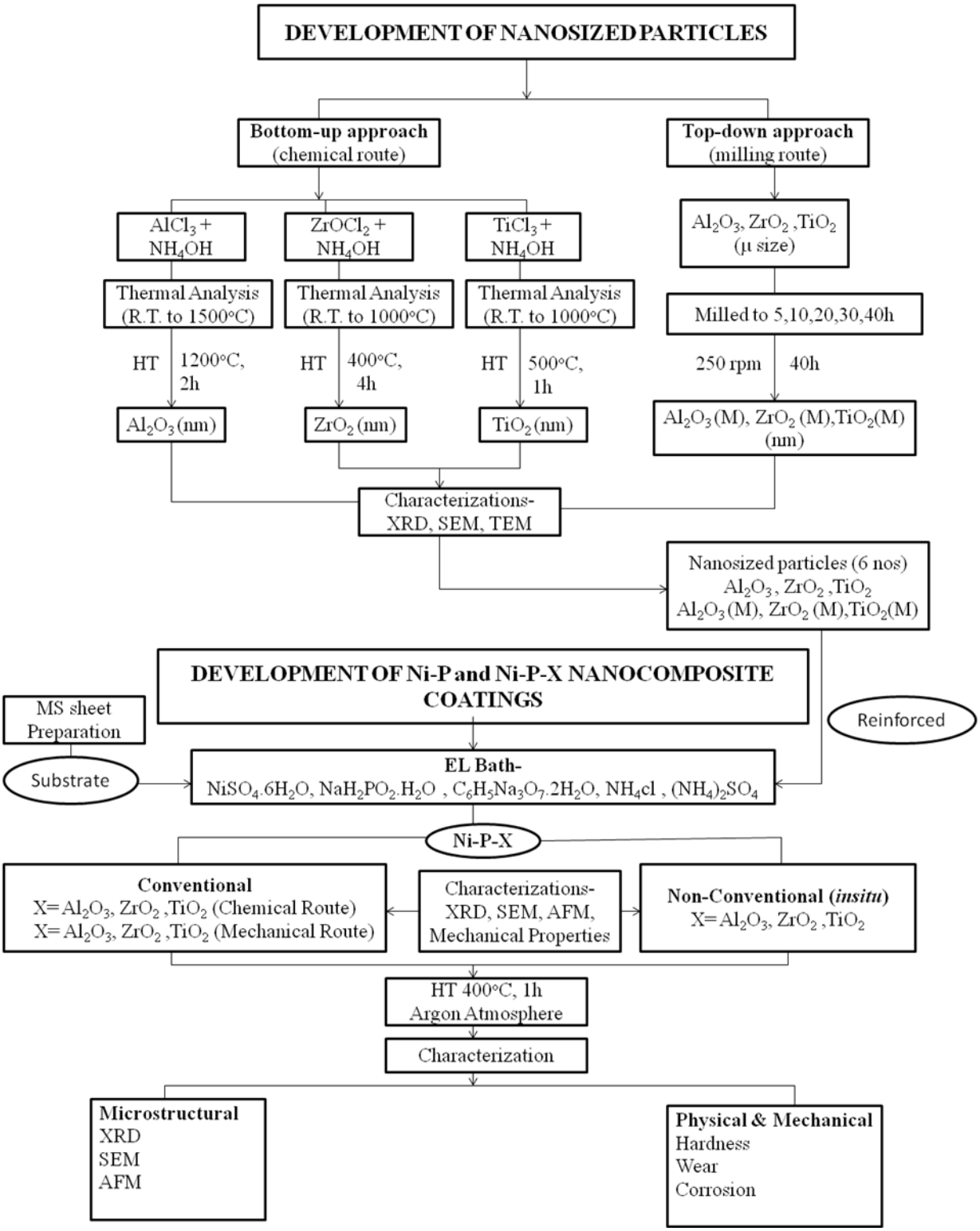

Fig 3.1- Flow chart showing the experimental details of proposed research plan.

CHAPTER 4

EXPERIMENTAL DETAILS

4.1 INTRODUCTION

The materials and the experimental techniques that are employed to achieve the objectives of the present investigation are discussed in this chapter. The details of the synthesis of Al_2O_3, ZrO_2 and TiO_2 nanoparticles by various routes, surface preparation of substrate, electroless nickel coatings bath, development of EL nanocomposite coatings and characterisation of nanoparticles and EL coatings with the equipments used are presented in the given sections. Nanoparticles of Al_2O_3, ZrO_2 and TiO_2 were separately synthesized by Bottom up approach i.e. chemical route using required chemical reagents and also separately by Top down approach i.e. mechanical milling using high energy ball mill. These synthesized nanoparticles of Al_2O_3, ZrO_2 and TiO_2 were used as the reinforcements to develop EL conventional Ni-P-X nanocomposite coatings. The non-conventional EL Ni-P-X nanocomposite coatings were also developed where Al_2O_3, ZrO_2 and TiO_2 nanoparticles are nucleated, grown and codeposited along with Ni-P within the coating bath. The three types of nanocomposite coatings were characterized before and after heat treatment for morphology, phase analysis, surface topography, microhardness, wear and corrosion characteristics. The features of developed nanocomposite coatings were compared with Ni-P alloy coatings.

4.2 SYNTHESIS OF NANOPARTICLES

The preparation of nanocrystalline metal oxide ceramic particles has gained much attention due to their unique features such as chemical stability, high surface to volume ratio, mechanical, magnetic and physical properties. The most promising nanocrystalline ceramics namely Al_2O_3, ZrO_2 and TiO_2 are highly required versatile materials widely used in refractories and surface protective coatings. Bottom up and Top down approaches are commonly employed to synthesize these nanoparticles.

4.2.1 Bottom up Approach (Chemical Route)

In the present work, Al_2O_3, ZrO_2 and TiO_2 nanopowders were synthesized using chemical precipitation technique where particles are generated atom by atom and grow in size. The chemical precipitation method is a simple and economical method of producing nanoparticles. Calcination of all the powders was carried out at temperatures depicted by DSC curves. Muffle furnace of accuracy ±2°C was employed and air was the medim used for all heat treatments.

The calcined powders of Al_2O_3, ZrO_2 and TiO_2 were used as the reinforcement for development of conventional EL Ni-P-Al_2O_3, Ni-P-ZrO_2 and Ni-P-TiO_2 nanocomposite coatings.

4.2.1.1 Synthesis of Al_2O_3 particles

Anhydrous aluminium chloride ($AlCl_3$) procured from Merck, India was used as the precursor for synthesis of alumina (Al_2O_3) nanopowder. Intially, 13.34gm of $AlCl_3$ was dissolved in 100mL of distilled water (1M) and the solution was continuously stirred (pH-1.8) at room temperature for 15min. The precipitating agent i.e., ammonia solution, NH_4OH, procured from Merck was then added dropwise into the continuously stirred solution until the complete precipitation occurred at pH-9. The precipitates were aged for 30h under continuous stirring at room temperature. The precipitates of $Al(OH)_3$ and NH_4Cl were obtained. The precipitates were washed with distilled water and dried in an oven at a temperature of 100^oC for 24h. The dried powder was calcinated in air at 1200^oC for 2h.

4.2.1.2 Synthesis of ZrO_2 particles

Zirconium oxychloride, $ZrOCl_2.8H_2O$ (Thomas baker) was used as the starting material for the synthesis of nanosized zirconia (ZrO_2) powder. Here $ZrOCl_2.8H_2O$ (11.27gm) was dissolved in distilled water (35mL) under continuous stirring to make 1M solution. Then the solution was hydrolyzed by dropwise addition of aqueous ammonia solution, NH_4OH (Merck) until got neutralized (pH-9). The precipitates were filtered and repeatedly washed with deionized water and ethanol in order to remove all chloride ions. The resulted precipitates were dried in oven at 100^oC for 24h. The calcination of dried powder was carried out at 400^oC for 4h in muffle furnace (air).

4.2.1.3 Synthesis of TiO_2 particles

The TiO_2 powder was synthesized using titanium trichloride ($TiCl_3$, Sigma Aldrich) and ammonia solution (NH_4OH, Merck) as the starting materials. Here $TiCl_3.8H_2O$ (50ml) was placed into a flask. Aqueous solution of concentrated ammonia solution (40mL) was mixed in 25mL of distilled water and then added dropwise to the flask containing $TiCl_3$ solution under continuous stirring at room temperature. The dark blue precipitates were observed and was aged under stirring for 16h during which the colour of the dispersion turned to white (pH -8.5). The precipitates were filtered and washed repeatedly with distilled water followed by washing with ethanol to remove all the chloride ions and oven dried at 100^oC for 24h. The dried powder was calcinated in air at 500^oC for 1h.

4.2.2 Top down Approach (Mechanical Milling Route)

In the present study, commercially purchased Al_2O_3, ZrO_2 and TiO_2 powders were reduced separately to nano level by mechanical milling using high energy planetary ball mill (Retsch, PM 400/2, Germany). The hardened steel grinding jars and grinding balls were provided by M/S Retsch GmbH, Germany. Micron-sized Al_2O_3, ZrO_2 and TiO_2 powders procured from Sigma Aldrich, Testbourne UK limited and Merck respectively with a purity of 99.99 % and approximate particle size of 40-42µm each was used as the starting charge for the mechanical grinding of Al_2O_3, ZrO_2 and TiO_2 nanoparticles. Hardened steel balls and jars were used as the media for mechanical milling and toluene was used as the process control agent for avoiding agglomeration of the powders in wet milling conditions. In the grinding experiment, 500ml jar was used for milling containing 30gm Al_2O_3, ZrO_2 and TiO_2 powder separately. While milling, the charge used was 1/3 of the jar i.e. about 200ml size was filled with balls and powder. The balls used have the diameter 20mm, 10mm and 5mm in weight ratio of 3:2:1 in each case. The milling of Al_2O_3, ZrO_2 and TiO_2 powders were carried out separately at 250rpm with ball to powder ratio 10:1 upto 40h, with intermittent milling time of 2h. Milling was stopped intermittently to avoid the overheating of the milling media and half an hour was given. The milled powder was dried in oven at 40^oC for about 2h after milling so that it dried completely.

4.3 CHARACTERIZATION OF NANOPARTICLES

The different techniques adopted for characterization of chemically and mechanically prepared Al_2O_3, ZrO_2 and TiO_2 nanopowders in the present study are outlined here. The thermal behavior of the dried powders was studied using TG/DTA. Morphological analyses of the above powders were observed by field emission scanning electron microscopy (FESEM). The phase structures of the powders were determined by X-Ray diffraction (XRD). The particle size of the powders was confirmed by transmission electron microscope (TEM). The details are briefly discussed in the following sub-sections.

4.3.1 Field Emission Scanning Electron Microscopy (FESEM)

The surface morphology of all the powders prepared separately by chemical and mechanical route was examined under field emission scanning electron microscope, FESEM (QUANTA FEG-200) using secondary electrons with accelerating voltage of 20kV. Before the morphological study, the powder samples were mounted onto the aluminium stubs using adhesive carbon tape. The powders were then gold coated using a gold discharge sputter. Different powder regions were observed and the average morphology was recorded. The elemental analyses of the powder were carried out by Energy dispersive X-ray spectroscopy,

EDAX (PENTA FET-200 Precision) as EDAX relies on the X-ray generated through interactions with the specimen.

4.3.2 Transmission Electron Microscopy (TEM)

The particle sizes of Al_2O_3, ZrO_2 and TiO_2 powders prepared by chemical and mechanical route along with its morphology was confirmed through transmission electron microscope, TEM (Tecnai G2-20 S-TWIN) operated at 200kV. All powders were first sonicated for 15min in isopropanol medium to remove agglomeration followed by drying. Dried powders were then put on the carbon coated TEM grids which were mounted on the specimen holder and were placed inside the electron beam chamber. The morphology was seen at different regions along with the selected area diffraction (SAD) patterns. SAD patterns were indexed to confirm the phases of the powders. Each ring radius (R) in SAD pattern is the characteristic of the interplanar spacing (d) of the reflecting planes in the crystal. The 'd' values were calculated using the relation $Rd= \lambda L$ where λL is the camera constant, 'λ' is the electron beam wavelength and 'L' is the distance between the specimen and the screen.

4.3.3 X-Ray Diffraction (XRD)

The phase analysis of Al_2O_3, ZrO_2 and TiO_2 powders prepared separately by chemical and mechanical route were carried out by X-ray diffraction (XRD) (D8 Bruker AXS Advance diffractometer) with copper (Cu) target, operating at an accelerating voltage of 40kV and 30 mA current. The diffracted beam intensity against 2θ was recorded on a graphical chart for all the powders for angle 2θ range from 20^o to 90^o at a goniometer speed of 1^o/min. All d (interplanar spacing) values were calculated from their corresponding 2θ peaks using Bragg's law of diffraction ($n\lambda = 2d \sin\theta$). The peaks of different phases present in the powders at the calculated 'd' values were identified with the help of JCPDS ASTM data cards (Using Panalytical X'Pert Highscore software using PAN-ICSD). The crystallite size (G) of the powders was calculated by the Scherrer's formula, ($G=0.9\lambda/\beta\cos\theta$). Here '$\lambda$' is the X-ray wavelength ($\lambda= 1.54A^o$, for Cu Kα), 'n' is order of diffraction (n=1), 'θ' is the Bragg's angle at the peak observed corresponding to a set of hkl planes. 'β' is the line broadening in radians given as $\beta = (\beta^2_M - \beta^2_I)^{1/2}$, where '$\beta_M$' is the full width at half maxima (FWHM), 'β_I' is the instrumental broadening correction factor.

4.3.4 Thermal Analysis

The thermal behaviour of chemically prepared Al_2O_3, ZrO_2 and TiO_2 powders were evaluated using thermal gravimetric and differential thermal analysers, TG/DTA (Perkin Elmer Pyris

Diamond). The powders were continuously heated at a rate of 10°C/min upto 1000°C each for ZrO_2 and TiO_2 powders and upto 1500°C for Al_2O_3 powder in a static air atmosphere. All three DTA, DTG and TG were carried out simultaneously under same experimental conditions on same sample. The DTA signal was recorded from the heat difference between the sample and inert reference material. This difference provides the information about the exothermic or endothermic reactions occurs within the sample. The microprocessor based DTA lineariser is included as a standard part of the equipment. 10mg powder was normally used for the thermal studies. The steps involved in the transformation of crystalline Al_2O_3, ZrO_2 and TiO_2 powders from its amorphous form were identified using DTA and the calcination temperatures for the formation of required phase was decided accordingly.

4.4 SUBSTRATE PREPARATION

Mild steel (MS) was used as the substrate material for electroless coatings employed for wear and corrosion applications. The composition analysis of the MS was carried out using spectrographic analysis. An optical emission spectrometer, T5A 181181 model suppliec Ash Corporation, USA was used. MS discs (42mm diameter x 3mm thickness) and MS plates (2.5mm x 2.5mm x 2mm) were used for wear and corrosion studies respectively. All substrates were first polished by emery paper(s) upto 1000 grit following the standard method before its surface preparation and pretreatment.

4.4.1 Degreasing and Etching of Substrate

Since EL is a chemical reduction process, the surface preparation of the substrate is essential. This can be achieved by using specific processes as per the literature. The steps involved for the surface preparation of MS substrates, are given below:

i. Degreasing with acetone for about 3min
ii. Rinse with distilled water
iii. Etching in dilute nitric or hydrochloric acid for 30sec
iv. Rinse with distilled water
v. Drying

4.4.2 Pretreatment of Substrate

To initiate the chemical reaction for coating to take place, pretreatment of the substrate is one of the crucial step after surface preparation. The steps followed for the pretreatment of the substrate are given below:

i. Sensitize the substrate by dipping into solution containing dilute hydrochloric acid and stannous chloride (0.5ml HCl + 0.1% $SnCl_2$) for about 1min.

ii. Activate the substrate by dipping in 0.01 % palladium chloride, $PdCl_2$, solution for 30sec.

iii. Dry the substrate

The pretreated substrate was then immersed in EL bath.

4.5 EL BATH

EL coatings are produced by the controlled chemical reduction of metallic ions onto a catalytic surface. For EL depositions, mainly two types of baths are used i.e. acidic and alkaline. In the present work, an alkaline EL bath was used. The schematic diagram of electroless set up used in the present study is shown in figure 4.1. EL bath components along with their composition are used in the present work is listed in table 4.1. The EL bath prepared (500ml glass beaker) was placed inside the copper beaker. The electrolyte was heated using constant temperature by an electrically heated silicon oil bath. The temperature and pH of the bath was controlled and maintained by using temperature controller and pH meter at accuracy of 90 ± 2°C and 9.0 ± 0.25 respectively to obtain coatings of similar composition. Operating conditions of EL bath used in work for sound EL coatings is given in table 4.2.

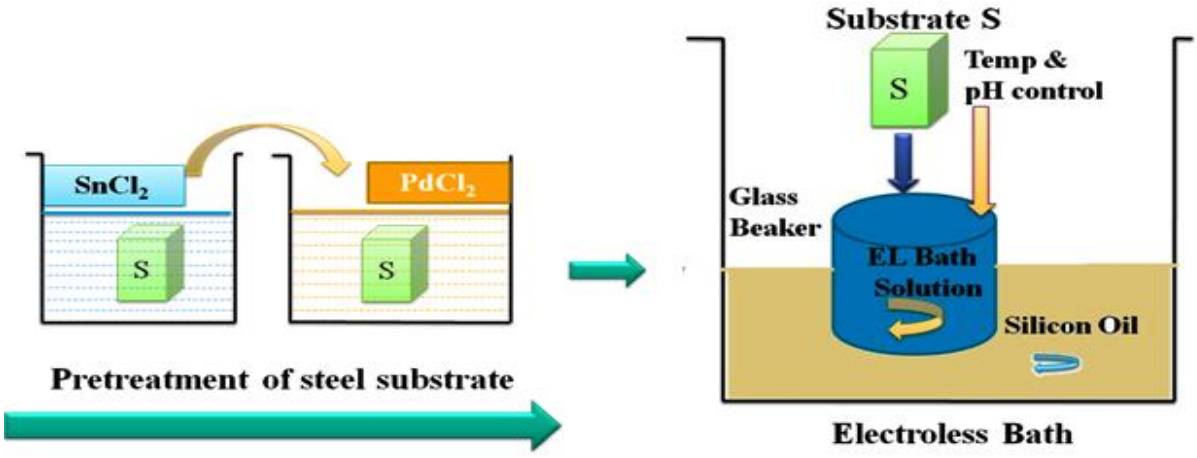

Fig4.1- Experimental set up For EL Coatings.

Table 4.1: Bath Components for EL Ni-P Based Coatings

EL BATH COMPONENTS	SALTS USED	AMOUNT(g/l)
Metal ion	Nickel sulphate, $NiSO_4.6H_2O$	30
Reducing agent	Sodium hypophosphite, $NaH_2PO_2.H_2O$	20
Complexing agent	Tri-sodium citrate, $Na_3C_6H_5O_7.2H_2O$	100
Stabilizer(s)	Ammonium sulphate, $(NH_4)_2SO_4$ Ammonium chloride, NH_4Cl	50 50
pH control Reagent	Ammonia solution, NH_4OH	(Few drops to make pH 9.0)
Second Phase powder for Ni-P-X Coatings (Conventional)	Alumina, Al_2O_3 Zirconia, ZrO_2 Titania, TiO_2	4
Co-precipitation elements for *Insitu* Ni-P-X Coatings (Non-Conventional)	Aluminium chloride, $AlCl_3$ Zirconium oxychloride, $ZrOCl_2$ Titanium trichloride, $TiCl_3$	19.2 5 50ml
Activated Substrate	Mild Steel, Fe	-

Table 4.2: Operating Conditions for EL Ni-P based coatings

OPERATING CONDITIONS	DESCRIPTION
Temperature	90^oC
pH	9.0
Plating Time	30 min
Bath Loading Factor	6000 mm^2/l

4.5.1 Ni-P Alloy Coating

The Ni-P alloy coating was developed on MS substrate. It involves an autocatalytic reduction of nickel ions onto the substrate with alternate layer of phosphorus without the use of electrical energy. The nature of reactions occurring during the EL Ni-P coating process has been discussed in section 2.3.2.2 via equations 2.1-2.4. EL Ni-P bath constituted of an aqueous solution of metal ions, reducing agent, complexing agent, bath stabilizer and an activated target substrate. The EL Ni-P alloy coatings were carried out by immersing pretreated substrate into the prepared bath as shown in figure 4.1. The bath temperature and pH were well adjusted at

90±2°C and 9.0 respectively before substrate immersion into the bath. The pH of the bath was continuously monitored and maintained at 9.0 by addition of sufficient quantity of ammonia solution during coating process. After the plating, the samples were taken out, rinsed with deionized water and were air dried at 45^{o}C for 15min and preserved for further characterizations in a desiccator.

4.5.2 Ni-P-X Composite Coating

Electroless Ni-P-X composite plating is a kind of surface treatment technology where the incorporation of hard particles 'X' improves the mechanical and tribological properties of EL Ni-P alloy coatings. According to past studies, EL composite coatings can be performed by two ways, depending upon the compatibility of reactions and the process parameters of EL bath namely conventional and non-conventional composite coatings. In the present investigation, both conventional and non-conventional, the fine precipitates of Al_2O_3, ZrO_2 and TiO_2 were physically entrapped in a growing Ni-P layer on the substrate surface and thus codeposited to form Ni-P-X nanocomposite coatings.

4.5.2.1 Conventional Composite Coating

The conventional Ni-P-X [X=Al_2O_3, ZrO_2 and TiO_2] nanocomposite electroless coatings was developed on mild steel substrate. In conventional route, the second phase(s) particles present in the composite coatings were added to the bath during the coating. Al_2O_3, ZrO_2 and TiO_2 nanoparticles prepared separately by chemical route and mechanical route were suspended (4g/l) into the prepared EL plating solution. The stirring was used for uniform suspension of particles in the solution, which were available for codeposition. The pH and temperature of the bath was continuously monitored during the coating process.

4.5.2.2 Non-Conventional Composite Coating

The *insitu* EL Ni-P-X [X= Al_2O_3, ZrO_2 and TiO_2] nanocomposite coatings were developed on mild steel substrate. In non-conventional (*insitu*) route, the second phase(s) particles were generated to nucleate and grow within EL bath (precipitation of nanosized particles). The *insitu* precipitation of Al_2O_3, ZrO_2 and TiO_2 has been carried out along with the Ni-P coating process. $AlCl_3$, $ZrOCl_2$ and $TiCl_3$ were dissolved separately in distilled water and dispersed in continuously stirred coating bath. The pH of the bath was maintatined by addition of NH_4OH solution as bath pH reduced on reaction with the added precursors.

4.5.3 Heat Treatment of EL Coatings

Heat treatment (HT) was conducted in a tubular furnace with an accuracy of ±2°C with control environment. All the coated steel samples were heat treated at 400°C in purified argon atmosphere for 1h. Argon gas with 99.993 % purity and 1.5 kg/cm^2 pressure was used for heat treatments of coated samples. After the heat treatment, the specimens were furnace cooled.

4.6 CHARACTERIZATION OF EL COATINGS BEFORE AND AFTER HT

The Ni-P alloy and Ni-P-X [X=Al_2O_3, ZrO_2 and TiO_2] nanocomposite coatings developed by conventional and non-conventional mode in 'as coated' and 'heat treated' conditions were characterized using different characterization techniques. The detalis are briefly discussed in the following sub-sections.

4.6.1 FESEM

The surface morphology of all EL coatings in 'as coated' and HT conditions were carried out by, FESEM and scanning electron microscope, SEM (Zeiss EVO-18). The compositional analysis of the coatings was studied by Energy dispersive X-ray spectroscopy, EDAX. The details are given in section 4.3.1.

4.6.2 XRD

The phases of EL Ni-P and Ni-P-X nanocomposite coatings were determined in 'as coated' and HT conditions using X-ray diffraction (XRD) with Cu Kα target. The details are given in section 4.3.3.

4.6.3 AFM

The surface topography of all the coated samples were examined by tapping mode imaging using atomic force microscopy (AFM, NT-MDT NTEGRA). AFM provides a surface three dimensional profile on a nanoscale. The forces between a sharp probe (<10nm) and surface area at shorter distances (0.2-5nm) were measured. The probe was supported on a flexible cantilever. The AFM probe gently touched the surface and the small force between the probe and the surface was recorded. A semiconductor diode laser was bounced off the back of the cantilever into a position sensitive photodiode detector. The bending of cantilever as the probe is scanned over the sample was measured by photodetector. The measured cantilever deflections were used to generate surface topography map of the sample.

4.6.4 Microhardness

Microhardness (VHN) of Ni-P and Ni-P-X nanocomposite coatings in 'as coated' and HT conditions were determined using microharness tester (402 MVD, Wilson Instruments) with dwelling time of 15sec under a 10gf load. An average of five measurements was determined along with standard deviation.

4.6.5 Wear and Friction Studies

To examine the friction coefficient and wear resistance of the coatings, ball-on-disc sliding contact method was employed using wear and friction testing machine (Ducom TR-201E-M2). The mild steel discs (42mm diameter x 3mm thickness) were used against hardened chromium 65 HRC steel ball (d = 6.0mm). Heat treated sample disc were used before wear test. Wear tests were performed at a linear sliding velocity of 0.1 and 0.2m/s under 1, 1.5 and 2N normal loads and 600m sliding distance in unlubricated, dry ambient environment with room temperature approx. 305K and humidity 40±5 %. 'Wear volume' of the coatings were evaluated by means of surface profilometer (Mitutoyo (SJ-401)) with maximum scan length 2.5mm. Using the 'wear volume', the specific wear rates of coatings, 'K' was calculated using $K=V/L.s$ ($m^3.N^{-1}m^{-1}$), where, 'V' is the wear volume (m^3) of coating, 'L' is the normal load (N), and 's' is the total sliding distance (m).

4.6.5.1 Wear Track Studies

The surface of wear tracks of Ni-P and Ni-P-X nanocomposite coatings in as coated and HT conditions were studied using field emission scanning electron microscope, FESEM.

4.6.6 Corrosion Studies

Corrosion behaviour of Ni-P alloy and Ni-P-X nanocomposite coatings in 'as coated' and heat treated conditions were examined using electrochemical polarization method. The details were discussed in the following sub-section.

4.6.6.1 Electrochemical Corrosion

The schematic arrangement of the electrochemical system includes a Gamry Interface 1000 potentiostat, a Pyrex® glass cell which consisted of counter electrode (platinum wire mesh), reference electrode (saturated Ag/AgCl electrode), steel samples as working electrode and electrolyte. The electrolyte used in the present investigation is acidic (pH-4.5) and alkaline (pH-8.0) solutions. In the set-up, the Luggin probe was kept as close as possible to the working electrode to minimize the effect of solution resistance. The coated samples were rinsed with

acetone, and were allowed to stabilize for 5400s to monitor OCP before polarization. The exposed area for testing was 1cm² x 1cm^2. Potentiodynamic Tafel testing was performed at room temperature (33^{o}C) from range of -250mV to +250mV about OCP at a scan rate of 1mV/s and the results were analyzed via Tafel extrapolation theory. Tafel plots were obtained from the data and the corrosion current density (I_{corr}) was determined by extrapolating the straight line section of the anodic and cathodic Tafel lines. Rate of corrosion of the coatings, 'CR' was calculated using CR (mpy) = 0.1288 I_{corr}.EW/ρ, where, 'EW' is Eq.wt of specimen and 'ρ' is its density (g/cm^3). The surface of all coated samples was analysed using field emission scanning electron microscope, FESEM.

4.7 SUMMARY

The present chapter discusses the details of synthesis of Al_2O_3, ZrO_2 and TiO_2 nanoparticles using different methods like chemical precipitation and ball milling. These nanoparticles were used as second phase for development of EL conventional Ni-P-X [X= Al_2O_3, ZrO_2 and TiO_2] nanocomposite coatings on mild steel substrate using electroless technique. EL *insitu* Ni-P-X [X= Al_2O_3, ZrO_2 and TiO_2] nanocomposite coatings were also developed. The characterisation details such as XRD, TG/DTA, SEM, TEM, EDAX, AFM, Microhardness, Wear and Corrosion used for the powders and coatings before and after heat treatment have been discussed.

RESULTS AND DISCUSSIONS

CHAPTER 5

SYNTHESIS AND CHARACTERIZATION OF NANOPARTICLES

5.1 INTRODUCTION

The present chapter deals with the synthesis and characterization of metal oxide nanoparticles such as Al_2O_3, ZrO_2 and TiO_2 employing Top down and Bottom up approaches. Section 5.2 includes the synthesis of Al_2O_3, ZrO_2 and TiO_2 nanoparticles separately using chemical precipitation method (Bottom up). Chemical route provides the precise size control and purity as particles are generated atom by atom and grow in size. The thermal studies and phase analysis of dried powders are carried out. The morphology, particle size and phase structures of calcined Al_2O_3, ZrO_2 and TiO_2 nanoparticles are discussed. Section 5.3 focuses about the preparation of Al_2O_3, ZrO_2 and TiO_2 nanoparticles separately by mechanical milling (Top down). Mechanical milling route is employed for economical mass production of nanoparticles as particles of micron size are reduced to nano size particles. The morphology, particle sizes and phase analysis of Al_2O_3, ZrO_2 and TiO_2 nanoparticles for different milling duration are analysed. Al_2O_3, ZrO_2 and TiO_2 nanoparticles produced by above methods are applied as the reinforcement for the development of surface protective nanocomposite coatings. In this chapter, the results based on chemical precipitation and mechanical milling processes are discussed in detail.

5.2 SYNTHESIS AND CHARACTERIZATION OF NANOPARTICLES BY BOTTOM UP APPROACH- (CHEMICAL PRECIPITATION ROUTE)

The Al_2O_3, ZrO_2 and TiO_2 nanoparticles are synthesized separately by chemical route employing precipitation technique using ammonia as the precipitating medium in all cases.

5.2.1 Alumina (Al_2O_3) nanoparticles

5.2.1.1 Thermal Analysis

Figure 5.1 shows the thermal analysis curves of the precursor $AlCl_3$ and dried Al_2O_3 powder from room temperature to 1500^{o}C. The Differential thermal analysis (DTA) curve [Fig 5.1a] of the precursor $AlCl_3$ has endothermic peak at 168^{o}C with energy loss of 6.27uV while the thermal gravitometry analysis (TGA) curve shows the weight loss of around 45% between temperatures 100^{o}C to 200^{o}C. It denotes the evaporation of maximum amount of chlorine from $AlCl_3$ at a rate of energy gain 78.3mJ/mg. The DTA curve of dried Al_2O_3 powder has endothermic peak at 297^{o}C with 64.8uV of energy loss. The TGA curve shows the weight loss

of ~60% in temperature range from 200 to 315°C which is due to the release of retained chlorine at a rate of 2.04J/mg of energy gain [Fig 5.1b]. The researchers have found that $Al(OH)_3$ transforms to mixed alumina phases above 400°C and calcinating at 1200°C for 2h results in the phase transformation to pure alpha (α) phase of alumina. Similar results have been observed by Hong et al. (1998) for α-Al_2O_3 powder.

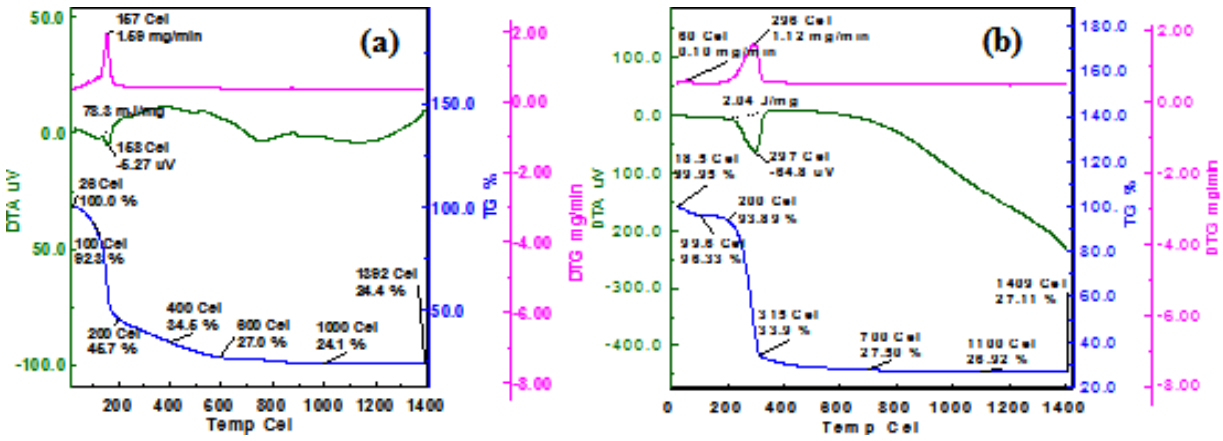

Fig 5.1- Thermal analysis of (a) Precursor $AlCl_3$ and (b) Dried Al_2O_3 powder from room temperature to 1500°C.

5.2.1.2 Morphological Study

The micrographs of calcined Al_2O_3 powders (1200°C, 2h) under FESEM and TEM are shown in figures 5.2a and 5.2b. In figure 5.2a, the agglomerates of Al_2O_3 particles are observed under FESEM. Aggregation of particles is apparent, indicating the continuous particulate network formation in the suspension structure. Spherical shaped Al_2O_3 particles are observed. The particle size distribution ranges from 9 to 15nm with an average particle size of 12nm is confirmed by figure 5.2b, TEM micrograph. SAD pattern supports the presence of Al_2O_3 particles [Fig 5.2b].

Figure 5.3 shows the compositional analysis of calcined Al_2O_3 powder via Energy Dispersive X-ray analysis, EDAX. The EDAX analysis reveals the elemental content of Al and O are in the ratio of 2:3 atomic% confirming the presence of Al_2O_3 particles.

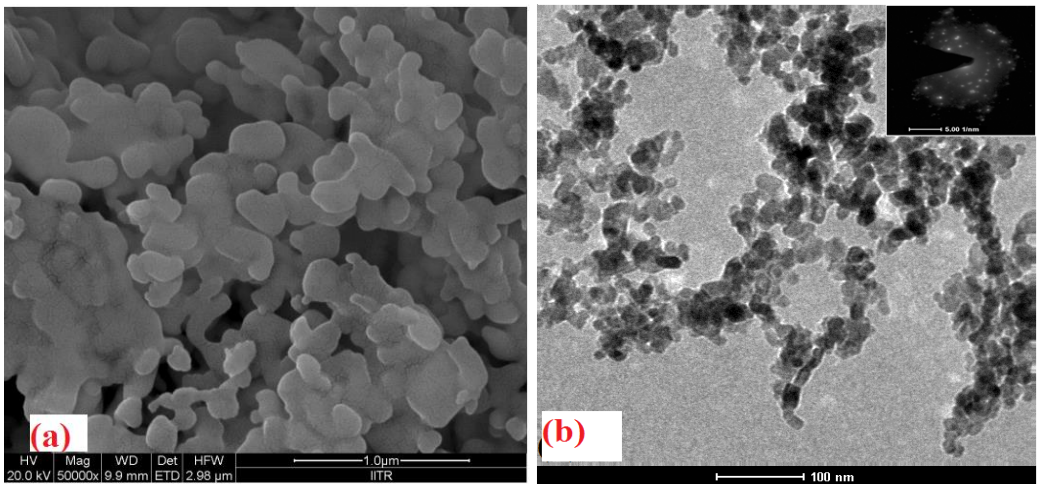

Fig 5.2- Microstructures of Al_2O_3 powder under, (a) FESEM and (b) TEM (*inset* SAD pattern).

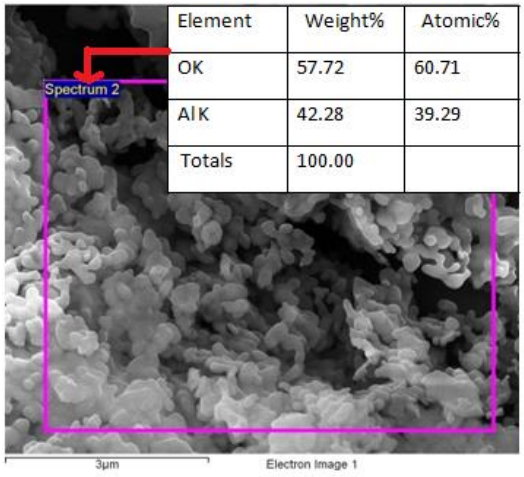

Fig 5.3- EDAX analysis along with surface morphology of calcined Al_2O_3 powder.

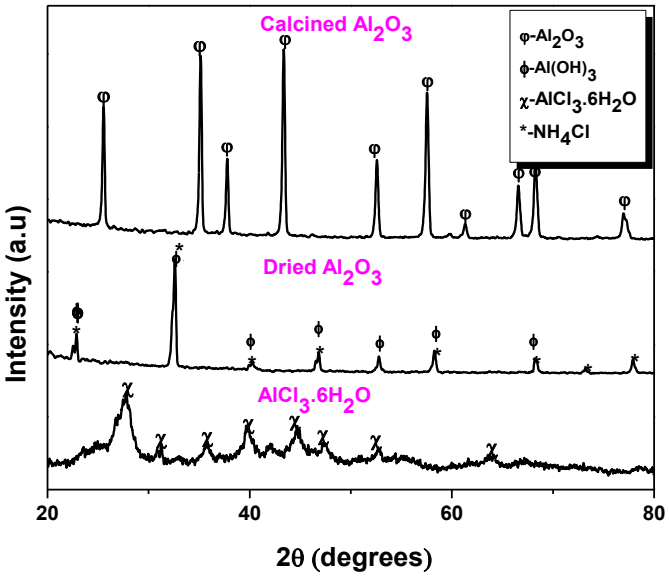

Fig 5.4- XRD patterns of $AlCl_3$, dried Al_2O_3 and calcined Al_2O_3 powder at 1200°C for 2h.

5.2.1.3 XRD Analysis

The XRD pattern of dried Al_2O_3 powder [Fig 5.4] shows mixed peaks of retained ammonium chloride (JCPDS ref no.: 01-073-0365) and precipitates of aluminium hydroxide (JCPDS ref no.: 01-074-1775). Calcination at 1200^{o}C for 2h results in pure alpha (α) phase of alumina (JCPDS ref no.: 01-083-2080) having rhombohedral crystal structure [Fig 5.4]. The calcined Al_2O_3 powder has mean crystalline size around 14nm as determined by Scherrer's formula. Alumina precipitates from aluminium chloride according to the following reactions [Hong et al. (1998)]:

$$2\ AlCl_3 + 6\ NH_4OH = 2\ Al(OH)_3 + 6\ NH_4Cl \quad (5.1)$$

On Dehydration

$$2\ Al(OH)_3 = Al_2O_3 + 3\ H_2O \quad (5.2)$$

5.2.2 Zirconia (ZrO_2) nanoparticles

5.2.2.1 Thermal Analysis

The Differential thermal analysis (DTA) curve [Fig 5.5a] of the precursor $ZrOCl_2$ have endothermic peaks at 100^{o}C and 145^{o}C with energy loss of 26.0µw and 28.5µw respectively while the TGA curve shows the weight loss of 20% between temperatures 50^{o}C to 150^{o}C which infers the evaporation of maximum amount of chlorine from $ZrOCl_2$ and energy gain of 675 mJ/mg. The DTA curve [Fig 5.5b] of dried ZrO_2 powder shows the exothermic peak at 234^{o}C and 434^{o}C with 48.7mJ/mg and 71.4mJ/mg of energy loss respectively. The TG traces of dried ZrO_2 shows the weight loss of ~25% in 31-200^{o}C temperature range [Fig 5.5b], it may be due to the evaporation of retained chlorine and can also be seen from the $ZrOCl_2$ behavior [Fig 5.5a]. $Zr(OH)_4$ transforms to tetragonal zirconia at 234^{o}C and calcination at 434^{o}C results in the transformation of tetragonal phase to monoclinic phase of zirconia. The similar results have been observed by Tyagi et al. (2006).

5.2.2.2 Morphological Study

FESEM and TEM micrograph reveals the morphology and the size ranges of ZrO_2 powders calcined at 400^{o}C for 4h [Fig 5.6]. The particles have an aspect ratio of ~1 and are agglomerated as seen in FESEM micrograph [Fig 5.6a]. TEM results confirm the spherical shape and the crystallite sizes ranging from 5 to 10nm with an average size of 7nm [Fig 5.6b]. SAD pattern shows the crystalline ZrO_2 particles.

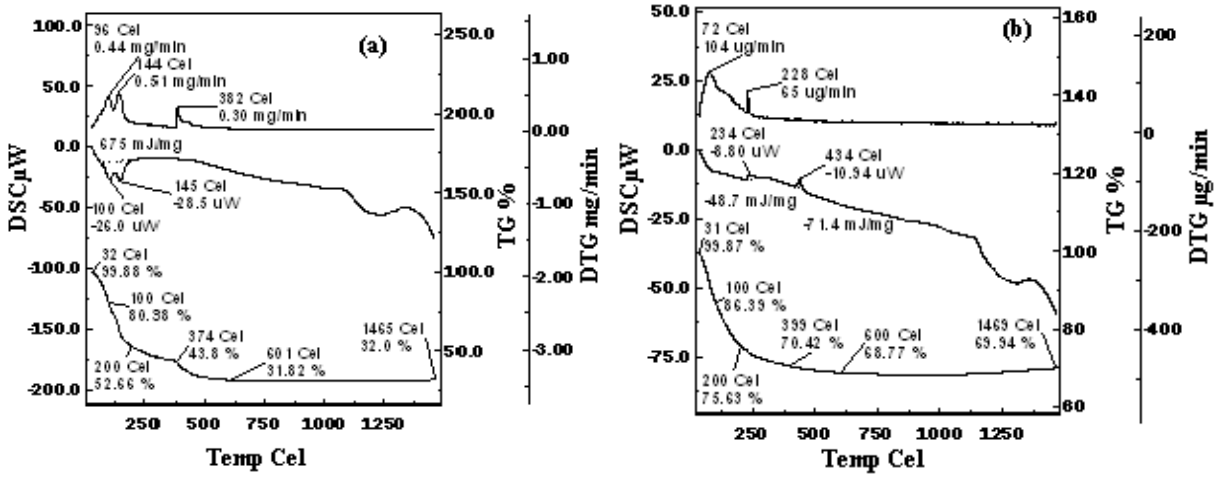

Fig 5.5- DTA/TG traces from room temperature to 1000°C of (a) Precursor $ZrOCl_2$ and (b) Dried ZrO_2 powder**.**

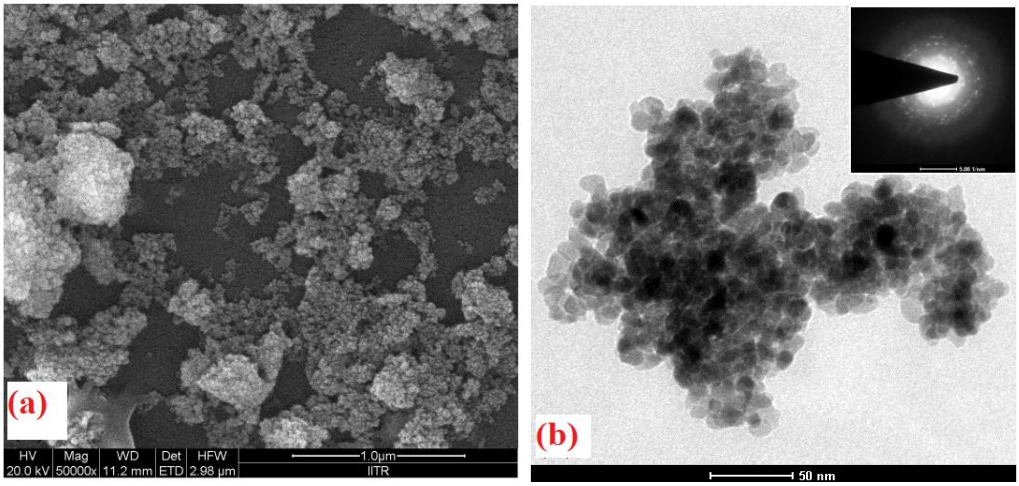

Fig 5.6- Micrographs of calcinated ZrO_2 powder (a) FESEM and (b) TEM (*inset* SAD pattern).

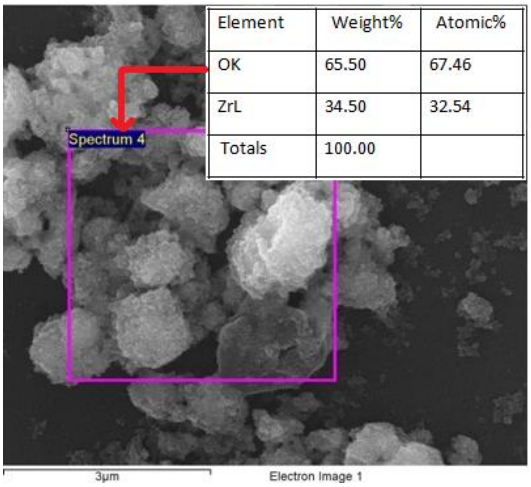

Fig 5.7- EDAX analysis and surface morphology of calcined ZrO_2 powder.

The quantitative analysis of the calcined ZrO_2 powder as determined by EDAX analysis is shown in figure 5.7. The elemental content of Zr and O in atomic% is in the ratio of 1:2 indicating the formation of ZrO_2 particles.

5.2.2.3 XRD Analysis

The X-ray diffraction pattern of precursor $ZrOCl_2.8H_2O$ confirms with JCPDS ref no.: 00-21-1499 [Fig 5.8]. Dried ZrO_2 powder shows broad peak of amorphous nature of precipitates of zirconia (JCPDS ref no.: 00-024-1164). XRD of hydrogel calcinated at 400^oC for 4h show monoclinic phase of zirconia (JCPDS ref no.: 01-078-0047) [Fig 5.8]. The crystalline size of the calcinated powder calculated by Scherrer's formula is found to be 8nm. Zirconia precipitates from zirconium oxychloride form according to the following reactions [Hong et al. (1998)]:

$$ZrOCl_2 + 2\ NH_4OH = ZrO(OH)_2 + 2\ NH_4Cl \quad (5.3)$$

On Dehydration

$$ZrO(OH)_2 = ZrO_2 + H_2O \quad (5.4)$$

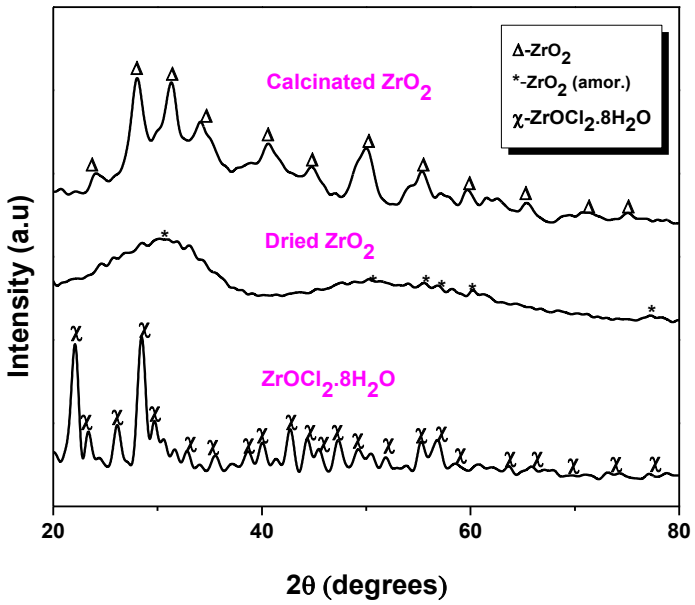

Fig 5.8- XRD patterns of precursor $ZrOCl_2$, dried ZrO_2 and calcined ZrO_2 powder at 400^oC for 4h.

5.2.3 Titania (TiO_2) nanoparticles

5.2.3.1 Thermal Analysis

The Differential thermal analysis (DTA) curve [Fig 5.9] of dried TiO_2 powder has the endothermic peak at 303^oC with energy loss of 2.15 J/mg of energy. The TG trace of dried

TiO_2 powder shows the weight loss of near about 69% between temperatures 200°C to 220°C, which indicates the evaporation of retained chlorine. Also exothermic peak is observed at 470°C which can be inferred as the anatase crystallite transformation. Thus, calcination of TiO_2 powder at 500°C for 1h results in the transformation to anatase phase of titania.

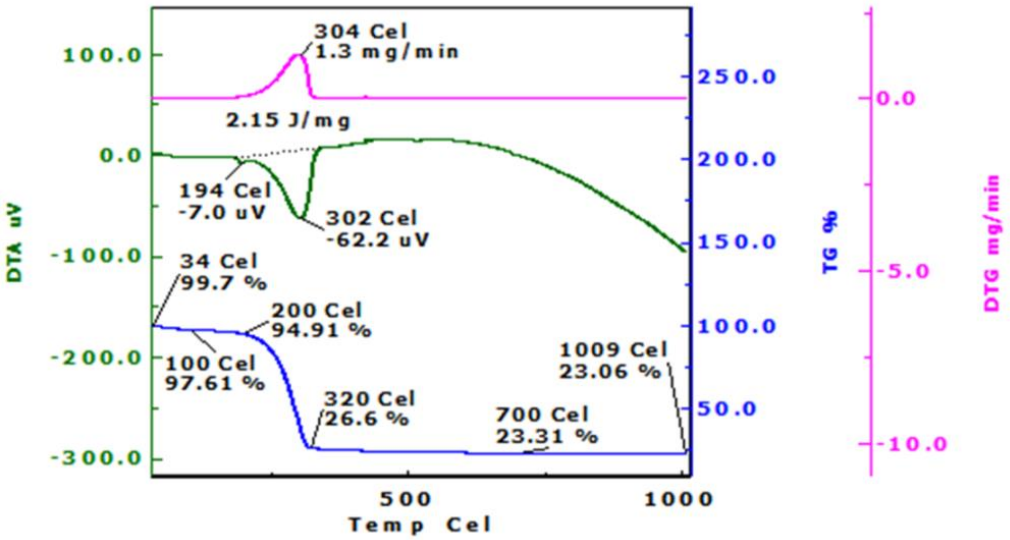

Fig 5.9- DTA/TG traces of dried TiO_2 powder from room temperature to 1000°C.

5.2.3.2 Morphological Study

FESEM and TEM micrographs of TiO_2 powders calcinated at 500°C for 1h are shown in figure 5.10. FESEM micrographs of the calcined titania powder show an agglomerated surface [Fig 5.10a]. TiO_2 particles have a spherical morphology as seen in TEM micrograph [Fig 5.10b]. The distribution of particle size varies from 9-12nm with an average particle size of 10nm. The crystalline TiO_2 formation is confirmed by SAD pattern (inset) [Fig 5.10b].

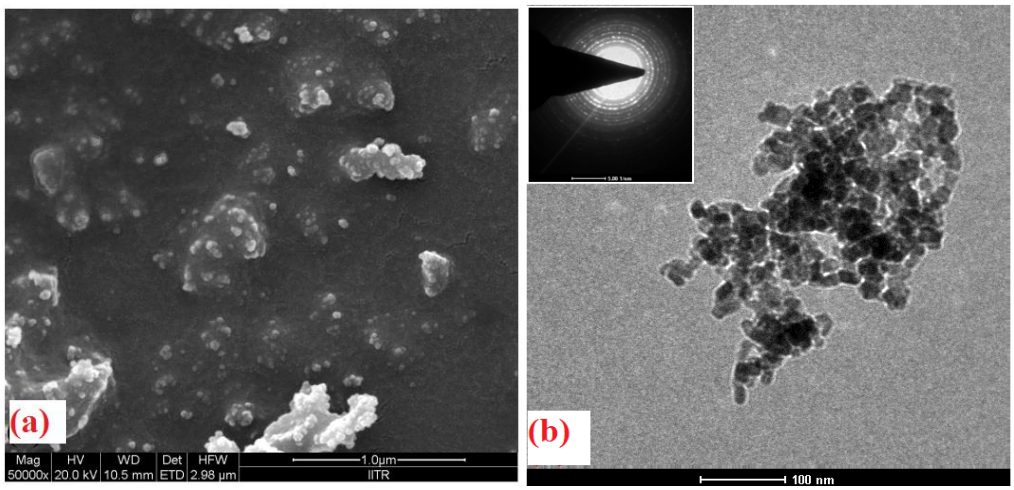

Fig 5.10- TiO_2 powder examined under (a) FESEM and (b) TEM with SAD pattern *(inset)*.

The elemental analysis of calcined TiO_2 powder is shown in figure 5.11. The elements Ti and O are observed in the (EDAX) spectrum. The atomic % of Ti & O is in the ratio of 1:2 supports the presence of TiO_2 particles.

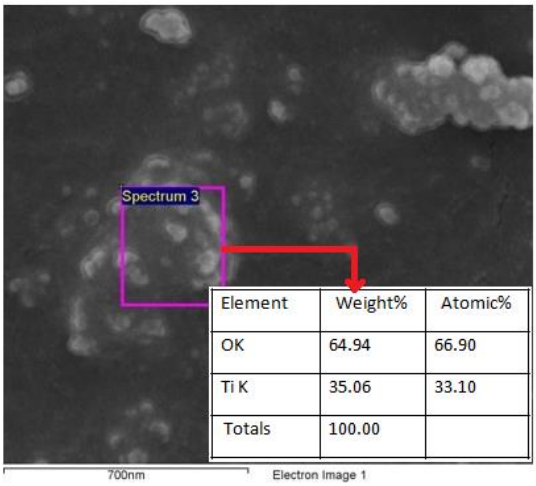

Fig 5.11- EDAX analysis along with surface morphology of calcined TiO_2 powder.

5.2.3.3 XRD Analysis

The X-ray diffraction pattern of dried TiO_2 powder shows ammine titanium chloride phase with JCPDS ref no.: 01-074-0508 [Fig. 5.12]. After mechanical milling of dried TiO_2 powder for a period of 4h, little amount of anatase phase of TiO_2 is observed due to the heat generated by milling. XRD pattern of TiO_2 powder calcinated at 500°C for 1h [Fig. 5.12] shows pure anatase phase of TiO_2 (JCPDS ref no.: 01-071-1166). The crystalline size of the calcinated powder calculated by Scherrer's formula is around 12nm.

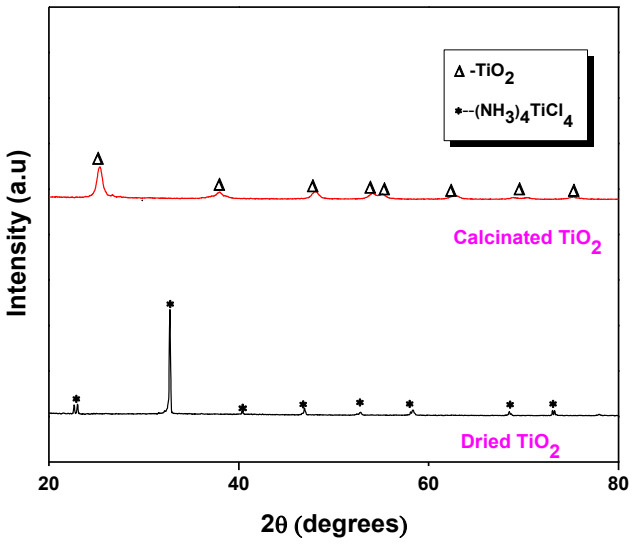

Fig. 5.12- XRD patterns of dried TiO_2 and calcined TiO_2 at 500°C, 1h.

5.3 SYNTHESIS AND CHARACTERIZATION OF NANOPARTICLES BY TOP DOWN APPROACH- (MECHANICAL MILLING ROUTE)

Ball Milling/Mechanical Milling process is the route where powder mixtures are subjected to high energy collision of balls. This method has been successfully used as a process by virtue of which a homogeneous mixture of powder with finer sizes is prepared. This process has advantages over chemical synthesis of nanopowders as it avoids the route where temperature as an external energy is mandatory. The nanosized Al_2O_3, ZrO_2 and TiO_2 powders are prepared separately by mechanical milling using high energy planetary ball mill. The ball mill parameters employed for milling in all the powders are listed in table 5.1.

Table 5.1: Milling and mixing parameters

Planetary High Energy Ball mill Details (Retsch PM 400/2)		
(1)	Balls	Hardened steel balls
(2)	Jars	Hardened steel jars
(3)	Jar capacity	500 ml
(4)	Milling Media	Toluene
(5)	Ball to charge ratio	10:1
(6)	Milling speed	250 rpm
(7)	Vial Speed	500 rpm
(8)	Total time of milling	5h,10h,20h,30h & 40h
(9)	Weight of initial charge	30gm

5.3.1 Alumina (Al_2O_3) nanoparticles

5.3.1.1 Morphological Study

The morphological characteristics of Al_2O_3 powder in 'as received' form and milled for various time extents is shown by FESEM micrographs [Fig 5.13a-e]. The Al_2O_3 powder was milled for 5h, 10h, 20h, 30h and 40h. The spherical morphology is observed in 'as recieved' powder and the starting particle size is almost 42µm [Fig 5.13a]. The milled powder exhibits irregular shaped morphology and seem to be agglomerated and flattened with fractured surfaces [Fig 5.13b-e]. It is due to plastic deformation by collisions between ball-particle-ball and ball-jar (wall)-ball. The approximate particle sizes of the milled powders are analysed by its volumetric analysis studies using FESEM micrographs. The average particle sizes attained after 5h, 10h and 20h of milling is around 5µm, 700nm and 220nm respectively. The work

hardened Al_2O_3 powder when milled further upto 40h, the particle size get lowered to the range of 13-18nm [Figs 5.13e-f]. The average particle size achieved after 40h of milling, Al_2O_3 $(M)_{40}$ is 15nm as observed by its TEM micrograph shown in figure 5.13f. The SAD pattern is displayed in the inset of TEM micrograph. The amorphous nature of Al_2O_3 $(M)_{40}$ powder contributes to the the diffused ring observed in SAD pattern. The variation in particle size with respect to the extent of milling is discussed in figure 5.14a. The lowering of particle size is observed with increase in milling time. This can be described on the basis of two comparative processes that involves during milling i.e. fracture and cold welding. The time of milling influence the charge (powder) by two means i.e. first, breaking of powder (fracture) followed by the agglomeration of the particles due to cold welding. Fracture contributes to the work hardening due to continuous plastic deformation and increase in Gibbs free energy of the system which facilitates fracture in order to attain its lowest stable energy. Cold welding, on the other hand, is attributed by the diffusion bonding that occurs due to the pressure developed by the impact of balls. The nascent surface formation after fracture raises the chance of cold welding, as it is short range order phenomenon where the system temperature is sufficiently high enough to facilitate welding of fine particles. Moreover, the higher free energy of the nascent surfaces frequently forms the cold welding which in turn results in the agglomeration of the powders. When the powders are subjected to higher duration of milling, the fracture overrules the cold welding phenomenon. Thus, the amount of fracturing of the surfaces increases in comparison to the simultaneous agglomeration process. Hence, the particle size is lowered with increase in milling time. However, at certain extent of milling, both the phenomena achieve an equilibrium, which inhibits further reduction of particle sizes [Mishra et al. (2013)].

The quantative compositional studies of Al_2O_3 powder milled for 40h, Al_2O_3 $(M)_{40}$, are carried out using EDAX analysis and shown in figure 5.14b along with its surface morphology. The EDAX studies reveal that the elements Al & O are present in the selected region. The atomic ratio of Al & O is almost 2:3 which confirms the presence of Al_2O_3 particles.

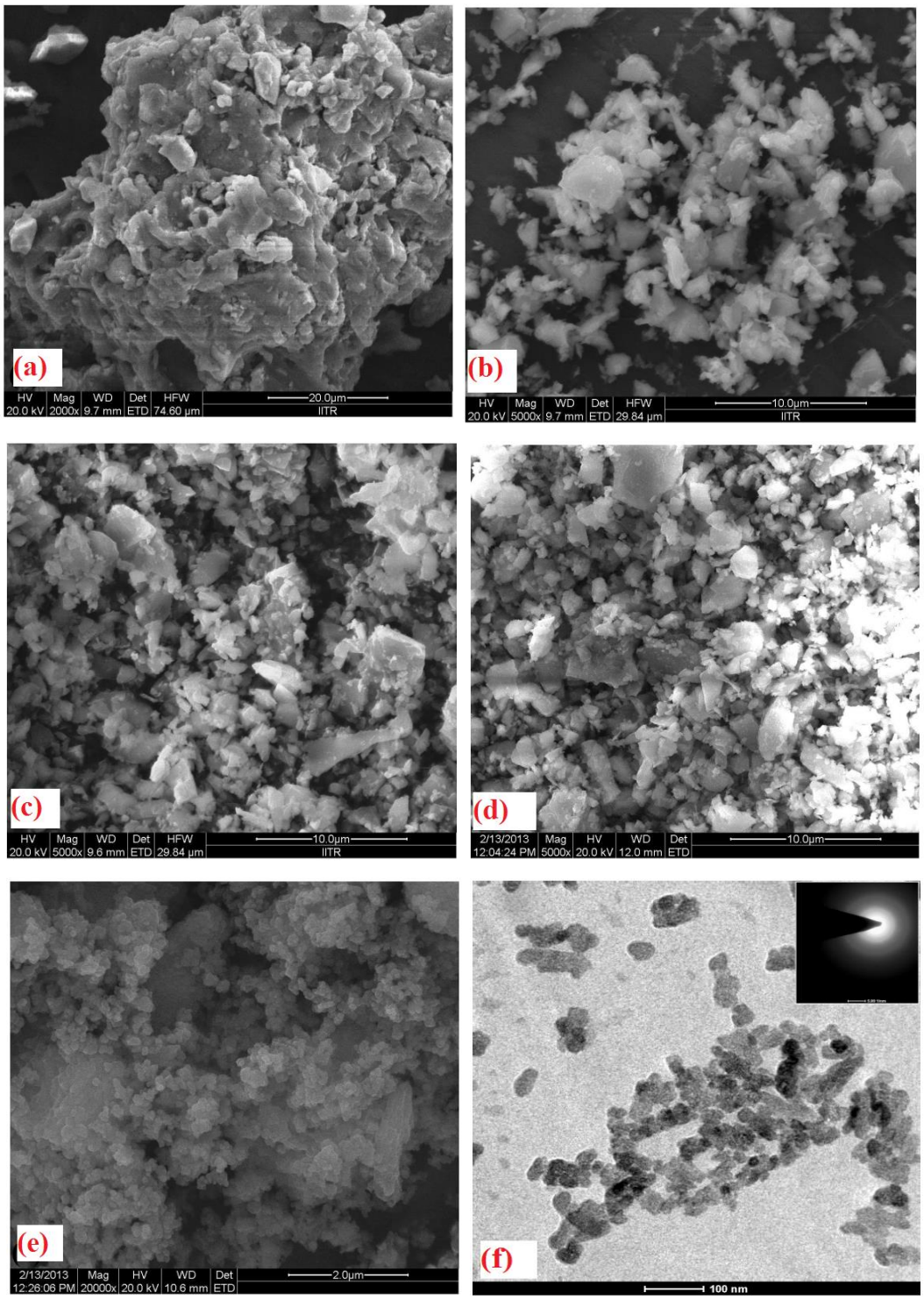

Fig 5.13- FESEM micrographs of Al_2O_3 powder (a) As received, milled for different extents of time (b) 5 h, (c) 10 h, (d) 20 h , (e) 40 h and (f) TEM micrograph of 40h milled Al_2O_3 powder with SAD pattern (*inset*).

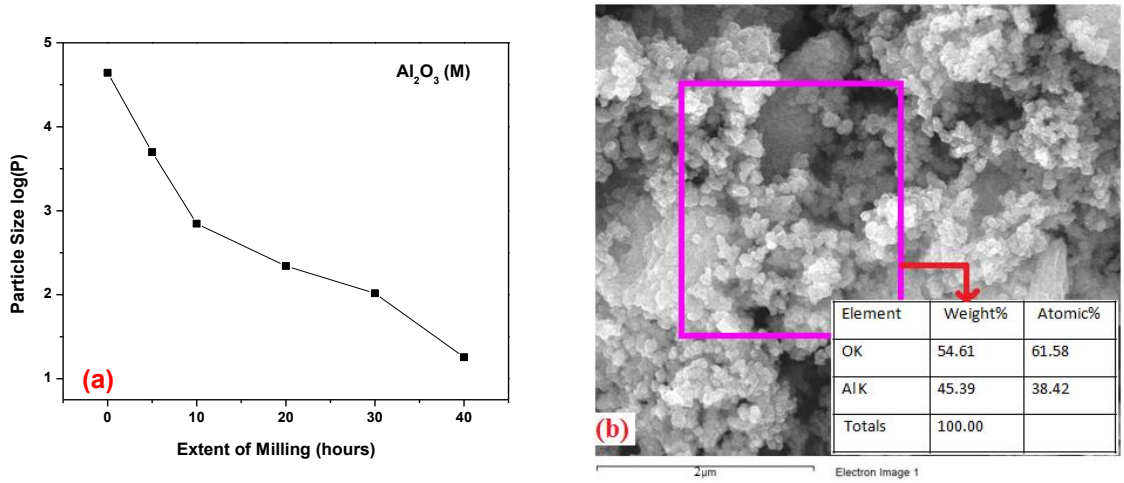

Fig 5.14- (a) Effect of milling time on the particle size of Al_2O_3 powder by FESEM quantitative analysis and (b) EDAX analysis along with surface morphology of 40h milled Al_2O_3 powder.

5.3.1.2 XRD Analysis

The diffraction patterns of Al_2O_3 powder in 'as recieved' and milled at different extents of time (5h, 10h, 20h, 30h and 40h) is displayed in figure 5.15. The pure alumina phase having rhombohedral system is confirmed by JCPDS ref no.: 00-042-1468 for 'as received' and all milled powders. The peak broadening and decrease in peak intensities are observed with increase in milling time [Fig 5.15]. It is due to the fact that milling introduces plastic deformation and thus renders the crystallinity to short range order.

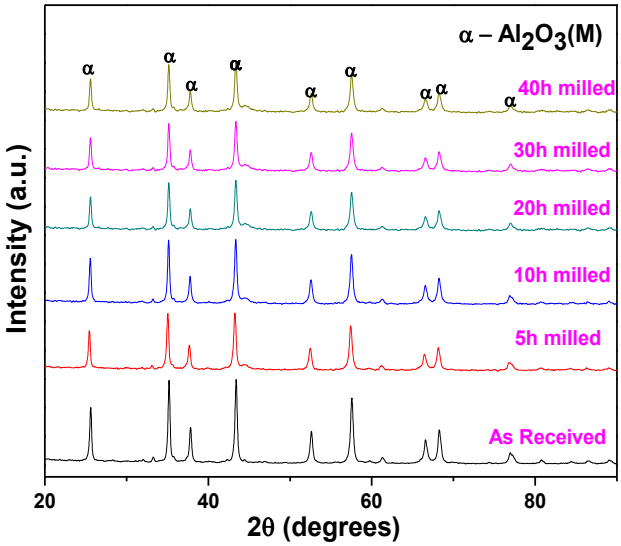

Fig 5.15- XRD patterns of 'As received' and Milled Al_2O_3 powder for 5h, 10h, 20h, 30h and 40h.

The effect of milling time with the crystallite size calculated using Scherrer's formula is shown in table 5.2. It is being observed that the crystallite size decreases with the increase in time of milling. The decrease in crystallite size can be described on the basis of collision during the milling within ball to ball and ball to jar, providing the external energy and work hardening to the materials and hence the breakage. The collisions introduce strain and hence the defects, vacancies, stacking faults and atomic disorder which in turn increase the Gibbs free energy of the system providing a way to fracture [Kumar et al. (2014)].

Table 5.2: Effect of milling hours on the crystallite size of Al_2O_3 (M) powder by XRD analysis (Scherrer's formula)

S.N.	Milling Time (h)	2θ (degree)	Interplanar Spacing (d) (A^o)	Phases Form	Grain Size by Scherrer Formula ($G=0.9\lambda/\beta\cos\theta$) (nm)
1.	0	43.34	2.08	Al_2O_3 (α)	55
2.	5	43.34	2.08		47
3.	10	43.34	2.08		42
4.	20	43.34	2.08		36
5.	30	43.34	2.08		25
6.	40	43.34	2.08		18

5.3.2 Zirconia (ZrO_2) nanoparticles

5.3.2.1 Morphological Study

FESEM micrograph reveals the morphology and particle size of the 'as received' and milled ZrO_2 powders for various time durations (5h, 10h, 20h, 40h) [Fig 5.16a]. The starting charge ('as received' powder), show spherical morphology with particle size of around 40μm [Fig 5.16a]. Milling of ZrO_2 powder at different durations show fractured and irregular morphology [Fig 5.17b-e] which is due to the external energy provided by milling during the collisions. Particle sizes of around 17μm, 743nm and 280nm are attained after 5h, 10h and 20h of milling of ZrO_2 powder respectively [Fig 5.16b-d]. FESEM [Fig 5.16e] and TEM [Fig 5.16f] analyses of the 40h milled powder, ZrO_2 $(M)_{40}$, reveals an irregular shape and the particle size variation of 17-25nm with an average particle size of 21nm. The diffused ring in SAD pattern (inset) [Fig 5.16f] supports the fact of amorphization during milling. The particle size variation of ZrO_2 powder with the milling time calculated by FESEM volumetric analysis is shown in figure 5.17a. The reduction in particle size is observed with increase in milling time as in higher extent of milling, fracture exceeds cold welding because of high hardness of the ZrO_2 powders. Fracture and cold welding are the basic processes taking place during milling. Cold welding is attributed by the formation of new surfaces of the powder during milling with

higher surface energy in order to decrease its free energy. With increase in extent of milling, the fracture of the surface overcome the free energy of new surfaces and agglomerated clumps and thus promotes lowering of particle size [Mishra et al. (2013)].

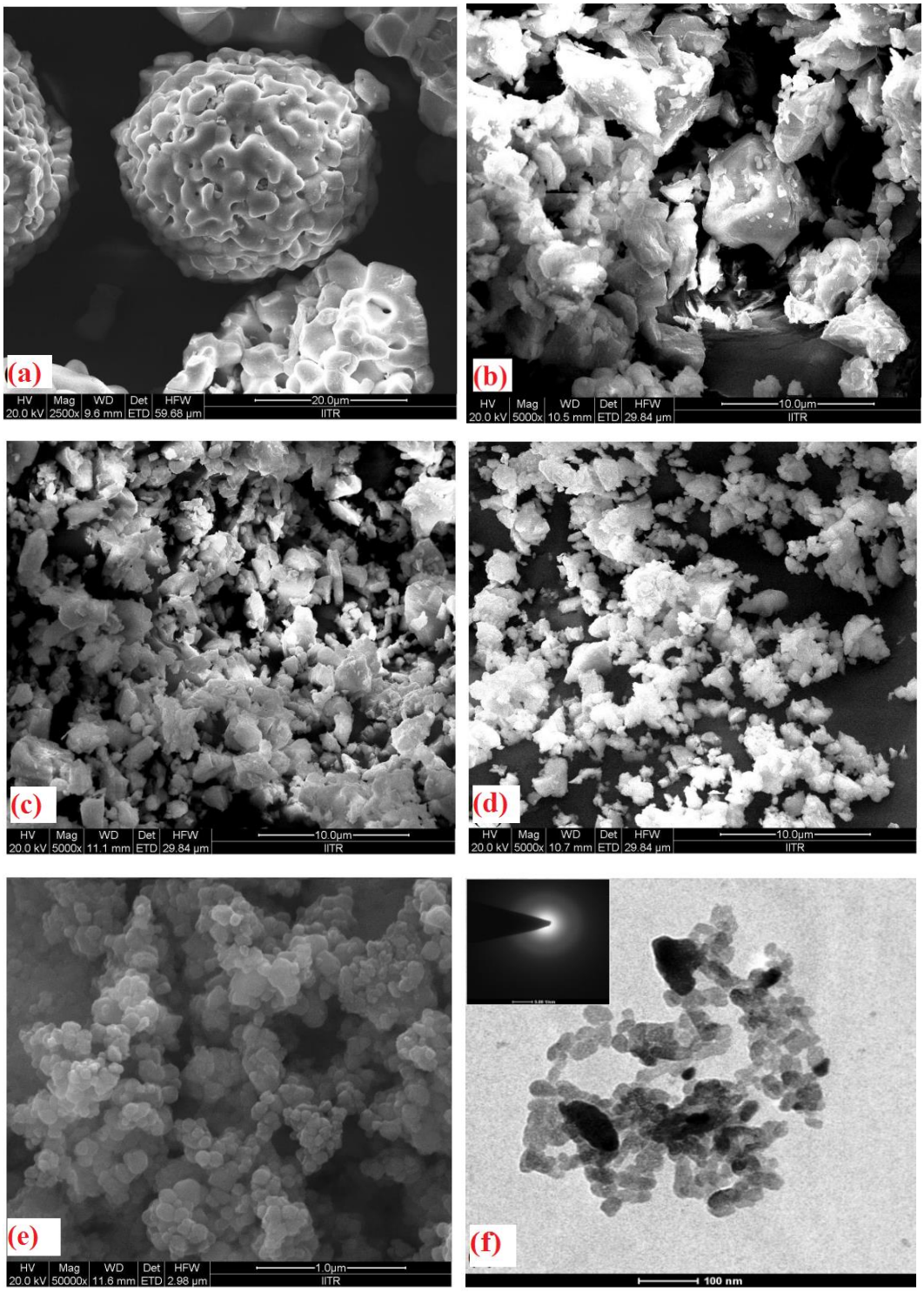

Fig 5.16- FESEM micrographs of ZrO_2 powder (a) As received, milled for different extents of time (b) 5 h, (c) 10 h, (d) 20 h, (e) 40 h and (f) TEM micrograph of 40h milled ZrO_2 powder with SAD pattern *(inset)*.

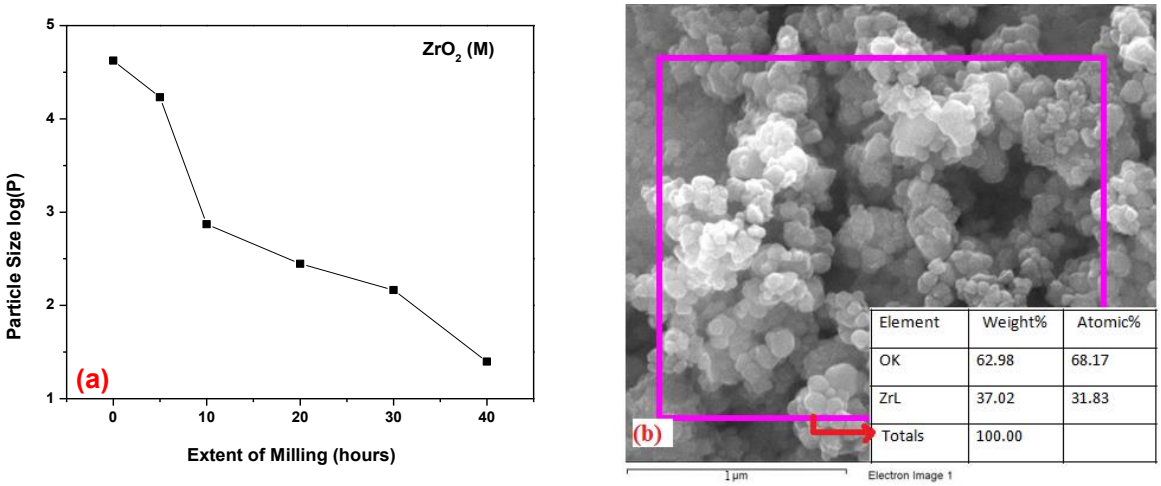

Fig 5.17- (a) Effect of milling time on the particle size of ZrO_2 powder by FESEM quantitative analysis and (b) EDAX analysis along with surface morphology of 40h milled ZrO_2 powder.

The compositional studies of 40h milled ZrO_2 powder, ZrO_2 $(M)_{40}$ is shown in figure 5.17b. The EDAX confirms the presence of Zr and O elements. The ratio of Zr & O in atomic percent is around 1:2 depicting the presence of ZrO_2 particles.

5.3.2.2 XRD Analysis

The X-ray diffraction patterns of 'as received' and milled for 5h, 10h, 20h, 30h and 40h ZrO_2 powders are shown in figure 5.18. The XRD patterns of 'as received' and milled powder reveal cubic phase of zirconia with JCPDS ref no.: 00-049-1642 [Fig. 5.18]. Peak broadening during mechanical milling depicts plastic deformation and amorphous nature of the charge. Extent of peak broadening is increased and intensity is reduced with increase in the duration of milling.

Table 5.3 shows the variation of milling time on the crystallite size of ZrO_2 powder calculated using Scherrer's formula. It is found that as the extent of milling increases, the crystallite size decreases. This is due to the collisions occurs during milling which gives the external energy to the material which results in breaking of particles and thus reduction in crystallite size [Gupta et al. (2012); Mishra et al. (2013)].

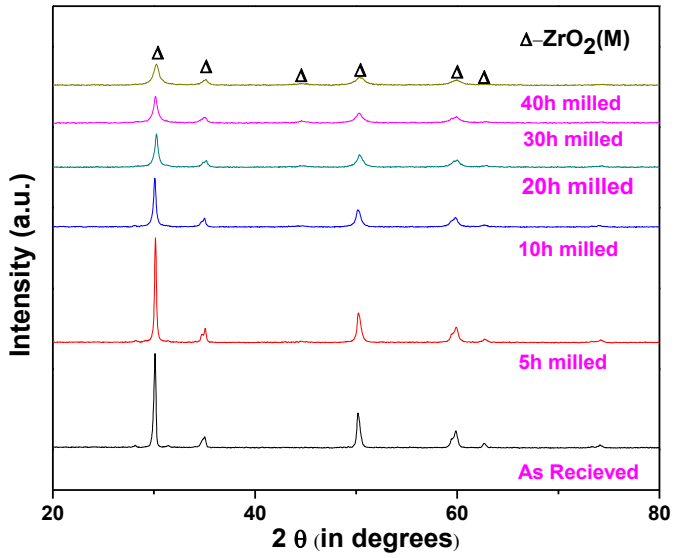

Fig 5.18- XRD patterns of As received and Milled ZrO_2 powder for 5h, 10h, 20h, 30h and 40h.

Table 5.3: Effect of milling hours on the crystallite size of ZrO_2 (M) powder by XRD analysis (Scherrer's formula)

S.N.	Milling Time (h)	2θ (degree)	Interplanar Spacing (d) (A°)	Phases Form	Grain Size by Scherrer Formula (G=0.9λ/βcosθ) (nm)
1.	0	25	3.52	ZrO_2 (Cubic)	51
2.	5	25	3.52		52
3.	10	25	3.52		47
4.	20	25	3.52		38
5.	30	25	3.52		26
6.	40	25	3.52		19

5.3.3 Titania (TiO_2) nanoparticles

5.3.3.1 Morphology Study

FESEM micrographs of the 'as received' and milled TiO_2 powders for different extents of time (5h, 10h, 20h, 40h) is shown in figure 5.19. The TiO_2 powder in 'as received' form is spherical in shape with particle size of about 42µm [Fig 5.19a]. The morphology of milled TiO_2 particles seems to be of irregular shape and have fractured surfaces showing the effect of external energy provided through milling, which is the characteristic of brittle materials [Figs 5.19b-e]. The particle sizes attained after 5h, 10h, 20h milling is in the range of 30µm, 12µm, 908nm respectively as calculated by volumetric analysis of the FESEM micrographs using ImageJ software [Fig 5.19b-d]. TiO_2 powder milled for 40h, TiO_2 $(M)_{40}$ exhibits irregular shape with particle size distribution found in a range of 33-45nm as examined by FESEM [Fig 5.19e] and

TEM micrographs [Fig 5.19f]. The average particle size of TiO_2 $(M)_{40}$ powder is 39nm. The diffused SAD pattern (inset) shows the amorphous nature of TiO_2 $(M)_{40}$ powder [Fig 5.19f]. The results of milling depict the brittle fracture rather than cold welding due to higher hardness of TiO_2 powders.

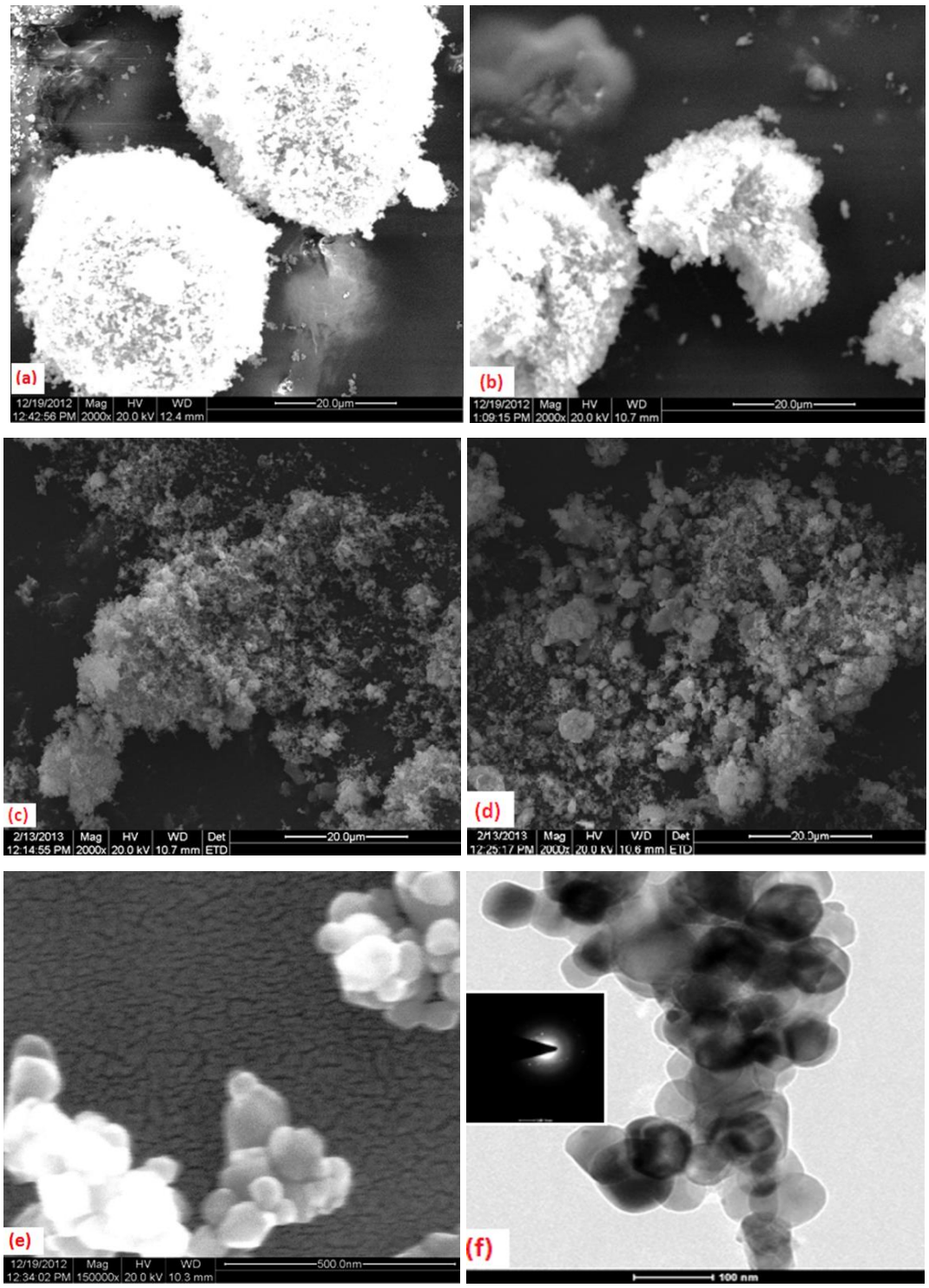

Fig 5.19- FESEM micrographs of TiO_2 powder (a) As received, milled for different extents of time (b) 5 h, (c) 10 h, (d) 20 h, (e) 40 h and (f) TEM micrograph of 40h milled TiO_2 powder with SAD pattern *(inset)*.

The effect of milling time on the particle size of TiO_2 powder determined by FESEM volumetric analysis is shown in figure 5.20a. It is observed that mechanical milling reduces the particle size from micron size to nanosize with time as milling time has two effects on the charge, first breaking of particles i.e. fracture and second, the agglomeration of particles occur by cold welding which takes place due to diffusion bonding by the pressure developed due to the impact of balls. When the amount of fracture overcomes cold welding, the reduction of particle size takes place [Kumar et al. (2014)].

The quantative analysis of TiO_2 powder milled for 40h, TiO_2 $(M)_{40}$ is shown in figure 5.20b. The EDAX spectrum in the selected region reveals the presence of Ti and O elements. The elemental ratio in atomic % of Ti & O is around 1:2 which infer the formation of TiO_2 particles.

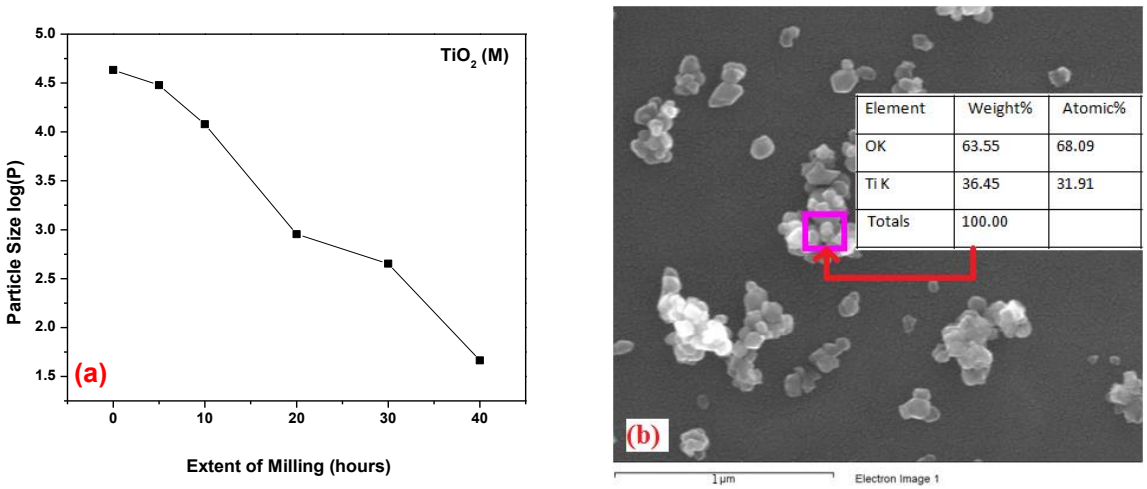

Fig 5.20- (a) Effect of milling hours on the particle size of TiO_2 powder by FESEM quantitative analysis and (b) EDAX analysis along with surface morphology of 40h milled TiO_2 powders.

5.3.3.2 XRD Analysis

The X-ray diffraction patterns of 'as received' and milled TiO_2 powder are shown in figure 5.21a. XRD patterns of 'as received' and milled TiO_2 powders for 5h, 10h, 20h, 30h and 40h confirms anatase phase of titania as per JCPDS ref no.: 01-073-1764 [Fig. 5.21]. The increase in amorphous nature of titania as shown by peak broadening and lowering the intensity as observed with increase in extent of milling time.

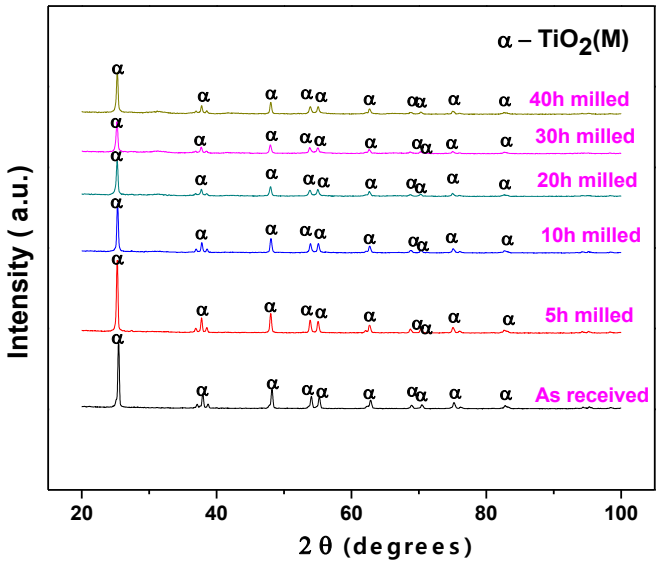

Fig 5.21- XRD patterns of As received and Milled TiO_2 powder for 5h, 10h, 20h, 30h and 40h.

Table 5.4: Effect of milling hours on the crystallite size of TiO_2 (M) powder by XRD analysis (Scherrer's formula)

S.N.	Milling Time (h)	2θ (degree)	Interplanar Spacing (d) (Aº)	Phases Form	Grain Size by Scherrer Formula (G) (nm)
1.	0	25	3.52	TiO_2 (Anatase)	54
2.	5	25	3.52		56
3.	10	25	3.52		49
4.	20	25	3.52		44
5.	30	25	3.52		40
6.	40	25	3.52		33

The effect of milling time on the crystallite size of TiO_2 powder is calculated from peak of XRD pattern using Scherrer's formula and given in table 5.4. It is observed that the crystallite size decreases with increase in milling time as the ball to ball collision, ball to jar (wall) collision provides external energy and hardening of the materials towards the breakage of the particles and hence reduction in size. It is due to the fact that collisions plastically deform the particles, which introduces defects thereby increases strain, which cause in the grain refinement by fracture [Muslimin and Yusoff (2009)]. The crystallite size of milled TiO_2 powder for 40h is found to be around 33 nm [Table 5.4].

5.4 SUMMARY

The synthesis of nanosized alumina, zirconia and titania particles using two different approaches such as Bottom up and Top down approach has been discussed in this chapter. The chemical precipitation method was employed to synthesize Al_2O_3, ZrO_2 and TiO_2 nanoparticles separately. The reagents used are aluminium chloride, zirconium oxychloride and titanium trichloride as precursor respectively. The thermal studies of the dried powders were carried out. Heat treatment at temperatures 1200^oC for 2h, 400^oC for 4h and 500^oC for 1h leads to formation of crystalline α-Al_2O_3, cubic ZrO_2 and anatase TiO_2 phase respectively in each case. Al_2O_3, ZrO_2 and TiO_2 nanoparticles of average particle size of 12nm, 7nm and 10nm were synthesized by chemical route. On the other hand, Al_2O_3, ZrO_2 and TiO_2 nanoparticles were also prepared separately by mechanical milling in high energy ball mill at 250 rpm for time extent upto 40 h. The variation of particle size with respect to different extents of milling time (5h, 10h, 20h, 30h and 40h) was also studied. Increase in milling time lowered the particle size and formed amorphous phases. Micron sized (40-42µm) Al_2O_3, ZrO_2 and TiO_2 particles was reduced into 15nm, 21nm and 39nm respectively through ball milling after 40h of milling. Al_2O_3, ZrO_2 and TiO_2 nanoparticles synthesized by the above two processes were used as the reinforcement for development of Ni-P-X [X= Al_2O_3, ZrO_2 and TiO_2] nanocomposite coatings using electroless technique as discussed in the next chapter.

CHAPTER 6

DEVELOPMENT OF Ni-P AND Ni-P-X NANOCOMPOSITE COATINGS USING ELECTROLESS TECHNIQUE

6.1 INTRODUCTION

Reinforcements play an important role in improving the physical and mechanical properties of the engineering materials [Balaraju et al. (2003); Wang and Zhou (1996); Wong and Gupta (2007)]. The present chapter includes the development of metal oxide reinforced Ni-P matrix nanocomposite coatings by electroless technique (EL Ni-P-X). The second phase particles 'X' used in the present investigation are nanosized alumina, zirconia and titania. The work focuses on the development of EL conventional Ni-P-X [X= Al_2O_3, ZrO_2 and TiO_2] nanocomposite coatings where 'X' reinforcements are synthesized by two different approaches i.e. chemical and mechanical route as discussed in chapter 5. An effort has been made to develop a novel EL Ni-P-X [X= Al_2O_3, ZrO_2 and TiO_2] nanocomposite coatings using non-conventional (*insitu*) route in this research work. Section 6.2 includes the synthesis of 'as coated' and heat treated Ni-P alloy coatings. The conventional and non-conventional synthesis of EL Ni-P-X [X= Al_2O_3, ZrO_2 and TiO_2] nanocomposite coatings and its subsequent heat treatment effect is explained in section 6.3. The concentration of the second phase particles is optimised for the development of sound nanocomposite coatings in non-conventional route in sub-section 6.3.2. The hardness studies of EL Ni-P and Ni-P-X [X= Al_2O_3, ZrO_2 and TiO_2] nanocomposite coatings are examined in section 6.4. In this chapter, the results based on morphology, phase structures and hardness studies of all developed nanocomposite coatings before and after heat treatment are discussed in detail and compared with Ni-P alloy coatings.

6.2 DEVELOPMENT OF EL Ni-P ALLOY COATINGS

6.2.1 Composition of Substrate Material

The chemical composition of mild steel used as substrate material in all the coatings as analysed through spectrographic method and are given in table 6.1.

Table 6.1: Composition of Mild steel (wt.%)

Element	C	Si	Mn	P	S	Cu
wt%	0.083	0.034	0.527	0.007	0.023	0.064

6.2.2 Morphological studies of 'as coated' and heat treated alloy coatings

FESEM micrographs of EL Ni-P alloy coatings in 'as coated' and heat treated conditions are given in figure 6.1. Plane Ni-P coating shows a hemispherical globular type structure [Fig 6.1a] with an average globular size of ~ 8μm. It is seen that the globules grow first laterally followed by the vertical growth on the substrate which results in almost non-porous deposits due to atom by atom deposition [Sharma et al. (2005)]. The coating is heat treated in argon atmosphere at 400°C for 1h in order to increase the adhesion of EL coatings with the substrate and to change it into crystalline phase [Mai et al. (1988)]. Heat treatment (HT) results in flattering of globules due to the diffusion of Ni atom at elevated temperature thus the globules seem to be relatively coarser than plane Ni-P coating as shown in figure 6.1b (region A). It is observed that heat treatment has only a slight influence on surface topography.

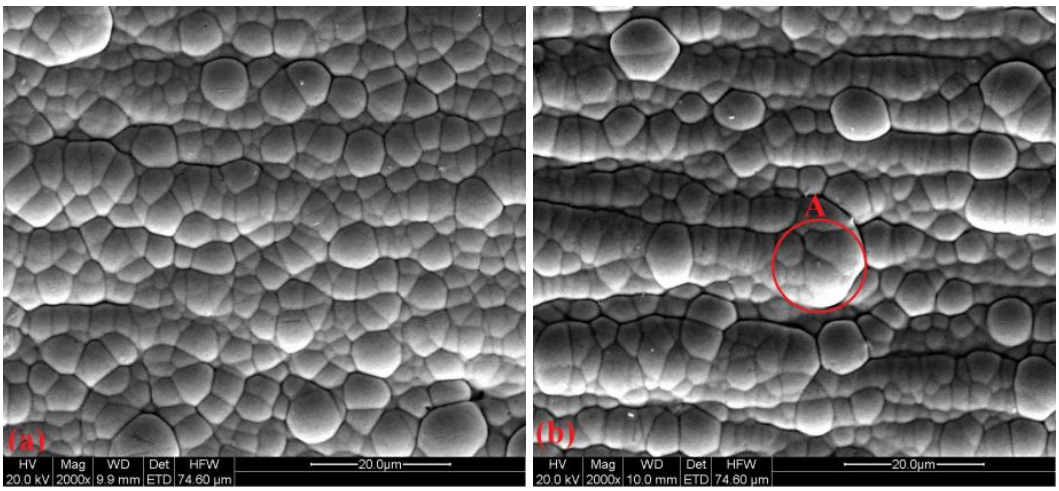

Fig 6.1- FESEM micrographs of EL Ni-P alloy coatings, (a) As coated and (b) HT conditions.

The three-dimensional AFM images of the surface of Ni–P coatings in as-deposited and after heat treatment with the scan area of 5x5 μm^2 are shown in figure 6.2. The Ni-P coating showed the globule like morphology and the average surface roughness (Ra) is found to be 10.82nm [Fig 6.2a]. It is noticed that on heat treatment at 400^oC for 1h, the surface morphology of the coatings showing compact globular structure and the surface roughness is decreased to 9.53nm [Fig 6.2b]. The results seem to be in resonance with FESEM micrographs shown in figure 6.1.

6.2.3 XRD Analysis of 'as coated' and heat treated alloy coatings

The X-Ray diffraction patterns of EL Ni-P alloy coating in 'as coated' and heat treated conditions are shown in figure 6.3. A single broad peak is observed in 'as coated' condition which corresponds to microcrystalline nickel, Ni (JCPDS ref no.: 00-045-1027). Heat treatment at 400^oC for 1h in argon atmosphere transforms microcrystalline nickel and Ni_xP_y

phases into crystalline Ni and stable Ni_3P phase (JCPDS ref no.: 01-074-1384) [Agarwala and Ray (1992); Alirezaei et al. (2004)]. The small peak of Fe (JCPDS ref no.: 00-006-0696) is noticed that may be due to the mild steel substrate used for coating.

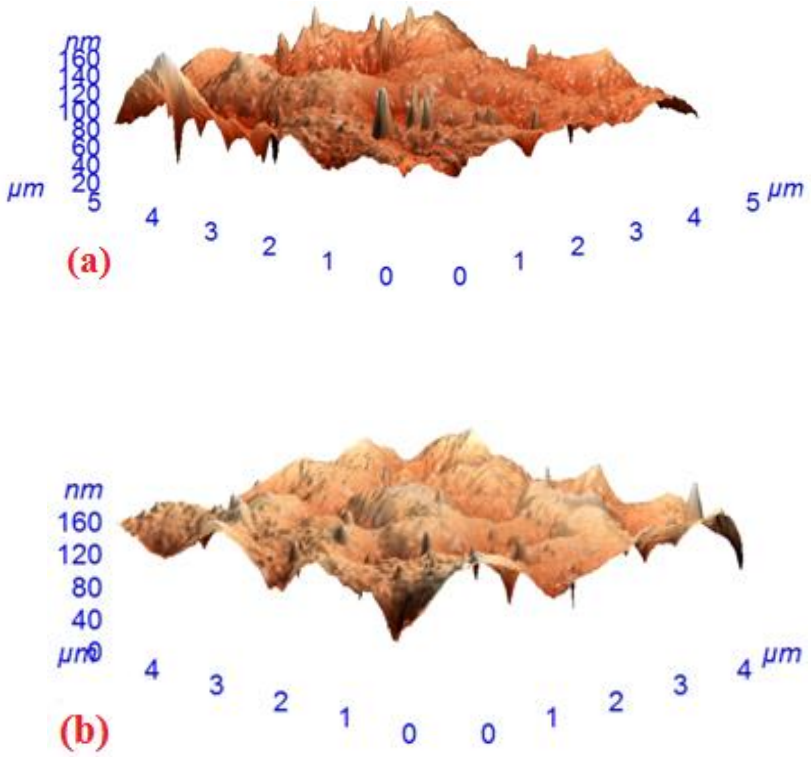

Fig 6.2- AFM morphologies of EL Ni-P alloy coatings, (a) As coated and (b) HT conditions.

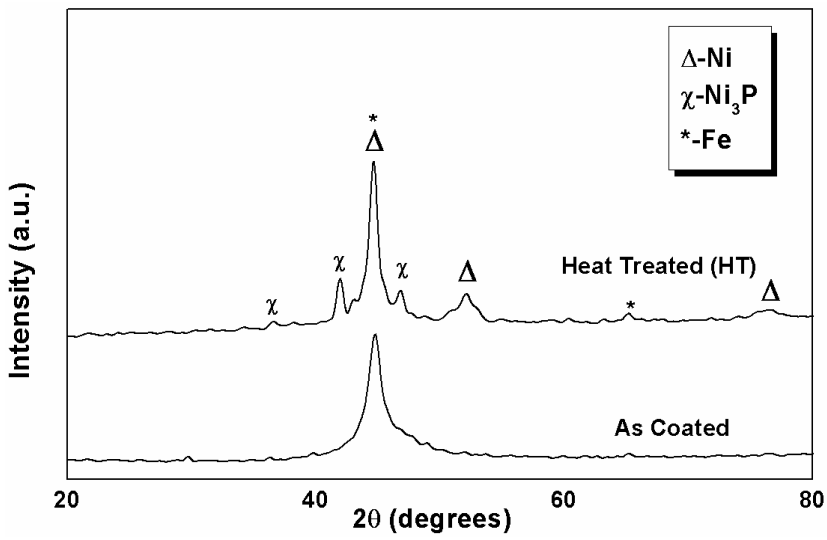

Fig 6.3- XRD patterns of EL Ni-P alloy coating in 'as coated' and HT conditions.

6.3 DEVELOPMENT OF EL Ni-P-X [X= Al_2O_3, ZrO_2, TiO_2] NANOCOMPOSITE COATINGS

Alumina, Zirconia and Titania are widely used as reinforcements due to their high strength, excellent wear resistance, high chemical stability, good corrosion resistance, low thermal expansion coefficient and ease of availability [Patnaik (2002)]. EL Ni-P-X [X= Al_2O_3, ZrO_2, TiO_2] nanocomposite coatings are prepared by conventional route where the second phase(s) 'X' can be added during the coating. In the present study, 'X' reinforcements are synthesized separately by chemical and mechanical milling route discussed in chapter 5. On the other hand, non-conventional route (*insitu*) is also employed to develop Ni-P-X [X= Al_2O_3, ZrO_2, TiO_2] nanocomposite coatings where the second phase(s) 'X' can be generated to nucleate and grow within the bath during coating [Sharma et al. (2005)]. From now, the convention for various Ni-P-X nanocomposite coatings where 'X' nanoparticles are prepared by chemical, milling and *insitu* route will be considered as prefixes of C, M, and I respectively. The different nanocomposite coatings are developed as listed in table 6.2.

Table 6.2: The details of Ni-P-X [X= Al_2O_3, ZrO_2, TiO_2] nanocomposite coatings developed by various routes with their sample IDs

S.No	EL Nanocomposite Coatings	Reinforcement 'X' [X=Al_2O_3, ZrO_2, TiO_2] prepared by various routes		
		Chemical Precipitation	Mechanical Milling	Insitu
1.	Ni-P-Al_2O_3	C_1	M_1	I_1
2.	Ni-P-ZrO_2	C_2	M_2	I_2
3.	Ni-P-TiO_2	C_3	M_3	I_3

6.3.1 Development of EL conventional Ni-P-Al_2O_3 nanocomposite coatings

6.3.1.1 Morphological studies of 'as coated' and heat treated (C_1 and M_1) nanocomposite coatings

FESEM micrographs of EL Ni-P-Al_2O_3 nanocomposite coatings where the second phase particle, Al_2O_3, are synthesized by two different routes are shown in figure 6.4. In Ni-P-Al_2O_3 nanocomposite coatings [Fig 6.4], it is seen that alumina particles are not only entrapped and dispersed on the surface (region A) but also the particles are seen to be themselves coated with the Ni-P (region B). It is also found that the smoothness of the Ni-P coating surface gets distorted on reinforcement by Al_2O_3 nanoparticles. The mechanically reduced $Al_2O_3(M)_{40}$

nanoparticles are seem to be more adherent onto the surface of Ni-P globules [Figs 6.4c,d] as compared to chemically synthesized nanosized Al_2O_3 particles [Figs 6.4a,b]. It is due to the fact that the increase in effective surface area of the powder after milling increases the surface energy hence better adherence with the matrix. Figures 6.4b,d show the micrograph of heat treated Ni-P-Al_2O_3 coated samples. Heat treatment allows coarsening of globules due to diffusion of Ni atom at elevated temperatures as discussed in previous section. Hence no significant effect on the surface topography of nanocomposite coatings is noticed in heat treated samples.

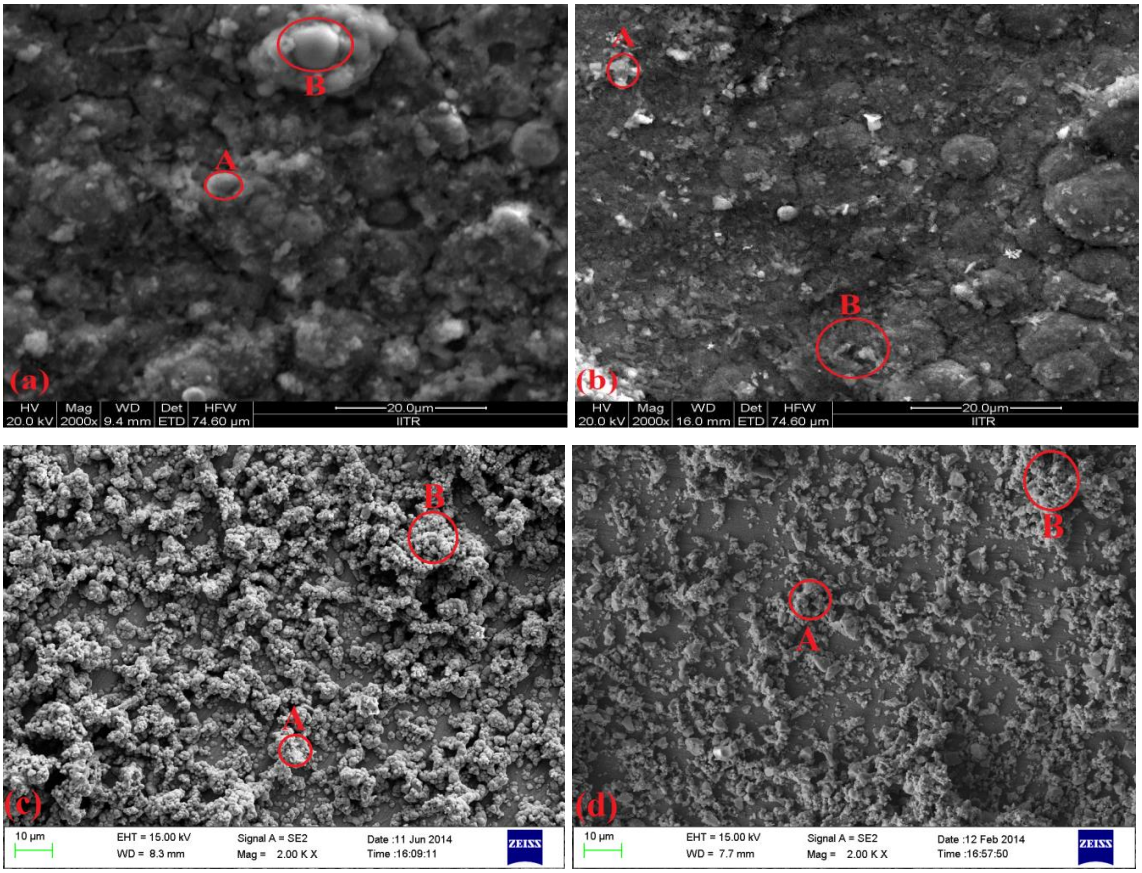

Fig 6.4- FESEM micrographs of EL conventional Ni-P-Al_2O_3 coatings, (a) C_1, (b) C_1 HT, (c) M_1 and (d) M_1 HT.

The EDAX as well as the X-Ray mapping studies of heat treated EL conventional Ni-P-Al_2O_3 nanocomposite coatings in the given region is shown in Fig 6.5. The EDAX and X-Ray mapping studies of two distinct nanocomposite coatings i.e. C_1 [Fig 6.5a] and M_1 [Fig 6.5b] reveals the presence of Ni, P, Al and O elements. The compositional analysis on a particle shows the elemental content of Al and O are in the ratio of almost 2:3 (atomic %) indicating the dispersion of Al_2O_3 particles in both the coatings on the surface of Ni-P globules and its entrapment within [Fig 6.5]. It is observed from the elemental mapping studies that Ni and P

are uniformly distributed throughout the matrix in both the composite coatings. Al and O regions are also seen in the required proportion for the formation of Al_2O_3 in each coating [Fig 6.5]. X-ray mapping supports the fact of entrapment of second phase strengthening in Ni-P globules. However, mechanically reduced Al_2O_3 nanoparticles are seem to be adsorbed in larger proportion on the Ni-P surface as compared with the chemically prepared particles. It is attributed to the better adhesion of milled particles in the Ni-P matrix due to high surface energy gained during milling.

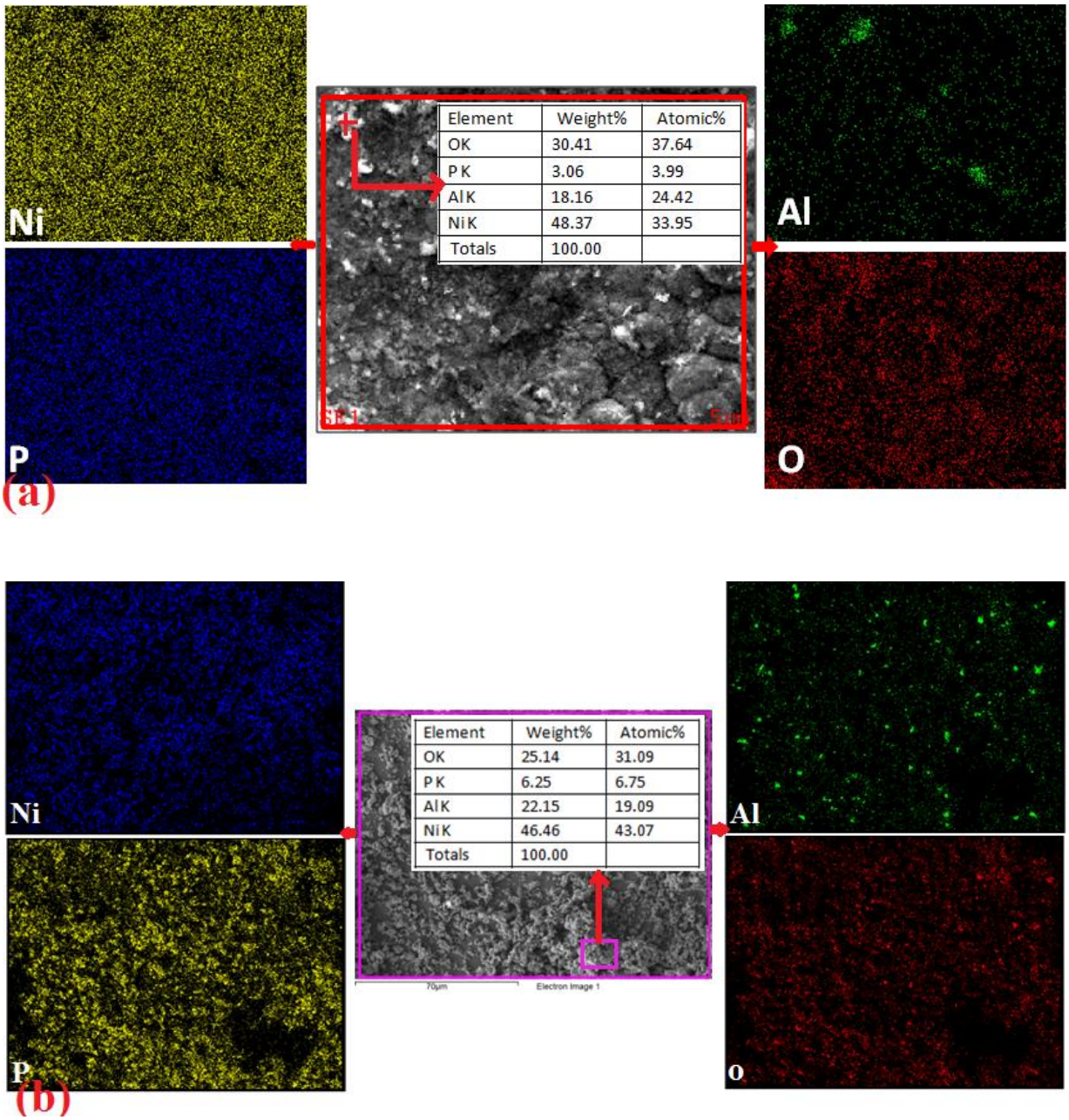

Fig 6.5- EDAX and X-ray Mapping analysis of heat treated EL Ni-P-Al_2O_3 nanocomposite coatings in the selected region under FESEM, (a) C_1 and (b) M_1 showing particle entrapment.

Figure 6.6 shows the three-dimensional AFM images for EL conventional Ni-P-Al_2O_3 nanocomposite coatings in 'as coated' and heat treated conditions. The surface topography of the two coatings C_1 [Fig 6.6a] and M_1 [Fig 6.6c] show a globule like morphology having nodules unlike Ni-P due to the reinforcement of Al_2O_3 nanoparticles. C_1 and M_1 coatings seems to represent different roughness values as the second phase Al_2O_3 particles incorporated in the coatings are prepared by two different methods. The average roughness value (Ra) of the nanocomposite coating with the inclusion of chemically synthesized Al_2O_3 nanoparticles (C_1) is found to be 18.16nm [Fig 6.6a]. Roughness value of Ni-P-Al_2O_3 nanocomposite coating (M_1) has been increased to 36.34nm with the presence of more nodules due to the codepositon of mechanically milled Al_2O_3 nanoparticles in Ni-P coating [Fig 6.6c] which provides better adhesion with the Ni-P coating surface. However, a reduction in roughness is observed on heat treatment in both the nanocomposite coatings. The average surface roughness (Ra) of the nanocomposite coatings after heat treatment at 400^{o}C for 1h determined from AFM images for C_1 [Fig 6.6b] and M_1 [Fig 6.6d] coatings is about 15.3nm and 32.15nm respectively. The results are in consistency with the FESEM micrographs where reinforcement of Al_2O_3 particles results in non-smooth surfaces.

6.3.1.2 XRD analysis of 'as coated' and heat treated (C_1 and M_1) nanocomposite coatings

The X-Ray diffraction patterns of EL conventional Ni-P-Al_2O_3 nanocomposite coatings using different mode of alumina as reinforcement in 'as coated' and heat treated conditions are shown in figure 6.7. XRD studies of Ni-P-Al_2O_3 nanocomposite coatings in 'as coated' condition found microcrystalline nickel, Ni (JCPDS ref no.: 00-045-1027) as the common phase just like in Ni-P coating along with the presence of Al_2O_3 (JCPDS ref no.: 01-083-2080) in both the coatings. However, the incorporation of mechanically reduced Al_2O_3 particles in the coating, M_1, results in a broader peak as compared with the coating where chemically synthesized Al_2O_3 particles are codeposited, C_1. This contributes to the reinforcement of milled alumina nanoparticles having amorphous nature which is entrapped in the matrix of Ni-P. On the other hand, the inclusion of crystalline phase of alumina, as prepared by chemical route, increases the crystallinity of the composite coating. The transformation of crystalline nickel from its microcrystalline form occurs as the coated samples were heat treated at 400^{o}C for 1h in argon atmosphere. During heat treatment, apart from the presence of Al_2O_3 phase (JCPDS ref no.: 01-083-2080), crystalline Ni and stable Ni_3P phase are also formed (JCPDS ref no.: 01-074-1384) as found in Ni-P alloy coating. This shows by incorporating Al_2O_3 nanoparticles in the Ni-P matrix, the structure of the coating remains unchanged. The Fe peaks (JCPDS ref no.:

00-006-0696) are noticed which may be diffracted from the steel substrate employed for coating [Fig 6.7].

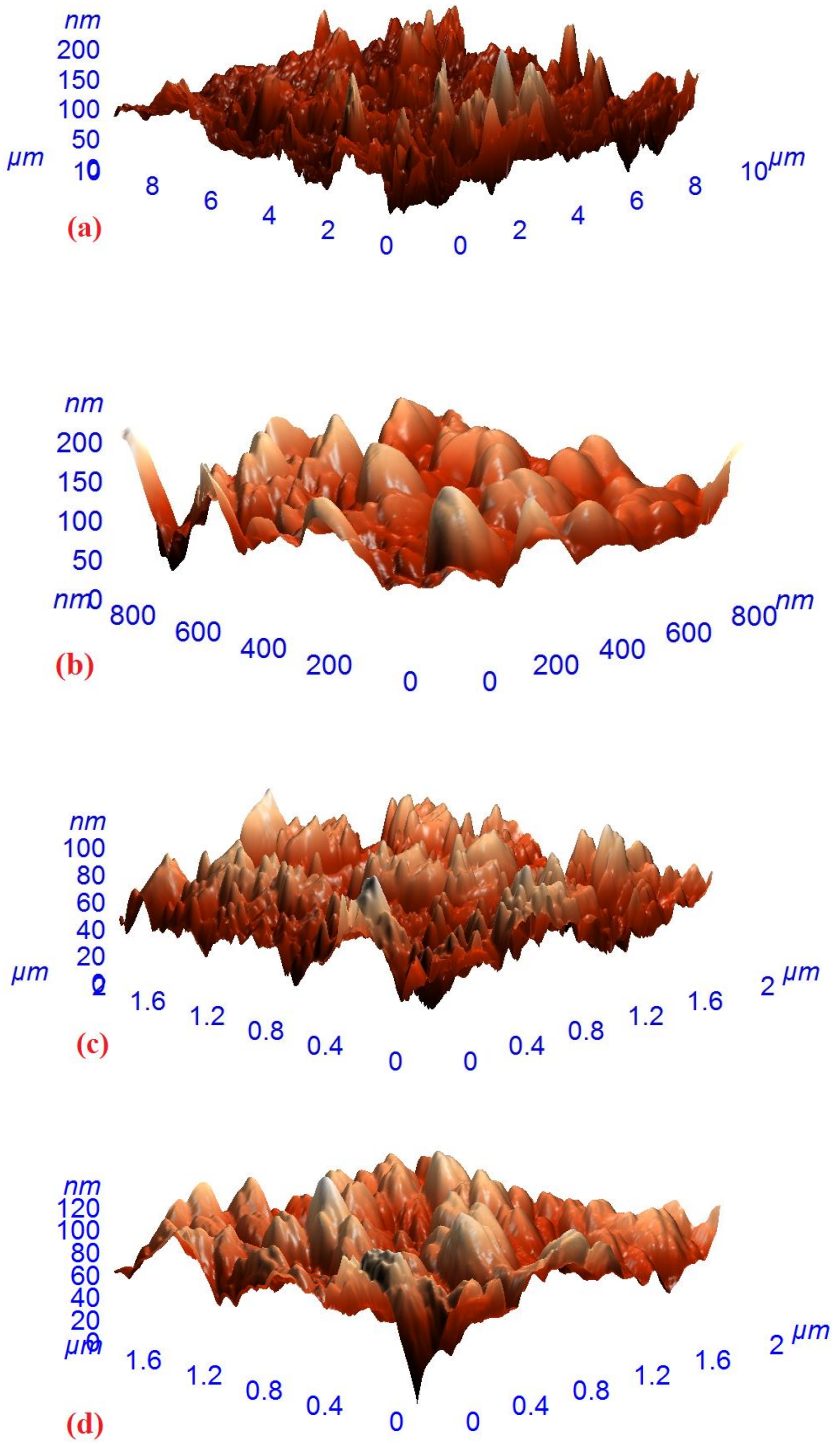

Fig 6.6- AFM studies of EL Ni-P-Al_2O_3 nanocomposite coatings, (a) C_1, (b) C_1 HT, (c) M_1 and (d) M_1 HT.

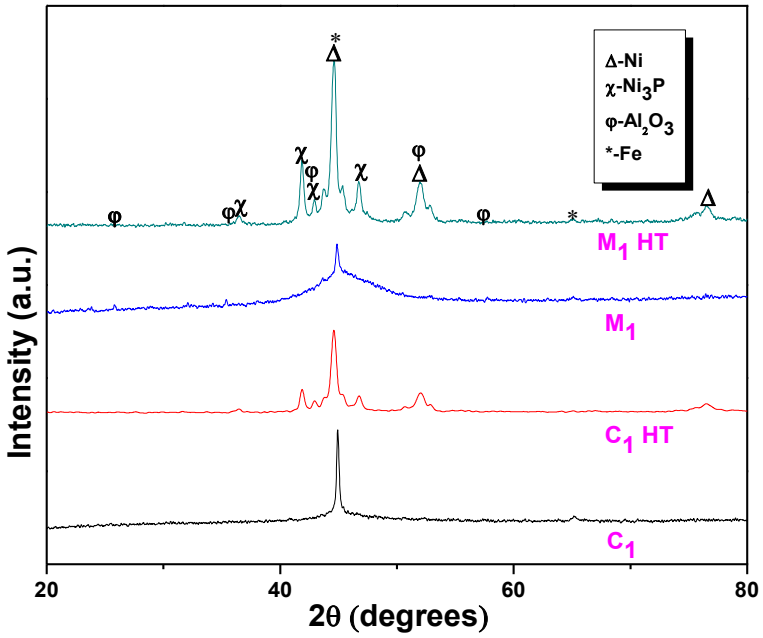

Fig 6.7- XRD patterns of EL Ni-P-Al_2O_3 nanocomposite coatings with different reinforced Al_2O_3 nanoparticles, C_1 and M_1 in 'as coated' and HT conditions.

6.3.2 Development of non-conventional (*insitu*) EL Ni-P-Al_2O_3 nanocomposite coatings and optimization of concentration of second phase particles

The precipitation of alumina can take place in an aqueous solution in the presence of ammonia, following the same conditions as for alkaline EL bath, therefore, this route has been used for the novel *insitu* precipitation of Al_2O_3 from $AlCl_3$ inside EL bath in the present study. Moreover, for comparison with the conventional method, the same precipitation reactions using precursor $AlCl_3$ occurs outside for the generation of Al_2O_3 nanoparticles as discussed in section 5.2.1. The non-conventional nanocomposite coatings results in precipitation of Al_2O_3 nanoparticles and its codeposition with Ni-P inside the EL bath. For development of sound EL *insitu* nanocomposite coatings, the concentration of the generated Al_2O_3 nanoparticles and its codeposition with Ni-P matrix is optimized by varying the amount of the precursor $AlCl_3$ accordingly inside the bath. The precipitation reaction occurs inside the bath and is given by equation 5.1. The balancing of this precipitation reaction can give the relative amounts of aluminium chloride ($AlCl_3$) as 26g/l, 39g/l and 52g/l for different concentrations of precipitation of alumina particles in a bath such as 10g/l, 15g/l and 20g/l repectively. The composite coatings with different concentrations of Al_2O_3 nanoparticles, for convenience, are indexed as listed in table 6.3.

Table 6.3: Concentrations of Al_2O_3 particles precipitated inside the bath for *insitu* method

S.N	Relative concentration of precipitation reactant $AlCl_3$ in the bath (g/l)	Concentration of *insitu* precipitated Al_2O_3 particles within the bath (g/l)	EL Coating Indexed
1.	26	10	A_1
2.	39	15	A_2
3.	52	20	A_3

6.3.2.1 Morphological studies of 'as coated' and heat treated (I_1) nanocomposite coatings

FESEM micrographs of novel EL Ni-P-Al_2O_3 nanocomposite coatings developed by non-conventional (*insitu*) mode with different concentrations of *insitu* precipitated alumina are presented in figure 6.8. All coatings show a typical morphology of a hemispherical globular structure with relatively uniform and dense coverage of the nanocomposite coating on mild steel substrate. The surface seems to be clean and no clusters or cracks can be seen on the surface of the coating [Fig 6.8]. No clear Al_2O_3 particles can be observed on the surface of the *insitu* Ni-P-Al_2O_3 nanocomposite coatings. This accounts for very fine size of Al_2O_3 particles. The extremely small sized particles probably physically absorbed/adsorbed on the coating surface and mixed uniformly in the emerging Ni-P matrix leading to their higher dispersion in the coating. However, the existence of nanosized Al_2O_3 particles can be confirmed by virtue of their EDAX analysis as discussed in the next section. It is observed that the average globule size of the *insitu* Ni-P-Al_2O_3 nanocomposite coating decline gradually with increase in the concentration of the Al_2O_3 particles in the bath solution as shown in figure 6.8. The mean globule size observed for nanocomposite coatings having different concentrations, A_1 A_2 and A_3 are ~ 10μm, 7μm and 4μm respectively as calculated by FESEM volumetric analysis using image J software [Fig 6.8]. The globule size refinement may be due to the highly dispersed Al_2O_3 nanoparticles in the coating. This may be interpreted as the concentration of precipitated Al_2O_3 nanoparticles rises in the bath solution, the increased amount of trapped Al_2O_3 nanoparticles either increases the nucleation sites or limit the lateral growth of the growing Ni-P layer and also itself gets distributed in grain boundaries which hinder the grain growth [Afroukhteh et al. (2012)]. Therefore, the globule size decreases with increase in the concentration of second phase Al_2O_3 particles leading to a grain refinement strengthening effect as evident in figure 6.8.

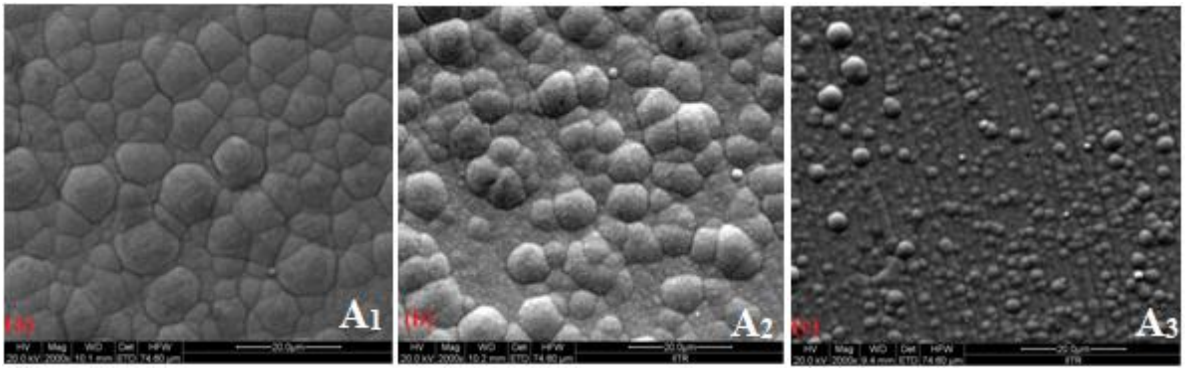

Fig 6.8- FESEM micrographs showing surface morphology of EL *insitu* Ni-P-Al_2O_3 nanocomposite coatings at different concentrations, (a) A_1, (b) A_2 and (c) A_3.

EDAX analysis reveals the quantative composition of *insitu* Ni-P-Al_2O_3 nanocomposite coatings in the selected region at various concentrations and is given in figure 6.9. The presence of Ni, P, Al and O elements are depicted by EDAX studies. The atomic % of Al and O indicates the entrapment of second phase Al_2O_3 nanoparticles in Ni-P matrix in all the three cases. However, it is observed by EDAX studies that the content of entrapped nanosized Al_2O_3 particles increases following with the concentration of its precipitation in the bath [Fig 6.9]. The sharp increase in alumina content is noticed in the coating for concentrations of Al_2O_3 nanoparticles upto 15 g/L whereas at higher concentrations, the increment rate slightly falls off [Fig 6.9c]. The increase in Al_2O_3 content with increase in its concentration in the bath can be described as more number of Al_2O_3 particles entrapped in the coating under the effect of agitation. However, the decrease in content beyond certain concentration, 15g/l, is probably due to the cogregation of Al_2O_3 particles in the solution as mean distance between them decreases. As a result, the floatability of Al_2O_3 particles weakens as the weight increases and they tend to settle down making fewer particles available for codeposition. Hence, relatively lower content is observed as seen in the EDAX studies at higher concentration [Fig 6.9c]. Similar results have been reported by Balaraju and Seshadri (1998); Alirezaei et al. (2004) for particle incorporation.

The relationship between concentration of the precipitation reactant, $AlCl_3$ in EL bath and Al_2O_3 incorporation (wt%) in Ni-P coating is derived from EDAX analysis and is shown in figure 6.10. It can be deduced from the figure that the weight percent incorporation of Al_2O_3 nanoparticles increases with an increase in concentration of reactant, $AlCl_3$ and achieves a maximum at a concentration of 39g/l and the rate of percentage incorporation decreases afterwards as explained above. When the precipitation reactant, $AlCl_3$, is added into the bath solution, well dispersed Al_2O_3 nanoparticles are *insitu* formed under the effect of ammonia.

These nanoparticles are then absorbed on the coating surface and embedded into the Ni-P matrix resulting in the formation of *insitu* Ni-P-Al_2O_3 nanocomposite coatings. The unifom distribution of Al_2O_3 nanoparticles leads to a good effect of second phase dispersion strengthening discussed in section 6.4. The Al_2O_3 concentration in the bath upto 15g/l ($AlCl_3$ (39g/l)) is consistent with improvement of mechanical properties. However, furher higher concentration of Al_2O_3 particles leads to deterioration of the mechanical properties. The details are discussed in sub-section 6.4.1. Hence the optimum concentration, A_2 (15g/l), is employed in the present work in all the cases, for sound *insitu* Ni-P-X [X=Al_2O_3, ZrO_2 and TiO_2] nanocomposite coatings.

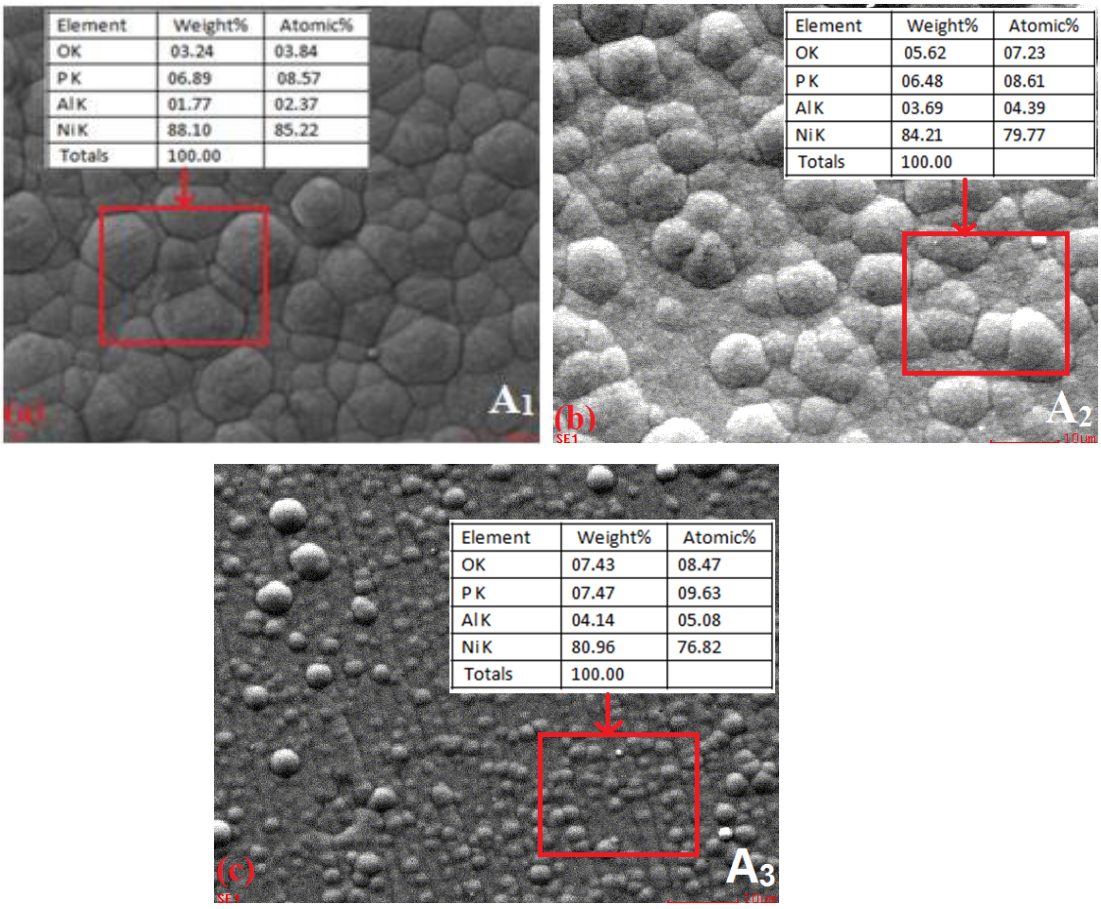

Fig 6.9- EDAX analysis of EL *insitu* Ni-P-Al_2O_3 nanocomposite coatings at different concentrations under FESEM, (a) A_1, (b) A_2 and (c) A_3.

The elemental mapping studies of optimized *insitu* Ni-P-Al_2O_3 (A_2) nanocomposite coating in heat treated condition is shown in figure 6.11 along with its surface morphology. The mapping analysis indicates the presence of Ni, P, Al and O elements in the coating. The uniform distribution of Ni and P elements is seen in the entire matrix. The Al and O elements are also

found to be uniform in the required proportion indicating the formation of Al_2O_3 particles entrapped throughout in the coating.

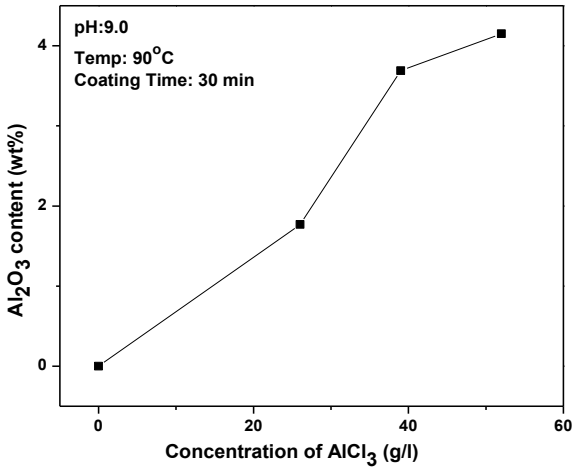

Fig 6.10- Effect of reactant, $AlCl_3$ concentration, in EL bath on Al_2O_3 content in the deposit.

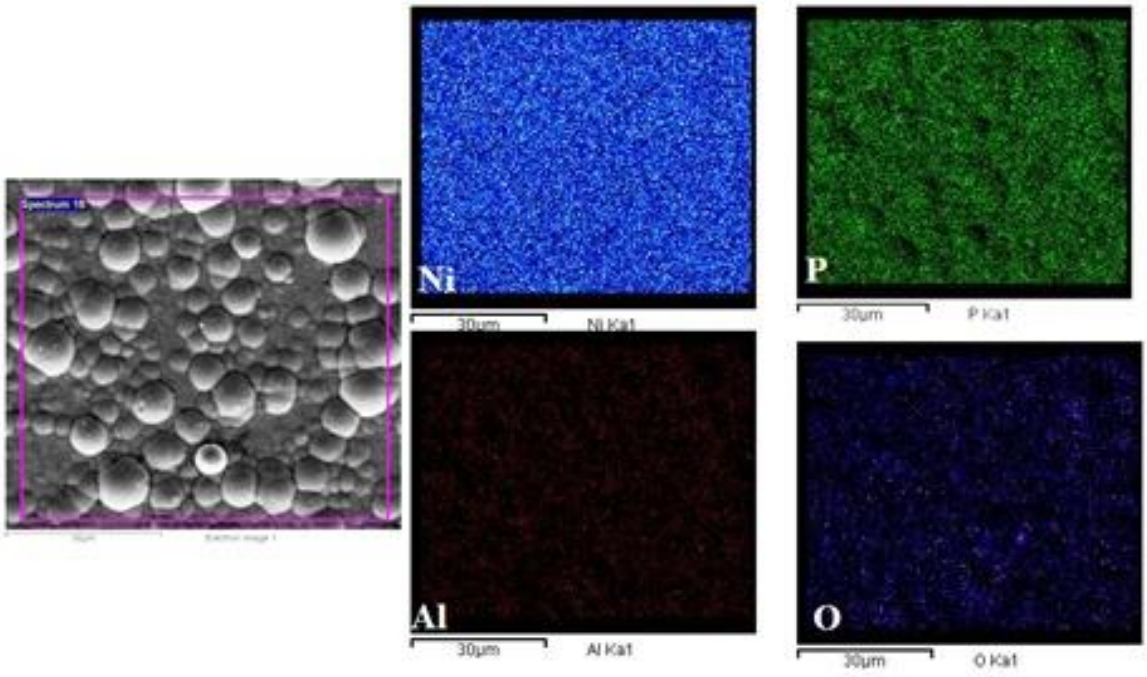

Fig 6.11- Area mapping studies of optimized heat treated EL *insitu* Ni-P-Al_2O_3 nanocomposite coating (A_2) in the selected region under FESEM showing particle entrapment.

The AFM images of the surface of the optimised *insitu* Ni-P-Al_2O_3 nanocomposite coatings (A_2) in 'as coated' and heat treated conditions are shown in figure 6.12. The figures reveal that non-conventional Ni-P-Al_2O_3 nanocomposite coating has a relatively smooth and compact surface morphology [Fig 6.12] than that of the conventional Ni-P-Al_2O_3 coatings [Fig 6.6]. Furthermore, the average roughness (Ra) of *insitu* Ni-P-Al_2O_3 nanocomposite coatings in 'as

coated' and heat treated conditions are calculated to be about 14nm [Fig 6.12a] and 12.21nm [Fig 6.12b] respectively. It can be concluded that the *insitu* codeposition of the Al_2O_3 nanoparticles in the Ni-P matrix increased the surface roughness as the presence of the metal oxide particles influenced the surface heterogeneity and enhances the boundaries between Ni and the particles in the matrix [Novakovic et al. (2006)].

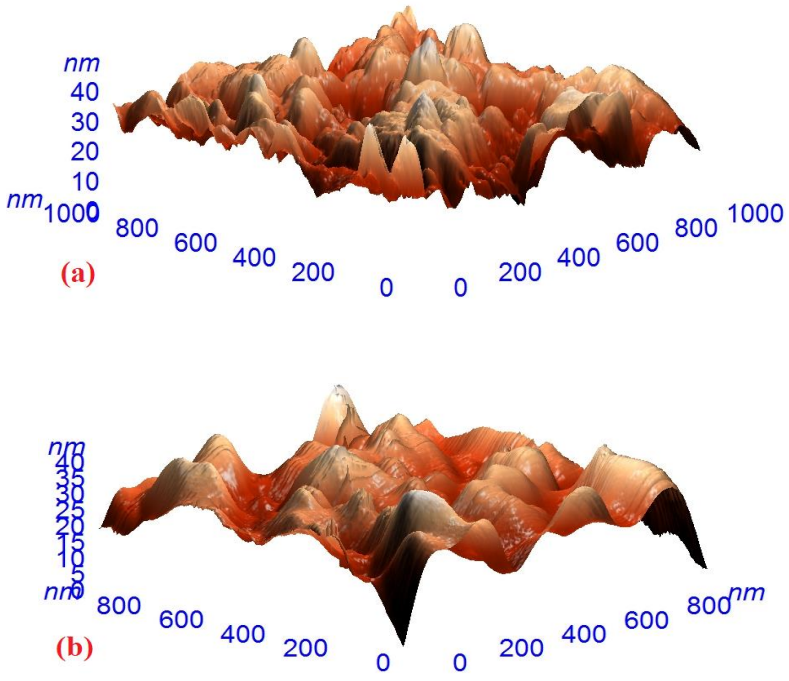

Fig 6.12- AFM micrographs of optimized EL *insitu* Ni-P-Al_2O_3 nanocomposite coating in (a) 'as coated' and (b) HT conditions.

6.3.2.2 XRD analysis of 'as coated' and heat treated (I_1) nanocomposite coatings

XRD patterns of EL *insitu* Ni-P-Al_2O_3 nanocomposite coating at different concentrations of the precipitating element Al_2O_3 in 'as coated' and heat treated conditions is shown in figure 6.13. XRD studies of Ni-P-Al_2O_3 coatings reveals that apart from single broad peak which corresponds to microcrystalline Ni (111) at 44.66^o (JCPDS ref no.: 00-045-1027), other peaks which correspond to Al_2O_3 (JCPDS ref no.: 00-001-1296) at 57^o, 43^o and 68^o are also present. However, due to the low quantity of Al_2O_3 particles and high intensity of other diffraction peaks, Al_2O_3 peaks have extremely small. As expected, it is seen that the particles incorporated into the electroless Ni-P coating doesnot vary its structure as the peaks corresponding to Ni and Ni_3P (JCPDS ref no.: 01-074-1384) remains the same. In the heat treated condition, crystalline phases of Ni, Ni_3P, Al_2O_3 and Fe are obtained. The peak from Fe (JCPDS ref no.: 00-006-

0696) present may be from the substrate used. The entrappment of higher content of alumina particles can also be seen by the higher crystalline nature of the A_2 nanocomposite coatings.

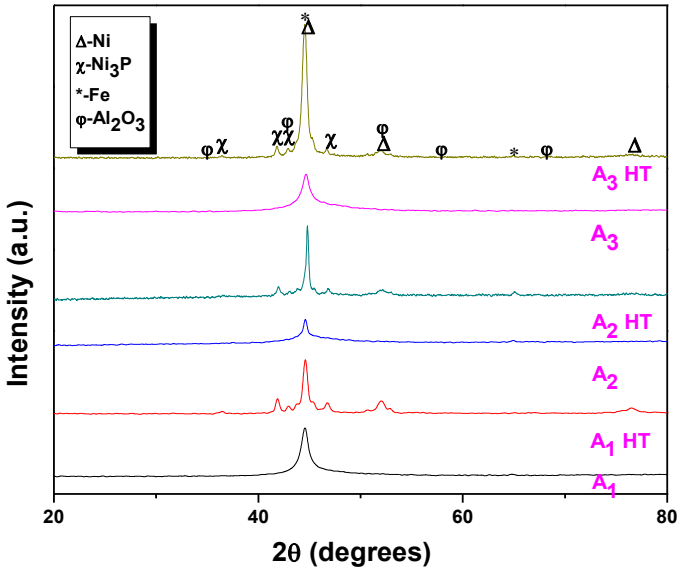

Fig 6.13- XRD patterns of EL *insitu* Ni-P-Al_2O_3 nanocomposite coatings at different concentrations, A_1, A_2 and A_3 in 'as coated' and HT conditions.

6.3.3 Development of Ni-P-ZrO_2 nanocomposite coatings

Zirconia particles are embedded in Ni-P matrix to form Ni-P-ZrO_2 nanocomposite coatings using conventional and non-conventional mode in the present work. The zirconia nanoparticles prepared by chemical and mechanical route as discussed in section 5.2.2 and 5.3.2 respectively are used as the second phase for the development of conventional Ni-P-ZrO_2 nanocomposite coatings. For non-conventional mode, zirconia is precipitated from zirconium oxychloride in the presence of ammonia solution in the similar manner as discussed in section 5.2.2.2 via equation 5.3 under alkaline conditions compatible with the alkaline EL bath employed for coating. Hence, *insitu* Ni-P-ZrO_2 nanocomposite coatings are developed where precipitation and codeposition of ZrO_2 nanoparticles occurs within EL bath only and compared with the respective conventional coatings.

6.3.3.1 Morphological studies of 'as coated' and heat treated (C_2, M_2 and I_2) nanocomposite coatings

FESEM micrograph of EL Ni-P-ZrO_2 nanocomposite coating in 'as coated' and heat treated conditions is shown in figure 6.14. It can be observed, in case of conventional EL Ni-P-ZrO_2 nanocomposite coatings [Figs 6.14 a-d], that the surface show many nodular protrusions as compared with smooth surface of plane Ni-P coating [Fig 6.1]. These nodules are of spherical

shape when chemically synthesized ZrO_2 nanoparticles are codeposited along with Ni-P [Figs 6.14a,b]. However, on inclusion of mechanically milled ZrO_2 nanoparticles in the Ni-P coatings, irregular shaped nodules are observed [Figs 6.14c,d]. In both cases, ZrO_2 particles are seen on Ni-P globules marked as region A and in certain regions, the particles are seen to be coated with the Ni-P (region B). It is clearly seen from the micrographs, that milled ZrO_2 $(M)_{40}$ nanoparticles show more adherence with Ni-P matrix [Figs 6.14c,d] as compared to ZrO_2 nanoparticles prepared by chemical route [Figs 6.14a,b]. This accounts for high surface energy of the powder gained via milling which promotes adherence with the surface easily unlike chemically synthesized particles. The FESEM micrograph of nonconventional (*insitu*) Ni-P-ZrO_2 nanocomposite coatings shows a clean hemispherical globular structure like Ni-P coating with extremely small zirconia particles entrapped within it which are supported by EDAX and X-ray mapping as discussed in next section [Figs 6.14e,f]. Heat treatment (HT) at 400°C for 1h in argon atmosphere as shown in figures 6.14b,d,f results in coarsening of globules. It is observed that heat treatment has only a slight influence on surface topography.

The EDAX and X-Ray mapping analysis of heat treated EL conventional [Figs 6.15a,b] and *insitu* [Fig 6.15c] Ni-P-ZrO_2 nanocomposite coatings in the selected region reveals the presence of Ni, P, Zr and O elements. The compositional quantative analysis as determined by EDAX studies specify that the elemental content of Zr and O are in the ratio of around 1:2 (atomic%) and thus indicates the presence of ZrO_2 particles embedded in the matrix in all developed nanocomposite coatings [Fig 6.15]. The entrappment is further supported by the elemental mapping studies which show the distribution of Zr and O in the proportion that promotes the formation of ZrO_2 in all the cases. Also, the uniform distribution of Ni and P are found throughout in all the coatings [Fig 6.15]. It is being noticed that the dispersion and embeddment of milled ZrO_2 nanoparticles [Fig 6.15b] are found to be higher among the other i.e. chemically prepared [Fig 6.15a] and *insitu* ZrO_2 nanoparticles [Fig 6.15c]. It accounts for the better adherence provided by the milled particles with the matrix due to its high effective surface area which gains higher surface energy as clearly seen by its FESEM micrograph [Figs 6.14c,d].

Figure 6.16 presents three dimensional AFM images of EL conventional (C_2, M_2) and non-conventional (I_2) Ni-P-ZrO_2 nanocomposite coatings. By comparing the three different images i.e. C_2, M_2 and I_2, it is clear that the coatings have different surface roughness due to distinct growth patterns of the coatings. The average roughness value (Ra) obtained for C_2 is 20.54nm [Fig 6.16a]. The incorporation of mechanically reduced ZrO_2 nanoparticles in the Ni-P matrix

(M_2) has resulted in more nodular and rougher deposit having a roughness of 29nm [Fig 6.16c]. It is observed that EL *insitu* Ni-P-ZrO_2 nanocomposite coating (I_2) has the smallest roughness value of 15.21nm than that of conventional C_2 and M_2 coatings [Fig 6.16e]. It correlates with the fact that the particles entrapped inside the matrix are of extremely small size depicted by the presence of very sharp nodules on the surface. The order of increasing roughness follows the trend- $M_2 > C_2 > I_2$. The reduction in surface roughness is observed on heat treatment (400^oC, 1h) with an average roughness of about 17nm, 26.11nm and 12.25nm for C_2, M_2 and I_2 nanocomposite coatings respectively [Figs 6.16b,d,f].

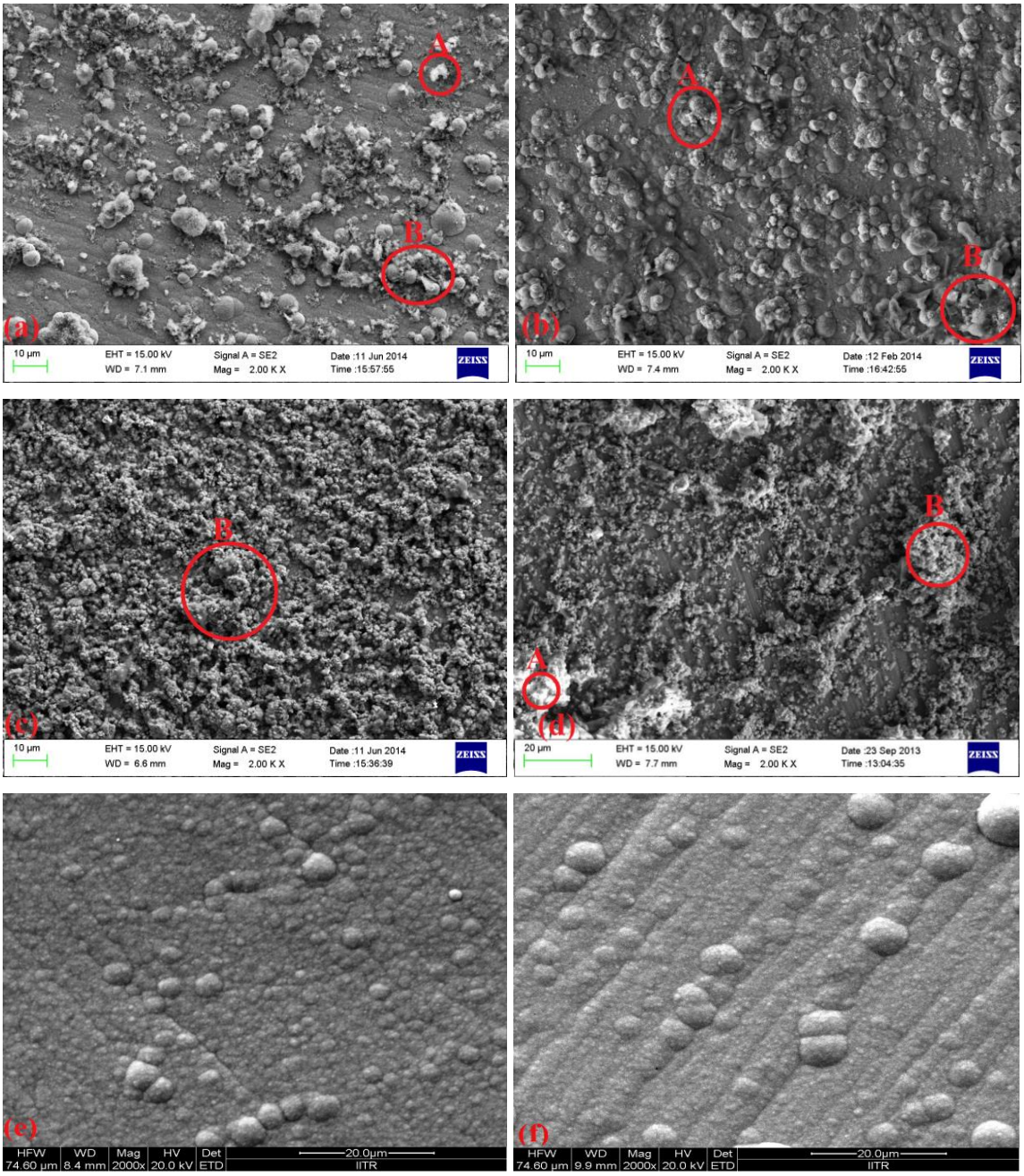

Fig 6.14- FESEM micrographs of EL Ni-P-ZrO_2 nanocomposite coatings, (a) C_2, (b) C_2 HT, (c) M_2, (d) M_2 HT, (e) I_2 and (f) I_2 HT.

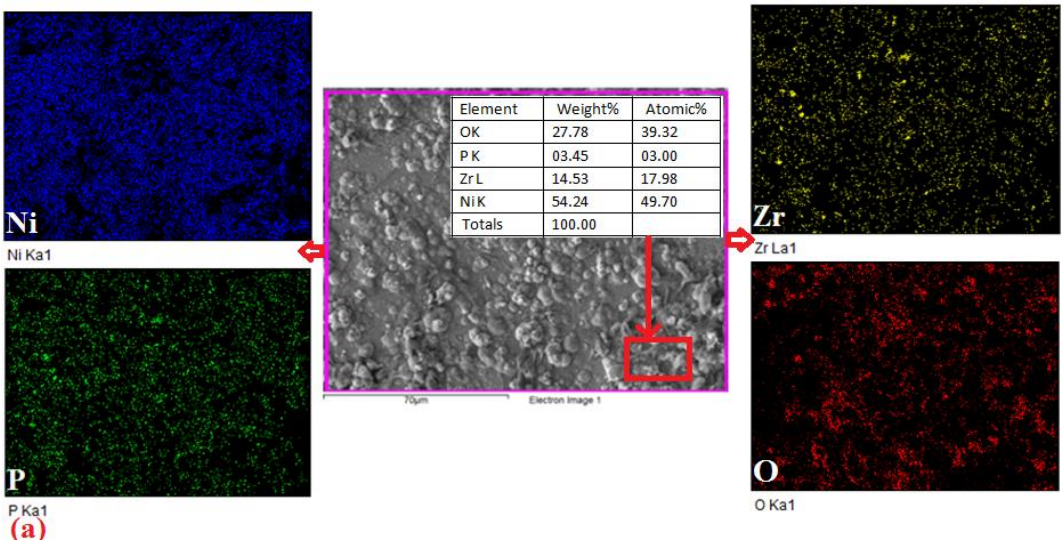

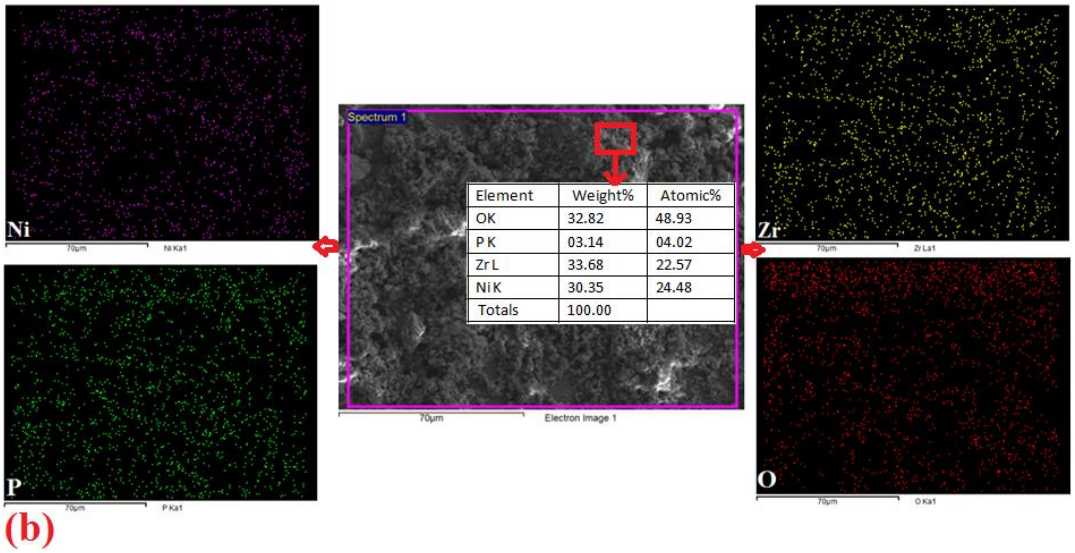

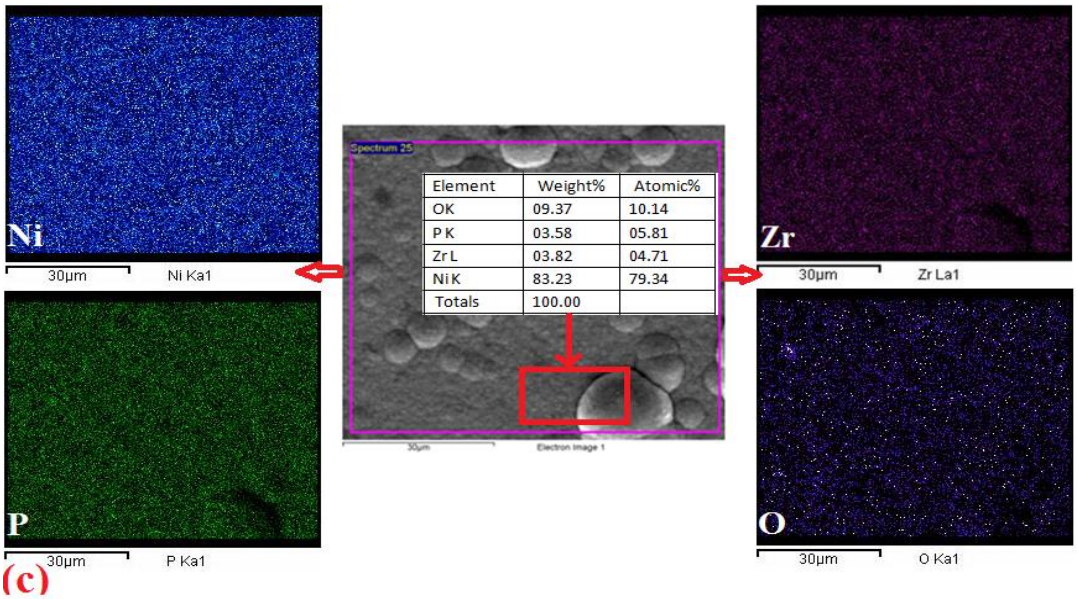

Fig 6.15- EDAX and X-ray Mapping analysis of heat treated EL Ni-P-ZrO_2 nanocomposite coatings in the selected region under FESEM, (a) C_2, (b) M_2 and (c) I_2.

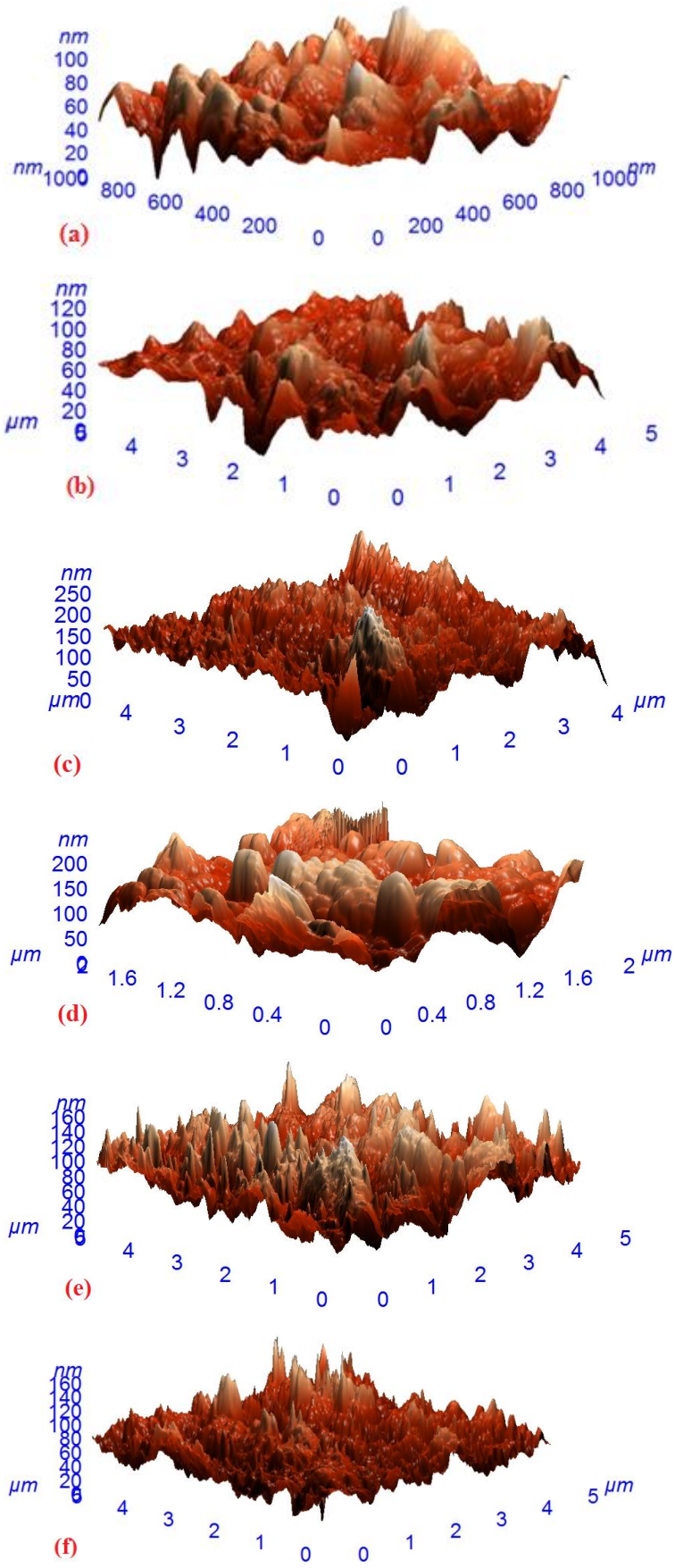

Fig 6.16- AFM studies of EL Ni-P-ZrO_2 nanocomposite coatings, (a) C_2, (b) C_2 HT, (c) M_2, (d) M_2 HT, (e) I_2 and (f) I_2 HT.

6.3.3.2 XRD analysis of 'as coated' and heat treated (C_2, M_2 and I_2) nanocomposite coatings

XRD analysis of EL Ni-P-ZrO_2 conventional (C_2, M_2) and non-conventional (I_2) coatings in 'as coated' and heat treated conditions are shown in figure 6.17. The single peak of microcrystalline nickel, Ni (111) at 44.6°C (JCPDS ref no.: 00-045-1027) as found in Ni-P along with other peaks which correspond to ZrO_2 (JCPDS ref no.: 00-037-1484) in monoclinic form at 28°, 32°and 50°C are present in case of C_2 and I_2 nanocomposite coatings. In case of codeposition of milled samples i.e. M_2 coatings, cubic form of ZrO_2 (JCPDS ref no.: 00-049-1642) is present as seen in peaks at 30°, 50° and 35°C as 40 h milled (cubic form) powder is used as reinforcement for the coating. However, the chemically prepared powder is heat treated first to get crystalline phase and then codeposit in the Ni-P coating. In the heat treated condition, crystalline phases of Ni, Ni_3P (JCPDS ref no.: 01-074-1384), ZrO_2 and Fe are obtained. The peak from Fe present (JCPDS ref no.: 00-006-0696) may be from the substrate used. As expected, it is seen that ZrO_2 particles incorporated into electroless Ni-P coating does not vary its structure as the peaks corresponding to Ni and Ni_3P remains the same.

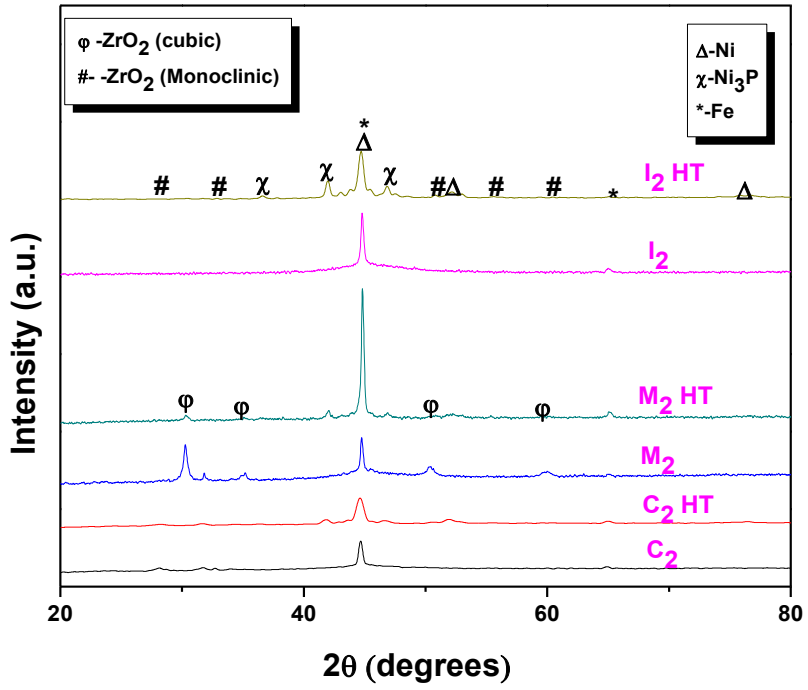

Fig 6.17- XRD patterns of EL Ni-P-ZrO_2 nanocomposite coatings with different mode of synthesis, C_2, M_2 and I_2 in 'as coated' and HT conditions.

6.3.4 Development of Ni-P-TiO_2 nanocomposite coatings

In the present study, TiO_2 nanoparticles are incorporated in Ni-P matrix following conventional and non-conventional route in the similar manner like Al_2O_3 and ZrO_2. The

conventional Ni-P-TiO_2 nanocomposite coatings are developed with the inclusion of chemically and mechanically prepared titania as discussed in sections 5.2.3 and 5.3.3 respectively. While for *insitu* preparation of Ni-P-TiO_2 nanocomposite coatings, the TiO_2 sol prepared using $TiCl_3$ with ammonia in the alkaline medium found appropriate with the alkaline EL coating bath conditions. Thus, titania is precipitated and codeposited with Ni-P matrix within EL bath to develop non-conventional Ni-P-TiO_2 nanocomposite coatings.

6.3.4.1 Morphological studies of 'as coated' and heat treated (C_3, M_3 and I_3) nanocomposite coatings

Figure 6.18 show FESEM micrographs of conventional (C_3, M_3) and *insitu* (I_3) EL Ni-P-TiO_2 nanocomposite coatings in 'as coated' and heat treated conditions. The conventional nanocomposite coatings show the presence of nodular protrusions along with the hemispherical globular structure. The surface topography of the conventional Ni-P-TiO_2 nanocomposite coatings change from a smooth state of Ni-P coating to the non-smooth state [Figs 6.18a-d] because of the presence of nodules which are due to the reinforcement of TiO_2 into the Ni-P matrix. The TiO_2 nanoparticles are seen on the surface of Ni-P globules whereas in nodular sites (marked as 2), the particles are seen to be themselves coated with Ni-P globules [Figs 6.18a-d]. The non-conventional Ni-P-TiO_2 nanocomposite coatings exhibit a clear globular structure with TiO_2 nanoparticles embedded in it [Fig 6.18e,f]. In order to increase the adhesion of the coatings with the substrate and to change it into crystalline phase, the coated samples are subjected to heat treatment at 400°C for 1h in argon atmosphere. It results in slightly flatter and coarser globules than 'as coated' ones due to the diffusion at higher temperature [Figs 6.18b,d,f].

The compositional analysis of heat treated EL Ni-P-TiO_2 nanocomposite coatings in terms of EDAX and X-ray mapping is shown in figure 6.19. The EDAX analysis on the selected region along with the X-ray mapping studies of heat treated EL conventional [Fig 6.19a,b] and *insitu* [Fig 6.19c] Ni-P-TiO_2 nanocomposite coatings supports the presence of TiO_2 nanoparticles apart from nickel and phosphorus and its entrapment in the Ni-P globules. It is also found from EDAX analysis that the elemental ratio of Ti & O is around 1:2 for all the developed nanocomposite coatings which further confirms the TiO_2 embeddment in Ni-P matrix. It is observed from mapping studies that, in all the cases, Ni and P are uniformly distributed all over the matrix. Although the higher content of TiO_2 nanoparticles are obtained in case of codeposition of milled particles with respect to other two coatings [Fig 6.19b]. It may be due to the fact that milling particles have higher surface energy. Each system wants minimum energy

for stability. Hence, particles adhere very easily in order to loose energy. Thus the adsorption of the particles apart from absorption is more likely in case of milled particles employed as the second phase in Ni-P coatings.

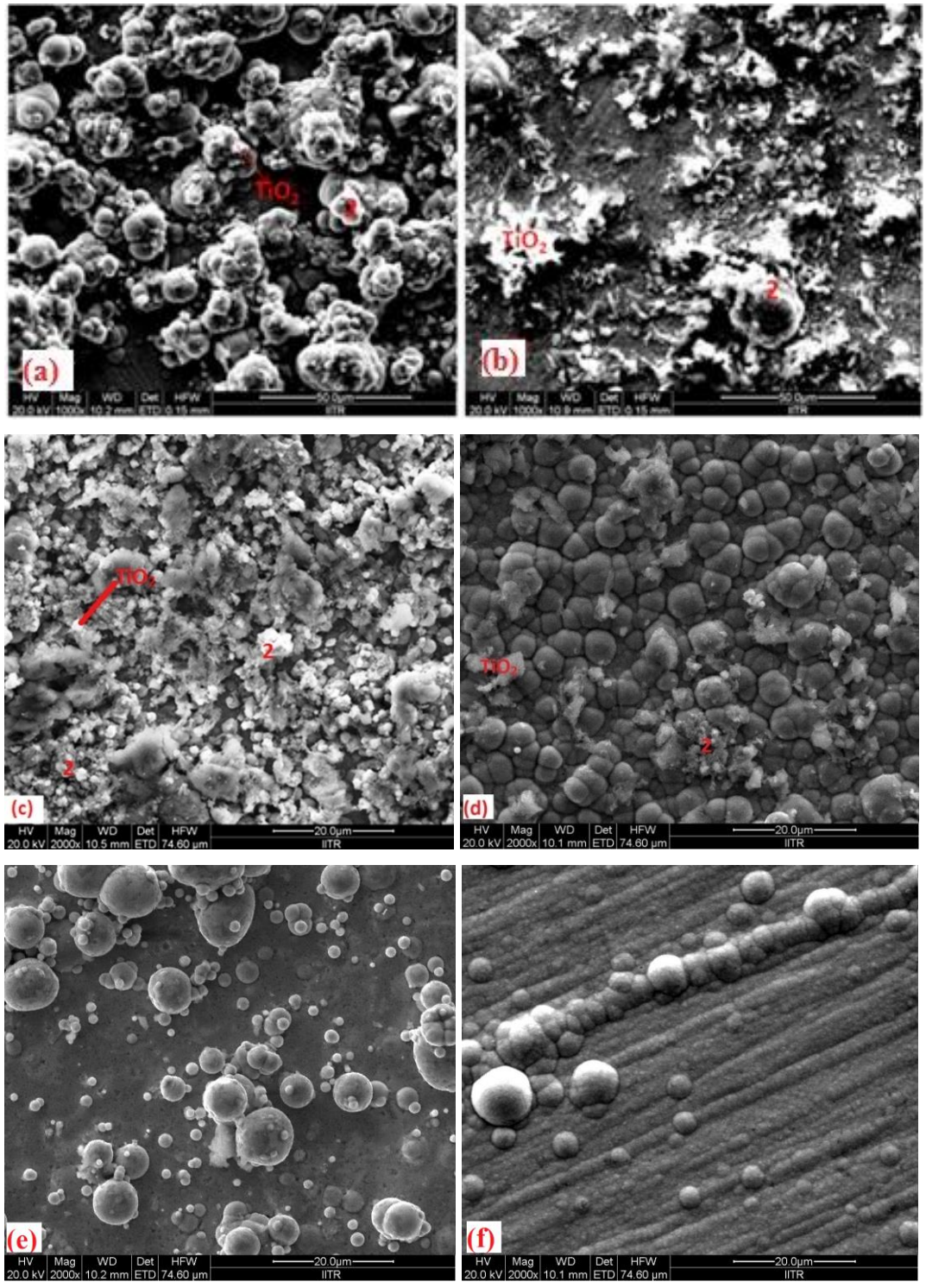

Fig 6.18- FESEM micrographs of EL Ni-P-TiO_2 nanocomposite coatings, (a) C_3, (b) C_3 HT, (c) M_3, (d) M_3 HT, (e) I_3 and (f) I_3 HT.

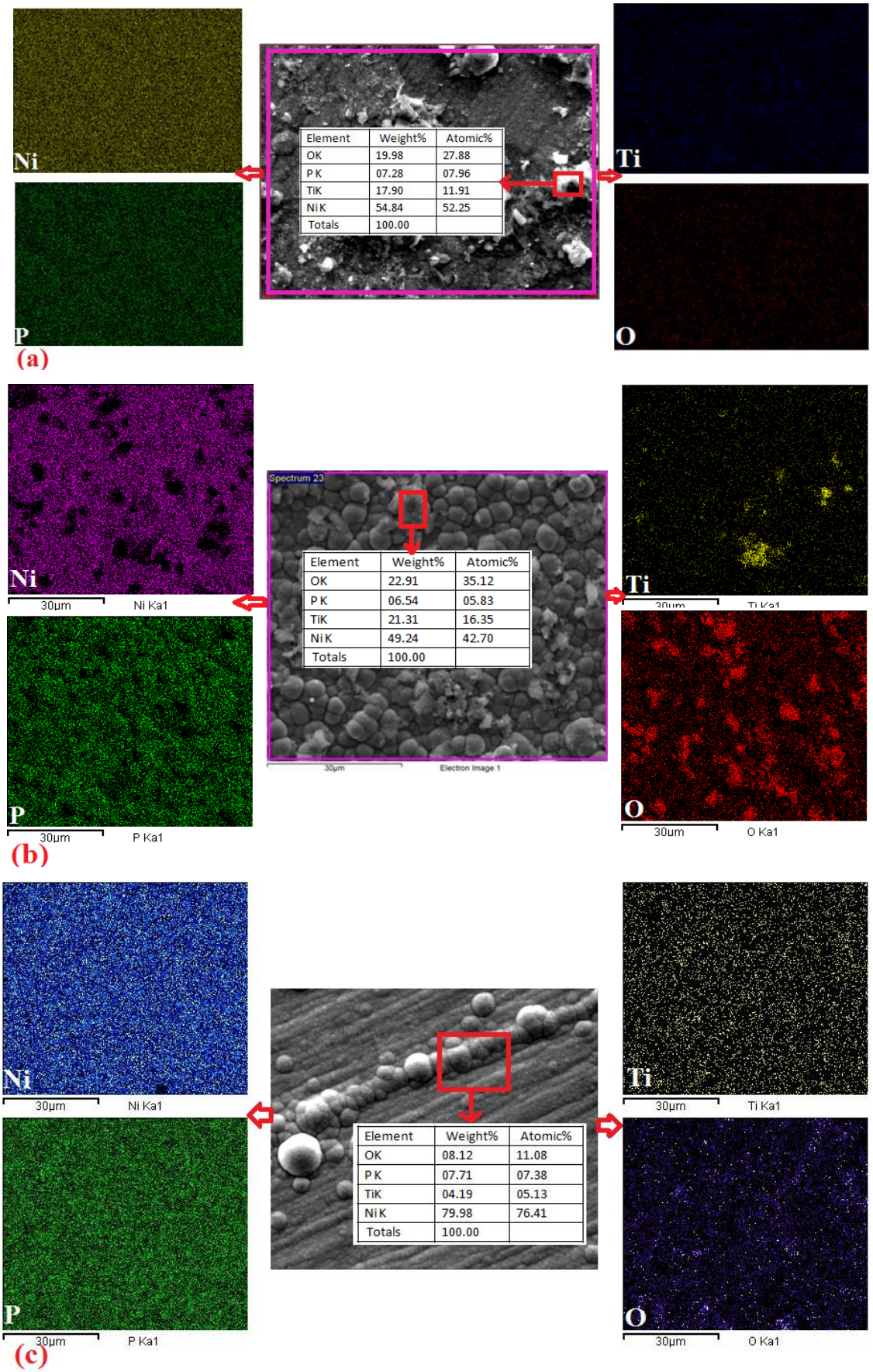

Fig 6.19- EDAX and X-ray Mapping analysis of heat treated EL Ni-P-TiO_2 nanocomposite coatings in the selected region under FESEM, (a) C_3, (b) M_3 and (c) I_3 showing particle entrapment.

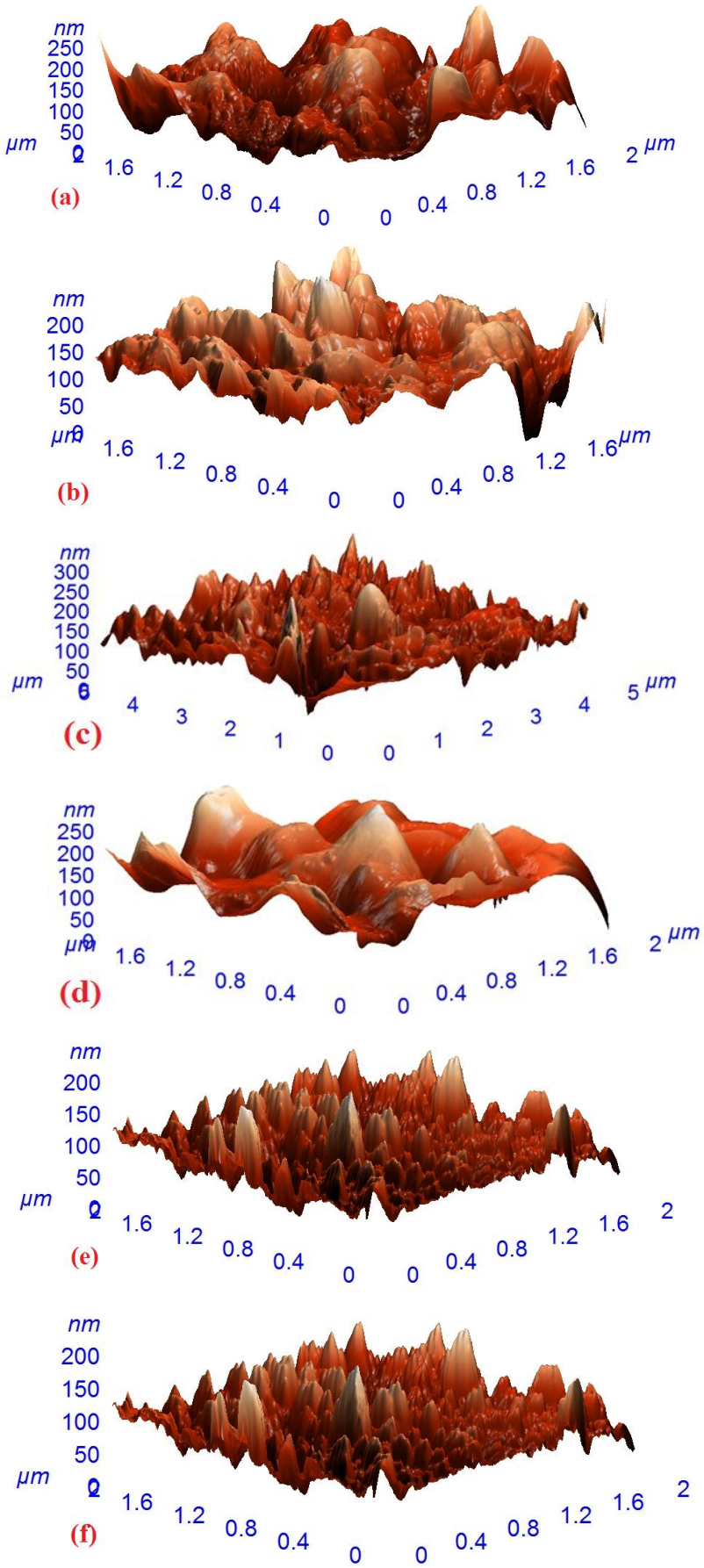

Fig 6.20- AFM studies of EL Ni-P-TiO_2 nanocomposite coatings, (a) C_3, (b) C_3 HT, (c) M_3, (d) M_3 HT, (e) I_3 and (f) I_3 HT.

The 3-D AFM images of EL Ni-P-TiO_2 nanocomposite coatings developed using conventional and non-conventional mode are displayed in figure 6.20. The AFM images clearly reveal that coating follows non-conventional route (I_3) [Fig 6.20e] has a relatively smooth surface as compared to conventionally developed coating i.e. C_3 and M_3 [Fig 6.20a,c]. It is due to the dispersion of fine TiO_2 particles. The average roughness values (Ra) obtained from AFM images for C_3, M_3 and I_3 coatings are about 18.86nm, 28.24nm and 14.8nm respectively. The highest roughness of M_3 coatings indicates to more number of milled TiO_2 particles are embedded into the Ni-P matrix as they adhere easily due its high surface energy. This creates larger sizes of island in case of M_3 coating [Fig 6.20c,d]. On the other hand, slight decrease in roughness is noticed on heat treatment. The Ra values evaluated for C_3, M_3 and I_3 coatings on heat treatment are 17.13nm, 27.02nm and 13.6nm respectively [Fig 6.20b,d,f].

6.3.4.2 XRD analysis of 'as coated' and heat treated (C_3, M_3 and I_3) nanocomposite coatings

The X-Ray diffraction patterns of EL Ni-P-TiO_2 nanocomposite coating in 'as coated' and heat treated conditions are displayed in figure 6.21. XRD studies reveals the presence of anatase form of TiO_2 peaks (JCPDS ref no.: 01-073-1764) at 25^{o}C, 47.7^{o}C and 53^{o}C apart from major microcrystalline peak of Ni (JCPDS ref no.: 00-045-1027) at 44^{o}C in all the developed nanocomposite coatings. As discusses in section 6.2.2, heat treatment induces transformation from microcrystalline nickel into crystalline Ni and the stable Ni_3P phase (JCPDS ref no.: 01-074-1384) at peaks at 42^{o}C, 36^{o}C and 46^{o}C. The heat treatment results in crystalline phases of Ni, Ni_3P, TiO_2 and Fe (JCPDS ref no.: 00-006-0696). The small peak of Fe may arise from the substrate used. It is clear that the the incorporation of TiO_2 particles into electroless Ni-P matrix shows no change in its structure as the peaks corresponding to Ni and Ni_3P remains the same.

6.3.5 Thickness of heat treated Ni-P based nanocomposite coatings

It is reported in literature that the thickness of electroless Ni-P coatings follow a linear relation with the coating time [Sorkhabi and Rafizadeh (2004)]. In the present study, all nanoccomposite coatings are developed for a fixed duration of 30 minutes. The thickness of the coatings are investigated by FESEM analysis from its transverse view using secondary [Fig 6.22a] and back scattered electrons [Fig 6.22b]. The crossectional morphology of all the nanocomposite coatings presents homogenous compact structure with thickness of ~ 30µm regardness of any surface irregularity. No pores, defects or cracks can be observed at the interface of the coating, giving an evidence of good adhesion between the mild steel substrate and the composite coating.

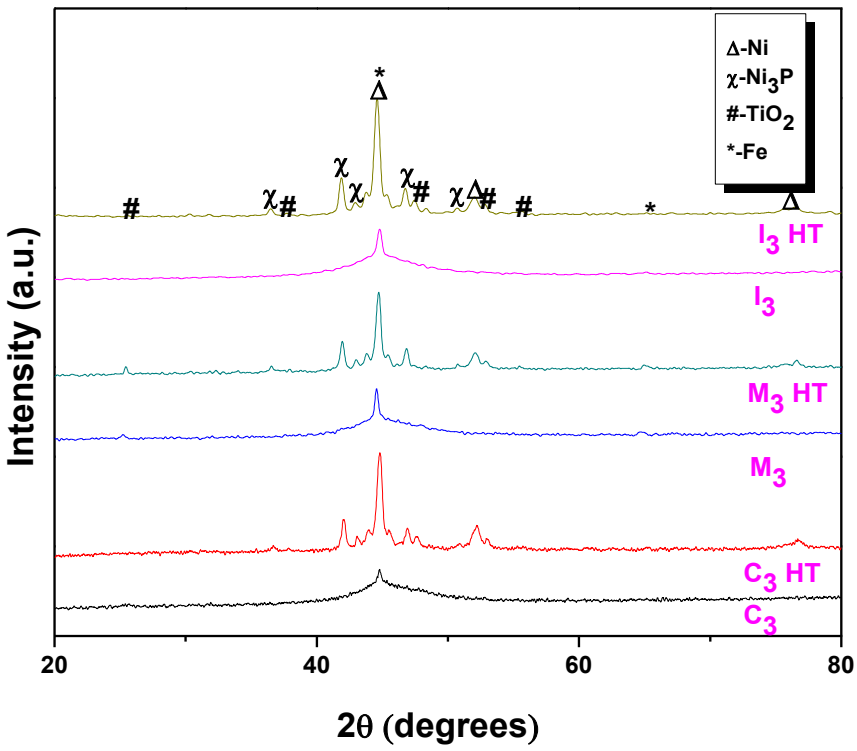

Fig 6.21- XRD patterns of EL Ni-P-TiO_2 nanocomposite coatings with different mode of synthesis, C_3, M_3 and I_3 in 'as coated' and HT conditions.

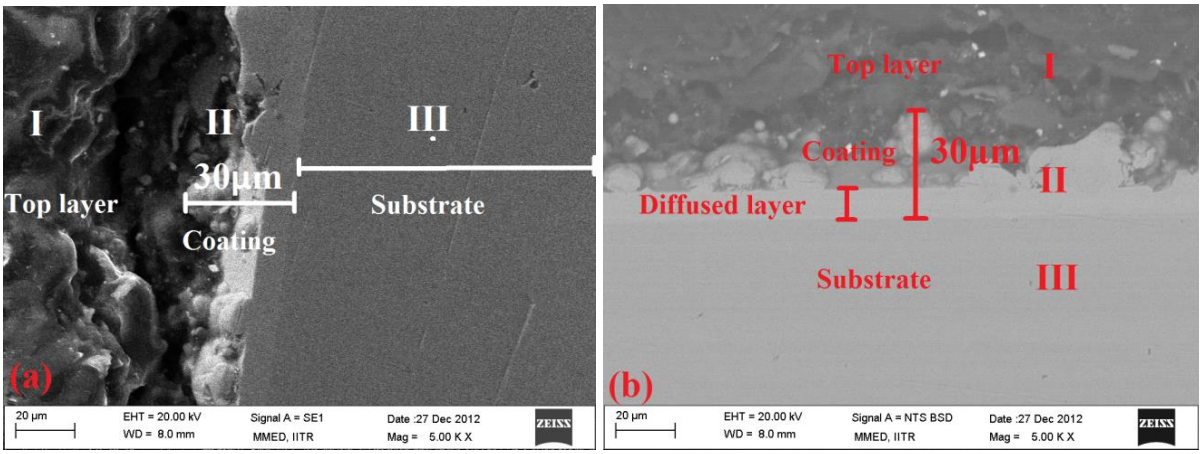

Fig 6.22- FESEM micrograph showing the crosssection of heat treated EL Ni-P based nanocomposite coating using (a) secondary electrons and (b) back scattered electrons.

6.4 HARDNESS STUDIES OF EL Ni-P ALLOY AND Ni-P-X NANOCOMPOSITE COATINGS

6.4.1 Hardness of EL *insitu* Ni-P-Al_2O_3 nanocomposite coatings developed at various concentrations

EL non-conventional Ni-P-Al_2O_3 nanocomposite coatings are developed at various concentrations as discussed in section 6.3.2.1. Figure 6.23 presents the microhardness value as a function of *insitu* precipitated Al_2O_3 particles concentration in the bath. The microhardness of Ni-P alloy coating without reinforcement is found to be 414 VHN. At lower concentrations, A_1 coating [Tabel 6.3], microhardness increases significantly upto 675 VHN. The *insitu* precipitation of 15g/l Al_2O_3 particles, A_2 nanocomposite coating, possesses the highest microhardness of 786 VHN. The upgradation in hardness upto 15g/l mainly attributed to two factors. The first one is the amount of hard or second phase particles embedded in Ni-P matrix which features the dispersion strengthening effect. The other one correlates with the microstructural change of Ni-P matrix as caused by the incorporation of second phase particles where grain refinement effect comes into picture. The strengthening mechanism evolved from particles dispersion hardening is termed as Orowan mechanism and expressed as following [Zhang and Chen (2006)]:

$$\sigma = 2\ Yb/t \qquad (6.1)$$

where 'Y' refers to the shear modulus of the coating, 'b' is the Burgers vector of the dislocation and 't' is the dispersed particles distance. According to equation 6.1, the yield stress 'σ' is evaluated by the amount of stress required for the dislocation to cross the adjacent two particles. The closer the dispersed particles distance, the efficient will be the strengthening effect. Thus, the crucial parameters that dominate the dispersion strengthening effect include particle size, particle spacing and volume fraction. An increased amount of Al_2O_3 nanoparticles precipitated in the EL bath leads to a higher entrapment of nanosized Al_2O_3 particles in the coating with shorter particle distance. The highly dispersed Al_2O_3 particles impede the dislocations mobility in the load bearing Ni-P matrix which inturn improves the hardness of the nanocomposite coatings. On the other hand, the yield stress is mathematically related with the grain size by the following Hall-Petch equation [Chen et al. (2010)]:

$$\sigma_y = \sigma_0 + k\ D^{-1/2} \qquad (6.2)$$

where 'σ_y' refers to the yield stress, 'σ_0' is the intial dislocation movement stress (material constant), 'k' corresponds to the strengthening coefficient and 'D' is the mean grain diameter. It is clear by equation 6.2 that the material strength enhances with the refining of grain size. During the coating process, as discussed earlier in section 6.3.2.1, that the embedded Al_2O_3 nanoparticles not only enhances the nucleation sites but also gets distributed in the grain

boundaries which acted as an obstacles and thus inhibit the globule (grain) growth. Hence, globule size (grain size) decreases with increase in concentration of Al_2O_3 nanoparticles as clearly shown by figure 6.8 and therefore leads to grain refinement strengthening effect. However, a larger amount of $AlCl_3$ (52g/l) in the solution or precipitation of 20g/l Al_2O_3 in the bath, A_3 coating, led to decrease in microhardness upto 523 VHN [Fig 6.23]. This decrease may be due to the fact that large number of precipitated Al_2O_3 nanoparticles starts to agglomerate and cause porous structure in the grain boundary areas which inturn reduces the dispersion strengthening and grain refinement strengthening effect. Therefore, in the present study, an optimize concentration, 15g/l, is used for sound *insitu* nanocomposite coatings in all the cases.

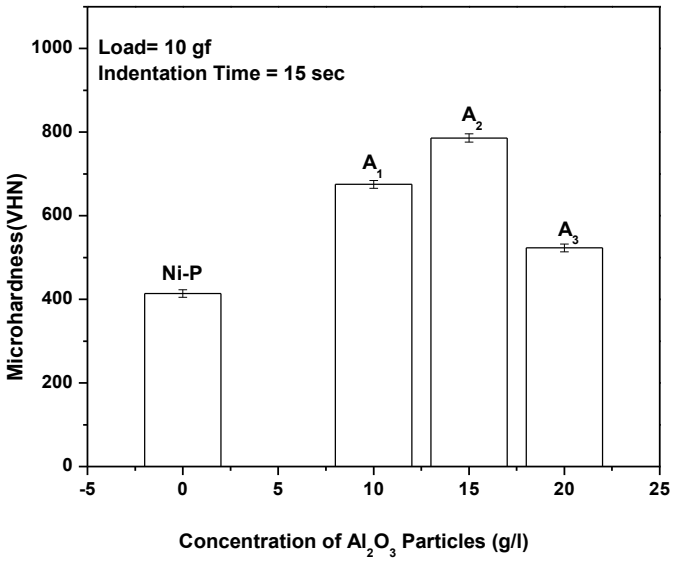

Fig 6.23- Microhardness of EL *insitu* Ni-P-Al_2O_3 nanocomposite coatings at various concentrations.

6.4.2 Hardness of EL Ni-P and Ni-P-X [Al_2O_3, ZrO_2 and TiO_2] nanocomposite coatings

Microhardness values of EL Ni-P alloy coatings, EL conventional and non-conventional Ni-P-Al_2O_3, Ni-P-ZrO_2 and Ni-P-TiO_2 nanocomposite coatings in 'as coated' and heat treated conditions is presented in figure 6.24. The average microhardness of EL Ni-P alloy coatings as listed in figure 6.24a is found to be 414 VHN. The hardness of the coating increased from 414 to 851 VHN when heat treated at 400^{o}C for 1h [Fig 6.24a]. The increment of 437 units, on heat treatment, may be due to phase transition occurring within the deposit. The transformation from amorphous Ni to crystalline Ni and precipitation of Ni_3P stable phase inturn cause Ni-P alloy to harden and produce maximum hardness like that of hard coatings [Alirezaei et al. (2004)]. The average hardness values of EL Ni-P-Al_2O_3 nanocomposite coatings developed by

conventional and non-conventional means is shown in figure 6.24b. It is observed that the incorporation of nanosized Al_2O_3 particles as reinforcement in Ni-P matrix either by conventional or *insitu* means shows an increase in hardness in 'as coated' condition. The hardness of the coatings is determined upto 618 VHN, 652 VHN and 786 VHN for C_1, M_1 and I_1 nanocomposite coatings respectively [Fig 6.24b]. The higher hardness of Al_2O_3 nanoparticles which are entrapped in Ni-P globules contributes to this increment in all the cases due to dispersion strengthening effect based upon the Orowan mechanism as explained in section 6.4.1 via equation 6.1. However, among all the coatings, the maximum hardness is noticed for *insitu* developed 'I_1' nanocomposite coating. This higher hardness is attributed to more effective dispersion strengthening effect and grain refinement as here Al_2O_3 nanoparticles with high density and very fine size are uniformly dispersed within the Ni-P matrix as discussed in section 6.4.1 [Hou et al. (2006); Zhang and Chen (2006)]. The conventional C_1 and M_1 nanocomposite coating possess comparatively lower hardness due to agglomeration of Al_2O_3 nanoparticles in certain areas resulting in non-uniform distribution of particles on Ni-P surface. Although, it is observed that the inclusion of mechanically milled Al_2O_3 nanoparticles into Ni-P matrix, M_1 coating, exhibits much higher hardness as compared to chemically synthesized nanoparticles reinforcement, C_1 coating [Fig 6.24b]. The milled particles have higher hardness due to high surface energy and adhere easily to the coating surface as evident by FESEM micrograph [Fig 6.4c,d]. So, the wettability of matrix and the reinforcement is comparatively higher and the adsorption of high number of hardened particles in Ni-P matrix results in higher hardness of the coating. The heat treatment further enhances the hardness of C_1, M_1 and I_1 nanocomposite coating to 1087 VHN, 1110 VHN and 1162 VHN respectively [Fig 6.24b]. The average hardness values of conventional and non-conventional Ni-P-ZrO_2 and Ni-P-TiO_2 nanocomposite coatings in 'as coated' and HT condition are displayed in figure 6.24c and 6.24d respectively. The hardness values of distinct Ni-P-ZrO_2 nanocomposite coatings i.e. C_2, M_2 and I_2 is found to be 570 VHN, 613 VHN and 714 VHN respectively in 'as coated' condition and 1011 VHN, 1032 VHN and 1078 VHN respectively in heat treated condition [Fig 6.24c]. The upgradation in hardness than Ni-P is attributed to the reinforcement of hard second phase ZrO_2 nanoparticles in Ni-P matrix. It is seen that the hardness values for different Ni-P-TiO_2 nanocomposite coatings i.e. C_3, M_3 and I_3 in 'as coated' condition is 510 VHN, 570 VHN and 688 VHN respectively. On heat treatment, hardness values for C_3, M_3 and I_3 nanocomposite coatings enhances to 935 VHN, 1010 VHN and 1045 VHN respectively [Fig 6.24d]. The presence of the second phase nano sized TiO_2 particles in Ni-P matrix accounts for the above increments. The same trend in hardness values are noticed by incorporation of different forms of ZrO_2 and TiO_2 nanoparticles in Ni-P matrix

as observed in Ni-P-Al_2O_3 nanocomposite coatings. The higher hardness values for M_2, M_3, I_2 and I_3 can be explained on the same basis as it can be explained for M_1 and I_1 coatings.

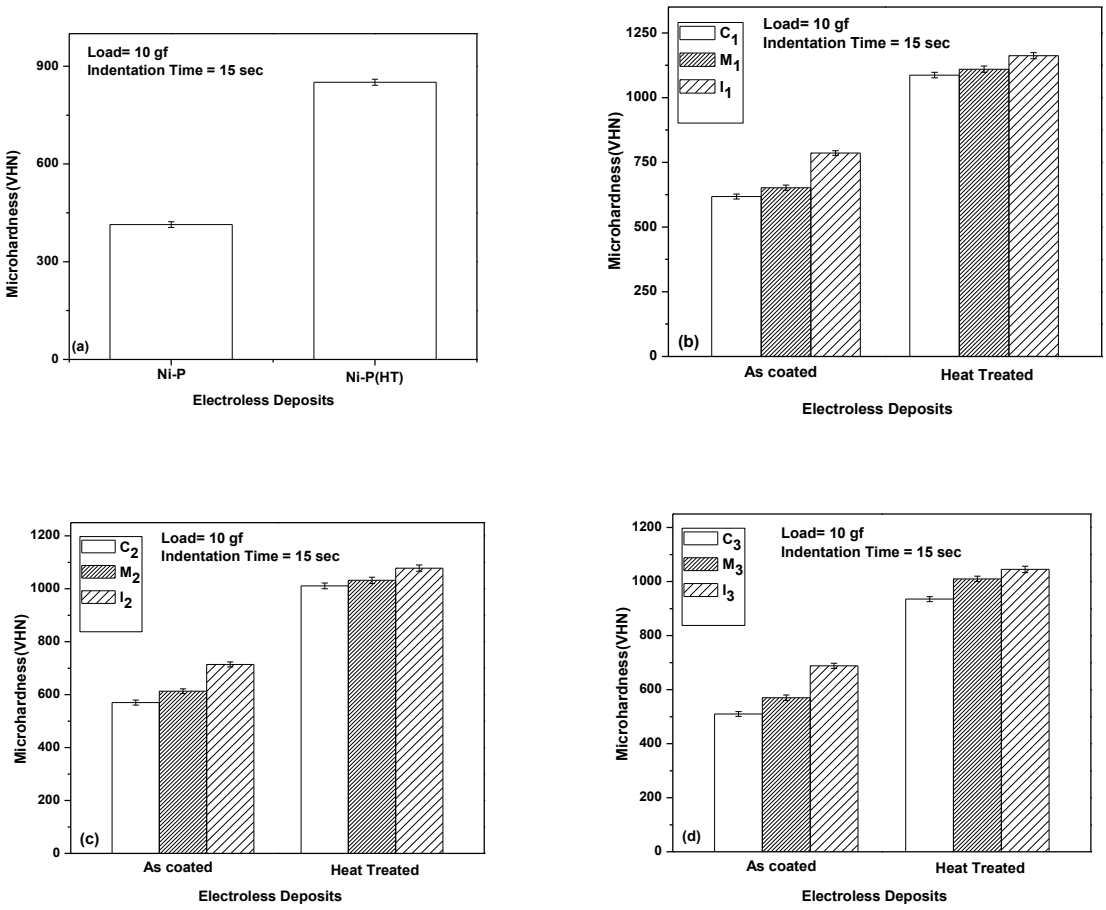

Fig 6.24- Hardness of EL coatings (a) Ni-P, (b) Ni-P-Al_2O_3 (C_1,M_1,I_1), (c) Ni-P-ZrO_2 (C_2,M_2,I_2), (d) Ni-P-TiO_2 (C_3,M_3,I_3) in 'as coated'and HT conditions.

6.5 SUMMARY

The development of conventional and non-conventional metal oxide reinforced Ni-P matrix i.e. Ni-P-X [X= Al_2O_3, ZrO_2 and TiO_2] nanocomposite coatings by electroless technique, its subsequent heat treatment and their hardness studies are discussed in this chapter. EL Ni-P alloy coatings with hemispherical globular structure are developed on mild steel substrate. Heat Treatment (400°C for 1h) causes amorphous to crystalline Ni transformation with stable Ni_3P phase. No significant change in surface morphology is observed on heat treatment. AFM studies reveal that the roughness of the coatings reduces after heat treatment. EL conventional Ni-P-X [X= Al_2O_3, ZrO_2 and TiO_2] nanocomposite coatings are developed where 'X' reinforcements used are chemically synthesized and/or mechanically milled powders. Codeposition of reinforcement 'X' into Ni-P matrix results in surface modification of the

coatings. The globular structure with the presence of nodular protrusions are analysed in FESEM micrographs and the evidence of their entrappment is determined via EDAX and X-ray mapping studies. The nanosized milled particles 'X' seems to exhibit good adherence with Ni-P matrix due to its higher surface energy. Phase analysis by XRD further confirms the presence of 'X' with Ni. The coatings have comparatively rougher surface with inclusion of milled particles in Ni-P matrix than chemically synthesized particles as reinforcement. A novel non-conventional Ni-P-X [X= Al_2O_3, ZrO_2 and TiO_2] nanocomposite coatings is also developed with the optimization of concentration of second phase particles 'X'. A typical globular structure with no clear 'X' particles [X= Al_2O_3, ZrO_2 and TiO_2] are seen on the surface of EL *insitu* Ni-P-X nanocomposite coatings. However, the existence of nanosized 'X' particles can be confirmed by virtue of their EDAX, X-ray mapping and XRD analysis. AFM studies depicts that non-conventional Ni-P-X nanocomposite coatings have relatively smooth surface than the conventional Ni-P-Al_2O_3 coatings. The thickness of the developed coatings is ~ 30µm showing good adhesion between the mild steel substrate and the coating. For optimization, EL *insitu* Ni-P-Al_2O_3 nanocomposite coatings are developed at different concentrations of alumina. The globule size decreases as Al_2O_3 content increases with increase in the concentration of second phase Al_2O_3 particles. The reactant concentration, $AlCl_3$ (39g/l) in the bath is consistent with improvement of hardness (786 VHN) due to the dispersion strengthening and grain refinement strengthening effect. Heat treatment enhances hardness of Ni-P coatings from 414 to 851 VHN due to the precipitation of Ni_3P phase. All developed EL Ni-P-X nanocomposite coatings exhibits higher hardness than Ni-P deposits due to the reinforcement of hard second phase in the Ni-P matrix. EL Ni-P-Al_2O_3 nanocomposite coatings following non-conventional (*insitu*) route are found to attain higher hardness (1162 VHN) as compared to conventionally developed coatings reinforced with milled (1110 VHN) and chemically synthesized Al_2O_3 particles (1087 VHN). It is probably due to the fine size uniform dispersion of Al_2O_3 particles without coagulation in the Ni-P matrix. Also, it is found that the inclusion of milled nanoparticles provides slightly higher hardness with respect to chemically synthesized nanoparticles due to the better adherence of milled particles on Ni-P surface. Similar trend is followed for hardness values in case of EL Ni-P-ZrO_2 and Ni-P-TiO_2 nanocomposite coatings.

CHAPTER 7

WEAR AND CORROSION STUDIES OF EL Ni-P AND Ni-P-X NANOCOMPOSITE COATINGS

7.1 INTRODUCTION

This chapter discusses the results obtained on the friction, wear and corrosion resistance of conventional and non-conventional EL Ni-P-X [X= Al_2O_3, ZrO_2 and TiO_2] nanocomposite coatings and compared with Ni-P alloy coatings. Section 7.2 includes the wear and friction characteristics of EL Ni-P alloy coatings. The wear and friction studies of all developed EL Ni-P-X nanocomposite coatings are discussed in section 7.3. The corrosion studies of EL Ni-P alloy coatings and Ni-P-X nanocomposite coatings before and after heat treatment are explained in section 7.4 and 7.5 respectively. The developed Ni-P-X nanocomposite coatings are indexed with the same notations as introduced in chapter 6 [Table 6.2].

7.2 WEAR AND FRICTION STUDIES OF EL Ni-P ALLOY COATINGS

7.2.1 Wear rate

The degree of wear is described by specific wear rate. The wear rate 'W' depends on the applied load 'F', nominal area 'An', sliding velocity 'v', materials properties and geometry of the surface [Lim and Ashby (1990)]. The variation in specific wear rate of EL Ni-P alloy coatings at varying loads and sliding velocities are shown in figure 7.1. The wear rate of Ni-P alloy coating is calculated to be 0.98, 2.87 and 4.3e-06 mm^3/Nm at 1, 1.5 and 2N loads [Fig 7.1a]. The wear rate of EL Ni-P alloy coatings at sliding velocities 0.1 and 0.2m/s under constant 1N load comes out to be 0.98 and 2.84e-06 mm^3/Nm [Fig 7.1b]. It is observed that with increase in the applied load and sliding velocity, the wear rate increases. The result is described empirically by Archard's law given as

$$W=K_aF \quad (7.1)$$

Where 'W' is the wear rate, 'K_a' is the constant and 'F' is applied load [Lim and Ashby (1990); Pathak et al. (2005)].

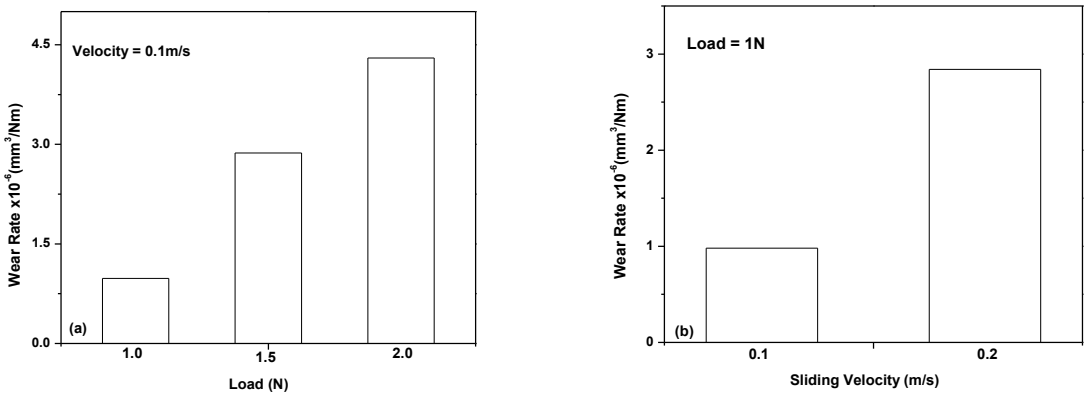

Fig 7.1- Variation in wear rate of heat treated EL Ni-P alloy coatings at varying (a) Loads and (b) Sliding velocities.

7.2.2 Friction studies

The studies of variation of friction coefficient with the sliding distance under 1, 1.5 and 2N loads at constant sliding speed of 0.1m/s for EL Ni-P alloy coatings is shown in figure 7.2a. The friction coefficient of EL Ni-P alloy coatings initially follows a linear behavior with the sliding distance followed by almost constant behavior. The friction coefficient of EL Ni-P coatings is found to increase (0.40 to 0.63) with increase in loads (1 to 2N). This accounts for the increase in the real contact area between the coating and testing counterface which increases with load [Dennis and Sagoo (1991); Dwivedi et al. (2011)]. It is noticed that the friction coefficient increases with increase in sliding velocities [Fig 7.2b]. The friction coefficient at varying velocities of 0.1m/s and 0.2m/s is found to be around 0.41 and 0.46 respectively.

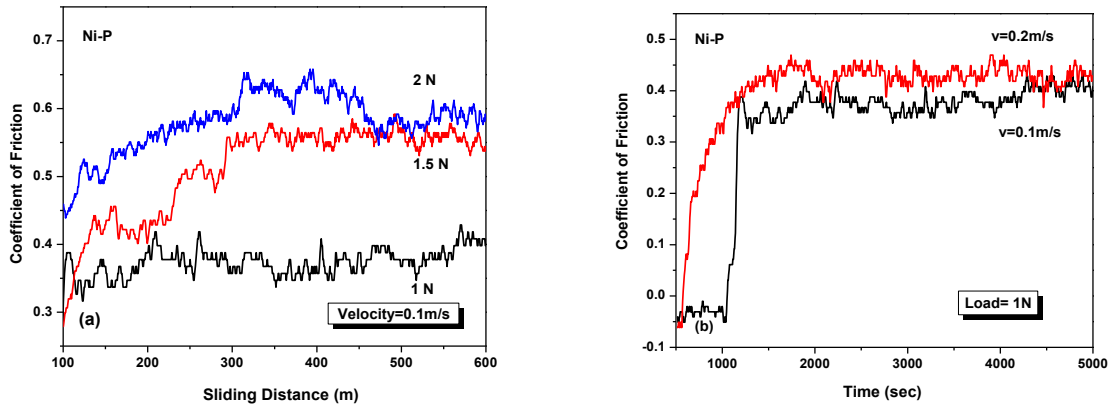

Fig 7.2- (a) Effect of sliding distance on the friction coefficient of EL Ni-P alloy coating at varying loads, (b) Variation of friction coefficient of EL Ni-P alloy coating with different sliding velocities.

7.2.3 Morphological studies of worn surfaces

The wear tracks of EL Ni-P alloy coatings at varying loads (1, 1.5, 2N) under 0.1m/s sliding velocity are shown by FESEM micrographs in figures 7.3a-c. The worn surface of Ni-P coating under 1N load at 0.2m/s sliding velocity is shown in figure 7.3d. Here, the worn surfaces are characterised by longitudinal grooves with partial irregular pits [Figs 7.3a-d] and cracks [Figs 7.3b-d] along the sliding direction. This symbolises the occurrence of microcutting and microploughing effect of the counterface, whereas pits indicate ductile fracture. When the contacting surfaces slide, nearly all the work done against friction shows up as heat. At lower sliding velocities (0.1 and 0.2m/s), no significant heat is generated and cold mechanisms are thus responsible for the wear which are dependent on material transfer by plasticity and crack growth [Lim and Ashby (1990)]. Adhesive wear mechanism is involved as indicated by worn surfaces of EL Ni-P alloy coatings [Gawne and Ma (1987)].

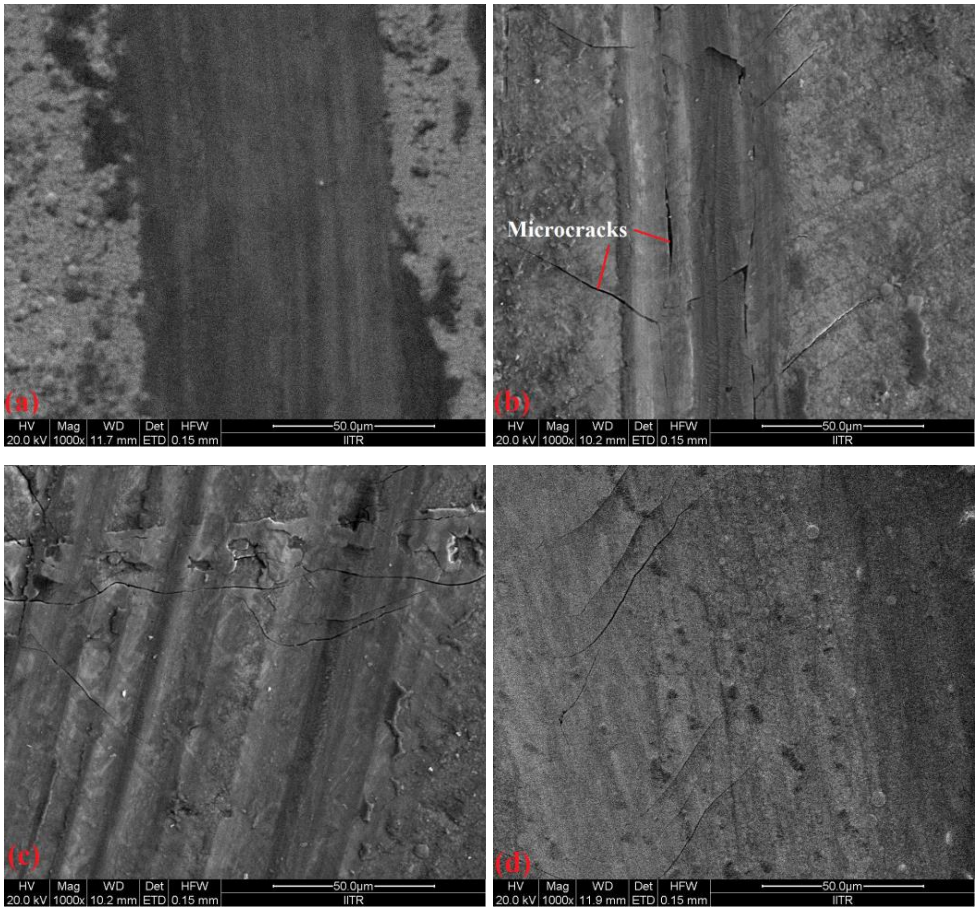

Fig 7.3- FESEM micrographs of EL Ni-P coatings under loads (a) 1 N, (b) 1.5 N, (c) 2 N at 0.1m/s sliding velocity and (d) Under 1 N load at 0.2m/s sliding velocity after wear tests.

7.3 WEAR AND FRICTION STUDIES OF EL Ni-P-X [Al_2O_3, ZrO_2 and TiO_2] NANOCOMPOSITE COATINGS

7.3.1 EL Ni-P-Al_2O_3 nanocomposite coatings (C_1, M_1 and I_1)

7.3.1.1 Wear Rate

The effect of loads (1, 1.5 and 2N) and sliding velocities (0.1 and 0.2m/s) on the specific wear rate of EL Ni-P-Al_2O_3 nanocomposite coatings developed by conventional and non-conventional means in HT condition are shown in figure 7.4 and indexed as C_1, M_1 and I_1 [Table 6.2]. At 0.1m/s sliding velocity, the wear rate of C_1 nanocomposite coatings under different loads of 1, 1.5 and 2N is calculated as 0.21, 0.72 and 1.56e-06 mm^3/Nm respectively. While for M_1 coatings, the wear rate comes out to be 0.18, 0.64 and 1.45e-06 mm^3/Nm respectively and for I_1 coatings, the wear rate is 0.14, 0.49 and 1.28e-06 mm^3/Nm respectively. The wear rate of I_1 nanocomposite coating developed by non-conventional mode is found to be minimal among all the coatings C_1 and M_1 developed by conventional mode [Fig 7.4a]. The uniform distribution of highly dispersed Al_2O_3 nanoparticles in case of I_1 coatings strengthens the Ni-P matrix more effectively as discussed in section 6.4.1. The excellent wear resistance is attributed to the higher hardness of I_1 nanocomposite coating [Fig 6.24b], which facilitates the coating to experience lesser wear as compared with C_1 and M_1 coatings. It seems that the wear resistance of C_1, M_1 and I_1 nanocomposite coatings is in resonance with the microhardness values. The wear rate of I_1 nanocomposite coatings under 1N constant load at sliding velocities of 0.1 and 0.2m/s are calculated as 0.14 and 0.52e-06 mm^3/Nm respectively and is found to be lower than C_1 (0.21 and 0.68e-06 mm^3/Nm) and M_1 (0.18 and 0.61e-06 mm^3/Nm) nanocomposite coatings [Fig 7.4b]. It is being noticed that the wear rate increases with increase in applied loads [Fig 7.4a] and velocities [Fig 7.4b] for all the developed coatings like Ni-P alloy coatings [Fig 7.1]. This can be explained on the basis of Archard's law given in equation 7.1. It is also observed that the wear rate of EL Ni-P-Al_2O_3 nanocomposite coatings [Fig 7.4] is found to lesser than that of Ni-P alloy coatings [Fig 7.1], both at different loads and sliding velocities. The higher hardness of Al_2O_3 reinforced Ni-P matrix nanocomposite coatings accounts for the reduced wear. It is reported that the presence of reinforcement can cause an improvement in the wear resistance of the composite material only if the dimensions of the particles damage in terms of extraction of particles from the matrix or cracking is almost negligible as compared with the effect due to the increase in hardness of the material [Colaco and Vilar (2003)]. The incorporation of nanosized Al_2O_3 particles may delay the movement of dislocations and thus inhibit plastic deformation which can be clearly seen by FESEM micrographs of the worn surfaces [Fig 7.7-7.9].

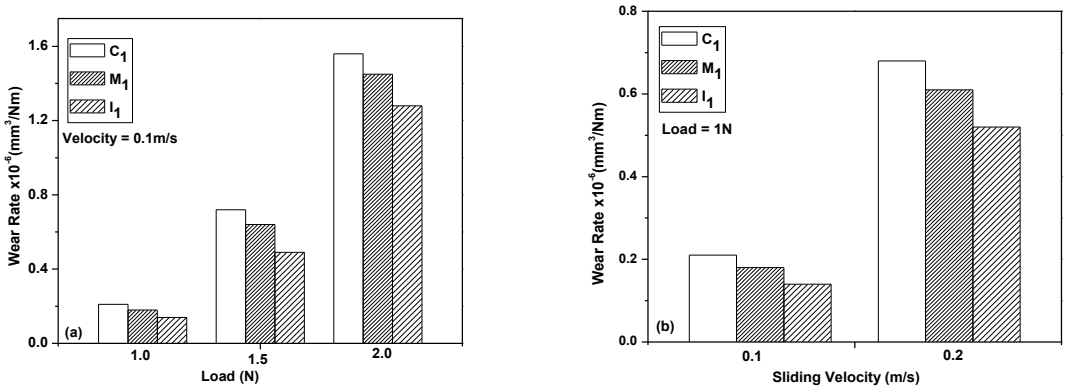

Fig 7.4- Variation in wear rate of heat treated EL C_1, M_1 and I_1 nanocomposite coatings at varying (a) Loads and (b) Sliding velocities.

7.3.1.2 Friction studies

Figure 7.5 reveals the variation of coefficient of friction with sliding distance of C_1, M_1 and I_1 nanocomposite coatings under 1, 1.5 and 2N loads. The composite coatings are greatly affected by the load and sliding velocity. The coefficient of friction for C_1, M_1 and I_1 nanocomposite coating increases with the increase in sliding distance, attains maximum value and then maintain at constant level [Fig 7.5]. The increment in coefficient of friction with sliding distance is attributed towards the mutual contributions from the adhesion between the surfaces as well as ploughing of the steel ball by hard second phase Al_2O_3 nanoparticles embedded in the electroless nickel matrix [Dennis and Sagoo (1991)]. The coefficient of friction increases from 0.18 to 0.36 for C_1 nanocomposite coatings with increase in load from 1N to 2N respectively as the real contact area between the nanocomposite coating and counterface steel ball increases with increase in load. Similarly, for M_1 and I_1 nanocomposite coatings, the increment in friction coefficient from 0.16 to 0.28 and 0.14 to 0.25 respectively are observed with varying loads from 1N to 2N. It is also found that the coefficient of friction of C_1 (0.18, 0.27), M_1 (0.17, 0.24) and I_1 (0.14, 0.22) nanocomposite coatings increases with increase in sliding velocity from 0.1m/s to 0.2m/s [Fig 7.6]. I_1 nanocomposite coatings show lowest coefficient of friction with respect to C_1 and M_1 coatings with sliding distance [Fig 7.5c]. It is due to the higher hardness of I_1 nanocomposite coatings achieved by highly dispersed Al_2O_3 reinforcement and presence of Ni_3P phase after annealing [Fig 6.24b]. Compared with Ni-P alloy coatings [Fig 7.2a], the friction coefficient of C_1, M_1 and I_1 nanocomposite coatings [Fig 7.5] is found to be lowered. The decrement may be due to the change in surface morphology on inclusion of Al_2O_3 nanoparticles or its rolling effect on the surface of the Ni-P matrix. The higher hardness of reinforced Al_2O_3 nanoparticles in Ni-P matrix probably contributes to this

decrement [Fig 6.24b]. It is reported that the impregnation of nanosized particles into the coating could modify the friction mechanism to adhesive one from a combined adhesive and abrasion mechanism [Liu et al. (2007)]. Similar results on Al_2O_3 reinforcement on Ni-P matrix was revealed by Li et al. (2013).

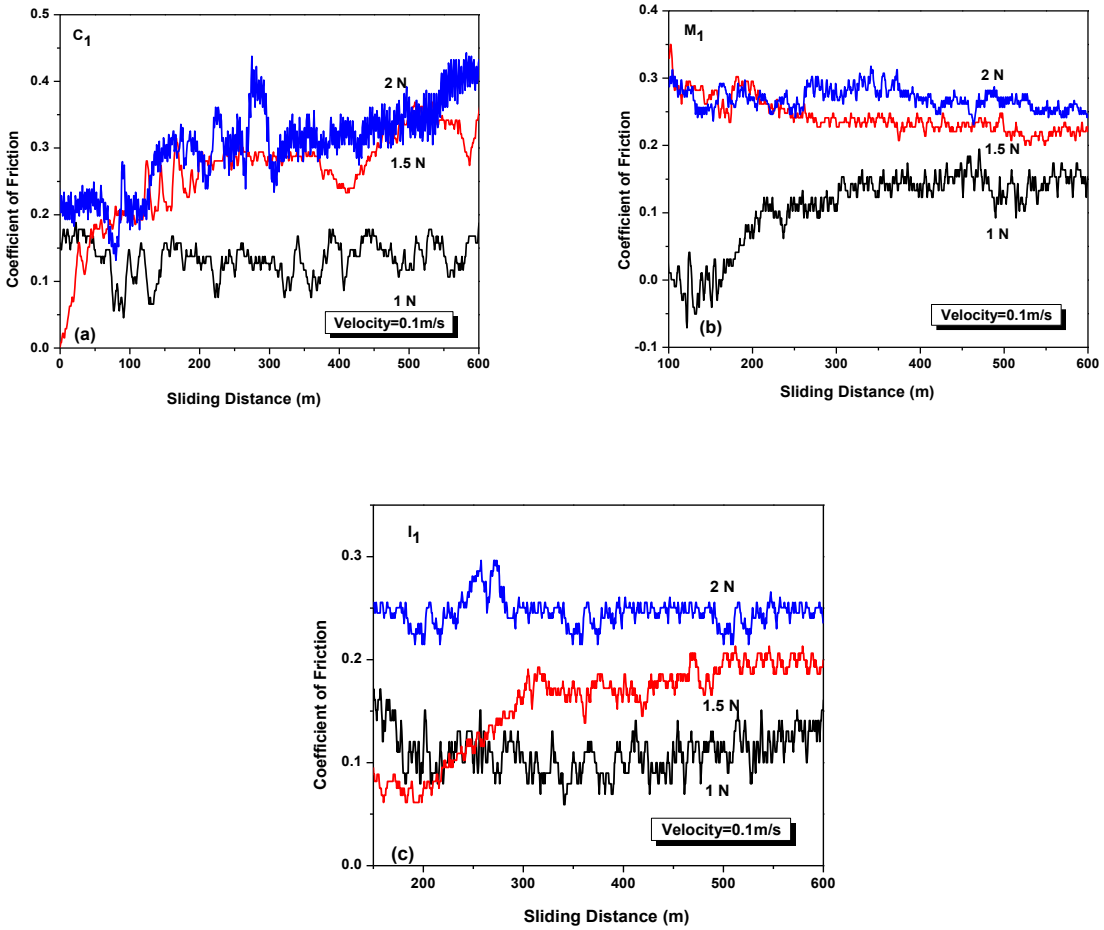

Fig 7.5- Effect of sliding distance on the coefficient of friction of (a) C_1, (b) M_1 and (c) I_1 nanocomposite coating at varying loads.

7.3.1.3 Morphological studies of worn surfaces

FESEM micrographs of the worn surfaces of C_1 nanocomposite coatings under 1N and 2N loads at sliding velocity of 0.1m/s is shown in figures 7.7a and 7.7b. Figure 7.7c shows the worn surface of C_1 coating under 1N load at sliding velocity of 0.2m/s. In the similar way, the worn surfaces of M_1 and I_1 nanocomposite coatings are displayed by figures 7.8 and 7.9 respectively. The wear tracks of C_1, M_1 and I_1 nanocomposite coatings is characterised by the presence of longitudinal grooves along the sliding direction. The presence of grooves indicates the microcutting and microploughing effect of the counterface. The worn surfaces of C_1, M_1 and I_1 nanocomposite coatings, unlike Ni-P coatings [Fig 7.3], seems to have wider grooves and is hard adhered may be due to the oxidation of the surface and severe wear of the

counterpart by the Al_2O_3 incorporated Ni-P matrix composite [Fig 7.7-7.9]. In case of I_1 nanocomposite coatings, it is seen that load is taken by some of the nodules as the globules are worn on the top only while the lower part remain undeformed which indicates that the coating is found to be most hard adhered [Fig 7.9]. This may be due to the fine dispersion of hardened Al_2O_3 particles reinforced in Ni-P matrix [Fig 6.24b]. Mild adhesive wear is the predominant mechanism taking place during wear for all the nanocomposite coatings. Similar mechanism was reported by Zhou et al. (2008) on inclusion of nano alumina on Ni-P matrix.

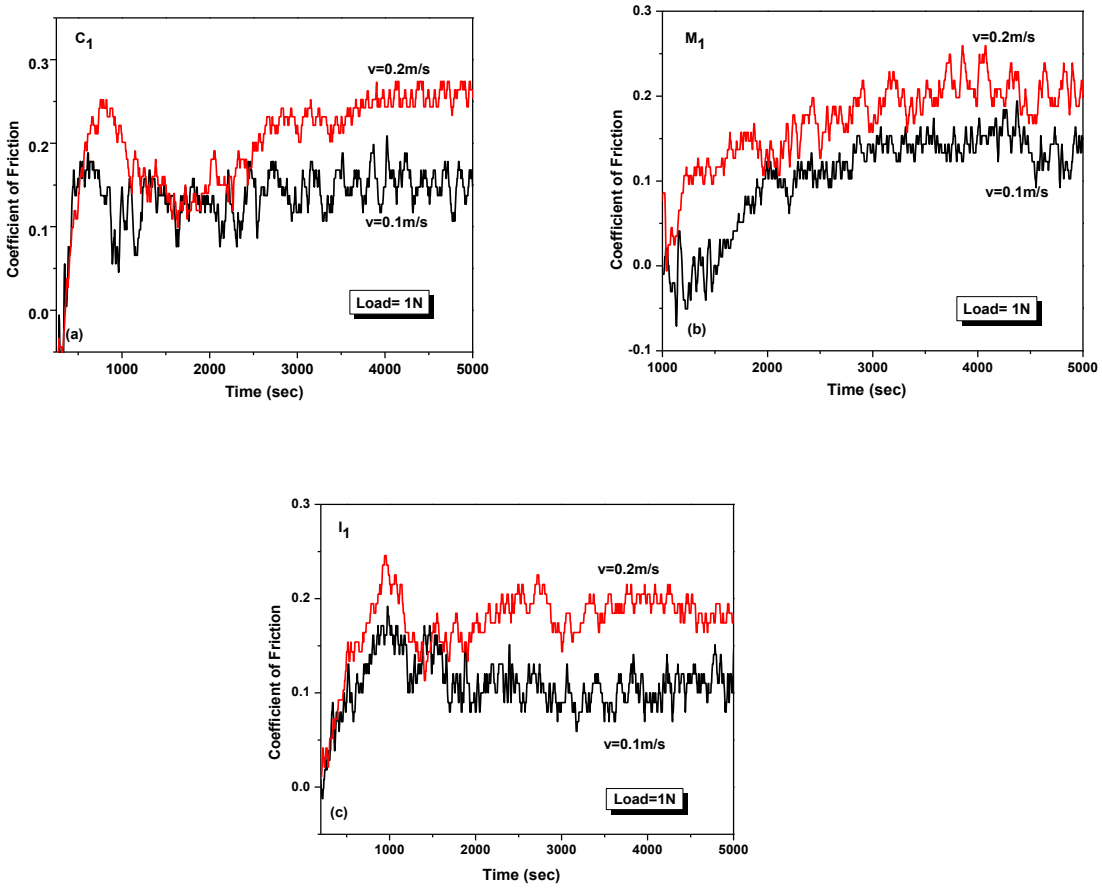

Fig 7.6- Variation of friction coefficient of (a) C_1, (b) M_1 and (c) I_1 nanocomposite coatings with sliding velocities.

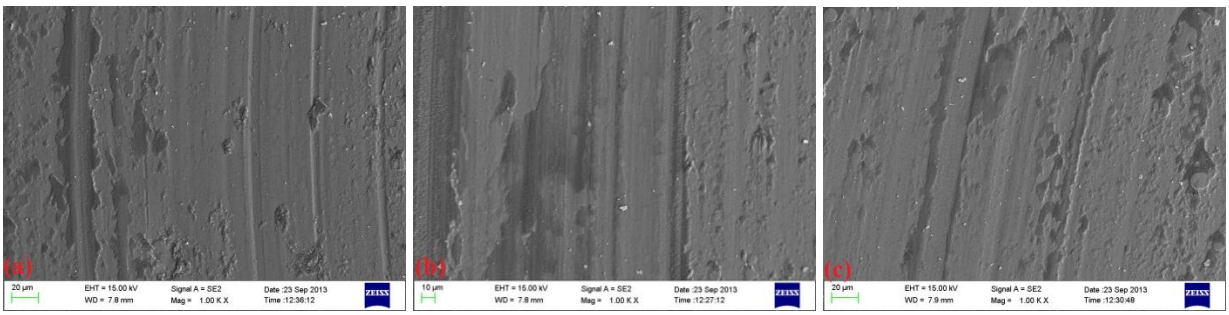

Fig 7.7- FESEM micrographs of C_1 nanocomposite coatings under loads, (a) 1N, (b) 2N at 0.1m/s velocity and (c) Under 1N load at 0.2m/s sliding velocity after wear tests**.**

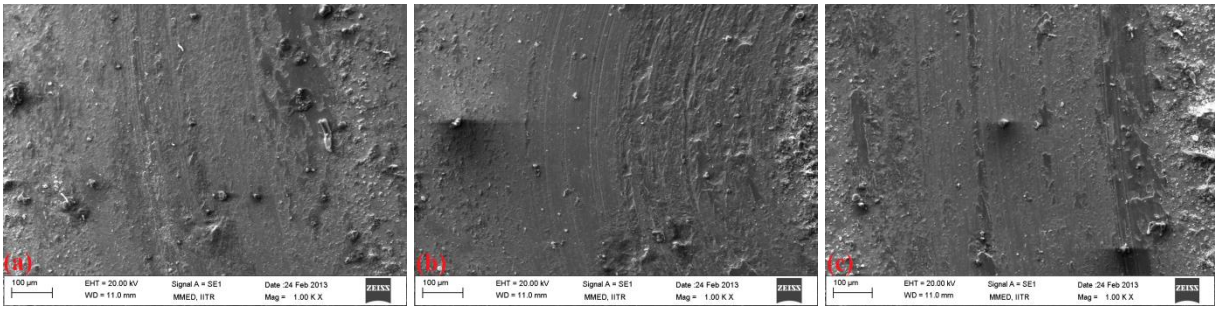

Fig 7.8- FESEM micrographs of M_1 nanocomposite coatings under loads, (a) 1N, (b) 2N at 0.1m/s sliding velocity and (c) Under 1N load at 0.2m/s sliding velocity after wear tests.

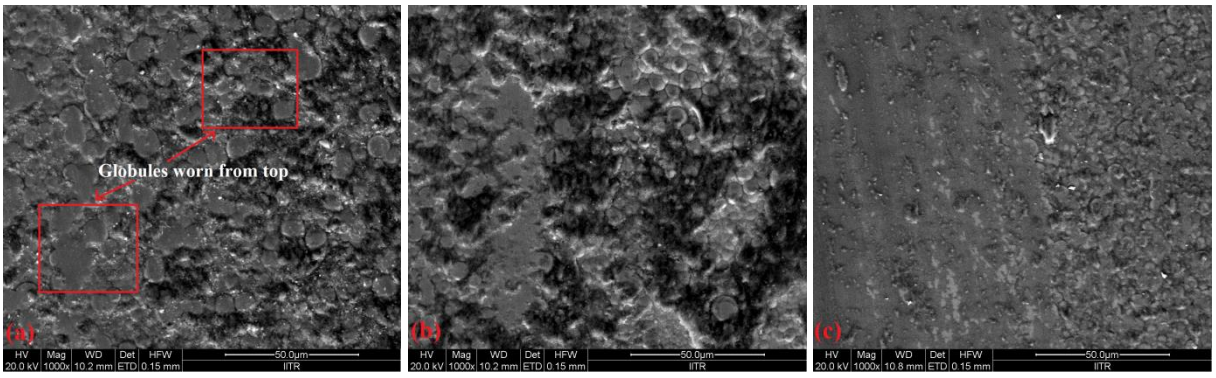

Fig 7.9- FESEM micrographs of I_1 nanocomposite coatings under loads, (a) 1N, (b) 2N at 0.1m/s sliding velocity and (c) Under 1N load at 0.2m/s sliding velocity after wear tests.

7.3.2 EL Ni-P-ZrO_2 nanocompositecoatings (C_2, M_2 and I_2)

7.3.2.1 Wear Rate

The variation in specific wear rate of heat treated EL conventional (C_2, M_2) and non-conventional (I_2) Ni-P-ZrO_2 nanocomposite coatings at varying loads and sliding velocities are shown in figure 7.10. The specific wear rate of nanocomposite coatings under 1, 1.5 and 2N loads at 0.1m/s sliding velocity is calculated as 0.29, 0.84, 1.72e-06 mm^3/Nm for C_2; 0.22, 0.75, 1.63e-06 mm^3/Nm for M_2 and 0.17, 0.62, 1.48e-06 mm^3/Nm for I_2 coatings respectively [Fig 7.10a]. The wear rate of nanocomposite coatings under 1N load at linear velocities of 0.1 and 0.2m/s is found to be 0.29 and 0.81e-06 mm^3/Nm for C_2; 0.22 and 0.72e-06 mm^3/Nm for M_2 and 0.17 and 0.60e-06 mm^3/Nm for I_2 nanocomposite coatings [Fig 7.10b]. It is observed that the wear rate of I_2 nanocomposite coating is lower than that of the C_2 and M_2 coatings at different loads [Fig 7.10a] and velocities [Fig 7.10b]. The higher hardness of the I_2 nanocomposite coatings is the main reason for rendering the coating to experience lower wear than C_2 and M_2 nanocomposite coatings. It is also seen that the calculated wear rates of heat

treated Ni-P-ZrO_2 (C_2, M_2, I_2) nanocomposite coatings [Fig 7.10a] are seemingly higher than that of plane Ni-P alloy coatings [Fig 7.1a]. It is attributed to the dispersion strengthening and load support function of ZrO_2 nanoparticles in the coating explained in section 6.4.2 [Yang et al. (2011)]. The movement of the dislocations is delayed due to the entrapment of ZrO_2 nanoparticles into the coating. The inhibition in the movement saves the substrate from plastic deformation, which is clearly noticed by FESEM micrographs of worn surfaces [Figs 7.13-7.15]. For C_2, M_2 and I_2 nanocomposite coatings, with increase in the applied loads [Fig 7.10a] and speeds [Fig 7.10b] the rate of wear increases following Archard's law given in equation 7.1.

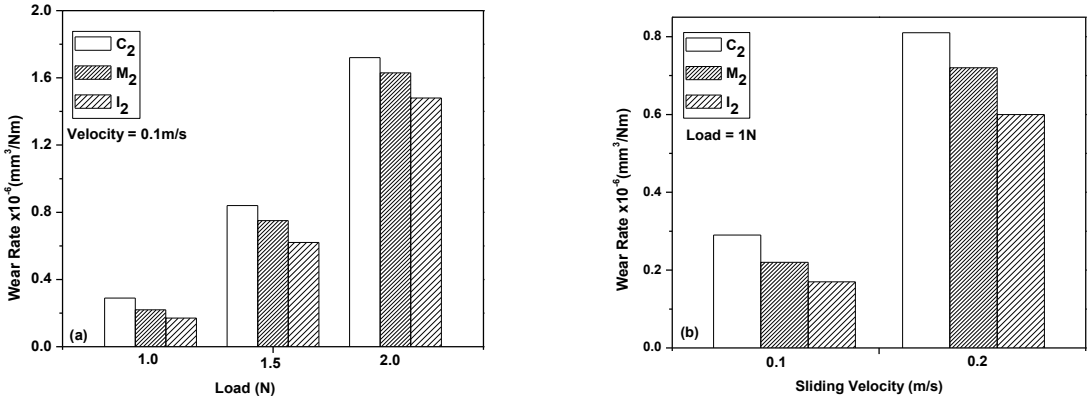

Fig 7.10- Variation in wear rate of heat treated C_2, M_2 and I_2 nanocomposite coatings at varying (a) Loads and (b) Sliding velocities.

7.3.2.2 Friction studies

The studies of variation of friction coefficient with the sliding distance under 1, 1.5 and 2N loads for C_2, M_2 and I_2 nanocomposite coatings at constant sliding speed of 0.1m/s is shown in figure 7.11. It is observed that the friction coefficient of C_2, M_2 and I_2 nanocomposite coatings initially increases with the sliding distance followed by constant behavior [Fig 7.11]. The average friction coefficient of nanocomposite coatings is found to increase for C_2 (0.23 to 0.36), M_2 (0.21 to 0.33) and I_2 (0.18 to 0.27) with increase in loads (1 to 2 N). It may be due to the fact that with increase in load, the real contact area between the nanocomposite coating and counterface steel ball increases. The lowest coeffient of friction is notified by I_2 nanocomposite coatings. It is attributed to the higher hardness of the I_2 coating with respect to effective dispersion of ZrO_2 particles in Ni-P matrix [Fig 6.24c]. It is also pointed out that the friction coefficient increases with increase in sliding velocities [Fig 7.12]. The friction coefficient at varying velocities of 0.1m/s and 0.2m/s is found to be around 0.23 and 0.32 for C_2; 0.21 and 0.29 for M_2 and 0.18 and 0.23 for I_2 respectively. It is found that the friction coefficients of the

C_2, M_2 and I_2 nanocomposite coating decreases with sliding distance [Fig 7.11] as compared with Ni-P alloy coating [Fig 7.2a]. The lower coefficient of friction accounts to higher hardness attained by heat treated C_2, M_2 and I_2 nanocomposite coating due to the trapping of zirconia particles in Ni-P matrix and precipitation of Ni_3P phase by heat treatment [Fig 6.24c]. Same observations were made by Gay et al. (2007) for inclusion of ZrO_2 particles in Ni-P matrix.

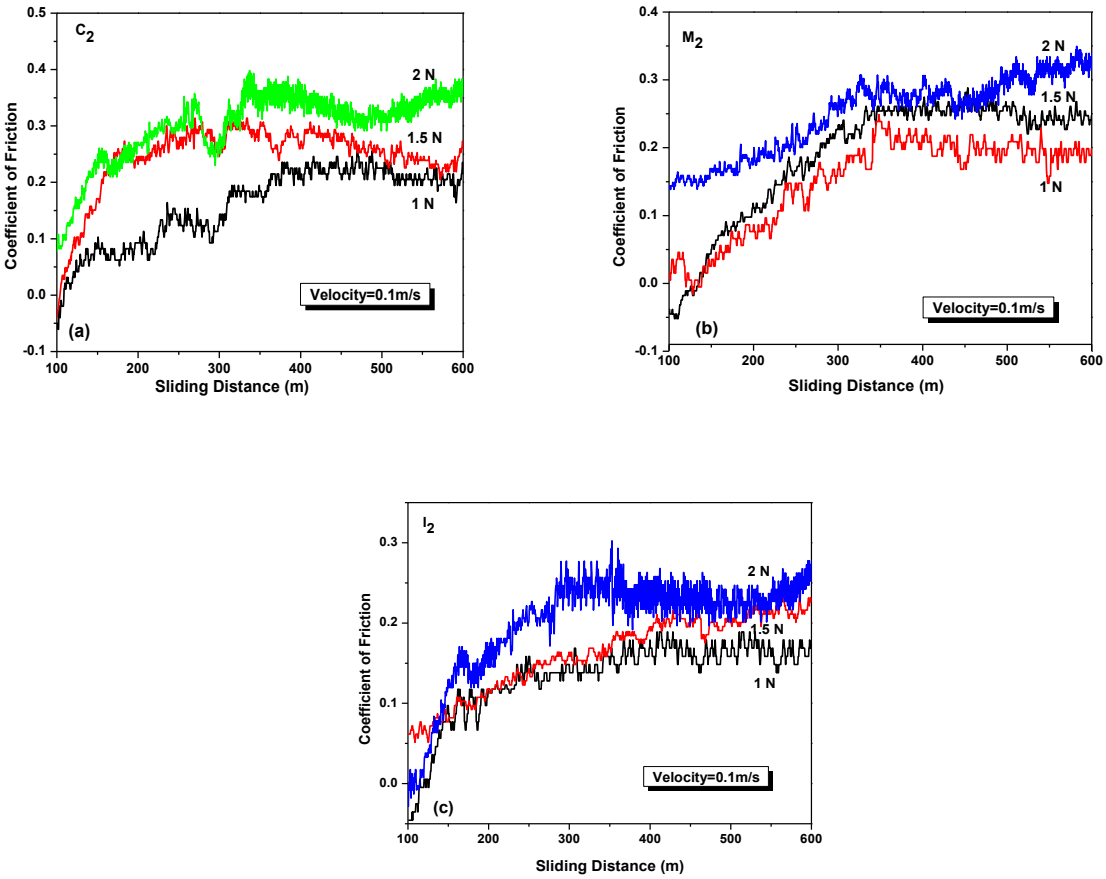

Fig 7.11- Effect of sliding distance on the coefficient of friction of (a) C_2, (b) M_2 and (c) I_2 nanocomposite coatings at varying loads.

7.3.2.3 Morphological Studies of worn surfaces

Figure 7.13 shows the wear tracks for the C_2 nanocomposite coating under different loads of 1N and 2N at 0.1m/s sliding velocity, also under 1N load at 0.2m/s sliding velocity. Similarly, the wear tracks of M_2 and I_2 nanocomposite coatings are presented in figure 7.14 and 7.15 respectively. The wear tracks of non-conventional I_2 nanocomposite coatings [Fig 7.15] seem lesser narrow with shallow plough lines than conventional C_2 [Fig 7.13] and M_2 [Fig 7.14] coatings. This indicates an improved wear resistance of the novel I_2 nanocomposite coatings compared to C_2 and M_2 nanocomposite coatings. This may be due to the uniform distribution of fine nanosized second phase ZrO_2 particles in Ni-P matrix without the agglomeration [Figs

6.14e,f]. The uniform dispersion of ZrO_2 nanoparticles can strengthen the Ni-P matrix more effectively than conventional ones as noticed in figure 6.24c. It is also shown from the wear tracks that the codeposition of ZrO_2 nanoparticlesin Ni–P matrix [Fig 7.13-7.15] leads to hard adhered coatings with lesser wear than plane Ni-P coating [Fig 7.3]. This infers to the higher hardness of the nanocomposite coatings due to the existence of ZrO_2 nanoparticles in the Ni-P coating [Fig 6.24c]. The predominant mechanism noticed for wear in all the nanocomposite coatings is mild adhesive wear.

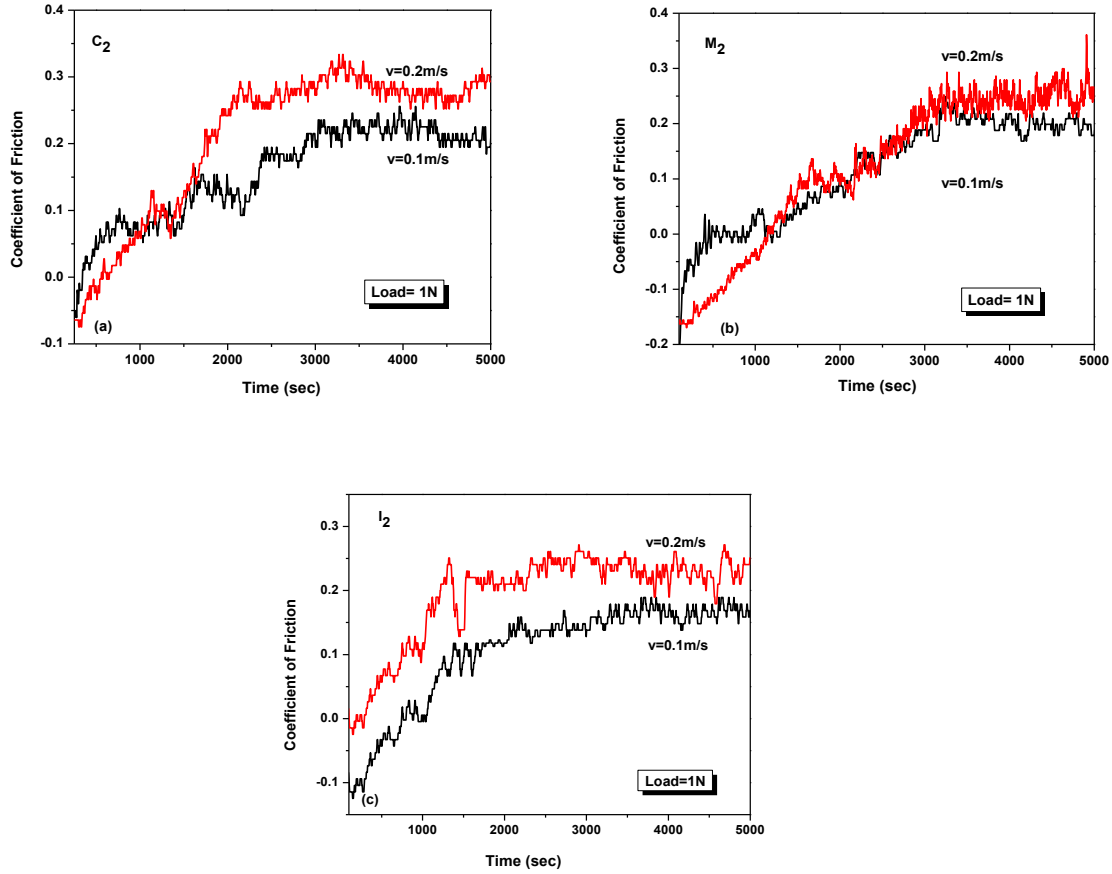

Fig 7.12- Variation of friction coefficient of (a) C_2, (b) M_2 and (c) I_2 nanocomposite coatings with sliding velocities.

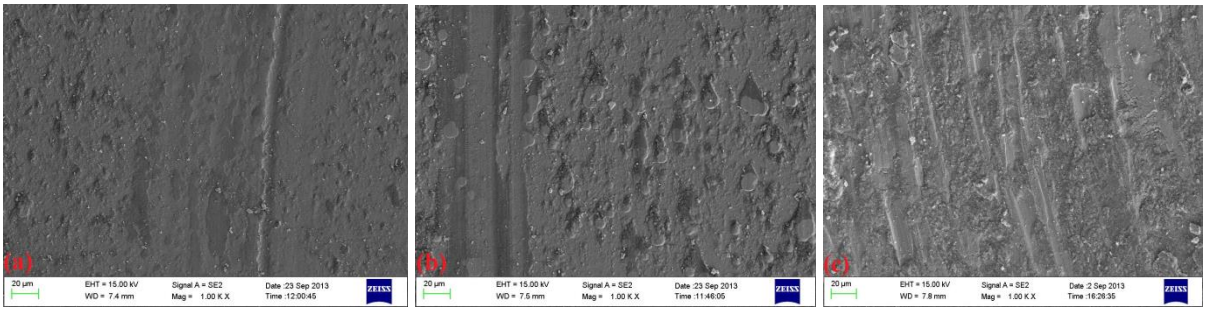

Fig 7.13- FESEM micrographs of C_2 nanocomposite coatings under loads, (a) 1N, (b) 2N at 0.1m/s velocity and (c) Under 1N load at 0.2m/s sliding velocity after wear tests.

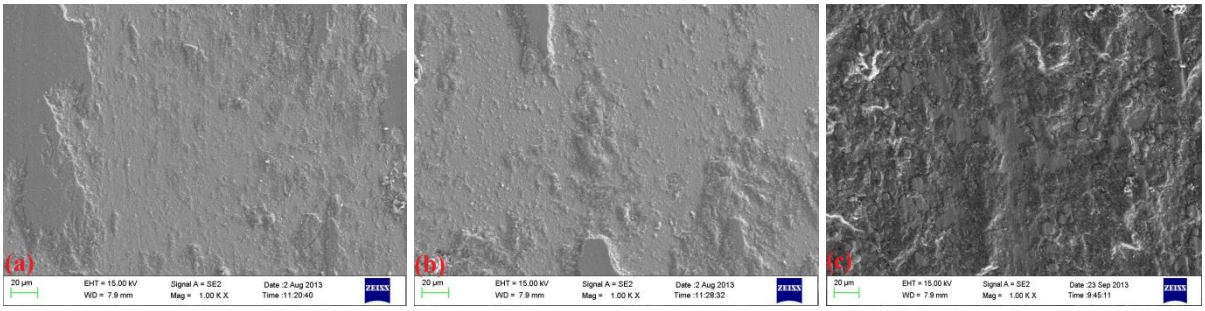

Fig 7.14- FESEM micrographs of M_2 nanocomposite coatings under loads, (a) 1N, (b) 2N at 0.1m/s sliding velocity and (c) Under 1N load at 0.2m/s sliding velocity after wear tests.

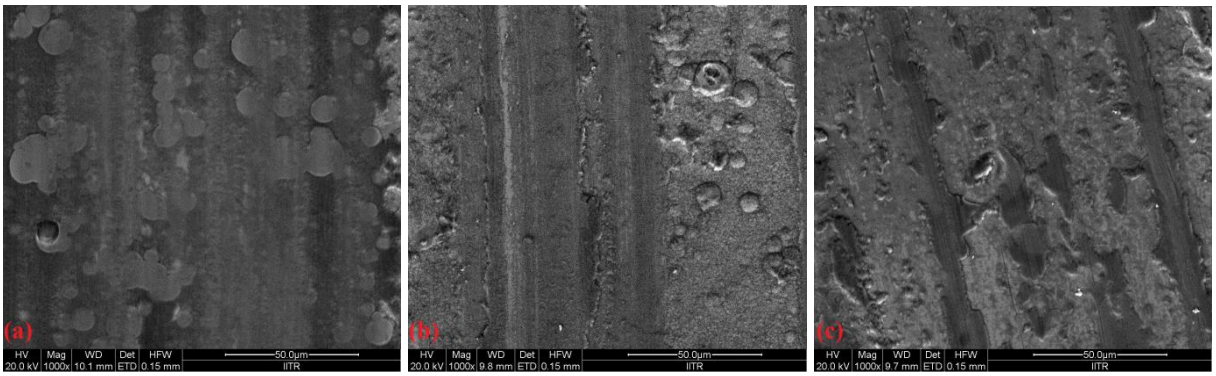

Fig 7.15- FESEM micrographs of I_2 nanocomposite coatings under loads, (a) 1N, (b) 2N at 0.1m/s sliding velocity and (c) Under 1N load at 0.2m/s sliding velocity after wear tests.

7.3.3 EL Ni-P-TiO_2 nanocompositecoatings (C_3, M_3 and I_3)

7.3.3.1 Wear Rate

Figure 7.16 shows the comparison of the specific wear rates of heat treated EL Ni-P-TiO_2 nanocomposite coatings developed by conventional (C_3, M_3) and non-conventional (I_3) modes at varying loads and sliding velocities. It is revealed that *insitu* developed I_3 nanocomposite coating offer lesser wear rate and hence better wear resistance than the conventional C_3 and M_3 coatings. At 0.1m/s sliding velocity, the wear rate of C_3 and M_3 nanocomposite coating at 1, 1.5 and 2N loads are found to be 0.40, 1.22, 2.18e-06 mm^3/Nm and 0.33, 1.16, 2.09e-06 mm^3/Nm respectively. While the wear rate of I_3 nanocomposite coatings is found to be the least, 0.24, 1.04, 1.97e-06 mm3/Nm at varying loads of 1, 1.5 and 2N [Fig 7.16a]. The wear rate of I_3 nanocomposite coatings are calculated as 0.24 and 0.98e-06 mm^3/Nm at linear velocities of 0.1 and 0.2m/s respectively under constant 1N load and is observed to be lower than C_3 (0.40 and 1.19e-06 mm^3/Nm) and M_3 (0.33 and 1.11e-06 mm^3/Nm) nanocomposite coatings [Fig 7.16b]. The uniform dispersion of TiO_2 nanoparticles in the Ni-P matrix, in case

of I_3 coating, leads to higher hardness [Fig 6.24d] which subsequently reduces the specific wear rate with respect to the conventional C_3 and M_3 coatings [Fig 7.16a]. The increment in wear rates are observed with the application of higher loads [Fig 7.16a] and velocities [Fig 7.16b] for all the developed C_3, M_3 and I_3 nanocomposite coatings. The results are in consistency with the Archard's law given by equation 7.1. Comparison of specific wear rate between Ni-P [Fig 7.1] and Ni-P-TiO_2 [Fig 7.16] coatings shows that the incorporation of TiO_2 particles in Ni-P matrix has improved the wear resistance of the coating. It is explained on account of the existence of hard TiO_2 particles which exhibit improved hardness than Ni-P alloy coatings [Fig 6.24c].

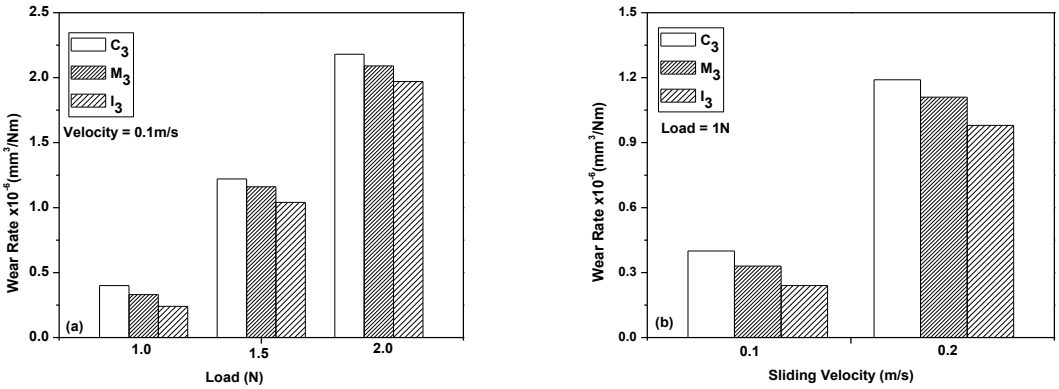

Fig 7.16- Variation in wear rate of heat treated C_3, M_3 and I_3 nanocomposite coatings at varying (a) Loads (b) Velocities.

7.3.3.2 Friction studies

Figure 7.17 presents the dependence of the average friction coefficients with the sliding distance for C_3, M_3 and I_3 nanocomposite coatings tested under 1, 1.5 and 2N loads. Load and speed of rotation are the main parameters that control the wear characteristics of nanocomposite coatings. Characteristic friction coefficients of heat treated C_3, M_3 and I_3 nanocomposite coatings, at first, behave linearly with the sliding distance and then reveal a constant behaviour [Fig 7.17]. This elevation in coefficients can be attributed towards the adhesion between the surfaces and ploughing of steel balls by nanosized TiO_2 reinforcements [Dennis and Sagoo (1991)]. It is found that when the load is increased from 1 to 2N, the average friction coefficient of C_3 (0.33-0.65), M_3 (0.29-0.45) and I_3 (0.25-0.40) nanocomposite coatings increases [Fig 7.17]. It can be explained on the basis that, real contact area within the nanocomposite coating and the substrate increase upon increasing the load. It is also noted that the lowermost coefficient of friction, among all, are shown by I_3 nanocomposite coatings [Fig 7.17c]. It is ascribed on the basis of the higher hardness attained by *insitu* reinforced TiO_2

nanoparticles owing to its uniform distribution in Ni-P matrix [Fig 6.24d]. Figure 7.18 describes that the friction coefficient behaviour in nanocomposite coatings seems to be directly proportional with the speeds of rotation i.e. higher friction coefficient is observed for 0.2m/s velocity as compared to 0.1m/s sliding velocity. The average friction coefficient at varying velocities of 0.1m/s and 0.2m/s is found to be around 0.33 and 0.41 for C_3; 0.29 and 0.39 for M_3 and 0.25 and 0.36 for I_3 nanocomposite coatings respectively [Fig 7.18]. It is also observed that the C_3, M_3 and I_3 nanocomposite coatings [Fig 7.17] display lesser coefficient of friction with sliding distance as compared to EL Ni-P alloy coatings [Fig 7.2a]. The precipitation of Ni_3P phase during heat treatment and the entrapment of nanosized TiO_2 strengthening in the globular matrix render the nanocomposite coating with higher hardness. This higher hardness leads to a decrease in the coefficient of friction in nanocomposite coatings.

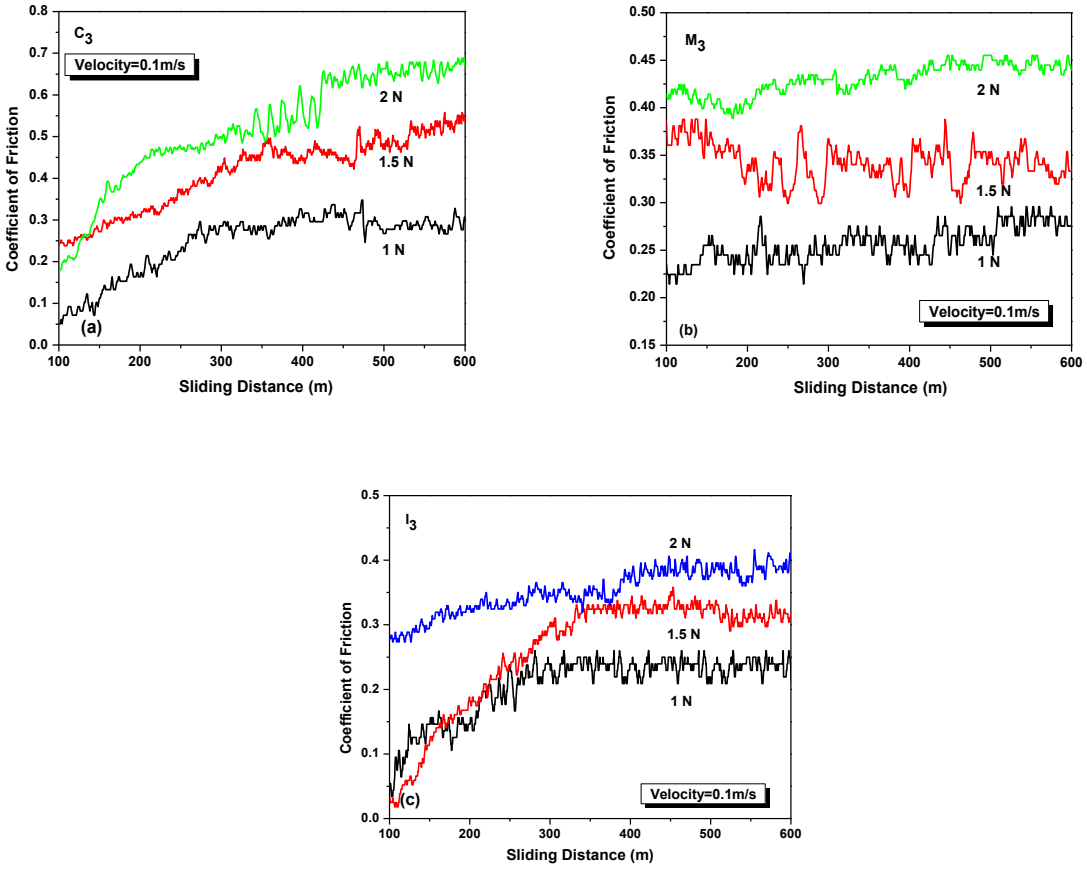

Fig 7.17- Effect of sliding distance on the coefficient of friction of (a) C_3, (b) M_3 and (c) I_3 nanocomposite coatings at varying loads.

7.3.3.3 Morphological Studies of worn surfaces

The morphologies of the wear tracks of Ni-P-TiO_2 nanocomposite coatings developed by different means like C_3, M_3 and I_3 nanocomposite coatings under varied loads of 1N and 2N with 0.1m/s sliding velocity also under 1N load at 0.2m/s sliding velocity are displayed in

figures 7.19, 7.20 and 7.21 respectively. Longitudinal grooves with adhesive tearing along the sliding direction are observed on the worn surface of C_3, M_3 and I_3 nanocomposite coatings. The narrower width and shallower plough lines of *insitu* TiO_2 reinforced coatings, I_3, characterizes its superior wear performance over C_3 and M_3 coatings owing to fine dispersion of TiO_2 nanoparticles in the Ni-P matrix. It is pointed out that the worn surfaces of all nanocomposite coatings are hard and adhered enough with shallower plough lines and hence exhibits improved wear resistance as compared with Ni-P alloy coatings [Fig 7.3]. This is ascribed by the higher hardness due to the impregnation of nanosized TiO_2 particles into the coating [Fig 6.24d]. Thus, the main wear mechanism notified in Ni-P-TiO_2 nanocomposite coatings is mild adhesive wear as sliding against hardened steel ball.

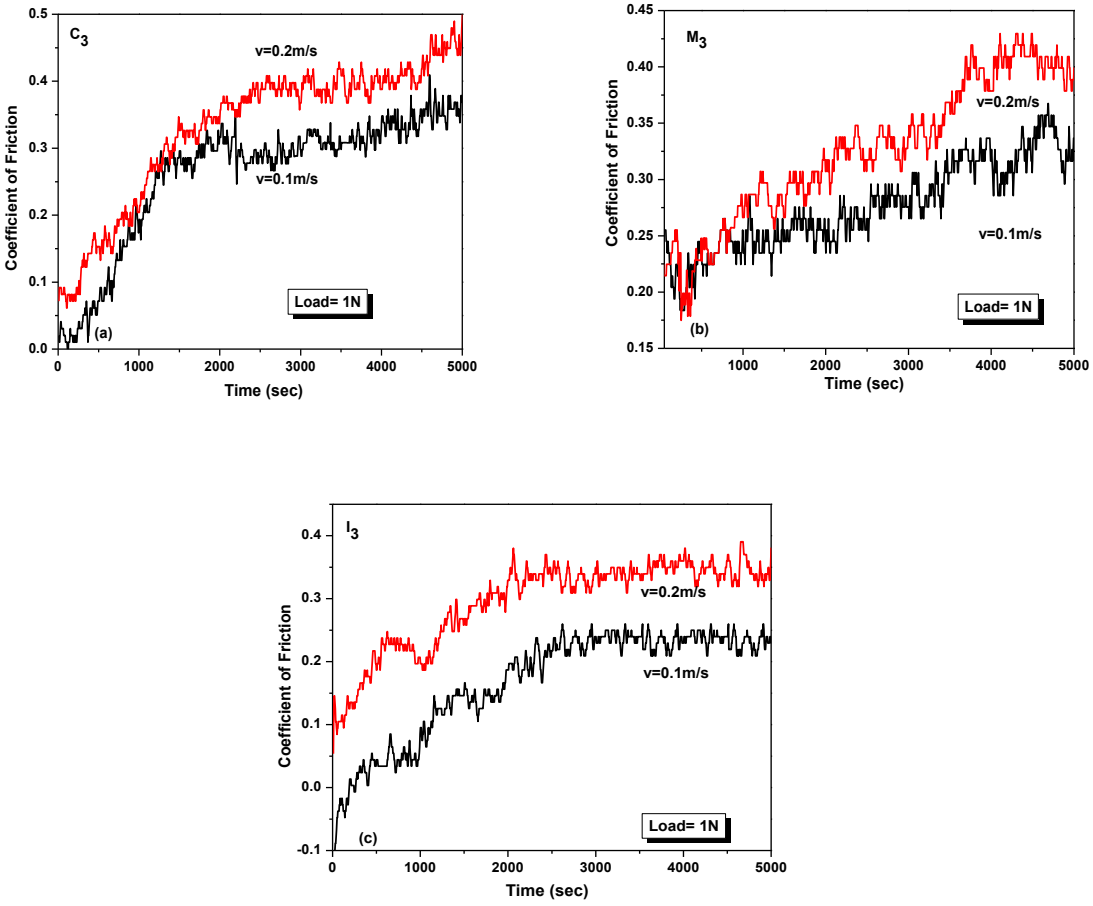

Fig 7.18- Variation of friction coefficient of (a) C_3, (b) M_3 and (c) I_3 nanocomposite coatings with sliding velocities.

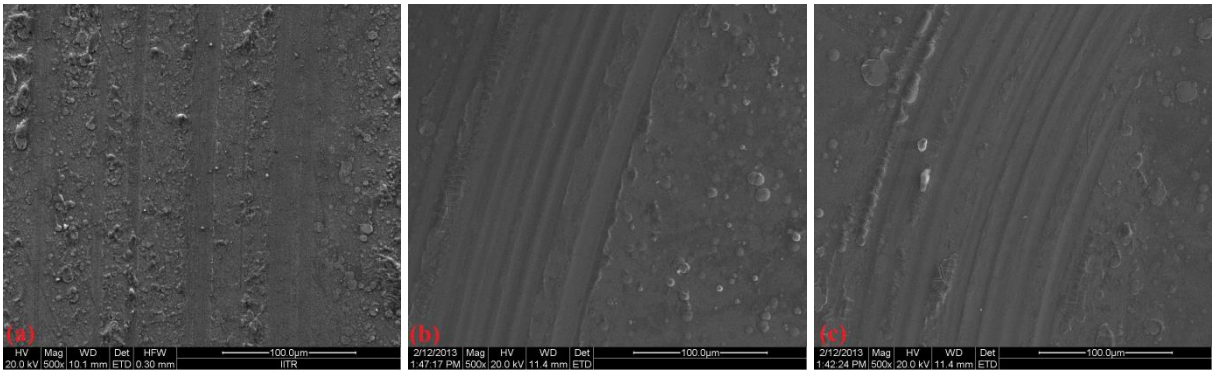

Fig 7.19- FESEM micrographs of C_3 nanocomposite coatings under loads, (a) 1N, (b) 2N at 0.1m/s sliding velocity and (c) Under 1N load at 0.2m/s sliding velocity after wear tests.

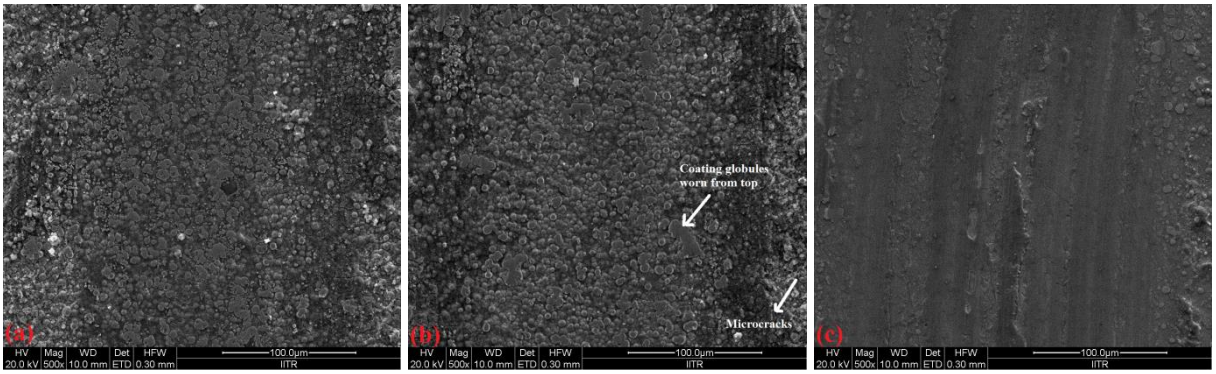

Fig 7.20- FESEM micrographs of M_3 nanocomposite coatings under loads, (a) 1N, (b) 2N at 0.1m/s sliding velocity and (c) Under 1N load at 0.2m/s sliding velocity after wear tests.

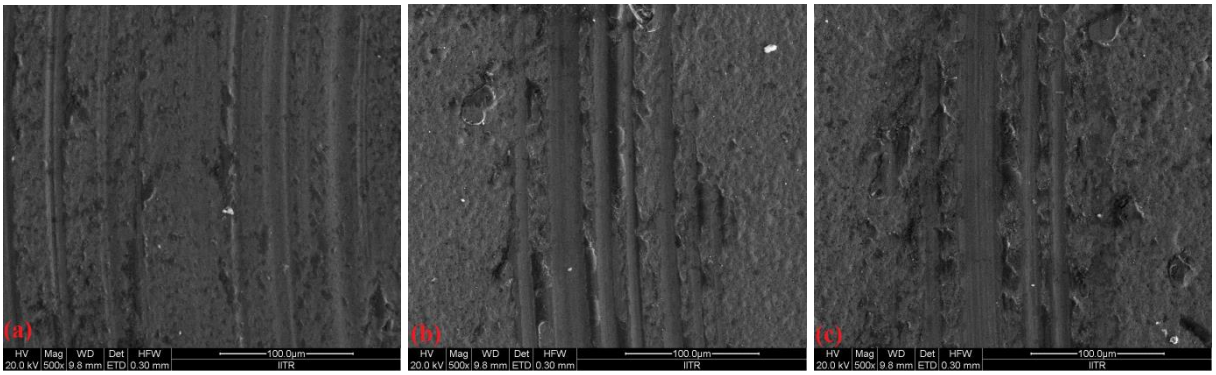

Fig 7.21- FESEM micrographs of I_3 nanocomposite coatings under loads, (a) 1N, (b) 2N at 0.1m/s sliding velocity and (c) Under 1N load at 0.2m/s sliding velocity after wear tests.

7.4 CORROSION STUDIES OF EL Ni-P ALLOY COATINGS

7.4.1 Potentiodynamic polarisation studies

The electrochemical polarization curves for EL Ni-P alloy coatings in 'as coated' and HT conditions for different pH compositions are shown in figure 7.22. The corrosion potential (E_{corr}) and the corrosion current density (I_{corr}) are calculated from the intersection of the cathodic and anodic Tafel curves extrapolated from the cathodic and anodic potentiodynamic polarization curves. The electrochemical corrosion characteristics obtained from the Tafel polarization curves before and after heat treatment under different pH conditions (pH-4.5 & 8) are tabulated in table 7.1. The values of corrosion current density (I_{corr}) and corrosion potential (E_{corr}) of plane Ni-P alloy coatings in acidic solution (pH-4.5) is around 1.89µA and 0.55V respectively whereas in alkaline solution (pH-8) is around 1.79 and 0.45 respectively. It is being noticed that the I_{corr} values obtained in alkaline media are lesser compared to an acidic one. The corrosion rate calculated for Ni-P coatings showed the similar trend [Table 7.1] showing better corrosion resistance in alkaline medium. Liang et al. (2009) reported that the steel coated with Ni-P alloy coating exhibits excellent corrosion resistance in alkaline solution.

In general, EL nickel coating improve the corrosion resistance due to formation of protective layer of metallic nickel and nickel phosphide that act as barrier to oxygen diffusion to the metal surface by sealing it off from the corrosive environments [Bozzoni et al. (2002); Hameed et al. (2010)]. As seen in figure 7.22 and table 7.1, the E_{corr} of Ni-P coatings is positively shifted from 0.55 to 0.50 V at pH-4.5 and 0.45 to 0.41 V at pH-8 when annealed at 400^{o}C for 1h. Moreover, I_{corr} and thus corrosion rate decreases, on heat treatment, from 1.14 to 0.95 mpy and 1.07 to 0.80 mpy in pH-4.5 and pH-8 electrolytes respectively. The reduction of corrosion rate of annealed sample may account for the phase transformation from amorphous to crystalline structure of Ni-P coating. The heat treatment also promotes the movement of Ni and P atoms at the surface, which results in formation of compact, smooth and homogenous coatings, with significant reduction in porosity. It may result into the reduction of corrosion current densities and corrosion rate. Similar results are reported by Bigdeli and Allahkaram (2009); Rabizadeh et al. (2010). It is evident from literature on Ni-P alloy coatings that preferential dissolution of nickel occurs at open circuit potential leading to phosphorus enrichment on the surface layer. The surface enriched with phosphorus then reacts with water to form a layer of adsorbed hypophosphite anions ($H_2PO_2^-$). This layer in turn will block the supply of water to the electrode surface. Thus preventing the hydration of nickel, which often considered being the first step to form either soluble Ni^{2+} ions or a passive nickel film [Balaraju et al. (2001); Crobu et al. (2008)].

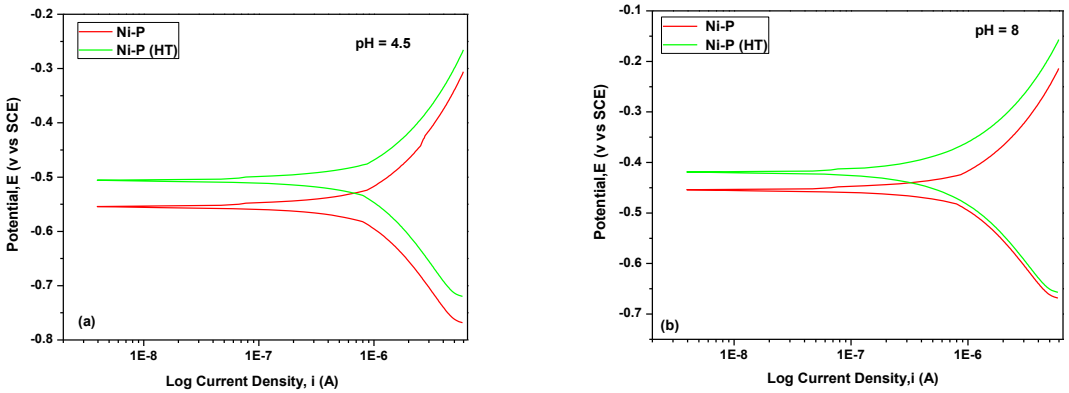

Fig 7.22- Tafel polarisation curves of EL Ni-P alloy coatings in varied environments with pH (a) 4.5 and (b) 8.0.

7.4.2 Microstructural analysis

Fig 7.23 shows the FESEM micrographs of EL Ni-P alloy coatings in 'as coated' and 'heat treated' conditions taken after the corrosion tests under different environments at pH-4.5 and pH-8. The micrographs reveal uniform distribution of metallic nickel and nickel phosphide layer over mild steel substrate [Fig 7.23]. However, the formation of large number of pits, microcracks and accumulation of corrosive products are seen on the coating surface exposed in acidic environment (pH-4.5) [Fig 7.23a]. The fewer pits with initiation of microcracks are noticed on the surface of coating introduced to alkaline environment (ph-8) [Fig 7.23c]. The picture depicts better resistance in alkaline atmosphere than acidic one. It is observed that heat treated Ni-P coatings (400^{o}C,1h) showed a much compact, uniform coating structure over the mild steel substrate with shallower pits [Fig 7.23b,d] and inturn enhance corrosion resistance.

Tabel 7.1: Corrosion characteristics of EL Ni-P alloy coatings in 'as coated' and heat treated conditions

Corrosion Characteristics	pH	Ni-P As coated	Ni-P (HT)
E_{corr} (V)	4.5	0.55	0.50
	8	0.45	0.41
I_{corr} (µA)	4.5	1.89	1.57
	8	1.79	1.34
CR (mpy)	4.5	1.14	0.95
	8	1.07	0.80

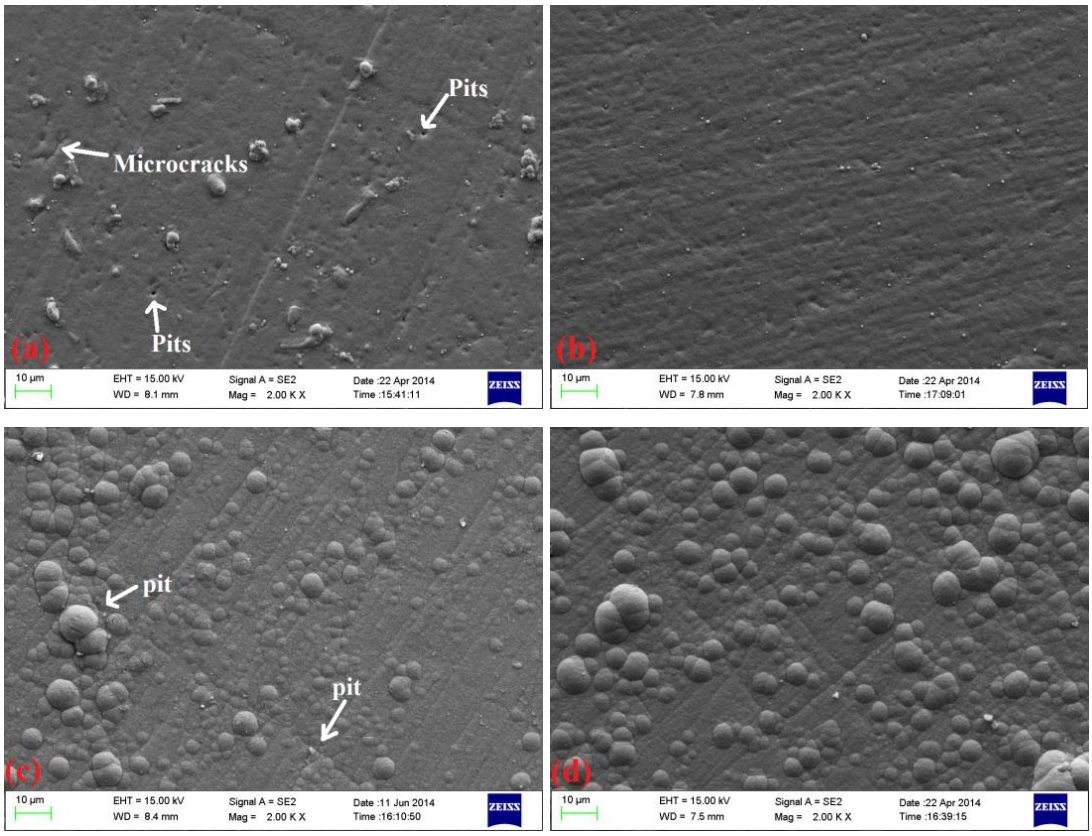

Fig 7.23- Morphologies of EL Ni-P alloy coatings after corrosion tests at pH-4.5, (a) As coated, (b) HT and at pH-8, (c) As coated, (d) HT conditions under FESEM.

7.5 CORROSION STUDIES OF EL Ni-P-X [Al_2O_3, ZrO_2 and TiO_2] NANOCOMPOSITE COATINGS

7.5.1 EL Ni-P-Al_2O_3 nanocomposite coatings (C_1, M_1 and I_1)

7.5.1.1 Potentiodynamic polarisation studies

The electrochemical polarization plots for EL Ni-P-Al_2O_3 nanocomposite coatings (C_1, M_1 and I_1) developed by various processes in 'as coated' and HT conditions in electrolytes having pH-4.5 and pH-8 are shown in figure 7.24. The corrosion parameters such as corrosion potential (E_{corr}), corrosion current density (I_{corr}), and corrosion rate (CR) are deduced from the polarization curves via Tafel extrapolation technique and listed in table 7.2. It is clearly noticed from table 7.2, that the incorporation of nanosized Al_2O_3 particles by any means into Ni-P matrix exhibited notable shift to more positive potentials (E_{corr}) and decrease in current density (I_{corr}) than those of the Ni-P alloy coatings [Table 7.1]. The results indicate that all C_1, M_1 and I_1 nanocomposite coatings can be employed for corrosion protection in both acidic (pH-4.5) and alkaline (pH-8) atmosphere. There was no passive area for a nanocomposite coating codeposited with Al_2O_3 (4g/l) similar to Ni-P coating because the effective metallic area prone to corrosion is decreased as the fine grains make the surface more uniform and compact with

lesser porosity. Also, Al_2O_3 particles act as inert physical barriers to the initiation and development of corrosion which contributes to isolating corrosive medium and decreasing corrosive area, increasing corrosion resistance [Bigdeli and Allahkaram (2009)]. Similar observations are made by research groups like Hamdy et al. (2007) and Yuan et al.(2011) on inclusion of alumina nanoparticles in nickel matrix. However, it was found that corrosion rate is minimal in non-conventional I_1 nanocomposite coating than that of the conventional C_1 and M_1 nanocomposite coatings [Table 7.2] in both acidic and alkaline electrolytes. This may be attributed to the fine dispersion of Al_2O_3 nanoparticles throughtout the matrix which blocks the pores especially around grain boundaries which are active corrosion paths and increased compactness of the coating hence exhibits better corrosion resistance. On the contrary, M_1 coatings showed highest corrosion rate among all [Table 7.2] in both the environments. It may be possibly due to the higher surface roughness of M_2 coatings [Fig 6.6c,d] which may cause the increase of the porosity at the interface of Al_2O_3 particles and Ni-P matrix and corrosion will be initiated at that site resulting in decreased corrosion resistance than C_1 and I_1 coatings. Heat treatment further exhibits the decrease in I_{corr} and has moved E_{corr} in noble direction than those of 'as coated' nanocomposite coatings [Table7.2] and the same trend is followed in both acidic and alkaline environments. Heat treatment at 400^{o}C for 1h significantly improves the coating density and results in less porous structure and thus enhanced corrosion resistance [Huang et al. (2004)]. The improvement of coating's corrosion resistance with heat-treatment is further confirmed by FESEM micrographs as discussed in section 7.5.1.2. Rabizadeh et al. (2010) reported that at 400^{o}C, grain growth triumph the formation of stable Ni_3P and Ni_xP_y intermediate compounds on the surface, which acts as barrier (passive film) and the corrosion resistance increases. It is also observed that the better anticorrosion properties are exhibited in alkaline medium than acidic environment for all the above nanocomposite coatings.

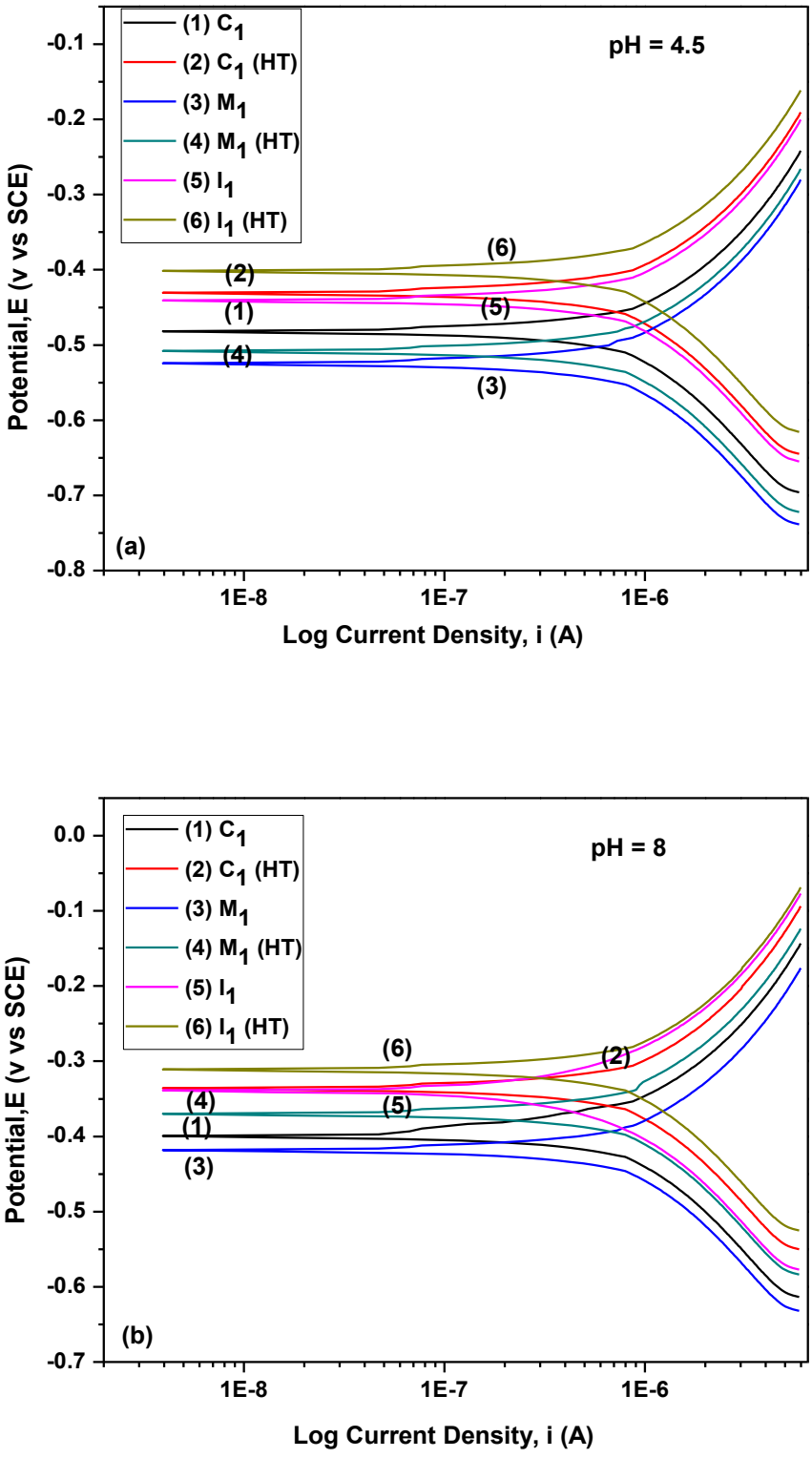

Fig 7.24- Tafel polarisation curves of C_1, M_1 and I_1 nanocomposite coatings in 'as coated' and HT conditions under environments with pH (a) 4.5 and (b) 8.0.

Tabel 7.2: Corrosion characteristics of EL Ni-P-Al_2O_3 nanocomposite coatings (C_1, M_1 and I_1) in 'as coated' and heat treated conditions.

Corrosion Charcteristics	pH	C_1 (as coat)	C_1 (HT)	M_1 (as coat)	M_1 (HT)	I_1 (as coat)	I_1 (HT)
E_{corr} (V)	4.5	0.48	0.43	0.52	0.50	0.44	0.40
	8	0.39	0.33	0.42	0.37	0.34	0.31
I_{corr}(µA)	4.5	1.41	0.95	1.56	1.09	1.15	0.84
	8	1.27	0.89	1.38	1.12	1.04	0.77
CR (mpy)	4.5	0.85	0.57	0.94	0.65	0.69	0.51
	8	0.77	0.53	0.83	0.67	0.63	0.46

7.5.1.2 Microstructural analysis

FESEM micrographs of EL Ni-P-Al_2O_3 (C_1, M_1 and I_1) nanocomposite coatings after corrosion tests at pH-4.5 and pH-8 environments are shown in figures 7.25 and 7.26 respectively. It is observed that when pH-4.5 (acidic) electrolyte is used, the layer of dispersed Al_2O_3 particles on 'as coated' C_1 and M_1 coatings is almost removed, leaving Ni-P matrix as the substrate [Figs 7.25a,c]. Fewer pits and pores are also seen, which results in accelerated electrochemical corrosion cells once they penetrated to the surface of the substrate. On the other hand, in pH-8 (alkaline) electrolyte, uniformly dispersed layer of Al_2O_3 particles are maintained over Ni-P matrix [Figs 7.26a,c] indicating better corrosion resistance than acidic environments. Further, in case of I_1 nanocomposite coatings, minute corrosion is observed on its surface as it contains only very shallow and small pits and hence stands superior over C_1 and M_1 coatings in both acidic [Fig 7.25d] and alkaline [Fig 7.26d] environments. The result is supported by the fact that there is a limited preferential corrosion path owing to uniform dispersion of fine grained Al_2O_3 in the nickel matrix which effectively fills up the Ni-P globule boundaries and thus enhanced resistance to corrosion. Figures 7.25b and 7.26b show the micrographs of the heat treated C_1 nanocomposite coatings after corrosion test in pH-4.5 and pH-8 electrolytes respectively. The smoother, dense and more compact structure is noticed on heat treatment (400^{o}C,1h) where Al_2O_3 layer is slightly etched away and no significant pitting defects are observed on the surface indicated the enhanced protective behaviour. The results further indicate that these C_1, M_1 and I_1 nanocomposite coatings can be used in both acidic and alkaline environments for corrosion protection applications.

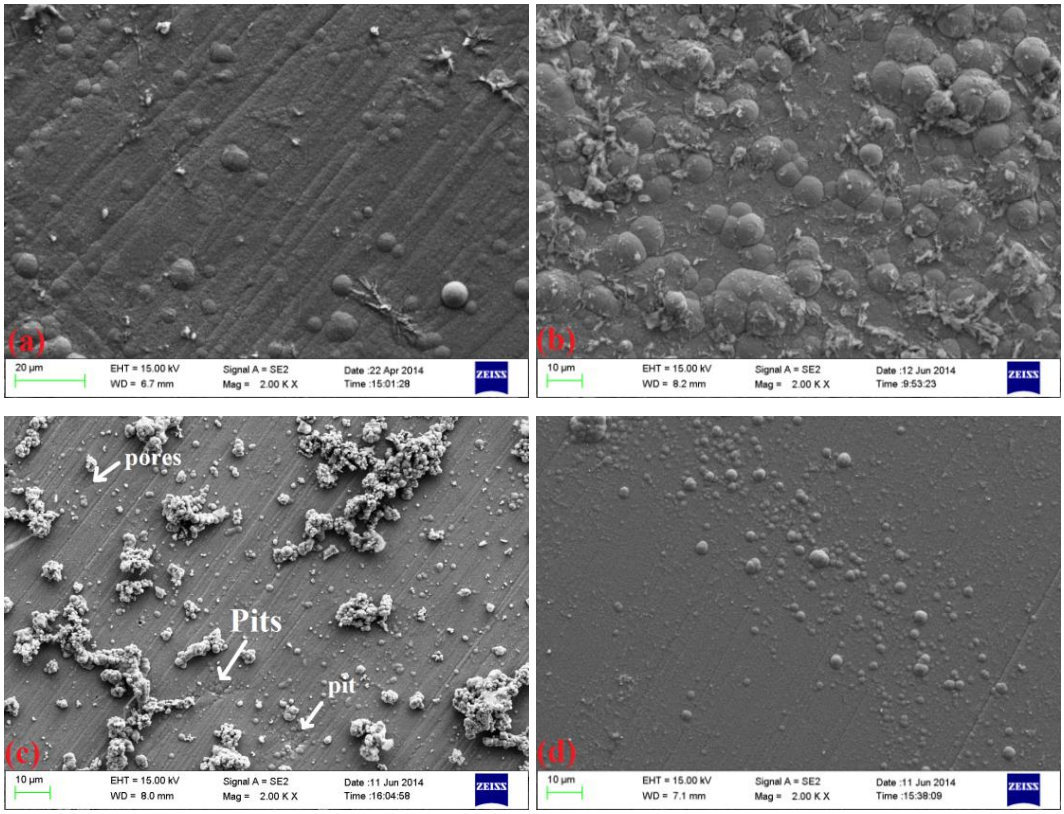

Fig 7.25- Morphologies of nanocomposite coatings after corrosion tests at pH-4.5, (a) C_1, (b) C_1 HT, (c) M_1 and (d) I_1 under FESEM.

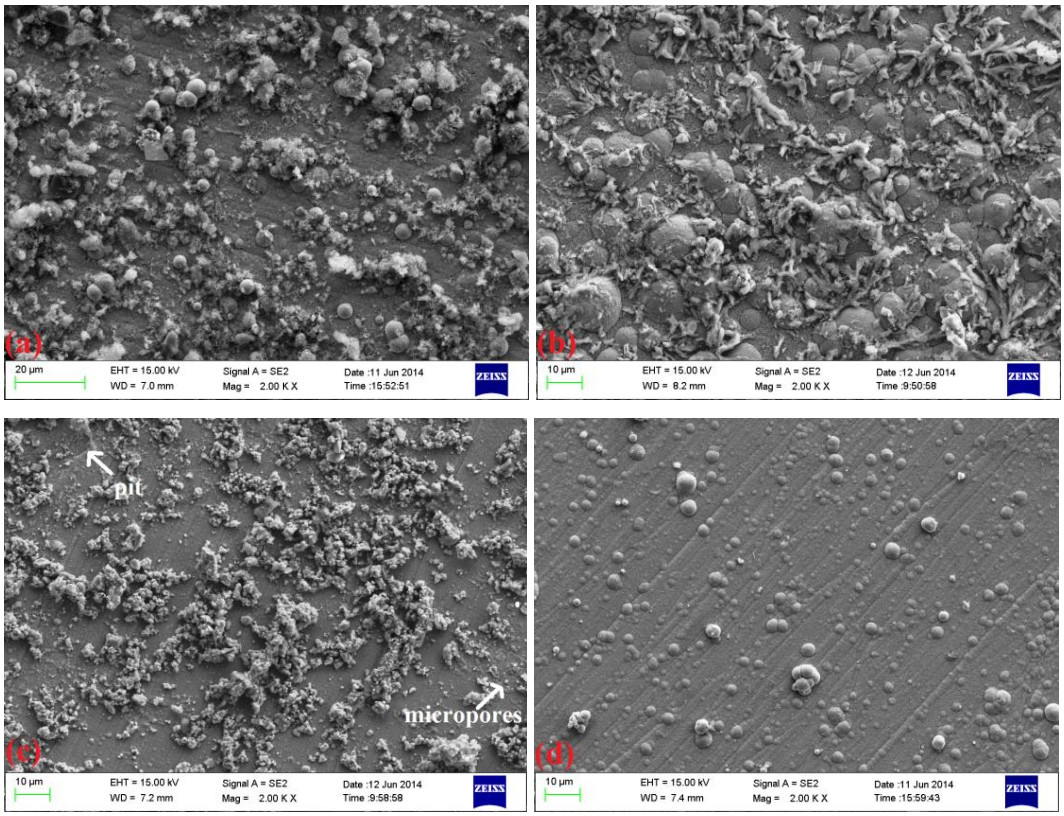

Fig 7.26- Morphologies of nanocomposite coatings after corrosion tests at pH-8, (a) C_1, (b) C_1 HT, (c) M_1 and (d) I_1 under FESEM.

7.5.2 EL Ni-P-ZrO_2 nanocomposite coatings (C_2, M_2 and I_2)

7.5.2.1 Potentiodynamic polarisation studies

Figure 7.27 shows the electrochemical polarization curves of EL Ni-P-ZrO_2 nanocomposite coatings developed by conventional (C_2, M_2) and non-conventional (I_2) means before and after heat treatment under environments with pH-4.5 and pH-8. The corrosion factors like E_{corr}, I_{corr} and rate of corrosion are calculated using Tafel extrapolation method from polarization curves [Fig 7.27] and summarized in table 7.3. It is observed that all the C_2, M_2 and I_2 nanocomposite coatings exhibited more positive E_{corr} and lower I_{corr} with respect to Ni-P alloy coatings [Table 7.1] indicating an improved corrosion resistance in both acidic (pH-4.5) and alkaline (pH-8) electrolytes [Table 7.3]. This effect probably due to the inclusion of second phase nanosized ZrO_2 particles which act as inert physical barriers by occupying minute pores in the Ni-P matrix and thus alters the Ni-P layer structure making it more uniform and compact as compared to the Ni-P coating. The effect is more pronounced in case of non-conventional I_2 nanocomposite coatings where ZrO_2 nanoparticles are uniformly distributed in the Ni-P matrix blocks the active corrosion sites more effectively and thus exhibited excellent corrosion resistance compared to C_2 and M_2 coatings [Table 7.3]. The worst corrosion resistance is shown in case of M_2 coatings may be on account of its higher surface roughness [Fig 6.16c,d] which probably raise the porosity and inturn increases the corrosion rate [Table 7.3]. Song et al. (2008) and Ranganatha et al. (2012) featured similar results on reinforcement of ZrO_2 nanoparticles in Ni-P matrix. All heat treated nanocomposite coatings (400^{o}C,1h) represented more positive E_{corr} and lower I_{corr} values [Table 7.3] depicting an improvement in corrosion resistance in both the acidic and alkaline environments. Proper heat treatment results in denser and less porous coating structure [Huang et al.(2004), Rabizadeh et al.(2011)] which is further cleared by FESEM micrographs [Fig 7.28b]. It is also found that C_2, M_2 and I_2 nanocomposite coatings imparts higher corrosion resistance in alkaline medium (pH-8) than acidic medium (pH-4.5).

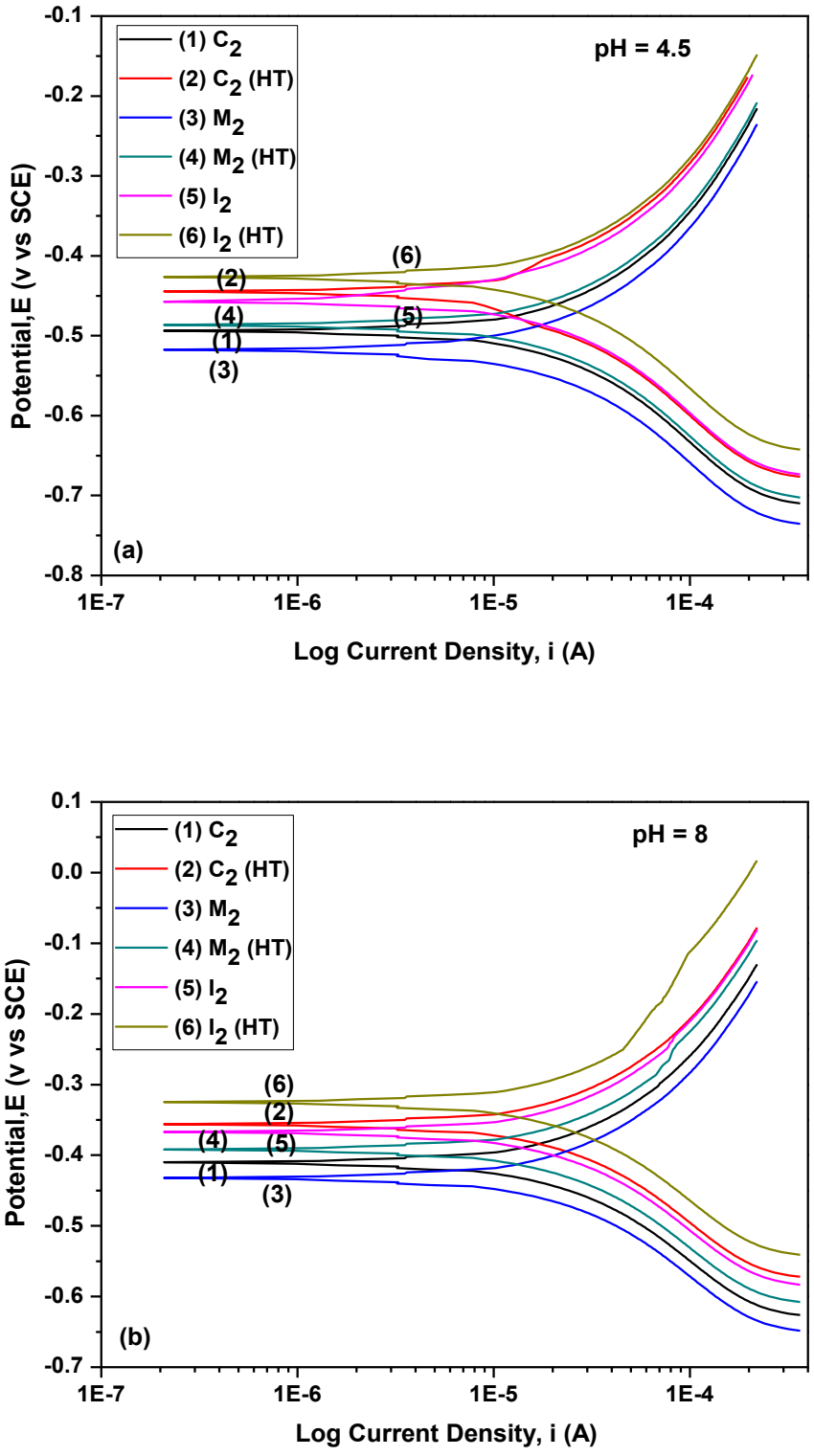

Fig 7.27- Tafel polarisation curves of C_2, M_2 and I_2 nanocomposite coatings in 'as coated' and HT conditions under environments with pH (a) 4.5 and (b) 8.0.

Tabel 7.3: Corrosion characteristics of EL Ni-P-ZrO_2 nanocomposite coatings (C_2, M_2 and I_2) in 'as coated' and heat treated conditions

Corrosion Charcteristics	pH	C_2 (as coat)	C_2 (HT)	M_2 (as coat)	M_2 (HT)	I_2 (as coat)	I_2 (HT)
E_{corr} (V)	4.5	0.49	0.44	0.52	0.48	0.46	0.42
	8	0.41	0.35	0.43	0.39	0.36	0.32
I_{corr} (µA)	4.5	1.52	1.07	1.68	1.21	1.25	0.95
	8	1.36	0.98	1.50	1.09	1.18	0.89
CR(mpy)	4.5	0.91	0.64	1.01	0.73	0.75	0.57
	8	0.82	0.59	0.90	0.65	0.68	0.54

7.5.2.2 Microstructural analysis

FESEM images of corroded surfaces of EL Ni-P-ZrO_2 (C_2, M_2 and I_2) nanocomposite coatings after exposure in acidic media (ph-4.5) and alkaline media (ph-8) is displayed in figures 7.28 and 7.29 respectively. Compared with the microscopic images of C_2 and M_2 coatings before [Fig 6.14a-d] and after corrosion [Figs 7.28a-c], it is noticed that most of the bonded ZrO_2 nanoparticles are etched away from the Ni-P surface in acidic media (pH-4.5) and tiny pits are seen on the coating surface [Figs 7.28a,c]. It is suggested that the uncovered nanosized ZrO_2 particles deposited with Ni-P when exposed in aggressive medium, corrosion will be initiated at the interface of these nanoparticles and Ni-P matrix. When more nickel disintegrates, a few particles may tumble off the coating and led the formation of corrosive pits [Ranganatha et al. (2012)]. On the contrary, the layer of dispersed ZrO_2 particles is some how maintained over Ni-P matrix in akaline media [Figs 7.29a,c] showing improved corrosion resistance of the coatings as compared to acidic media. It is also observed that very shallow pits are seen on the clean surface of I_2 nanocomposite coatings which signifies higher corrosion resistance in acidic [Fig 7.28d] as well as alkaline [Fig 7.29d] electrolytes. It is due to the effective adsorption of *insitu* ZrO_2 nanoparticles at nodule boundaries which are prime sites of corrosion. The less etched layer of ZrO_2 particles and presence of no significant pits on the surface of heat treated C_2 nanocomposite coatings show an enhanced corrosion resistance in acidic [Fig 7.28b] and alkaline medium [Fig 7.29b] than 'as coated' coatings. It is also revealed that C_2, M_2 and I_2 nanocomposite coatings can be sustained in both acidic (ph-4.5) and alkaline (ph-8) atmospheres.

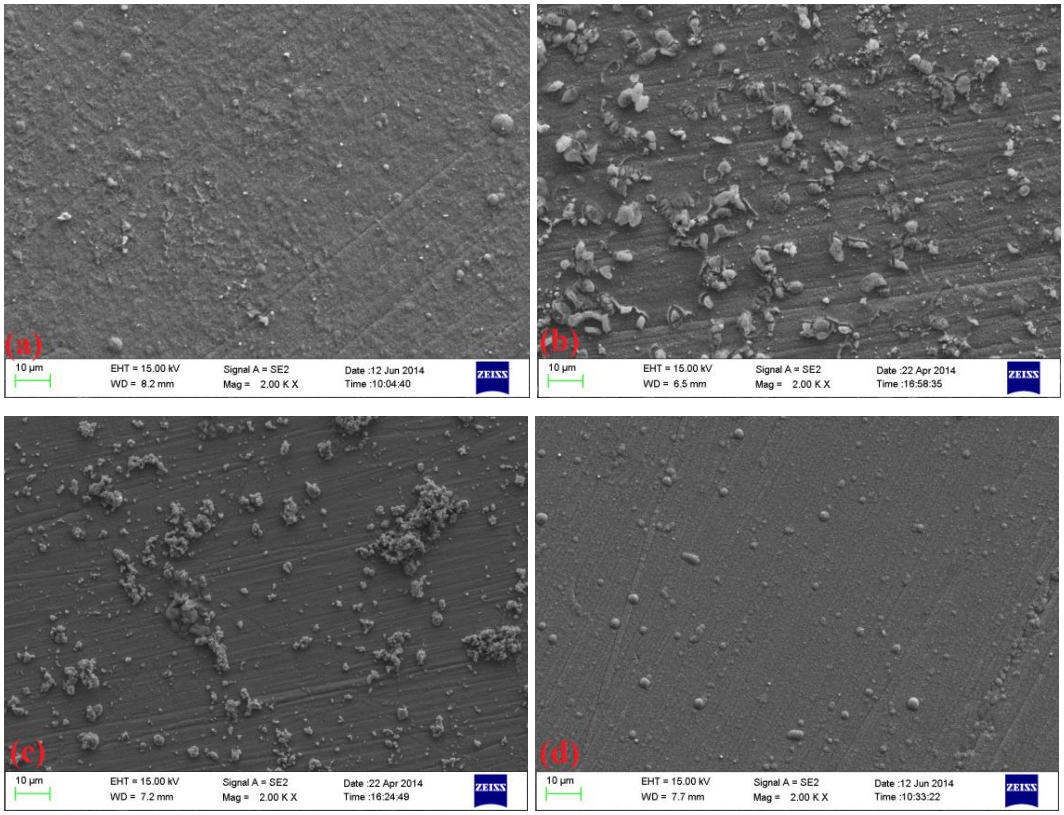

Fig 7.28- Morphologies of nanocomposite coatings after corrosion tests at pH-4.5, (a) C_2, (b) C_2 HT, (c) M_2 and (d) I_2 under FESEM.

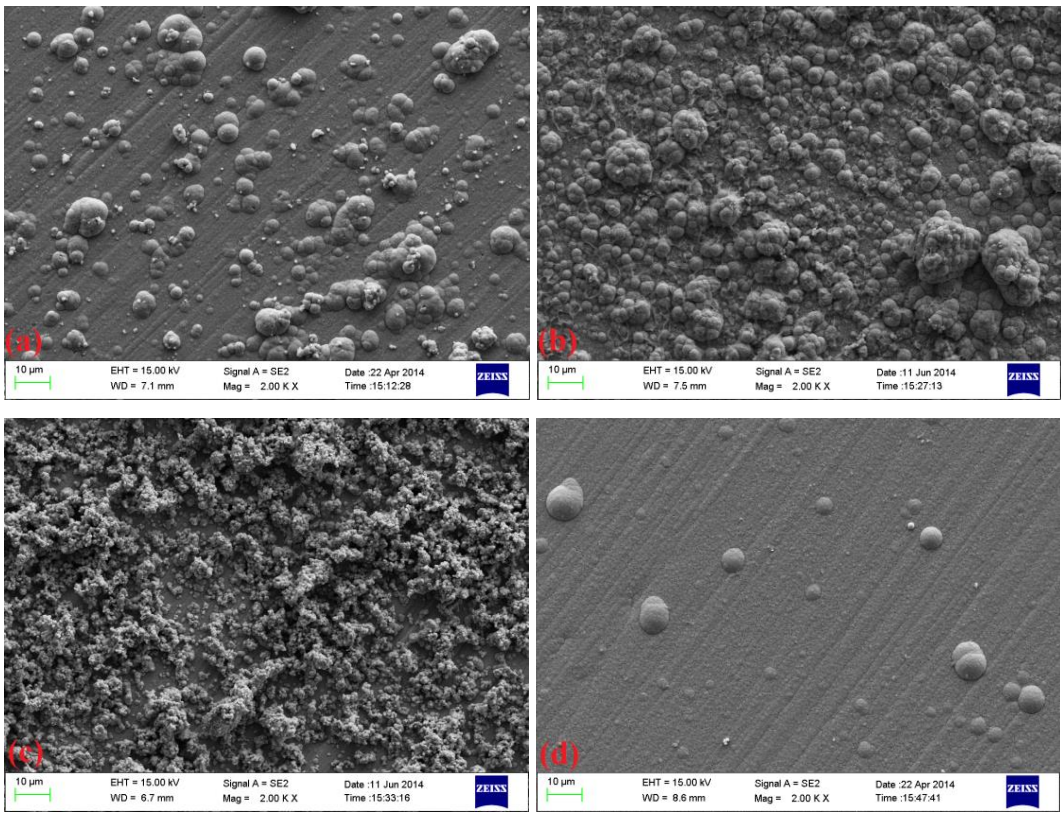

Fig 7.29- Morphologies of nanocomposite coatings after corrosion tests at pH-8, (a) C_2, (b) C_2 HT, (c) M_2 and (d) I_2 under FESEM.

7.5.3 EL Ni-P-TiO_2 nanocomposite coatings (C_3, M_3 and I_3)

7.5.3.1 Potentiodynamic polarisation studies

The electrochemical polarization curves of Ni-P-TiO_2 (C_3, M_3 and I_3) nanocomposite coatings in varied pH environments (pH-4.5 and 8) before and after heat treatment is shown in figure 7.30. The corrosion characteristics namely E_{corr}, I_{corr} and corrosion rate are determined from the polarization curves [Fig 7.30] using Tafel extrapolation method and is given in table 7.4. Figure 7.28 and table 7.4 reveal the slight positive shift in E_{corr} and a small decrement in I_{corr} values, in case of conventionally developed C_3 and M_3 nanocomposite coatings with respect to Ni-P coatings [Table 7.1] in acidic and alkaline environments. This indicates slight improvement in corrosion resistance on inclusion of nanosized TiO_2 particles. However, it should also be pointed out that the non-conventionally (*insitu*) developed I_3 nanocomposite coatings show better corrosion behavior in terms of lesser I_{corr} and more positive E_{corr} values and lowest corrosion rate amongs all [Table 7.4] in both the environments. The increment in corrosion resistance is ascribed by the factor that TiO_2 serves as inert physical barriers that blocks the pores in the Ni-P matrix. In other words, the incorporation of TiO_2 nanoparticles retrained the anodic dissolution reaction of the deposit by means of reduction in its active metallic surface available for corrosion and inturn enhanced the barrier effect of the coating [Ranganatha et al. 2010]. Hence, this factor can contribute to higher corrosion resistance attained in I_3 nanocomposite coatings as more number of TiO_2 nanoparticles is incorporated via non-conventional mechanism [Fig 6.19c]. The results on enhancement of corrosion resistance by *insitu* precipitation of TiO_2 nanoparticles in Ni-P matrix are supported by research groups like Song et al. (2004, 2008) and Guo et al. (2011). The higher corrosion rate is observed by M_3 coatings compared with C_3 and I_3 coatings. The higher adsorption of milled particles on Ni-P surface may generate porosity resulting in poorer corrosion resistance than C_3 and I_3 coatings [Table 7.4]. It is also noticed from table 7.4 that the heat treatment (400^{o}C, 1h), shifted the polarization curves of all C_3, M_3 and I_3 coatings to more positive E_{corr} and lower I_{corr} values. This signifies the improvement in corrosion protection on proper heat treatment by all the nanocomposite coatings in both acidic (pH-4.5) and alkaline environments (pH-8). The formation of a compact Ni_3P film with lesser porosity due to better adhesion of the coating with substrate at this temperature may result in reduction of corrosion resistance [Bigdeli and Allahkaram (2009)]. It is also found that the coatings are more resistant to corrosive attack in alkaline atmosphere than acidic one. It is seen that the inclusion of Al_2O_3, ZrO_2 and TiO_2 nanoparticles by any means in Ni-P matrix follows the same trend in alkaline (pH-8) and acidic (pH-4.5) environments [Table 7.2, 7.3 and 7.4] and showed an improvement in corrosion resistance than Ni-P alloy coating [Table7.1].

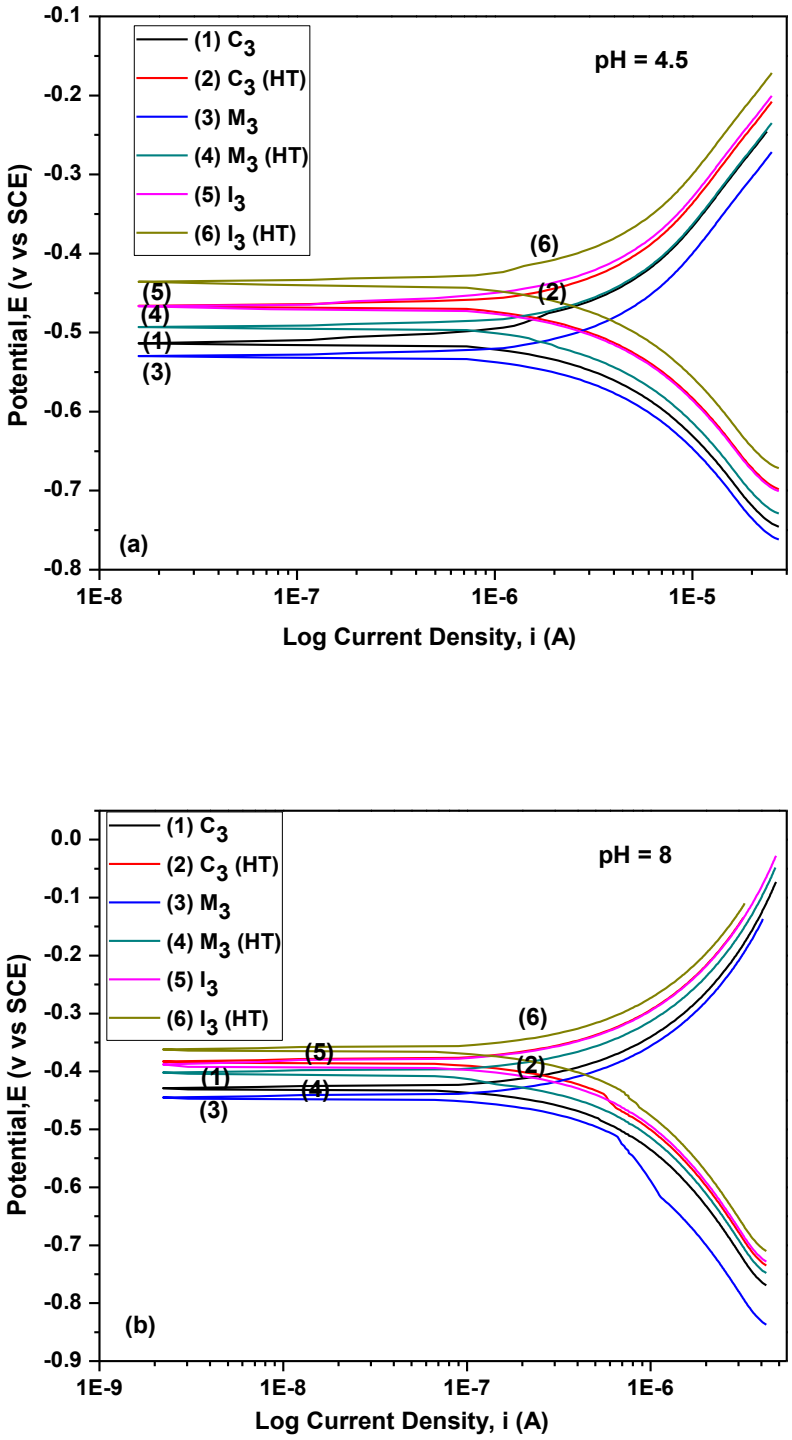

Fig 7.30- Tafel polarisation curves of C_3, M_3 and I_3 nanocomposite coatings in 'as coated' and HT conditions under environments with pH (a) 4.5 and (b) 8.0.

Tabel 7.4: Corrosion characteristics of EL Ni-P-TiO_2 nanocomposite coatings (C_3, M_3 and I_3) in 'as coated' and heat treated conditions

Corrosion Charcteristics	pH	C_3 (as coat)	C_3 (HT)	M_3 (as coat)	M_3 (HT)	I_3 (as coat)	I_3 (HT)
E_{corr} (V)	4.5	0.51	0.46	0.53	0.49	0.47	0.43
	8	0.43	0.38	0.44	0.40	0.39	0.36
I_{corr} (µA)	4.5	1.66	1.20	1.81	1.35	1.39	1.07
	8	1.48	1.11	1.60	1.26	1.22	1.00
CR (mpy)	4.5	1.01	0.72	1.09	0.81	0.84	0.65
	8	0.89	0.67	0.96	0.76	0.73	0.60

7.5.3.2 Microstructural analysis

FESEM micrographs of EL Ni-P-TiO_2 (C_3, M_3 and I_3) nanocomposite coatings taken after the corrosion tests in acidic (ph-4.5) and alkaline (ph-8) environments is shown in figures 7.31 and 7.32. It is observed that most of the TiO_2 particles is fallen off in C_3 and M_3 nanocomposite coatings when expose to acidic (ph-4.5) atmosphere [Figs 7.31a,c]. Apart from these small pits and slight intiation of microcracks on particle and Ni-P interface are also observed on surface. However, the adherence of TiO_2 particles with Ni-P matrix is still maintained in alkaline (ph-8) atmosphere [Figs 7.32a,c] with signs of its more resistance in alkaline atmosphere. Small pits are seen on the surface of I_3 nanocomposite coatings in both acidic [Fig 7.31d] and alkaline [Fig 7.32d] atmosphere. More compact and denser coatings with lesser removal of TiO_2 particles are observed on heat treated surface of C_3 nanocomposite coatings in both acidic [Fig 7.32b] and alkaline [Fig 7.32b] atmospheres.

The comparative results obtained on wear and corrosion behavior of EL Ni-P-X [X= Al_2O_3, ZrO_2 and TiO_2] nanocomposite coatings developed by conventional and non-conventional approaches with respect to EL Ni-P alloy coatings are summarized in table 7.5 and 7.6 respectively.

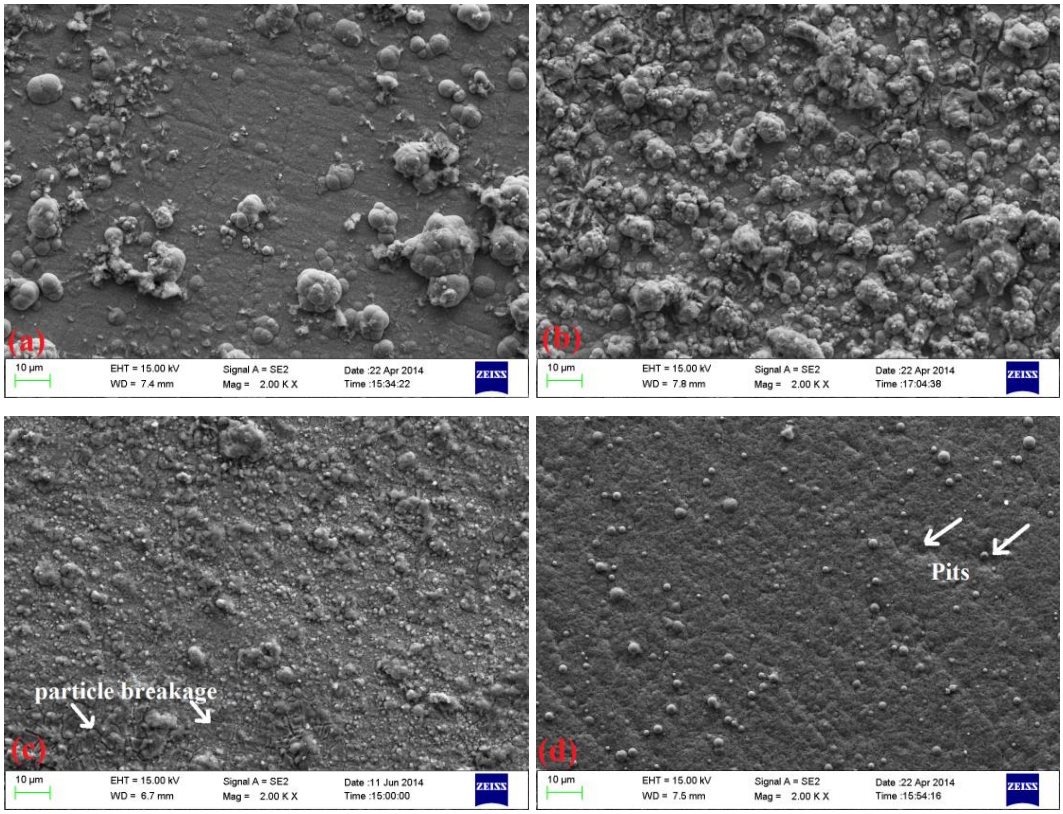

Fig 7.31- Morphologies of nanocomposite coatings after corrosion tests at pH-4.5, (a) C_3, (b) C_3 HT, (c) M_3 and (d) I_3 under FESEM.

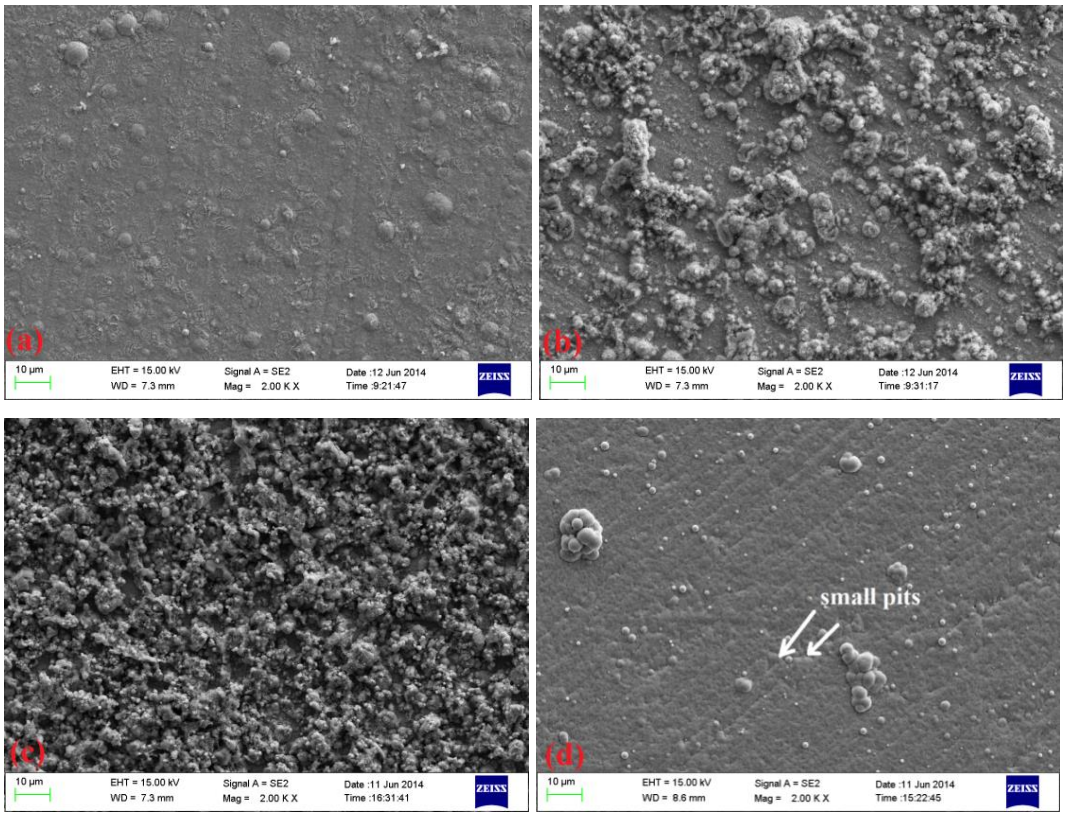

Fig 7.32- Morphologies of nanocomposite coatings after corrosion tests at pH-8, (a) C_3, (b) C_3 HT, (c) M_3 and (d) I_3 under FESEM.

Tabel 7.5: Wear resistance of EL Ni-P and Ni-P-X nanocomposite coatings in heat treated condition

EL Coatings (HT condition)		Wear Rate (mm^3/Nm)				
		Loads (N) (at constant 0.1m/s sliding velocity)			Sliding velocity (m/s) (at constant 1N load)	
		1	2	3	0.1	0.2
Ni-P		0.98	2.87	4.3	0.98	2.84
$Ni\text{-}P\text{-}Al_2O_3$	C_1	0.21	0.72	1.56	0.21	0.68
	M_1	0.18	0.64	1.45	0.18	0.61
	I_1	0.14	0.49	1.28	0.14	0.52
$Ni\text{-}P\text{-}ZrO_2$	C_2	0.29	0.84	1.72	0.29	0.81
	M_2	0.22	0.75	1.63	0.22	0.72
	I_2	0.17	0.62	1.48	0.17	0.60
$Ni\text{-}P\text{-}TiO_2$	C_3	0.40	1.22	2.18	0.40	1.19
	M_3	0.33	1.16	2.09	0.33	1.11
	I_3	0.24	1.04	1.97	0.24	0.98

***Conventional nanocomposite coatings (C, M)** where second phase particles employed is 'C'- Chemically synthesized nanopowders, 'M'- Mechanically milled nanopowders.

***Non-Conventional nanocomposite coatings (I)** where second phase particles employed is *insitu* synthesized nanopowders within EL bath.

Tabel 7.6: Corrosion resistance of EL Ni-P and Ni-P-X nanocomposite coatings in 'as coated' and heat treated conditions

EL Coatings		Corrosion Rate (mpy)			
		pH- 4.5 (acidic)		pH- 8 (alkaline)	
Conditions		As coat	HT	As coat	HT
Ni-P		1.14	0.95	1.07	0.80
Ni-P-Al_2O_3	C_1	0.85	0.57	0.77	0.53
	M_1	0.94	0.65	0.83	0.67
	I_1	0.69	0.51	0.63	0.46
Ni-P-ZrO_2	C_2	0.91	0.64	0.82	0.59
	M_2	1.01	0.73	0.90	0.65
	I_2	0.75	0.57	0.68	0.54
Ni-P-TiO_2	C_3	1.01	0.72	0.89	0.67
	M_3	1.09	0.81	0.96	0.76
	I_3	0.84	0.65	0.73	0.60

***Conventional nanocomposite coatings (C, M)** where reinforcements used is 'C'- Chemically synthesized nanopowders, 'M'- Mechanically milled nanopowders.

***Non-Conventional nanocomposite coatings (I)** where reinforcements used is *insitu* synthesized nanopowders within EL bath.

7.6 SUMMARY

The present chapter discuss the results obtained from the evaluation of the various properties, namely, wear, friction and corrosion of EL Ni-P-X [X= Al_2O_3, ZrO_2 and TiO_2] nanocomposite coatings developed by conventional and non-conventional *(insitu)* routes and compared with Ni-P alloy coatings. The effect of loads (1, 1.5 and 2N) and sliding velocities (0.1 and 0.2m/s) on the specific wear rate and coefficient of friction of heat treated EL Ni-P and Ni-P-X nanocomposite coatings are discussed. The results indicate an improvement in wear resistance and lower coefficient of friction for all Ni-P-X nanocomposite coatings with respect to Ni-P alloy coatings, both at different loads and sliding velocities. This is attributed to the higher hardness of EL Ni-P-X nanocomposite coatings over Ni-P alloy coatings. The lower wear rate and friction coefficient is observed by Ni-P-X nanocomposite coatings following *insitu* (I) route compared to conventional route (C,M). The higher hardness achieved due to uniform dispersion of nanosized 'X' particles without coagulation in Ni-P matrix contributes to the above. Also, it is found that, in case of conventional nanocomposite coatings, the inclusion of milled nanoparticles on Ni-P surface imparts slightly lower friction coefficient and wear rate with respect to chemically prepared nanoparticles. It is being noticed that the wear rate and friction coefficient increases with increase in applied loads (1 to 2N) and velocities (0.1, 0.2m/s) for all the coatings. The worn surfaces of Ni-P and Ni-P-X nanocomposite coatings under different loads and sliding velocities are characterised using FESEM analysis. Mild adhesive wear is the predominant mechanism noticed during wear for all the nanocomposite coatings. The electrochemical polarization curves for EL Ni-P and Ni-P-X [X=Al_2O_3, ZrO_2, TiO_2] nanocomposite coatings in 'as coated' and heat treated conditions under different environments (pH-4.5 & 8) are analysed. EL Ni-P-X nanocomposite coatings are found to have higher corrosion potentials (E_{corr}) and lower corrosion currents (I_{corr}) than those of Ni-P coating, indicating an improved corrosion protection in both acidic (pH-4.5) and alkaline (pH-8) atmosphere. The heat treatment also promotes the reduction of corrosion current densities and corrosion rate due to the formation of compact, smooth and homogenous coatings and the trend is followed in both acidic and alkaline environments. It is observed that EL Ni-P-X nanocomposite coatings following *insitu* route exhibits lower corrosion rate over the conventional (C, M) route. In conventional route, the usage of milled nanoparticles as reinforcements in Ni-P matrix showed slight decrease in corrosion resistance over the chemically prepared nanoparticles. The increase in porosity due to the higher roughnesss of the coating (M) may account for the above decrement. The corroded surfaces are analysed with the help of FESEM micrographs. It is observed that EL Ni-P-X nanocomposite coatings are more corrosion resistant to alkaline (pH-8) atmosphere as compared to acidic (pH-5) one.

CHAPTER 8

CONCLUSION

The following conclusions can be ascribed in the present investigation on the "Development of EL Ni-P-X nanocomposite coatings on mild steel substrate for wear and corrosion applications".

8.1 SYNTHESIS AND CHARACTERISATION OF REINFORCEMENTS 'X' USED TO MAKE Ni-P-X SYSTEM

1. Nanoparticles of Al_2O_3, ZrO_2 and TiO_2 with average particle size of 12nm, 7nm and 10nm were synthesized by chemical precipitation route (Bottom up approach).
2. Nanosized Al_2O_3, ZrO_2 and TiO_2 powders of size range 15nm, 21nm and 39nm respectively were also prepared by Top down approach using mechanical milling in high energy ball mill at 250 rpm for 40 h.
3. The milled powders show lowering in particle size and formation of amorphous phases upon increase in extent of milling time.

8.2 SYNTHESIS AND CHARACTERISATION OF EL Ni-P ALLOY AND Ni-P-X NANOCOMPOSITE COATINGS

1. Electroless Ni-P alloy coatings with hemispherical globular structure were developed on mild steel substrate. The layer developed by lateral and vertical growth of globules and autocatalytically covers the substrate surface to form pore free deposits.
2. EL conventional Ni-P-X [X= Al_2O_3, ZrO_2 and TiO_2] nanocomposite coatings were developed where 'X' reinforcements used were chemically synthesized and mechanical milled powders.
3. Codeposition of reinforcement 'X' into Ni-P alloy matrix resulted in surface modification of the coatings with presence of nodular protrusions.
4. No significant change in surface morphology has been observed on heat treatment (400°C for 1h) of both Ni-P and Ni-P-X coatings.
5. The XRD patterns of 'as coated' condition for both Ni-P alloy and Ni-P-X nanocomposite coatings displayed amorphous nature, but upon heat treatment, the diffraction pattern reveal the precipitation of harder Ni_3P phase along with crystalline Ni formation.

6. Phase analysis of Ni-P-X nanocomposite coatings confirms the presence of 'X' apart from Ni. The incorporation of nanoparticles donot varies Ni-P coating structure.
7. The nanosized milled particles 'X' exhibit good adherence with Ni-P matrix due to its high surface energy compared to reinforcements prepared by chemical route.
8. A novel EL non-conventional Ni-P-X [X= Al_2O_3, ZrO_2 and TiO_2] nanocomposite coatings were also developed using *insitu* precipitation reactions within the EL bath.
9. Globular morphology with no clear 'X' nanoparticles can be observed on the surface of *insitu* Ni-P-X nanocomposite coatings. However, the existence of nanosized 'X' particles can be confirmed by virtue of their EDAX, X-ray mapping and XRD analysis.
10. EL *insitu* Ni-P-Al_2O_3 nanocomposite coatings were optimised by varying precipitation reactant, $AlCl_3$, content in the EL bath. The globule size decreases and Al_2O_3 content increases with increase in the precipitated concentration of Al_2O_3 particles. The $AlCl_3$ content (39g/l) is consistent with improvement of hardness (786VHN) due to the dispersion strengthening and grain refinement effect. Hence, the same amount was used in present study to develop *insitu* Ni-P-ZrO_2 and Ni-P-TiO_2 nanocomposite coatings.
11. The thickness of the all Ni-P-X developed coatings was around 30 µm showing good adhesion between the mild steel substrate and the coating.

8.3 PROPERTIES OF EL Ni-P AND Ni-P-X NANOCOMPOSITE COATINGS

1. All developed EL Ni-P-X nanocomposite coatings exhibits higher hardness than Ni-P alloy coatings and it achieve maximum on heat treatment due to the reinforcement of hard second phase 'X' in Ni-P matrix and precipitation of stable Ni_3P phase.
2. EL Ni-P-X nanocomposite coatings developed by non-conventional route attain higher hardness as compared to conventionally developed coatings due to uniform distribution of non-coagulated second phase 'X' particles in Ni-P matrix.
3. The codeposition of milled particles provides higher hardness than chemically synthesized particles due to the higher embeddement of 'X' nanoparticles in EL Ni-P matrix.
4. The specific wear rate and friction coefficient of EL Ni-P-X nanocomposite coating is found to be lower than Ni-P alloy coatings at different loads (1, 1.5, 2N) and sliding velocities (0.1, 0.2 m/s).
5. The lower wear rate and friction coefficient is showed by EL Ni-P-X nanocomposite coatings developed by *insitu* route compared to conventional ones owing to its highest hardness.

6. In case of EL conventional coatings, the inclusion of milled nanoparticles on Ni-P surface imparts slightly better wear resistance and lower friction coefficient with respect to chemically prepared nanoparticles.
7. The wear rate and coefficient of friction increases with increase in load from 1N to 2N respectively and increase in sliding velocity from 0.1m/s to 0.2m/s in all the coatings.
8. Mild adhesive wear is the predominant mechanism observed by worn surfaces for all developed Ni-P-X nanocomposite coatings.
9. EL Ni-P-X nanocomposite coatings demonstrated an improvement in corrosion resistance in both acidic (pH-4.5) and alkaline (pH-8) atmosphere over Ni-P alloy coatings.
10. Heat treatment ($400^{o}C$, 1h) further enhanced the corrosion resistance of Ni-P-X nanocomposite coatings due to its improved coating density and structure.
11. EL Ni-P-X coatings following *insitu* route showed lower corrosion rate over the conventional route. Moreover, the use of milled nanoparticles as reinforcement exhibited a slight decrease in corrosion resistance over the chemically prepared nanoparticles.
12. EL Ni-P-X coatings are found to be more corrosion resistant in alkaline (pH-8) atmosphere as compared to acidic (pH-4.5) one.
13. Top down approach using milling can be used successfully for developing Ni-P based nanocomposite coatings for wear resistance but affect corrosion resistance over the chemical methods.
14. The order of wear and corrosion resistance in Ni-P-X [X= Al_2O_3, ZrO_2 and TiO_2] nanocomposite coatings follows the trend- $Al_2O_3 > ZrO_2 > TiO_2$.

CHAPTER 9

SUGGESTIONS FOR FUTURE WORK

Design and development of nanocomposite coatings for wear and corrosion resistance applications has opened the door to develop newer variants of nanocomposite coatings and understanding of their tribological and corrosion behaviour. There are still tremendous opportunities to work in the era of nanocomposite coatings and some of them are listed as follows:

- For development of non-conventional coatings, in order to to yield better properties, control of insitu precipitation reaction is required. This is attributed by use of suitable dispersants within the EL bath which is expected to form non-coagulated particles. Hence, uniform distribution of particles in Ni-P matrix can be consummated.
- The newer variants or their combinations with different volume fraction can be employed as reinforcement in Ni-P coating to form nanocomposite coatings may lead to tailored properties. The mechanical, tribological and corrosive performance of such Ni-P-X nanocomposite coatings can be determined for better exploitation of EL Ni-P based composite technology.
- The wear and friction behavior could be assessed for varying parameters like sliding speeds and loads. Moreover, wear, friction and corrosion performance of EL Ni-P-X coatings can be studied under different environments and also by the use of different wear and corrosion testing geometries. The further understanding of tribological and corrosion responses in the Ni-P-X nanocomposite coatings may be used to gain knowledge regarding its commercial capabilities for specific engineering applications.

REFERENCES

1. Abraham S., Pai B.C., Satyanarayana K.G. and Vaidyan V.K., (1990), "Studies on Nickel Coated Carbon Fibers and their Composites", J. Mater. Sci., Vol. 25, pp. 2839-2845.
2. Adam J., Drumm R., Klein G. and Veithw M., (2008), "Milling of Zirconia Nanoparticles in a Stirred Media Mill", J. Am. Ceram. Soc., Vol. 91, No.9, pp. 2836-2843.
3. Afroukhteh S., Dehghanian C., Emamy M., (2012), "Preparation of electroless Ni-P composite coatings containing nano-scattered alumina in presence of polymeric surfactant", Prog. Nat. Sci. Mater. Inter., Vol. 22(4), pp. 318–325.
4. Agarwala R. C., (1987), "Structural Studies and Crystallization Behaviour of Electroless Ni-P Films", Ph.D. Thesis, University of Roorkee, Roorkee (India).
5. Agarwala R. C. and Ray S., (1992), "Crystallization Behaviour of Electroless Ni-P Films Part II: A Kinetics Study", Z. Metallkd., Vol. 83, No. 3, pp. 203-207.
6. Alirezaei S., Monirvaghefi S.M., Salehi M., Saatchi A., (2004), "Effect of alumina content on surface morphology and hardness of Ni-PAl_2O_3(α) electroless composite coatings", Surf. Coat. Technol., Vol. 184, pp. 170–175.
7. Alirezaei S., Monirvaghefi S.M., Salehi M., Saatchi A., (2007), "Wear behavior of Ni-P and Ni-P-Al_2O_3 electroless coatings", Wear, Vol. 262, pp.978–985.
8. Alishahi M., Monirvaghefi S. M., Saatchi A., Hosseini S. M., (2012), "The effect of carbon nanotubes on the corrosion and tribological behavior of electroless Ni-P-CNT composite coating", Appl. Surf. Sci., Vol. 258, pp. 2439-2446.
9. Allahkaram S.R., Nazari M.H., Mamaghani S., Zarebidaki A., (2011), "Characterization and Corrosion behavior of electroless Ni-P/ nano-SiC coating inside the CO_2 containing media in the presence of acetic acid", Mater. Des, Vol. 32, pp. 750–755.
10. Allahkaram S.R., Salmi S., Tohidlou E., (2012), "An investigation on effects of TiO_2 nanoparticles incorporated in electroless Ni-P coatings properties", Inter. J Modern Phys.: Confer. Ser., Vol. 5, pp. 833–840.
11. Ambrus Z., Bala´zs N., Alapi T., Wittmann G., Sipos P., Dombi A., Mogyoro´si K., (2008), "Synthesis, structure and photocatalytic properties of Fe (III)-doped TiO_2 prepared from $TiCl_3$", Appl. Catal. B Environ., Vol.81, pp. 27–37.

12. Apachitei I., Duszczyk J., Katgerman L., Overkamp P.J. B., (1998/1), "Electroless Ni-P Composite Coatings: The Effect of Heat Treatment on the Microhardness of Substrate and Coating", Scripta Mater., Vol. 38, No. 9, pp. 1347-1353.
13. Apachitei I., Duszczyk J., Katgerman L., Overkamp P.J. B., (1998/2), "Particles Co-deposition by Electroless Nickel", Scripta Mater., Vol. 38, No. 9, pp. 1383-1389.
14. Apachitei I., Duszczyk J., (1999), "Hydrogen Evolution, Incorporation and Removal in Electroless Nickel Composite Coatings on Aluminium", J. of Appl. Electrochem., Vol. 29, pp. 837-843.
15. Apachitei I., Duszczyk J., (2000), "Autocatalytic Nickel Coating on Aluminium with Improved Abrasive Wear Resistance", Surf. Coat. Technol., Vol. 132, pp. 89-98.
16. Balaraju J.N., Kalavati, Rajam K.S. (2006), "Influence of particle size on the microstructure, hardness and corrosion resistance of electroless Ni-P-Al_2O_3 composite coatings", Surf. Coat. Technol., Vol. 200, pp. 3933-3941.
17. Balaraju J .N., Narayanan TSN Sankara, Seshadri S.K., (2001), "Evaluation of the corrosion resistance of electroless Ni-P and Ni-P composite coating by electrochemical impedance spectroscopy", Solid State Electrochem, Vol.5, pp. 334–8.
18. Balaraju J.N., Narayana TSN Sankara, Seshadri S.K., (2003), "Electroless Ni–P composite coatings", J Appl Electrochem, Vol. 33, pp. 807–816.
19. Balaraju J.N., Narayanan T.S.N. Sankara, Seshadri S.K., (2006), "Structure and phase transformation behaviour of electroless Ni–P composite coatings", Mater. Res. Bull., Vol. 41, pp. 847-860.
20. Balaraju J.N., Rajam K.S., (2008), "Preparation and characterization of autocatalytic low phosphorus nickel coatings containing submicron silicon nitride particles" J Alloy Compd, Vol. 459, pp. 311-319.
21. Balaraju J.N., Selvi V.E. and Rajam K. S. (2010), "Electrochemical behaviour of high phosphorus electroless Ni-P-Si_3N_4 composite coatings", Trans. IMF, Vol. 88, Iss. 6, pp. 311-316.
22. Balaraju J.N., Seshadri S.K., (1998), "Synthesis and corrosion behavior of electroless Ni-P-Si_3N_4 composite coatings", J. Mater. Sci. Lett., Vol. 17, pp. 1297-1299.
23. Bangwei Z., Haowen X., (2000), "Effect of alloying elements on the amorphous formation and corrosion resistance of electroless Ni-P based alloys", Mater. Sci. Eng., A Vol. 281, pp. 286-291.

24. Basu S. and Chakravorty D., (2006), "Optical Properties of Nanocomposites with Iron Core-Iron Oxide Shell Structure", J. Non-Cryst. Solids, Vol. 352, No.5, pp. 380-385.
25. Baudrand D.W., (1994), "Electroless Nickel Plating", ASM Handbook, Surf Eng., Vol. 5, pp. 290-310.
26. Bedingfield P. B., Lewis D.B., Datta P. K., Gray J. S., Wells P.B., (1991), "Studies of Electroless Nickel-Boron Alloy Coatings", Trans. Inst. Metal Finish., Vol. 70, No. 1, pp. 19-23.
27. Bigdeli F., Allahkaram S. R., (2009), "An investigation on corrosion resistance of as-applied and heat treated Ni–P/nanoSiC coatings", Mater. Des., Vol. 30, pp. 4450-4453.
28. Bin S. M., Leyland A., James A. S., Matthew A., Housden J., Garside B., (1996), "Substrate Surface Finish Effects in Duplex Coatings of PAPVD TiN and CrN with Electroless Nickel-Phosphorus Interlayers", Surf. Coat. Technol., Vol. 81, No. 2-3, pp. 215-224.
29. Bjgrkval J., Sichen D., Seetharaman S., (2000), "Thermodynamic description of $A1_2O_3$-CaO-MnO and $A1_2O_3$-FeO-MnO melts - a model approach", Calphad, Vol. 24, No. 3, pp. 353-376.
30. Bozzini B., Cavallotti P.L., (1997), "Evidence of Clustering in X-ray Amorphous Ni-P Prepared by Autocatalytic Chemical Deposition", Scripta Mater., Vol. 36, No.1, pp. 1245-1248.
31. Bozzini B., Lenardi C., Serra M., Faniglulio M., (2002), "Electrochemical and X-ray photoelectron spectroscopy investigation into anodic behaviour of electroless Ni–9.5 wt% P in acidic chloride environment", Brit Corros J, Vol. 37, pp. 173-81.
32. Bozzini B., Martini C., Cavallotti P.L., Lanzoni E., (1999), "Relationships among Crystallographic Structure, Mechanical Properties and Tribological Behavior of Electroless Ni-P (9%)/B_4C Films", Wear, Part-2, Vol. 225-229, pp. 806-813.
33. Brenner A., Riddell G., (1946), "Nickel Plating on Steel Chemical Reduction", Res. Nat. U. S. Bur. Stand., Vol. 37, pp. 31.
34. Brenner A. and Riddell G., (1947), "Nickel Plating on Steel by Chemical Reduction", Res. Nat. U. S. Bur. Stand, Vol. 39, pp. 385.
35. Bull S. J., (1997), "Tribological and Micro-Tribological Phenomena in Coatings", Mater. Sci. Forum, Vol. 246, pp. 105-152.
36. Casanova J.R., Fabregas I.O., Lamas D.G., Reca N.E.W., Lascalea G.E., Kempf R., Craievichd A.F. and Santillie C.V., (2007), "Structure of Nanoporous Zirconia-Based Powders Synthesized by Different Gel-Combustion Routes", J. Appl. Cryst., Vol.40, pp. s147-s152.

37. Chen W., Gao W., He Y., (2010), "A novel electroless plating of Ni-P-TiO_2 nano-composite coatings", Surf. Coat. Tech., Vol. 204, pp. 2493–2498.
38. Chen W., Gao W., He Y., (2010), "Sol-enhanced triple-layered Ni–P–TiO_2 composite coatings", J Sol-Gel Sci Technol, Vol. 55, pp. 187–190.
39. Chitty J., Pertuz A., Hintermann H., Staia M. H., Puchi E.S., (1997), "Influence of Electroless Ni-P Deposits on the Corrosion Fatigue Properties of an AISI 1045 Steel", Thin Solid Films, Vol.308-309, pp. 430-435.
40. Colaco R., Vilar R., (2003), "A model for the abrasive wear of metallic matrix particle-reinforced materials", Wear, Vol. 254, Iss. 7, pp. 625-634.
41. Colin S.B., Caër G. L., Villieras F., Devaux X., Simonnot M. O., Girot T., Weisbecker P., (2002), "From high-energy ball-milling to surface properties of TiO_2 powders", JMNM, Vol. e, pp. 27-36.
42. Crobu M., Scorciapino A., Elsener B., Rossi A., (2008), "The corrosion resistance of electroless deposited nanocrystalline Ni-P alloys", Electrochim. Acta., Vol. 53, pp. 3364–3370.
43. Debsikdar J.C., (1987), "Influence of Synthesis Chemistry on Alumina-Zirconia Powder Characteristics", J. Mater. Sci., Vol. 22, pp. 2237-2247.
44. Dennis J.K., Sagoo K.S., (1991), "Wear behavior of engineering coatings and surface treatments", Met. Finish, Vol. 89, pp. 111–121.
45. Dong D., Chen X.H., Xiao W.T., Yang G.B., Zhang P.Y., (2009),"Preparation and properties of electroless Ni-P-SiO_2 composite coatings", Appl. Surf. Sci., Vol. 255, pp. 7051-7055.
46. Duchnaiya R.K., Sharma A., Totlani M.K., Upadhyay S., (2011),"Morphology and corrosion study of electroless Ni-P coating on commercial aluminium alloys", Mater. Sci. Res. Int., Vol. 81, pp. 301-307.
47. Dwivedi D.K., Sharma A., Rajan T.V., (2011), "Friction and wear behavior of cast hypereutectic Al-Si alloy (LM28) at low sliding velocities", Indian Ins. Met., Vol. 54 , pp. 247-254.
48. Elsener B., Crobu M., Scorciapino M.A., Rossi A., (2008), "Electroless deposited Ni-P alloys: corrosion resistance mechanism", J Appl Electrochem, Vol. 38, pp.1053–60.
49. Eriksson R., Seetharaman S., (2004), "Thermal Diffusivity Measurements of Some Synthetic CaO-Al_2O_3-SiO_2 Slags", Metall. Mat. Transac. B, Vol. 35B, pp.461.
50. Feldstein N., (1983), "Electroless (Autocatalytic) Plating" and "Electroless Composite Plating", Met. Finish, Vol. 82, 1A, pp. 408-416 and pp. 417-420.

51. Feldstein N., Lancsek T., Lindsay D., Salerno L., (1983), “Electroless Composite Plating”, Met. Finish, Vol. 81, No. 8, pp. 35-41.
52. Ganesan V., Ganesan V., (1998), “Corrosion of annealed AISI 316 stainless steel in sodium environment”, J. Nucl. Mater., Vol. 256, pp.69-77.
53. Ganesan V., Ganesan V., Borgstedt H.U., (2003), “Analysis of CREVONA sodium loop material”, J. Nucl. Mater., Vol. 312, pp. 174–180.
54. Ganesan V., Seetharaman V., Raghunathan V.S., (1984), “Interdiffusion In The Nickel-Iron System”, Mater. Lett., Vol. 2, pp. 257-626.
55. Gadhikar A.A., Sharma A., Goel D.B., Sharma C.P., (2014), "Effect of carbides on erosion resistance of 23-8-N steel”, Bull. Mat. Sci., Vol. 37, pp. 315-319.
56. Gaurilow G.G., (1979), “Chemical (Electroless) Nickel Plating”, Porticullis Press, Redhill, England.
57. Gawad S.A.A., Baraka A.M., Morsi M.S. and Eltoum M.S.A., (2013), “Development of Electroless Ni-P-Al_2O_3 and Ni-P-TiO_2 Composite Coatings from Alkaline Hypophosphite Gluconate Baths and their Properties”, Int. J. Electrochem. Sci., Vol. 8, pp. 1722 – 1734.
58. Gawne D.T., Ma U., (1987), “Wear Mechanisms in Electroless Nickel Coating”, Wear, Vol. 120, pp. 125-149.
59. Gawne D.T., Ma U., (1989), “Friction and Wear of Chromium and Nickel Coatings”, Wear, Vol. 129, pp. 123-142.
60. Gay P.A., Limat J.M., Steinmann P.A., Pagetti J., (2007), “Characterisation and mechanical properties of electroless Ni-P–ZrO_2 coatings”, Surf. Coat. Technol., Vol. 202, pp. 1167–1171.
61. Georgiza E., Novakovic J., Vassiliou P., (2013), “Characterization and corrosion resistance of duplex electroless Ni–P composite coatings on magnesium alloy”, Surf. Coat. Technol., Vol. 232, pp. 432–439.
62. Gerasopoulos K., Chen X., Culver J., Wang C., Ghodssi R., (2010), “Self-assembled Ni/TiO_2 nanocomposite anodes synthesized via electroless plating and atomic layer deposition on biological scaffolds”, Chemical Communication, Vol. 46, Iss. 39, pp. 7349.
63. Giampaolo A.R, Ordonez J.G., Gugliemacci J.M., Lira J., (1997), “Electroless Nickel-Boron Coatings on Metal Carbides’, Surf. Coat. Technol., Vol. 89, pp. 127-131.
64. Gillespie P., (1997), “EL Nickel Coatings: Case Study. In Surface Engineering Casebook”; Burnell-Gray, J. S., Datta, P. K., (eds), Woodhead Publishing Limited, pp. 49.

65. Graham A.H., Lindsay R.W., Read H.J., (1962), "Structure of Electroless Nickel", J. of Electrochem. Soc., Vol. 109, No. 12, pp. 1200-1201.
66. Graham, A.H., Lindsay R.W., Read H.J., (1965), "The Structure and Mechanical Properties of Electroless Nickel", J. of Electrochem. Soc., Vol. 112, No. 4, pp. 401-413.
67. Groshart E.A., (1983), "Design for Finishing: Electroless Nickel Coating - its Use in Design", Met. Finish., Vol. 81, No. 11, pp. 19-21.
68. Grosjean A., Rezrazi M., Tachez M., (1997), "Study of the Surface Charge of Silicon Carbide (SiC) Particles for Electroless Composite Deposits: Nickel-SiC", Surf. Coat. Technol., Vol. 96, No. 2-3, pp. 300-304.
69. Guo X., Guo M., Zhang M., Wang X., Chou K.C., (2010), "Effects of pretreatment of substrates on the preparation of large scale ZnO nanotube arrays", Rare Met., Vol. 29,Iss.1, pp. 21-25.
70. Guo X.W., Wang S.H., Yang H.Y., Peng L.M., Ding W.J., (2011), "Characterization of Ni-P/TiO_2 MMC Coatings Prepared by Electroless Plating Process on Mg-Nd-Zn-Zr Magnesium Alloys" Mater. Sci. Forum, Vol. 690, pp. 422-425.
71. Gupta R.K., Pant B., Agarwala V., Ramkumar P., Sinha P.P., (2010), "Development of TiB_2 reinforced in-situ Ti aluminide matrix composite through reaction synthesis" Trans. Indian Inst. Met., Vol 63, Issue 4, pp. 715-718.
72. Gupta R.K., Pant B., Agarwala V., Sinha P.P., (2012), "Differential scanning calorimetry and reaction kinetics studies of $\gamma + \alpha_2$ Ti aluminide", Mater. Chem. Phys., Vol. 137, Iss. 2, pp. 483–492.
73. Gupta R.K., Pant B., Agarwala V., Sinha P.P., (2012), "Effect of Ti particle size on reaction synthesis of Ti aluminide", Mater. Sci. Forum, Vol. 710, pp. 314-319.
74. Gutzeit G., (1959), "Outline of the Chemistry Involved in the Process of Catalytic Nickel Deposition from Aqueous Solution", Plat. Surf. Finish., Vol. 46, pp. 1158, 1275, 1377.
75. Habig K.H., (1989), Wear behaviour of surface coatings on steels, Tribol Int., Vol 22 , pp.2.
76. Hamdy A.S., Shoeib M.A., Hady H., Salam O.F. Abdel, (2007), "Corrosion behavior of electroless Ni-P alloy coatings containing tungsten or nano-scattered alumina composite in 3.5% NaCl solution", Surf Coat Tech, Vol. 202, pp. 162–171.
77. Hameed Abdel R.M., Fekry A.M., (2010), "Electrochemical impedance studies of modified Ni-P and Ni-Cu-P deposits in alkaline medium", Electrochem. Acta, Vol. 55, pp. 5922–5929.

78. Hamid Z.A., Elkhair M.T.A., (2002), "Development of electroless nickel–phosphorous composite deposits for wear resistance of 6061 aluminum alloy", Mater. Lett., Vol. 57, pp. 720–726.
79. Harris S.J., Overs M. P., Gould A. J., (1985), "The Use of Coatings to Control Fretting Wear at Ambient and Elevated Temperatures", Wear, Vol. 106, pp. 35-52.
80. Hazan Y., Zimmermann D., Z'graggen M., Roos S., Aneziris C., Bollier H., Fehr P., Graule T., (2010), "Homogeneous electroless Ni–P/SiO_2 nanocomposite coatings with improved wear resistance and modified wear behavior " Surf. Coat. Technol., Vol. 204, pp. 3464-3470.
81. He Y.J., Winnubst A.J.A., Schipper D.J., Burggraaf A.J., Verweij H., (1997), "Effects of a second phase on the tribological properties of Al_2O_3 and ZrO_2 ceramics", Wear, Vol. 210, pp.178-187.
82. Henry J., (1985), "Electroless (Autocatalytic, Chemical) Plating", Met. Finish., Vol. 83, pp. 372-387.
83. Hogmark S., Hedenqvist P., Jacobson S., (1997), "Tribological Properties of Thin Hard Coatings: Demand and Evaluation", Surf. Coat. Technol., Vol. 90, No. 3, pp. 247-257.
84. Holmberg K., Mathews A., Ronkainen H., (1998), "Coatings Tribology - Contact Mechanisms and Surface Design", Trib. Int., Vol. 31, No. 1-3, pp. 107-120.
85. Hong J.S., Torre S.D. De la, Miyamoto K., Miyamoto H., Gao L., (1998), "Crystallization of Al_2O_3/ZrO_2 solid solution powders prepared by coprecipitation", Materials Letters, Vol.37, pp. 6–9.
86. Hou F, Wang W, Guo H, (2006), "Effect of the dispersibility of ZrO_2 nanoparticles in Ni-ZrO_2 electroplated nanocomposite coatings on the mechanical properties of nanocomposite coatings", Appl Surf Sci, Vol. 252, pp. 3812–3817.
87. Huang Y.S., Zeng X.T., Hu X.F., Liu F.M., (2004), "Corrosion resistance properties of electroless nickel composite coatings", Electrochem. Acta, Vol. 49, pp. 4313–4319.
88. Hur K.H., Jeong J.H., Lee D.N., (1990), "Microstructures and Crystallization of Electroless Ni-P Deposits", J. Mater. Sci., Vol. 25, pp. 2573-2584.
89. Husheng G., Haicheng G., Huijiu Z., (1991), "Sliding Wear and Fretting Fatigue Resistance of Amorphous Ni-P Coatings", Wear, Vol.142, pp. 291-301.
90. Indris S., Bork D. and Heitjans P., (2000), "Nanocrystalline Oxide Ceramics Prepared by High-Energy Ball Milling" J. Mater. Synth. Process., Vol. 8, Nos. 3/ 4.
91. Ivanov M. V., (2001), "Electroless Nickel-Boron-Phosphorus Coatings: Protective and Functional Properties", Prot. Met, Vol. 37 (6), pp. 592-596.

92. Jiaqiang G., Yating W., Lei L., Wenbin H., (2005), "Crystallization behavior of nanometer-sized Al_2O_3 composite coatings prepared by electroless deposition", Mater. Lett., Vol. 59, pp. 391–394.
93. Jiaqiang G., Lei L., Yating W., Bin S., Wenbin H., (2006), "Electroless Ni-P-SiC composite coatings with superfine particles", Surf. Coat. Technol., Vol. 200, pp. 5836–5842.
94. Juarez J.C., Morales R., (2008), "Reduction Kinetics of Ag_2MoO_4 by Hydrogen", Met. Mater. Trans. B, Vol. 39, Iss. 5, pp.738-745.
95. Karthikeyan S. , Ramamoorthy B., (2014), "Effect of reducing agent and nano Al_2O_3 particles on the properties ofelectroless Ni–P coating", Appl. Surf. Sci., Vol. 307, pp. 654–660.
96. Karwan B.J., (2011), "The Properties of Fe-Ni-Mo-Cu-B materials produced via liquid phase sintering", Archives Metall. Mater., Vol. 56.
97. Karwan B.J., Dymkowski T., Sobiecki J.R., Formanski. T, (2010), "Processing and surface properties based on iron sintered alloys after plasma nitriding treatment", Archives Metall. Mater., Vol. 55.
98. Karwan B.J., Gotman I., Gutmanas E.Y. , (2003), "Processing of dense Fe–based alloys with fine microstructure via short distance infiltration of low melting phase", Powder Metall. Prog., Vol. 3, pp. 175.
99. Karwan B.J., M. Rosso, (2006), "The effect of boron on the properties of Fe-Mo PM sintered alloys", Powder Metall. Prog., Vol. 6, pp.11.
100. Khalifa O.R.M., Wahab E.A.E. and Tilp A.H., (2011),"The effect of Sn and TiO_2 Nano Particles added in Electroless Ni-P Plating Solution on the Properties of Composite Coatings", Aus. J. Bas. App. Sci., Vol. 5(6), pp. 136-144.
101. Kikandi S., Brito J., Sadik O.A, (2007), "Electroless deposition of TiO_2/Ti onto aluminum substrates", J Electrochem. Soc., Vol.154.
102. Krishnan K.H., John S., Srinivasan K.N., Praveen J., Ganesan M., Kavimani P.M., (2006), "An overall aspect of electroless Ni-P depositions: a review article", Metall. Mater. Trans. A, Vol. 37A, pp. 1917–1926.
103. Kumar A., Agarwala V. and Singh D., (2014), "Effect of milling on dielectric and microwave absorption properties of SiC based composites", Ceram. Int., Vol. 40, pp.1797–1806.
104. Lanzoni, E., Martini, C., Ruggeri, O., Bertoncello, R. and Glisenti, A., (1997), "Structure and Corrosion Behaviour of Electroless Ni Coatings Deposited from

Differently Stabilised Baths", Published for European Fedration of Corrosion, the Institute of Materials, Edited by Fedrizzi, L. and Bonora, Vol. 672, pp. 232-243.

105. León C., Ochoa E.G., Guerra J.G., Sánchez J.G., (2010), "Annealing temperature effect on the corrosion parameters of autocatalytically produced Ni-P and Ni–P–Al_2O_3 coatings in artificial seawater" Surf. Coat. Technol., Vol. 205, pp. 2425–2431.
106. Levy D. J., (1963), "Thin Nickel Films by Hydrazine Autocatalytic Reduction", Electrochem. Tech., Vol. 1, p. 38.
107. Lee C.K., (2012), "Comparative Corrosion Resistance of Electroless Ni-P/nano-TiO_2 and Ni-P/nano-CNT Composite Coatings on 5083 Aluminum Alloy", Int. J. Electrochem. Sci., Vol. 7, pp. 12941-12954.
108. Li C., Wang Y., Pan Z., (2013), "Wear resistance enhancement of electroless nanocomposite coatings via incorporation of alumina nanoparticles prepared by milling", Mater. Des., Vol. 47, pp. 443–448.
109. Li J., Hu X., Wang D., (1996), "Effects of Codeposited Tungsten on the Properties of Low-Phosphorus Electroless Nickel Coatings", Plat. Surf. Finish., Vol. 83, No. 8, pp. 62-64.
110. Li J.G., Sun X.D., (2000), "Synthesis and sintering behavior of a nanocrystalline α-alumina powder", Acta Mater., Vol. 48 (12), pp. 3103-3112.
111. Li Y., (1997), "Investigation of Electroless Ni-P-SiC Composite Coatings", Plat. Surf. Finish., Vol. 84, No. 11, pp. 77-81.
112. Li Y., Guo M., Zhang M., Wang X., (2009), "Hydrothermal synthesis and characterization of TiO_2 nanorod arrays on glass substrates", Mater. Res. Bull., Vol. 44, Iss.6, pp. 1232-1237.
113. Lin J.F., Lian J.C., Li K.Y., (1997), "The effect of electroless nickel film on the tribological characteristics of alumina coatings", Wear, Vol. 209, pp.199-212.
114. Lim S.C., Ashby M.F., (1990), "Wear mechanism maps", Scripta Metall Mater, Vol. 24, Iss. 5, pp. 805-810.
115. Liang T., Sun J., Zhang L. L. and Ji Z. Z., (2009), "Corrosion behavior of electroless Ni-P deposits", Surf. Technol., Vol. 38, pp. 28–29.
116. Liu Y.Y., Yu J., Huang J., Xu B.H., Liu X.L., Gao Y., Dong X.L., (2007),"Synthesis and tribological behavior of electroless Ni-P-WC nanocomposite coatings", Surf. Coat. Technol., Vol. 201, pp. 7246-7251.
117. Lu J.H., Sun W.C., Zhu M., Tan M.F., Zhou Q, (2010), "Effects of Content of Al_2O_3 Particles and Heat Treatment on Corrosion Resistance of Ni-P-Al_2O_3 Composite Coatings", Adv. Mater. Res., Vol. 105-106, pp. 441-443.

118. Luo L., Yao J., Li J., Yu J., (2009), "Preparation and characterization of sol-gel Al_2O_3/Ni–P composite coatings on carbon steel", Ceram. Int., Vol. 35, pp. 2741–2745.
119. Mafi I.R., Dehghanian C., (2011), "Studying the effects of the addition of TiN nanoparticles to Ni–P electroless coatings", Appl. Surf. Sci., Vol. 258, pp. 1876-1880.
120. Mahoney M.W., Dynes P.J., (1985), "The Effects of Thermal History and Phosphorus Level on the Crystallization Behavior of Electroless Nickel", Scr. Metall., Vol. 19, pp. 539-542.
121. Mai Q.X., Daniels R.D., Harpalani H.B., (1988), "Structural Changes Induced by Heating in Electroless Nickel-phosphorus Alloys", Thin Solid Films, Vol. 166, pp. 235-247.
122. Mallory G. O., (1974), "Influence of the Electroless Plating Bath on the Corrosion Resistance of the Deposits", Plating, Vol. 61, pp. 1005-1014.
123. Mallory, G.O., (1979), "The Electroless Nickel Plating Bath", Reprinted Courtesy Allied Kellite Products Division, The Richardson Company, Des Plaines, Illinois 60018. Originally presented at Electroless Nickel Conference, Nov. 1979, Cincinnati, Ohio.
124. Mazaheri H., Allahkaram S.R., (2012), "Deposition, characterization and electrochemical evaluation of Ni-P-nano diamond composite coatings", Appl. Surf. Sci., Vol. 258, pp. 4574-4580.
125. Miao X. and Ben B.N., (2000), "Microstructure and Properties of Zirconia-Alumina Nanolaminate Sol-Gel Coatings", J. Mater. Sci., Vol.35, No.2, pp. 497-502.
126. Michalski J., Konopka K., Trzaska M., (2003), "Description of Al_2O_3 powders coated by Ni–P particles obtained through an electroless chemical reaction and possibilities to obtain an Al_2O_3/Ni–P composite", Mater. Chem. Phys., Vol. 81, pp. 407–410.
127. Mirjalili F., Hasmaliza M., Abdullah L.C., (2010), "Size-controlled synthesis of nano α-alumina particles through the sol-gel method", Ceram. Int., Vol.36, pp.1253–1257.
128. Mishra D., Agarwala V. and Agarwala R.C., (2013), "Synthesis of Nanograined Ti-Al-Cr-Nb-X [X = Ni-P-Coated Graphite and Carbon] Intermetallic Matrix Composites by Mechanical Alloying", Particul Sci Technol, Vol. 31, Iss. 4.
129. Momenzadeh M., Sanjabi S., (2011), "The effect of TiO_2 nanoparticle codeposition on microstructure and corrosion resistance of electroless Ni P coating", Mater. Corros, Vol. 10, pp. 1002.
130. Moonir S.M., Saatchi A., Hedjazi J., (1997), "Tribological Behaviour of Electroless Ni-P-MoS_2 Composite Coatings", Z. Mettalkd., Vol. 88, No 6, pp. 498-501.

131. Morales R., Albiter A., Salazar M., (2005), "Corrosion behavior of uniaxially cold-pressed Fe_2Mo intermetallic in 0.5M H_2SO_4", Mater. Sci. Eng. A, Vol. 397, Iss. (1-2), pp. 1-7.
132. Morales R., Francisco J. T., Ragnhild E. A., (2005), "Hydrogen reduction of complex oxides-a novel route toward the production of nanograined alloys and intermetallics", Scand. J. Metall., Vol 34, Iss. 2, pp. 108-115.
133. Muslimin M. and Yusoff M., (2009), "The effect of high energy milling on the crystallite size of alumina", JNRT, Vol. 6, No. 1, (Special Edition).
134. Nai SML, Wei J, Gupta M, (2006), "Development of lead-free solder composites containing nanosized hybrid (ZrO_2 + 8 mol.% Y_2O_3) particulates", Solid State Phenom., Vol. 11, pp. 59-62.
135. Narayanan T.S.N. Sankara, Selvakumar S., Stephen A., (2003), "Electroless Ni-Co-P ternary alloy deposits: preparation and characteristics", Surf Coat Tech, Vol. 172, pp. 298-30.
136. Nováka M., Vojtěcha D., Vı´tu˚ T., (2010), "Influence of heat treatment on tribological properties of electroless Ni-P and Ni-P-Al_2O_3 coatings on Al-Si casting alloy", Appl. Surf. Sci., Vol. 256, pp. 2956-2960.
137. Nováka M., Vojtěcha D., Vı´tu˚ T., (2010), "Influence of heat treatment on microstructure and adhesion of Al_2O_3 fiber-reinforced electroless Ni–P coating on Al-Si casting alloy", Mater. Charact., Vol. 6 1, pp. 668-673.
138. Novakovic J., Vassiliou P., Samara K., Argyropoulos T., (2006), "Electroless Ni-P-TiO_2 composite coatings: Their production and properties", Surf Coat Tech, Vol. 201, pp. 895–901.
139. Novakovic J., Vassiliou P., (2009), "Vacuum thermal treated electroless Ni-P-TiO_2 composite coatings", Electrochem. Acta, Vol. 54, pp. 2499–2503.
140. Odekerken, (1966), Brit. Pat. 1,041,753, U. S. Pat. 3,644,183 and DDR Pat. Vol. 41, pp. 406.
141. Oulladj M., Saidi D., Chassaing E., Lebaili S., (1999), " Preparation and properties of electroless Ni–Zn–P alloy films" J. Mater. Sci., Vol. 34, pp. 2437-2439.
142. Padmanabhan K.A, (2001), "Mechanical Properties of Nanostructured Materials", Mater. Sci. Eng. A, Vol. 304-306, pp. 200-205.
143. Panchula M.L., Ying J.Y., (2007), "Mechanical synthesis of nanocrystalline α-Al_2O_3 seeds for enhanced transformation kinetics", Nanostruct. Mater., Vol. 9 (1–8), pp. 161–164.

144. Park S. H., Lee D.N., (1988), "A Study on the Microstructure and Phase Transformation of Electroless Nickel Deposits", J. Mater. Sci., Vol. 23, pp. 1643-1654.
145. Pathak J.P., Mohan S., (2005), "Wear of Conventional and Experimental Aluminium Bearing Alloys Sliding Under Lubrication", MetaIlkd., Vol. 96, pp.297.
146. Pathak J.P., Mohan S., Rai D., (2005), "Dry Sliding Wear Behaviour of Martensitic Ni-Cr-Mo-V Steel Under Different Operating Loads", Met. Mater. Processes, Vol. 17(1), pp.43-54.
147. Patnaik P., (2002), "Handbook of Inorganic Chemicals", Kenneth, McComb McGraw-Hill, New York.
148. Pedraza, A. J., Godbole M.J., (1990), "Recrystallization and Mechanical Properties of Electroless Copper", Scripta Metall., Vol. 24, pp. 1185-1189.
149. Ping Ho Lo, Wen Ta Tsai, Ju Tung Lee and Ming Pan Hung, (1997), "The study of interdiffusion phenomena of Ni-P/steel interface", Scripta Metall Mater, Vol. 29, pp. 37-42.
150. Puchi, E. S., Staia, M. H., Hintermann, H, Pertuz, A. and Chitty, J., (1993), "Influence of Ni-P Electroless Coating on the Fatigue Behavior of Plain Carbon Steels", Thin Solid Films, Vol. 290-291, pp. 370-375.
151. Pushpavanam M., (1992), "Electroless Ni-P-Al_2O_3 Composites", Bull. Electrochem., Vol. 8 (8), pp. 399-401.
152. Rabinowicz E., (1965), Friction and Wear of Metals, John Wiley and Sons, Inc., New York, USA.
153. Rabizadeh T., Allahkaram S.R., (2011), "Corrosion resistance enhancement of Ni–P electroless coatings by incorporation of nano-SiO_2 particles", Mater. Des., Vol. 32, pp. 133-138.
154. Rabizadeh T., Allahkaram S.R., Zarebidaki A., (2010), "An investigation on effects of heat treatment on corrosion properties of Ni–P electroless nano-coatings", Mater. Des., Vol. 31, pp. 3174–3179.
155. Ramasubramanian M., Popov B.N., White R.E., Chen K.S., (1999), "A Mathematical Model for Electroless Copper Deposition on Planar Substrates", Electrochem. Soc., Vol. 146, No. 1, pp. 111-116.
156. Ranganatha S., Venkatesha T.V., Vathsala K., (2010), "Development of electroless Ni–Zn–P/nano-TiO_2 composite coatings and their Properties", Appl. Surf. Sci., Vol. 256, pp. 7377–7383.

157. Ranganatha S.,Venkatesha T.V., Vathsala K., (2012), "Process and properties of electroless Ni-Cu-P-ZrO_2 nanocomposite coatings", Mater. Res. Bull., Vol. 47, pp. 635–645.
158. Reddy V.V.N., Ramamoorthy B., and Nair P. K., (2000), "A study on the wear resistance of electroless Ni-P/diamond composite coatings", Wear, Vol. 239, No. 1, pp. 111-116.
159. Reid C. B., Forrester J. S., Goodshaw H. J., Kisi E. H., Suaning G. J., (2008), "A study in the mechanical milling of alumina powder", Ceram. Int., Vol. 34, pp. 1551-1556.
160. Sahoo P, Das S.K., (2011), "Tribology of electroless nickel coatings – A review", Mater Des, Vol. 32, pp. 1760–1775.
161. Segal D., (1997), "Chemical synthesis of ceramic materials", J. Mater. Chem.**,** Vol. **7**, pp. 1297-1305.
162. Seo D.S. and Kim H., (2003), "Synthesis and characterization of TiO_2 nanocrystalline powder prepared by homogeneous precipitation using urea", J. Mater. Res., Vol. 18, No. 3.
163. Šepelák V., Colin S.B. and Caërc G.L., (2012), "Transformations in oxides induced by high-energy ball-milling", Dalton Trans., Vol. 41, pp. 11927-11948.
164. Shahbazian F., Sichen D., Seetharaman S., (2002), "The effect of addition of Al_2O_3 on the viscosity of CaO-FeO-SiO_2-CaF_2 slags", Vol. 42, pp.155-162.
165. Sharma R., Agarwala R.C., Agarwala V., (2006), "Electroless Ni-P based Nanocoating Technology-A review", Synth. React. Inorg. Met. Org. Chem., Vol. 36, pp. 493-515.
166. Sharma S. B., Agarwala R.C., Agarwala V., (2003), "A Study on Synthesis and Empirical Model Development of Electroless Ni-P based Composite Coating", Trans. Indian Inst. Metals, Vol. 56 No. 6, pp. 583-590.
167. Sharma S. B., Agarwala R.C., Agarwala V., Ray S., (2002), "Application of Ni-P-ZrO_2-Al_2O_3-Al_3Zr Electroless Composite Coatings and their Characteristics", Int. J. Surf Eng., Vol. 18 No. 05, pp. 344-349.
168. Sharma S. B., Agarwala R.C., Agarwala V., Ray S., (2002), "Dry Sliding Wear and Friction Behaviour of Ni-P-ZrO_2-Al_2O_3 Composite Electroless Coatings on Aluminium", Int. J. Mater. Manuf. Process. , Vol. 17 (05), pp. 637-649.
169. Sharma S. B., Agarwala R.C., Agarwala V., Satyanarayana K.G., (2005), "Development of Electroless Composite Coatings by using In-Situ Co-precipitation followed by Co-deposition Process", Met. and Mat. Trans., Vol. 36B, pp. 23-31.
170. Sharma A. and Singh A.K., (2013), "Electroless Ni-P and Ni-P-Al_2O_3 Nanocomposite Coatings and Their Corrosion and Wear Resistance", J. Mater. Eng. Perform, Vol. 22, pp. 176-183.

171. Shibli S.M.A., Dilimon V.S., (2007), "Effect of phosphorous content and TiO_2-reinforcement on Ni–P electroless plates for hydrogen evolution reaction", Int. J. Hydrogen Energy, Vol. 32, pp. 1694-1700.
172. Shibli S.M.A., Dilimon V.S., Deepthi T., (2006), "ZrO_2 reinforced Ni–P plate: An effective catalytic surface for hydrogen evolution", Appl. Surf. Sci., Vol. 253, pp. 2189–2195.
173. Shrestha N. K., Hamal D. B., Saji T., (2004), "Composite plating of Ni-P-Al_2O_3 in two steps and its anti-wear performance", Surf. Coat. Technol., Vol. 183, pp. 247–253.
174. Sidky P.S., Hocking M.G., (1999), "Review of inorganic coatings and coating processes for reducing wear and corrosion, Corros. Eng. Sci. Technol., Vol. 34, pp. 171-183.
175. Song L., Wang Y., Lin W., Li Q., (2008), "Primary investigation of corrosion resistance of Ni-P/TiO_2 composite film on sintered NdFeB permanent magnet", Surf. Coat. Technol., Vol. 202, pp. 5146-5150.
176. Song Y.W, Shan D.Y., Chen R.S., Han E.H., (2007), "Study on electroless Ni–P–ZrO_2 composite coatings on AZ91D magnesium alloys", Surf. Engg., Vol. 23, No. 5, pp. 334-338.
177. Song L., Song S., Gao Z., (2004), "Formation of TiO_2 modified film on carbon steel", J. Mater. Sci. Technol., Vol.20, No. 5.
178. Song Y.W., Shan D.Y. and Han E.H., (2007), "Comparative study on corrosion protection properties of electroless Ni-P-ZrO_2 and Ni-P coatings on AZ91D magnesium alloy", Mater. Corros., Vol. 58, Iss. 7, pp. 506-510.
179. Song Y.W., Shan D.Y., Han E.H., (2008), "High corrosion resistance of electroless composite plating coatings on AZ91D magnesium alloys", Electrochim. Acta, Vol. 53, pp. 2135-2143.
180. Song L., Wang Y., Lin W., Liu Q., (2008), "Primary investigation of corrosion resistance of Ni-P/TiO_2 composite film on sintered NdFeB permanent magnet", Surf. Coat. Technol., Vol. 202, pp. 5146–5150.
181. Sorkhabi H.A., Rafizadeh S.H., (2004), "Effect of coating time and heat treatment on structures and corrosion characteristics of electroless Ni–P alloy deposits", Surf. Coat. Technol., Vol. 176, pp. 318–326.
182. Srivastava A., Mohan S., Agarwala V., Agarwala R.C., (1992), "Factors Influencing the Deposition Rate of Ni-B Electroless Films", and "On the Crystallization Behaviour of an Amorphous Ni-17.8 at.% B Electroless Deposit", Z. Metallkd., Vol. 83, No. 4, pp. 254-257, and 251-253.

183. Staia M.H., Castillo E.J., Puchi, E.S., Lewis B., Hintermann H.E., (1996), "Wear Performance and Mechanism of Electroless Ni-P Coating", Surf. Coat. Technol., Vol. 86-87, pp. 598-602.
184. Staia M.H, Enriquez C., Puchi E.S., (1997), "Influence of the Heat Treatment on the Abrasive Wear Resistance of Electroless Ni-P", Surf. Coat. Technol., Vol. 94-95, pp. 543-548.
185. Strafford K.N., Dutta P.K., Gray J.S., (1990), "Applications and Performance of Coatings: Some Perspectives and Prospects", Surf. Eng. Prac., Ellis Horwood Publishers, U.K., pp. 397-419.
186. Sun W.C., Tan M.F., Lu J.H., Zhang L., Zhou Q, (2010), "Corrosion and Oxidation Resistance of Electroless Ni-P-Al_2O_3 Composite Coatings on Carbon Steel", Appl. Mech. Mater., Vol. 34-35, pp. 831-835.
187. Szczygieł B. and Turkiewicz A., (2008), "The effect of suspension bath composition on the composition, topography and structure of electrolessly deposited composite four-component Ni–W–P–ZrO_2 coatings", Appl. Surf. Sci., Vol. 254, pp. 7410–7416.
188. Szczygieł B., Turkiewicz A., Serafińczuk J., (2008), "Surface morphology and structure of Ni–P, Ni–P–ZrO_2, Ni–W–P, Ni–W–P–ZrO_2 coatings deposited by electroless method", Surf. Coat. Technol., Vol. 202, pp.1904–1910.
189. Tabriz S.A.H., Nassaj E.T., (2009), Economical synthesis of Al_2O_3 nanopowder using a precipitation method, Mater. Lett., Vol. 63 , pp. 2274–2276.
190. Tan M.F., Sun W.C., Zhang L., Zhou Q. and Ding J., (2011), "High-Temperature Oxidation Resistance of Electroless Ni-P-ZrO_2 Composite Coatings" Mater. Sci. Forum, Vol. 686, pp. 569-573.
191. Tyagi B., Sidhpuria K., Shaik B., Jasra R., (2006), "Synthesis of Nanocrystalline Zirconia Using Sol-Gel and Precipitation Techniques", Ind. Eng. Chem. Res., Vol.45, pp. 8643-8650.
192. Valova E., Armyanov S., Franquet A., Hubin A., Steenhaut O., Delplancke J-L. and Vereecken J., (2001), "Electroless deposited Ni-Re-P, Ni-W-P and Ni-Re-W-P alloys", J. Appl. Electrochem., Vol. 31, pp. 1367-1372.
193. Vaben R. and Stover D., (1999), "Processing and Properties of Nanophase Ceramics", J. Mater. Process. Technol., Vol.92, No.93, pp.77-84.
194. Varma H.K., Mani T.V., Damodran A.D., (1994), "Characteristics of alumina powders prepared by spray-drying of boehmite sol", J. Am. Ceram. Soc., Vol. 77 (6), pp. 1597–1600.

195. Vasudvan R., Narayanan S., Karthik P.R., (1998), "Some Investigations on the Effect of Ultrasonic Agitation on the Properties of Nickel-Phosphorous and Nickel-Boron Electroless Deposits", Trans. Indian Inst. Met., Vol. 51, No. 5, pp. 445-448.
196. Vidacak B., Sichen D., Seetharaman S., (2001), "An Experimental Study of the Viscosities of Al_2O_3-CaO-"FeO" Slags", Metall. Mater. Transac. B, Vol 32B, pp. 679.
197. Wang L., Zhao L., Huang G., Yuan X., Zhang B., Zhang J., (2000), "Composition, structure and corrosion characteristics of Ni-Fe-P and Ni-Fe-P-B alloy deposits prepared by electroless plating", Surf. Coat. Tech., Vol. 126, pp. 272-278.
198. Wang L., Huang W., Huang G., and Zhao L., (2002), "Study of Magnetic Properties of Ni-Fe-P and Ni-Fe-P-B Chemical Films", Z Metallkd, Vol. 93, No. 4, pp. 298-302.
199. Wang L.Y., Tu J.P., Chen W.X., Wang Y.C., Liu X.K., Olk C., Cheng D.H., Zhang X.B., (2003), "Friction and wear behavior of electroless Ni-based CNT composite coatings", Wear, Vol. 254, pp. 1289-1293.
200. Wang S., Li X., Wang S., Li Y., Zhai Y., (2008), "Synthesis of γ-alumina via precipitation in ethanol" Mater. Lett., Vol. 62, pp. 3552–3554.
201. Wang S.H., Yang H.Y., Peng L.M., Ding W.J., (2011), "Characterization of Ni-P/TiO_2 MMC Coatings Prepared by Electroless Plating Process on Mg-Nd-Zn-Zr Magnesium Alloys", Mat. Sci. Forum, Vol. 690, pp 422.
202. Wang Y.Q., Zhou B.L., (1996), "Behaviour of Coatings on Reinforcements in Some Metal Matrix Composites", Composites, part A, Vol. 27A, pp. 1139-1145.
203. Wang Y.W., Xiao C.C., Deng Z.G., (1992), "Structure and corrosion resistance of electroless Ni-Cu-P", Plat. Surf. Finish, Vol 79 (3), pp. 57–59.
204. Wong W. L. E., Gupta M., (2007), "Improving Overall Mechanical Performance of Magnesium Using Nano-Alumina Reinforcement and Energy Efficient Microwave Assisted Processing Route", Adv. Eng. Mat., Vol. 9, Iss.10, pp. 902–909.
205. Wu Y.C., Zhang Z.M., Huang X.M., Shan C.L., Lin Z.P., (2009), "Study on photocatalytic Degradation of Electroless Ni-P-TiO_2 Composite Coating", Adv. Mater. Res., Vol. 75, pp.13-18.
206. Xu H., Yang Z., Li M.K., Y.Li. Shi, Y. Huang, H.L. Li,(2005), "Synthesis and properties of electroless Ni-P-nanometer diamond composite coatings", Surf. Coat. Tech., Vol. 191, pp. 161-165.
207. Yang W., Fu Y., Xia A., Zhang K., Wu Z., (2012),"Microwave absorption property of Ni-Co-Fe-P-coated flake graphite prepared by electroless plating", J. Alloy Compd., Vol. 518, pp. 6-10.

208. Yang Y., Chen W., Zhou C., Xu H., Gao W., (2011), "Fabrication and characterization of electroless Ni-P-ZrO_2 nano-composite coatings", Appl Nanosci., Vol.1, pp.19-26.
209. Yu L., Huang W., Zhao X., (2011), "Preparation and characterization of Ni-P-nanoTiN electroless composite coatings", J. Alloys Compd., Vol. 509, pp. 4154-4159.
210. Yu Z.X., He Q. H., Hui L., Liu H., Zhang S.G., (2007), "Electroless composite coatings of Ni-P-nano-TiO_2 (anatase-type) and its corrosion resistance", Mat Chem Eng, pp. 1005.
211. Yuan F.L., Chen C.H., Kelder E.M. and Schoonman J., (1998), "Preparation of Zirconia and Yttria-Stabilized Zirconia (YSZ) Fine Powders by Flame-Assisted Ultrasonic Spray Pyrolysis (FAUSP)", Solid State Ionics, Vol.109, No.1-2, pp. 119-123.
212. Yuan X.T., Hua Z.Q., Wang L., Sun D.B., and Chen S.L., (2011), "Effect of Nano Al_2O_3 Particles on the Ni-P-Al_2O_3 Nanocomposite Coatings Properties", Appl. Mech. Mater., Vol. 66-68, pp. 1668–1675.
213. Yuxiang L., Mei Z., Min G., Xidong W., Wang X., (2010), "Preparation and Characterization of TiO_2 Nanorod Arrays via Hydrothermal Approach", Rare Met. Mater. Eng., Vol. 38, pp. 1060-1063.
214. Zhang Q., Yao J., Pan Y., (2010), "Study of nanometer Al_2O_3 composite electroless deposit strengthened by different laser power", Mater. Des., Vol. 31, pp. 1695-1699.
215. Zhang Z., Chen D.L., (2006), "Consideration of Orowan strengthening effect in particulate-reinforced metal matrix nanocomposites: a model for predicting their yield strength", Scr Mater, Vol. 54, pp. 1321–1326.
216. Zhao C. and Yao Y., (2014), "Preparation and Mechanical Properties of Electroless Nickel- Phosphorus-Tungsten Carbide Nanocomposite Coatings", J. Mater. Eng. Perform., Vol. 23, pp. 193-197.
217. Zhong X., Gupta M., (2005), "High Strength Lead-Free Composite Solder Materials using Nano Al_2O_3 as Reinforcement", Adv. Eng. Mat., Vol. 7, Iss.11, pp. 1049–1054.
218. Zhou G-H, Ding H-Y, Fe Z., Zhou F. and Zhang Yue, (2008), "Structure and Mechanical Properties of Ni-P-Nano Al_2O_3 Composite Coatings Synthesized by Electroless Plating, J. Iron Steel Res. Inter., Vol. 15(1), pp. 65-69.
219. Zhou M.J., Zhang N., Zhang L., Yan J.H, (2012), "Photocathodic protection properties of Ni-P/TiO_2 bilayer coatings by a combined electroless plating and sol-gel method", Mater. Corros., Vol. 63, No. 8.

220. Zielin´ska K., Stankiewicz A., Szczygieł I., (2012), “Electroless deposition of Ni–P–nano-ZrO_2 composite coatings in the presence of various types of surfactants”, J. Colloid Interface Sci., Vol. 377, pp. 362–367.